

# 励起子系のエネルギー緩和と位相緩和

(課題番号59460024)

昭和60年度科学研究費補助金(一般B)  
研究成果報告書

昭和61年3月

研究代表者 舛本泰章

(東京大学物性研究所)

昭和60年度科学研究費補助金（一般研究B）

励起子系のエネルギー緩和と位相緩和  
（研究課題番号59460024）

研究組織

研究代表者	舩本 泰章	（東京大学物性研究所	助手）
研究分担者	高河原俊秀	（東京大学工学部	助手）

研究経費

昭和59年度	7,500	千円
昭和60年度	500	千円
計	8,000	千円

## はじめに

近年、超短パルスレーザー、超高速分光法の進歩は著しく、物質の種々の励起状態の緩和過程の研究もピコ秒領域からフェムト秒領域が可能になりつつある。一方、イオン結晶、半導体における基本的な最低電子励起状態である励起子は永く、光物性物理の中心的研究対象であり、この超高速分光法を用いて、励起子系の動的挙動の解明は待望されている。実際直接許容型の物質中の励起子の発光寿命は、ナノ秒程度であり、それより速い時間スケールで起る励起子の生成、緩和等のダイナミクスを直接、探る為には、ピコ秒分光法は唯一、必須の方法である。本研究では、このピコ秒分光法を主な実験研究手法として、励起子の緩和の原理的な問題から出発して、現代の固体物理学において、その役割の早急な解明が要請されている諸特性——次元性、ランダム性、局在性、界面——を、それらが励起子緩和に及ぼす影響を調べるという側面を通して研究する事を企画した。我々は、この様な問題意識にもとづき、励起子系のエネルギー緩和および位相緩和を、典型的モデル物質としてCuCl, CdSe, GaAs-AlAs超格子の三種類の物質を選び、実験、理論両面から多角的に研究した。CuClの励起子ポラリトンの位相緩和については、励起子ポラリトンの位相緩和とは何かという概念的問題から検討し、実験的には、ピコ秒時間分解非縮退四光波混合法をみだし、これにより研究した。強度依存性まで含めた実験により、励起子ポラリトンの位相緩和の要因としては、フォノン散乱よりはポラリトン相互の衝突によるものが重要である事を推論した。続いてII-VI族半導体の典型例としてCdSeの励起子系のエネルギー緩和の研究を、ピコ秒時間分解発光の方法により行い、三種の励起子-格子相互作用(変型ポテンシャル型、ピエゾ型およびフレリッヒ型)が、励起子系のエネルギー緩和へどう寄与するかを明かにした。二次元性と不均一性をあわせ持っている半導体超格子中の励起子の緩和は、CuClやCdSeの様な典型的な三次元結晶半導体中の励起子系の緩和とは、異なる様相を示す事が期待できる。この為、GaAs-AlAs, AlGaAs-AlAs超格子中の励起子の緩和をピコ秒時間分解発光の方法および、共鳴レイリー型光混合の方法により研究した。エネルギー緩和としては、励起子の状態密度スペクトルに依存する異常に遅いエネルギー緩和を見出した。これは、量子井戸内の厚さの不均一性により局在した励起子が、フォノンを放出しながら、状態密度スペクトルの裾の状態間を遷移するというモデルにより説明でき、その際あわせて、二次元励起子と音響型フォノンとの相互作用の一般理論を確立した。このモデルに従い量子井戸内の励起子の位相緩和を、励起子の局在性の指標としてとらえ、状態密度スペクトル中の移動度端近傍での位相緩和の様相、局在性の様相をしらべた。更に、量子井戸中での励起子波動関数の二次元的収縮を初めて実験的に明かにし、次に、垂直電場下でのGaAs-AlGaAs超格子中の励起子発光のピコ秒時間応答を調べる事により、半導体超格子中の光生成担体のトンネル過程のダイナミクスを初めて明かにした。又、量子井戸中の励起子が示す大きな光学的非線形分極率の原因について考察し、普通考えられている様な励起子の二次元性によるものより、むしろ量子井戸中の励起子のもつ局在性による巨大振動子効果のほうが寄与が大きい事を示した。

研究発表

<報文>

LIST OF PUBLICATIONS

- Y.Masumoto, Y.Unuma and S.Shionoya:  
"Picosecond Dynamics of Excitonic Polaritons and Excitonic Molecules"  
in "Semiconductor Processes Probed by Ultrafast Laser Spectroscopy" vol.I ed. R.R.Alfano (Academic Press, 1984) p.307.
- \*Y.Masumoto, S.Shionoya and T.Takagahara:  
"Optical Dephasing of Excitonic Polaritons in CuCl Studied by Time-Resolved, Nondegenerate Four Wave Mixing"  
Phys. Rev. Letters 51 923 (1983).
- \*Y.Masumoto, S.Shionoya and H.Kawaguchi:  
"Picosecond Time-Resolved Study of Excitons in GaAs-AlAs Multi-Quantum-Well Structures"  
Phys. Rev. B 29 2324 (1984).
- \*Y.Masumoto and S.Shionoya:  
"Picosecond Energy Relaxation Processes of Excitons in CdSe"  
Phys. Rev. B 30 1076 (1984).
- Y.Unuma, Y.Abe, Y.Masumoto and S.Shionoya:  
"Dynamical Behavior of High Density Electron-Hole System in CdSe"  
Phys. status solidi (b) 125 735 (1984).
- Y.Masumoto, H.Kunitomo, S.Shionoya, H.Munekata and H.Kukimoto:  
"Polarization Memory of Luminescence from Photo-Generated Carriers in a-Si<sub>1-x</sub>C<sub>x</sub>:H (x~0.2)"  
Solid State Commun. 51 209 (1984).
- Y.Masumoto:  
"Picosecond Dephasing and Energy Relaxation of Excitons in Semiconductors"  
in "Ultrafast Phenomena IV" ed. D.H.Auston and K.B.Eisenthal (Springer, 1984) p.156; Proc. 4th Int. Conf. on Ultrafast Phenomena (Monterey, 1984).
- \*Y.Masumoto, S.Shionoya and H.Okamoto:  
"Slow Energy Relaxation of Excitons in GaAs-AlAs Multi-Quantum-Well Structures"  
Proc. 17th Int. Conf. on the Physics of Semiconductors (San Francisco, 1984) p.349.
- Y.Masumoto:  
"Picosecond Studies on Phase and Energy Relaxation of Excitons in Semiconductors"  
J. Lumines. 31/32 385 (1984); Proc. Int. Conf. on Luminescence-1984 (Madison, 1984).
- Y.Masumoto:  
"Energy- and Time-Resolved Studies on Exciton Luminescence in CdSe"  
Proc. IXth Int. Conf. on Raman Spectroscopy (Tokyo, 1984), p.666.
- T.Takagahara, Y.Masumoto and S.Shionoya:  
"Optical Dephasing Relaxation of Excitonic Polaritons and Excitonic Molecules"  
Proc. IXth Int. Conf. on Raman Spectroscopy (Tokyo, 1984), 376.
- \*Y.Masumoto:  
"Picosecond Spectroscopy of the Two-Dimensional Exciton System in

GaAs-AlAs Superlattices"

Solid State Physics (Kotai Butsuri) 20 52 (1985) (in Japanese).

Y.Masumoto, S. Shionoya and H. Okamoto:

"Ultrafast Relaxation of Excitons in GaAs-AlAs Multi-Quantum-Well Structures Studied by Resonant Rayleigh-Type Optical Mixing"  
Opt. Commun. 53 385 (1985).

\*Y.Masumoto, M.Matsuura, S.Tarucha and H.Okamoto:

"Direct Experimental Observation of Two-Dimensional Shrinkage of the Exciton Wavefunction in Quantum Wells"  
Phys. Rev. B 32 4275 (1985).

Y.Masumoto, S.Tarucha and H.Okamoto:

"Picosecond Spectroscopy of Two-Dimensional Excitons in GaAs-AlAs and Al<sub>x</sub>Ga<sub>1-x</sub>As-AlAs Multi-Quantum-Well Structures"  
To be published in Proc. 2nd Int. Conf. on Modulated Semiconductor Structures (Kyoto, 1985).

Y.Masumoto, M.Matsuura, S.Tarucha and H.Okamoto:

"Two-dimensional Shrinkage of the Exciton Wavefunction in Quantum Wells Probed by Optical Absorption"  
To be published in Proc. on Electronic Properties of Two-Dimensional Systems" (Kyoto, 1985).

Y.Masumoto, S.Tarucha and H.Okamoto:

"Absorption Saturation of Excitons in GaAs-AlAs Multi-Quantum-Well Structures"  
J. Phys. Soc. Jpn. 55 57 (1986).

\*Y.Masumoto, S.Tarucha and H.Okamoto:

"Tunneling Dynamics of Photo-Generated Carriers in Semiconductor Superlattices"  
Phys. Rev. B 33, ~~No. 6~~ (1986) (in press).

T.Takagahara

"Proposed Method for Measuring the Dephasing Relaxation Constant of Excitonic Molecules"  
Phys. Rev. B 29 4160 (1984).

T.Takagahara

"Picosecond Relaxation in Solids and Nonlinear Spectroscopy"  
in "Semiconductor Probed by Ultrafast Laser Spectroscopy" vol.II ed. R.R.Alfano (Academic Press, 1984) p.331.

\*T.Takagahara:

"Theoretical Study of Population Dynamics of Two-Dimensional Excitons in GaAs-AlAs Quantum Well Structures"  
Proc. 17th Int. Conf. on the Physics of Semiconductors (San-Francisco, 1984), p.355.

\*T.Takagahara:

"Localization and Energy Transfer of Quasi-Two-Dimensional Excitons in GaAs-AlAs Quantum Well Heterostructures"  
Phys. Rev. B 31 6552 (1985).

\*T.Takagahara:

"Theory of Dephasing Relaxation of Excitonic Polaritons"  
Phys. Rev. B 31 8171 (1985).

\*T.Takagahara:

"Localization and Homogeneous Dephasing Relaxation of Quasi-Two-

Dimensional Excitons in Quantum-Well Heterostructures"

Phys. Rev. B 32 7013 (1985).

T.Takagahara:

"Localization and Homogeneous Dephasing Relaxation of Quasi-Two-Dimensional Excitons in Quantum Well Heterostructures"

To be published in Proc. on Electronic Properties of Two-Dimensional Systems" (Kyoto, 1985).

T.Takagahara and E.Hanamura:

"Giant Oscillator Strength Effect on Exciton Optical Nonlinearities"

submitted for publication.

\* Papers reproduced in this booklet.

<口答発表>

舛本泰章, 塩谷繁雄, 河口仁司

GaAs/AlAs 超格子中の二次元励起子系のピコ秒分光 I I

日本物理学会 (1984年4月)

高河原俊秀

付加的境界条件の微視的理論

日本物理学会 (1984年4月)

舛本泰章, 樽茶清悟, 岡本紘

GaAs/AlAs 超格子中の二次元励起子系のピコ秒分光 I I I

日本物理学会 (1984年10月)

高河原俊秀

量子井戸内二次元励起子のエネルギー緩和の理論

日本物理学会 (1984年10月)

舛本泰章, 松浦清, 樽茶清悟, 岡本紘

超格子中の励起子の波動関数の二次元性の直接的実験検証

日本物理学会 (1985年4月)

高河原俊秀

付加的境界条件の微視的理論

日本物理学会 (1985年4月)

舛本泰章, 樽茶清悟, 佐久規, 岡本紘

混晶量子井戸AlGaAs/AlAs中の励起子のピコ秒緩和

日本物理学会 (1985年10月)

舛本泰章, 樽茶清悟, 岡本紘

垂直電場下での多重量子井戸中の励起子のピコ秒分光

日本物理学会 (1985年10月)

高河原俊秀

量子井戸中準二次元励起子の位相緩和の理論

日本物理学会 (1985年10月)

舛本泰章, 樽茶清悟, 岡本紘

半導体超格子中の光励起担体のトンネル過程のダイナミクス

日本物理学会 (1986年3月 発表予定)

高河原俊秀, 花村栄一

量子井戸構造中の励起子による非線形光学応答

日本物理学会 (1986年3月 発表予定)

## Optical Dephasing of Excitonic Polaritons in CuCl Studied by Time-Resolved, Nondegenerate Four-Wave Mixing

Yasuaki Masumoto and Shigeo Shionoya

*The Institute for Solid State Physics, The University of Tokyo, Roppongi, Minato-ku, Tokyo 106, Japan*

and

Toshihide Takagahara

*Department of Applied Physics, Faculty of Engineering, The University of Tokyo, Hongo, Bunkyo-ku, Tokyo 113, Japan*

(Received 9 June 1983)

Optical dephasing of excitonic polaritons in CuCl is directly measured for the first time in the picosecond time domain by means of time-resolved, nondegenerate four-wave mixing. Dephasing of the  $\omega_1$  polariton pulse is probed by an interrogation  $\omega_2$  polariton pulse whose group velocity is faster than that of the  $\omega_1$  polariton pulse. It is found that the dephasing damping constant  $\Gamma/2$  of excitonic polaritons is of order of 0.01 meV and increases as  $\hbar\omega_1$  approaches the exciton resonance energy from below.

PACS numbers: 71.36.+c, 42.65.-k, 78.20.-e

Recent studies in the picosecond time domain have revealed dynamical aspects of excitonic polaritons. By studying the transient induced absorption from the excitonic polariton state to the excitonic molecule state, energy relaxation processes of excitonic polaritons have been clarified.<sup>1</sup> In solids, it is considered that the phase relaxation is generally much faster than the energy relaxation. However, there has been no direct experimental information in the time domain about the phase relaxation of excitonic polaritons. In addition, the concept of the optical dephasing of excitonic polaritons has not been made clear yet.

Dephasing of localized excitation can be directly measured in the ultrashort time domain by means of time-resolved, degenerate four-wave mixing which is a generalized modification of the photon echo.<sup>2</sup> Under irradiation by two light pulses,  $(\vec{k}_1, \omega_1)$  and  $(\vec{k}_2, \omega_1)$ , which are resonant with some material excitation, the output of the  $(2\vec{k}_2 - \vec{k}_1, \omega_1)$  pulse is measured as a function of the time separation between the two pulses. This measurement is based on the principle that the third-order nonlinear polarization which generates the  $(2\vec{k}_2 - \vec{k}_1, \omega_1)$  pulse depends on the nondephased part of excitation generated by the first  $(\vec{k}_1, \omega_1)$  pulse at the time when the second, delayed  $(\vec{k}_2, \omega_1)$  pulse reaches the excitation. In the study of the phase relaxation of excitonic polaritons, on the other hand, it is important to note that excitonic polaritons are composite particles of excitons and photons. Incident photons  $(\vec{k}_1, \omega_1)$  and  $(\vec{k}_2, \omega_1)$  are converted to polaritons  $(\vec{k}_1, \omega_1)$  and  $(\vec{k}_2, \omega_1)$  inside the crystal. As they propagate at the same group velocity  $v_g(\omega_1)$ , the excitonic

polariton pulse  $(\vec{k}_1, \omega_1)$  cannot be caught up with by the second, delayed pulse  $(\vec{k}_2, \omega_1)$ . Therefore, it is necessary to modify this technique. If the delayed interrogation pulse  $(\vec{k}_2, \omega_2)$  is suitably chosen so that its group velocity is faster than that of the first pulse  $(\vec{k}_1, \omega_1)$ , this  $(\vec{k}_2, \omega_2)$  pulse catches up with the  $(\vec{k}_1, \omega_1)$  pulse, and the third-order nonlinear polarization which now emits a  $(2\vec{k}_2 - \vec{k}_1, 2\omega_2 - \omega_1)$  pulse is generated in proportion to the nondephased part of the  $(\vec{k}_1, \omega_1)$  pulse. Therefore, we can obtain information about the optical dephasing of the  $(\vec{k}_1, \omega_1)$  polariton pulse by measuring the  $2\omega_2 - \omega_1$  output as a function of the relative time delay between the two pulses. To confirm the above mentioned ideas, we have tried an experiment for excitonic polaritons in CuCl. As mentioned below, it is demonstrated for the first time that the optical dephasing of excitonic polaritons can be directly measured in the picosecond time domain by use of this time-resolved, nondegenerate four-wave mixing.

Tunable picosecond light pulses  $\omega_1$  and  $\omega_2$  were generated in the following way. Two temperature-controlled LiNbO<sub>3</sub> parametric oscillators were pumped by the second-harmonic radiation of a repetitively mode-locked Nd<sup>3+</sup>-doped yttrium aluminum garnet laser,<sup>3</sup> and  $\omega_1$  and  $\omega_2$  pulses were obtained by taking the second harmonics of parametric signals. The temporal widths of the  $\omega_1$  and  $\omega_2$  pulses were about 20 ps. The peak powers of the  $\omega_1$  and  $\omega_2$  pulses were kept at 130 kW and 85 kW, respectively. Flakes of CuCl single crystals having {111} faces were grown from the vapor phase. They were directly immersed in superfluid helium. Two beams,  $(\vec{k}_1, \omega_1)$  and  $(\vec{k}_2, \omega_2)$ ,

were focused on a CuCl crystal with a spot size of 140  $\mu\text{m}$  in diameter. One of them, the  $\omega_1$  beam, was variably delayed by use of an optical delay. When the temporal coincidence as well as the spatial overlap were optimum, a signal of  $2\omega_2 - \omega_1$  was clearly observed in the direction of  $2\vec{k}_2 - \vec{k}_1$ . The  $2\omega_2 - \omega_1$  signal can always be kept in the transparent region of the crystal, in contrast to the  $2\omega_1 - \omega_2$  signal, since  $2\omega_2 - \omega_1 = \omega_2 - (\omega_1 - \omega_2) < \omega_2$ . Thus the measurement of the  $2\omega_2 - \omega_1$  signal is quite feasible. The angle between the  $\omega_1$  and  $\omega_2$  beams was  $15^\circ$ . The  $2\omega_2 - \omega_1$  signal was highly directional (solid angle  $\approx 1.1 \times 10^{-4}$  sr), so that it was spatially separated from the background scattering by use of a diaphragm. It was detected by a photomultiplier and a boxcar integrator through a monochromator. The spectral width [full width at half maximum (FWHM)] of  $\omega_1$  and  $\omega_2$  was 1.8 meV while that of  $2\omega_2 - \omega_1$  was about 4.6 meV. The central spectral part of the  $2\omega_2 - \omega_1$  signal with a spectral width (FWHM) of 0.5 meV was selected.

In Fig. 1, the output intensity of  $2\omega_2 - \omega_1$  pulses is shown as a function of the relative time delay  $t_2 - t_1$ . The positive direction of  $t_2 - t_1$  means that the slower  $\omega_1$  pulse is ahead of the faster  $\omega_2$  pulse. Here  $\omega_2$  was kept almost constant at  $\sim 3.178$  eV. It is very helpful to note the group velocity and the transit time of the excitonic polaritons  $\omega_1$  and  $\omega_2$  in order to interpret the results of Fig. 1. In Fig. 2, the experimentally confirmed dispersion relation and the group velocity of excitonic polaritons in CuCl are illustrated together with the calculated transit time of the ex-

citonic polariton pulse through the sample of 14.15  $\mu\text{m}$  thickness.<sup>4</sup> The transit time of the  $\omega_2$  pulse through the sample is 1.4–1.5 ps, while that of the  $\omega_1$  pulse varies from 3.88 ps to several hundred picoseconds. The correlation traces 1 to 6 show asymmetry tailed toward  $t_2 - t_1 > 0$ . This asymmetry grows as we go from 1 to 3, and then decreases from 3 to 8. Then, the correlation traces 8 to 10 are sharp and almost symmetric. The asymmetric tail toward  $t_2 - t_1 > 0$  suggests that the phase of the  $\omega_1$  polariton pulse survives for a while and then it is probed by the  $\omega_2$  polariton pulse when the latter catches up with the  $\omega_1$  polariton pulse. The reason why the asymmetry grows in going from 1 to 3 is that the transit time of the  $\omega_1$  polariton pulse increases. Because the dephasing damping of the  $\omega_1$  polariton pulse increases, the asymmetry decreases in going from 3 to 8.

Dispersion of excitonic polaritons including the damping term  $\Gamma$  is written as<sup>5</sup>

$$\begin{aligned} \left(\frac{ck}{\omega}\right)^2 &= \epsilon(k, \omega) \\ &= \epsilon_\infty \left(1 + \frac{\omega_i^2 - \omega_t^2}{\omega_i^2 + (\hbar\omega_i/M)k^2 - \omega^2 + i\omega\Gamma}\right). \end{aligned} \quad (1)$$

This damping term  $\Gamma$  has always been introduced phenomenologically. However, we can give a physical meaning to  $\Gamma$ . Equation (1) is derived from the coupled equations described below:

$$\begin{aligned} P + \Gamma\dot{P} + [\omega_i - (\hbar/2M)\nabla^2]^2 P &= \beta\omega_i^2 E, \\ \epsilon_\infty \ddot{E} - c^2 \nabla^2 E &= -4\pi\ddot{P}, \\ \epsilon(k, \omega)E &= \epsilon_\infty E + 4\pi P, \end{aligned} \quad (2)$$

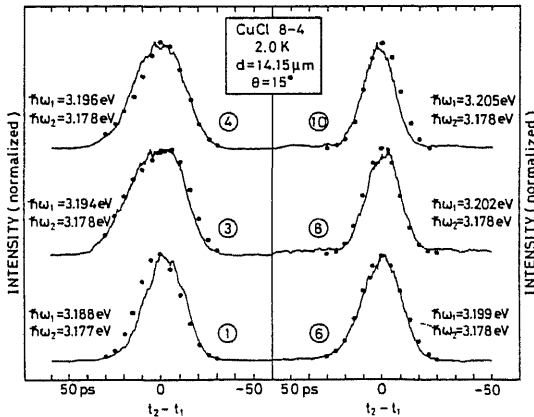


FIG. 1. Intensity of the  $2\omega_2 - \omega_1$  beam emitted from a CuCl crystal as a function of the relative time delay between the  $\omega_2$  and  $\omega_1$  pulses,  $t_2 - t_1$ .

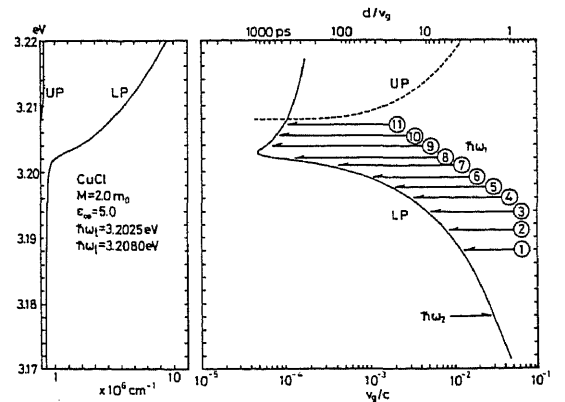


FIG. 2. Left: Dispersion relation of excitonic polaritons in CuCl. Right: Corresponding group velocity of excitonic polariton pulses normalized by  $c$  (light velocity in vacuum) and the calculated transit time of the pulses through a CuCl crystal of 14.15  $\mu\text{m}$  thickness.

where  $\beta$  is defined by  $4\pi\beta\omega_i^2/\epsilon_\infty = \omega_i^2 - \omega_p^2$ . The first equation, that is, the equation of motion of macroscopic polarization  $P$  due to excitonic polaritons, is the same as a familiar equation of polarization in a semiclassical laser theory<sup>6</sup> except for the spatially dispersive term. In the laser theory the equation of motion of macroscopic polarization is derived from the density matrix formalism for the two-level system. In the density matrix formalism,  $\Gamma/2$  is defined as the dephasing damping (transverse relaxation) con-

stant.<sup>7</sup> Therefore, it is reasonable to identify  $\Gamma/2$  as the dephasing damping constant of excitonic polaritons.

In CuCl the third-order nonlinear polarization  $P_{NL}^{(3)}$  is generated through a four-polariton parametric process around the exciton resonance or a two-photon resonance of excitonic molecules.<sup>8</sup> As a result,  $P_{NL}^{(3)}(2\omega_2 - \omega_1)$  is proportional to the product of macroscopic polarizations due to excitonic polaritons,  $[P(z, t|k_2, \omega_2)]^2 P^*(z, t|k_1, \omega_1)$ , where the macroscopic polarization in the crystal is given by

$$P(z, t|k, \omega) = (\frac{1}{4}\pi)[\epsilon(k, \omega) - \epsilon_\infty]\{p(\omega) \exp[-ik(\omega)z] E(t - z/v_g(\omega)) + q(\omega) \exp[ik(\omega)z] E(t + z/v_g(\omega))\}. \quad (3)$$

Here,  $z$  is the coordinate perpendicular to the sample surface,  $k(\omega)$  is the complex wave vector determined by Eq. (1),  $v_g(\omega)$  is the group velocity of polaritons  $\omega$ ,  $E$  is the envelope of the electric field of the incident pulse, and  $pE$  and  $qE$  are the envelopes of the electric field associated with polaritons propagated forward and backward in the crystal, respectively. The electric field outside the crystal  $E(\gamma, t)$  generated by  $P_{NL}^{(3)}(2\omega_2 - \omega_1)$  is proportional to<sup>9</sup>

$$\int_0^d dz \exp[i(2\omega_2 - \omega_1)(z - d)/v_p] [P(z, t - t_2 + t_1 + (z - d)/v_p|k(\omega_2), \omega_2)]^2 P^*(z, t + (z - d)/v_p|k(\omega_1), \omega_1), \quad (4)$$

where  $d$  is the thickness of the crystal and  $v_p$  is the phase velocity at  $2\omega_2 - \omega_1$ . The correlation trace is calculated by the time integral of the absolute square of  $E(\gamma, t)$ . A numerical calculation was done based on the dispersion relation of excitonic polaritons in CuCl shown in Fig. 2. The results are plotted by the closed circles in Fig. 1. Here, adjustable parameters are limited to  $k(\omega_1)$  and  $k(\omega_2)$  which are implicitly determined by  $\Gamma(\omega)$ . As a result,  $k(\omega_1)$  and  $\Gamma(\omega_1)$  can be almost uniquely determined, because  $\omega_2$  is fixed as is shown in Fig. 1. Obtained values of  $\Gamma$  are plotted as a function of  $\hbar\omega_1$  in Fig. 3. The right vertical axis indicates the dephasing time  $\hbar/(\Gamma/2)$  of the macroscopic polarization  $P$  due to the  $\omega_1$  polariton. As is seen in Fig. 3,  $\Gamma/2$  is of the order of 0.01 meV and increases as  $\hbar\omega_1$  approaches the resonance energy of the exciton,  $\hbar\omega_x$ . In the energy region above 3.200 eV,  $\Gamma(\omega)$  could not be definitely determined, because the correlation trace was insensitive to the value of  $\Gamma(\omega)$ .

The order of  $\Gamma/2$  cannot be explained by the LA phonon interaction, because the scattering rate of excitonic polaritons due to LA phonons is by far slower than the observed  $\hbar/(\Gamma/2)$ .<sup>4,10</sup> The most probable mechanism of dephasing is polariton-polariton collision. It is known that four-polariton parametric scattering occurs efficiently in CuCl and even the superbroadened distribution of excitonic polaritons was observed.<sup>11</sup> A model calculation of the rate of polariton-polariton scattering was performed with neglect of the wave-vector dependence of the collision matrix ele-

ment. The absolute value of  $\Gamma$  was fitted to the experimental value at 3.188 eV. The calculated result is shown by a dashed line in Fig. 3. The increasing trend of experimental  $\Gamma$  with polariton energy is interpreted by the calculation. This model suggests that correlation traces should depend on the intensity of the incident light. In fact, experimental data were found to depend on the intensity of the incident light. The details will be described in a forthcoming paper.

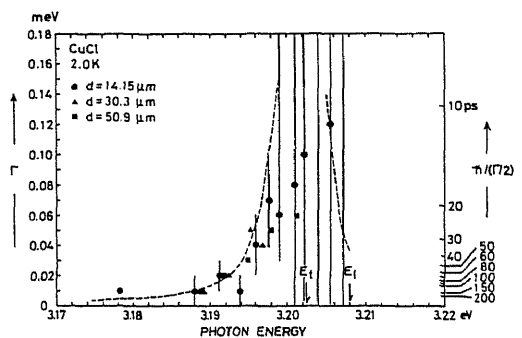


FIG. 3. Dephasing damping constant  $\Gamma$  as a function of the energy of excitonic polaritons. The three data symbols correspond to samples of different thicknesses. Very long error bars above 3.200 eV mean that  $\Gamma$  cannot be definitely determined. The dashed line is the calculated energy dependence of the dephasing damping constant based on a model of polariton-polariton scattering.

It is instructive to compare the population decay with the phase decay of excitonic polaritons and to clarify the difference. The population decay was measured by the time-resolved induced absorption (IA) from the excitonic polariton state to the excitonic molecule state.<sup>4,11,12</sup> It was found that the  $\omega_1$  ( $=3.199$  eV) polaritons survive in the crystal of  $51.9$   $\mu\text{m}$  thickness as long as  $200$  ps after the injection of the  $\omega_1$  pulse.<sup>11</sup> However, the signal of  $2\omega_2 - \omega_1$  is exactly zero at  $50$  ps in the same sample, since the correlation trace shows almost the same temporal profile as is seen in 6 of Fig. 1. In the IA case, all the polaritons which are scattered in various directions but almost elastically can contribute to the signal. The decay time constant of the IA reflects the energy relaxation of the ensemble of injected polaritons. In the case of four-wave mixing, on the other hand, even the elastically scattered polaritons do not contribute to the signal, because the signal arises from the coherent mixing of polariton waves and the detection is spatially well colimated. Thus the momentum relaxation due to the polariton-polariton scattering which is much faster than the energy relaxation contributes dominantly to the dephasing damping of excitonic polaritons.

In summary, we have demonstrated that the optical dephasing of excitonic polaritons in CuCl is directly measurable in the picosecond time domain by time-resolved, nondegenerate four-wave mixing at  $2.0$  K. The observed dephasing damp-

ing constant  $\Gamma/2$  is of the order of  $0.01$  meV and increases as the energy approaches the resonance energy of the transverse exciton from below. This energy dependence suggests that the optical dephasing of excitonic polaritons is attributable to the process of polariton-polariton scattering.

<sup>1</sup>Y. Masumoto and S. Shionoya, *J. Phys. Soc. Jpn.* **51**, 181 (1982).

<sup>2</sup>T. Yajima and Y. Taira, *J. Phys. Soc. Jpn.* **47**, 1620 (1979).

<sup>3</sup>Y. Tanaka, T. Kushida, and S. Shionoya, *Opt. Commun.* **25**, 273 (1978), and **41**, 459 (1982).

<sup>4</sup>Y. Masumoto, Y. Unuma, Y. Tanaka, and S. Shionoya, *J. Phys. Soc. Jpn.* **47**, 1844 (1979).

<sup>5</sup>J. J. Hopfield and D. G. Thomas, *Phys. Rev.* **132**, 563 (1963).

<sup>6</sup>K. Shimoda, T. Yajima, Y. Ueda, T. Shimizu, and T. Kasuya, *Quantum Electronics* (Shokabo, Tokyo, 1970) (in Japanese).

<sup>7</sup>N. Bloembergen, *Nonlinear Optics* (Benjamin, New York, 1965).

<sup>8</sup>Y. Masumoto and S. Shionoya, *J. Phys. Soc. Jpn.* **49**, 2236 (1980), and **50**, 1035 (1981); B. Honerlage, R. Levy, and J. B. Grun, *Opt. Commun.* **43**, 443 (1982).

<sup>9</sup>Y. Masumoto, S. Shionoya, and T. Takagahara, unpublished.

<sup>10</sup>M. Aihara, private communication.

<sup>11</sup>Y. Masumoto and S. Shionoya, *Solid State Commun.* **41**, 147 (1982).

<sup>12</sup>Y. Segawa, Y. Aoyagi, and S. Namba, *Solid State Commun.* **39**, 535 (1981).

## Theory of dephasing relaxation of excitonic polaritons

T. Takagahara

*Department of Applied Physics, The University of Tokyo, Tokyo, 113 Japan*

(Received 2 January 1985)

A detailed theory is developed for the dephasing relaxation of the excitonic polariton which was measured recently by Masumoto, Shionoya, and Takagahara [Phys. Rev. Lett. 51, 923 (1983)] in samples of CuCl crystal by means of nondegenerate four-wave mixing. The concept of dephasing (transverse) relaxation of the excitonic polariton is clarified for the first time and the conceptual difference between the dephasing relaxation of the localized excitation and of the excitonic polariton is emphasized. A method of analysis of the experimental data of the nondegenerate four-wave mixing is presented in detail. The various mechanisms of dephasing relaxation of the excitonic polariton are discussed and examined quantitatively. It is found that the mutual collision among excitonic polaritons is the most probable mechanism that gives the correct order of magnitude of the dephasing relaxation rate and leads to reasonable energy dependence of the relaxation rate in agreement with the experimental results.

### I. INTRODUCTION

Recently the dephasing relaxation constant of the excitonic polariton in CuCl was measured by Masumoto, Shionoya, and Takagahara<sup>1</sup> by means of nondegenerate four-wave mixing. The relaxation constant was found to be on the order of 0.01 meV and to increase as the polariton energy approached the exciton resonance from below. Before details are given, it is important to note that there is a conceptual difference between the dephasing relaxation of the localized excitation and of the propagating elementary excitation. In the former case the excitation is localized on an atom or a molecule under consideration. The dephasing relaxation of the localized excitation is related to the decay of the coherence of the relevant optical or nonoptical transition or, in other words, the decay of the off-diagonal component of the density matrix associated with the transition. This dephasing relaxation constant can be directly measured in the time domain by means of time-resolved, degenerate four-wave mixing,<sup>2-5</sup> which is a generalized version of the photon echo.<sup>6</sup> Under irradiation by two light pulses with wave vector and frequency denoted by  $(\vec{k}_1, \omega_1)$  and  $(\vec{k}_2, \omega_1)$ , respectively, which are resonant with some material excitation, the intensity of the output pulse with  $(2\vec{k}_2 - \vec{k}_1, \omega_1)$  is measured as a function of the time separation between the two pulses. This measurement is based on the principle that the third-order nonlinear polarization which generates the signal pulse is proportional to the nondephased part of the excitation due to the first pulse at the time when the second delayed pulse reaches the excitation. Thus, the decay of the coherence of the localized excitation can be probed by means of time-resolved, degenerate four-wave mixing.

On the other hand, the proper elementary excitation in solids propagates throughout the crystal with a definite wave vector. Furthermore, it should be noted that the excitonic polariton is a composite particle of exciton and photon. Thus, there arises a conceptual question: What is

the dephasing relaxation of the excitonic polariton? The interpretation is not so straightforward as in the case of the localized excitation. The definiteness of the wave vector is one of the salient features of the excitonic polariton which make a remarkable contrast with the case of the localized excitation. The wave vector of the excitonic polariton is primarily determined by the incident light pulse. This wave vector is disturbed by any scattering process, such as impurity scattering, phonon scattering, and polariton-polariton collision. A change of wave vector will lead to the decay of the polarization wave with a definite wave vector. In addition, the electron-hole relative motion of the exciton is also one of the degrees of freedom of the excitonic polariton. The electron-hole relative motion of the exciton may be changed in the scattering processes. This change of the internal degree of freedom leads to the fluctuation and relaxation of the polarization wave, since the oscillator strength of the exciton depends on the exciton internal state. Thus, the concept of dephasing or transverse relaxation of the excitonic polariton is quite different from that of the localized excitation. As a consequence of the definiteness of the wave vector, the wave packet of excitonic polaritons propagates in the crystal with a definite group velocity and there arises an interesting situation from the experimental point of view. The incident photons  $(\vec{k}_1, \omega_1)$  and  $(\vec{k}_2, \omega_1)$  are converted to the excitonic polaritons  $(k_1, \omega_1)$  and  $(k_2, \omega_1)$  inside the crystal. The incident photons with the same energy propagate in the crystal with the same group velocity. Thus, in degenerate four-wave mixing, the second delayed polariton pulse  $(k_2, \omega_1)$  cannot catch up with the first polariton pulse  $(k_1, \omega_1)$ . In order to make the spatial overlap between the two pulses as large as possible, it is essential to make use of nondegenerate four-wave mixing in which the energy of the delayed probe pulse  $(k_2, \omega_2)$  is suitably chosen so that its group velocity is larger than that of the first pulse  $(k_1, \omega_1)$ . Then the third-order nonlinear polarization will be generated in proportion to the nondephased part of the  $(k_1, \omega_1)$  pulse and the signal beam with wave

vector and frequency  $(2k_2 - k_1, 2\omega_2 - \omega_1)$  will be emitted. One can obtain information about the dephasing relaxation of the  $(k_1, \omega_1)$  polariton pulse by measuring the intensity of the output pulse  $(2k_2 - k_1, 2\omega_2 - \omega_1)$  as a function of the relative time delay between the two pulses. To realize the above idea an experiment was carried out for the excitonic polariton in CuCl.<sup>1</sup> It was demonstrated for the first time that the dephasing relaxation of the excitonic polariton could be measured directly in the picosecond time domain by time-resolved, nondegenerate four-wave mixing. The experimental details are given in Ref. 1.

This paper is organized as follows. In Sec. II the propagation dynamics of the excitonic polariton are formulated. The third-order nonlinear polarization in the crystal is calculated perturbationally and the signal intensity of the nondegenerate, four-wave mixing is derived in a suitable form for analysis of the experimental data. In Sec. III experimental data of the correlation trace of nondegenerate four-wave mixing are analyzed to determine the dephasing relaxation constant of the excitonic polariton as a function of energy. In Sec. IV, the various mechanisms of the dephasing (momentum) relaxation of the excitonic polariton are discussed and the relaxation rate due to each mechanism is estimated quantitatively. It is found that mutual collision among excitonic polaritons is the most probable mechanism to cause the dephasing relaxation of the excitonic polariton. In Sec. V, the basic equations of

motion for the excitonic polariton are derived quantum mechanically and also the damping constant of the polarization field, which is identified with the dephasing relaxation constant of the excitonic polariton, is derived by the standard statistical mechanical method using the projection operator. Finally in Sec. VI, a few proposals are presented to overcome the difficulty of nondegenerate, four-wave mixing, that the dephasing relaxation constant in the resonance region cannot be determined precisely. In addition a few interesting problems are pointed out for future study.

## II. NONDEGENERATE FOUR-WAVE MIXING VIA EXCITONIC POLARITONS

Let us now present the theoretical scheme used to analyze the experimental data. Of main interest is the propagation of excitonic polaritons and their nonlinear interaction in the crystal. Since the excitonic polariton is a composite elementary excitation of exciton and photon, one has to treat the polarization of the material system and the electromagnetic field on an equal footing. The basic equations of motion are given by the constitutive equations for the material polarization due to the exciton and the Maxwell equations for the electromagnetic field. They are written explicitly as

$$\frac{\partial^2}{\partial t^2} P(r, t) + \int_{-\infty}^{\infty} dt' \Gamma(t-t') \frac{\partial}{\partial t'} P(r, t') + \left[ \omega_t^2 - \frac{\hbar \omega_t}{M} \nabla^2 \right] P(r, t) = -\beta \omega_t^2 E(r, t) I(r, t), \quad (2.1)$$

$$\frac{\partial}{\partial t} I(r, t) + \gamma_{\parallel} [I(r, t) - I_0] = \frac{2E(r, t)}{\hbar \omega_t} \left[ \frac{\partial}{\partial t} P(r, t) + \frac{1}{2} \int_{-\infty}^{\infty} dt' \Gamma(t-t') P(r, t') \right], \quad (2.2)$$

$$\epsilon_{\infty} \frac{\partial^2}{\partial t^2} E(r, t) - c^2 \nabla^2 E(r, t) = -4\pi \frac{\partial^2}{\partial t^2} P(r, t), \quad (2.3)$$

with

$$4\pi\beta\omega_t^2/\epsilon_{\infty} = \omega_1^2 - \omega_t^2, \quad (2.4)$$

where  $P$ ,  $I$ , and  $E$  denote, respectively, the polarization field, the population inversion of the material system, and the electric field; and  $\omega_t$  ( $\omega_1$ ),  $M$ ,  $\epsilon_{\infty}$ ,  $I_0$ , and  $\gamma_{\parallel}$  are the transverse (longitudinal) exciton frequency, the exciton effective mass, the background dielectric constant, the thermal equilibrium value of  $I$ , and the longitudinal (population) relaxation rate, respectively. The damping function  $\Gamma(t)$  is related to the dephasing relaxation of the excitonic polariton and its time dependence leads to the frequency-dependent damping constant  $\Gamma(\omega)$ . Equations (2.1) and (2.2), for the polarization field and the population inversion due to the exciton, are taken from the well-known equations of motion in laser theory<sup>7,8</sup> with modification to include spatial dispersion. In Sec. V, these equations are derived microscopically and their use for the case of excitonic polaritons can be justified. As a matter of course, this set of equations leads to the familiar expression for the dielectric function  $\epsilon(k, \omega)$  defined by

$$\epsilon(k, \omega) E(k, \omega) = \epsilon_{\infty} E(k, \omega) + 4\pi P(k, \omega), \quad (2.5)$$

where the spatial and temporal Fourier transforms of the electric and polarization fields are considered. In a situation with no excitation, it is calculated as<sup>9</sup>

$$\epsilon(k, \omega) = \epsilon_{\infty} + \frac{4\pi\beta\omega_t^2}{\omega_t^2 - \omega^2 + \hbar\omega_t k^2/M + i\omega\Gamma(\omega)}. \quad (2.6)$$

The frequency-dependent or -independent damping constant  $\Gamma(\omega)$  is usually introduced phenomenologically. However, as is clear from the above argument, it has the meaning of a damping of the polarization field. In this sense  $\Gamma(\omega)$  can be called the dephasing relaxation constant of the excitonic polariton. Our main interest in this paper is how to determine  $\Gamma(\omega)$  from the experimental data of nondegenerate four-wave mixing. This is possible because the other material constants  $\epsilon_{\infty}$ ,  $\beta$ ,  $\omega_t$ , and  $M$  are determined fairly precisely by hyper-Raman scattering<sup>10,11</sup> and time-of-flight<sup>12,13</sup> measurements.

The spatial distribution of the electric field is shown schematically in Fig. 1 when a monochromatic elec-

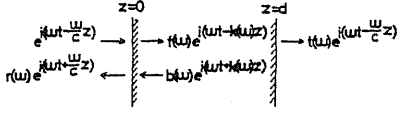


FIG. 1. Schematic representation of the electric field distribution inside and outside a slablike crystal.

tromagnetic field with unit amplitude enters the crystal. The incident laser beam is assumed to propagate normal to the crystal surface. This assumption can be justified because of the small angle of incidence and the large dielectric constant of CuCl. The slablike crystal occupies the region from  $z=0$  to  $z=d$ . The complex wave vector  $k(\omega)$  is determined by the dielectric function through the relation

$$\left[ \frac{ck}{\omega} \right]^2 = \epsilon(k, \omega), \quad (2.7)$$

$$\begin{aligned} E_{\alpha}(t) \cos \omega_{\alpha} t &= \int_{-\infty}^{\infty} d\omega g_{\alpha}(\omega) e^{i\omega t} (e^{i\omega_{\alpha} t} + e^{-i\omega_{\alpha} t}) / 2 \\ &= \frac{1}{2} \int_{-\infty}^{\infty} d\omega [g_{\alpha}(\omega + \omega_{\alpha}) + g_{\alpha}(\omega - \omega_{\alpha})] e^{i\omega t} \\ &= \text{Re} \left[ \int_0^{\infty} d\omega [g_{\alpha}(\omega + \omega_{\alpha}) + g_{\alpha}(\omega - \omega_{\alpha})] e^{i\omega t} \right] = \text{Re} \left[ \int_0^{\infty} d\omega G_{\alpha}(\omega) e^{i\omega t} \right], \end{aligned} \quad (2.11)$$

with

$$G_{\alpha}(\omega) = g_{\alpha}(\omega + \omega_{\alpha}) + g_{\alpha}(\omega - \omega_{\alpha}), \quad (2.12)$$

where  $\omega_{\alpha}$  is the carrier frequency,  $E_{\alpha}(t)$  the pulse envelope, and  $g_{\alpha}(\omega)$  its Fourier transform. The electric field and the polarization field in the crystal can be written as the superposition of monochromatic waves:

$$E(z, t | k(\omega_{\alpha}), \omega_{\alpha}) = \text{Re} \left[ \int_0^{\infty} d\omega G_{\alpha}(\omega) [f(\omega) e^{-ik(\omega)z} + b(\omega) e^{ik(\omega)z}] e^{i\omega t} \right], \quad (2.13)$$

$$P(z, t | k(\omega_{\alpha}), \omega_{\alpha}) = \text{Re} \left[ \int_0^{\infty} d\omega G_{\alpha}(\omega) [\epsilon(k(\omega), \omega) - \epsilon_{\infty}] [f(\omega) e^{-ik(\omega)z} + b(\omega) e^{ik(\omega)z}] e^{i\omega t} / 4\pi \right]. \quad (2.14)$$

When two light pulses with wave vector and frequency denoted by  $(k_1, \omega_1)$  and  $(k_2, \omega_2)$ , respectively, enter the crystal, the third-order nonlinear polarization with wave vector  $2k_2 - k_1$  and frequency  $2\omega_2 - \omega_1$  will be generated and emit the signal beam to be measured in the experiment. The nonlinear polarization can be calculated perturbationally from the equations of motion (2.1)–(2.3). Starting from the state with no excitation, one has, apart from a proportionality factor,

$$E_{\alpha}(z, t) = \text{Re} \left[ \int_0^{\infty} d\omega G_{\alpha}(\omega) f(\omega) e^{i\omega t - ik(\omega)z} \right], \quad (2.15)$$

$$P_{\alpha}(z, t) = \text{Re} \left[ \int_0^{\infty} d\omega \frac{\beta \omega_r^2 G_{\alpha}(\omega) f(\omega) e^{i\omega t - ik(\omega)z}}{\omega_r^2 - \omega^2 + \hbar \omega_r k^2(\omega) / M + i\omega \Gamma(\omega)} \right], \quad (2.16)$$

where only the forward-propagating parts in (2.13) and (2.14) are retained and the subscript  $\alpha$  ( $=1, 2$ ) indicates the first or second laser pulse. Substituting (2.15) and (2.16) into the right-hand side of (2.2) and extracting the term proportional to  $\exp[i(\omega_2 - \omega_1)t]$ , one obtains

$$\begin{aligned} &\frac{2}{\hbar \omega_r} \int_0^{\infty} d\omega \int_0^{\infty} d\omega' \exp\{i(\omega - \omega')t - i[k(\omega) - k^*(\omega')]z\} G_2(\omega) G_1^*(\omega') f(\omega) f^*(\omega') \\ &\quad \times \{ [i\omega + \Gamma(\omega)/2] D(\omega, k(\omega)) + [-i\omega' + \Gamma(\omega')/2] D^*(\omega', k(\omega')) \}, \end{aligned} \quad (2.17)$$

with

and is taken to be in the lower half of the complex plane. The coefficients  $f(\omega)$  and  $b(\omega)$  correspond to the forward- and backward-propagating polariton waves, respectively, and their expressions are obtained from the Maxwell boundary conditions as

$$f(\omega) = \frac{2(\sqrt{\epsilon} + 1)}{(\sqrt{\epsilon} + 1)^2 - (\sqrt{\epsilon} - 1)^2 e^{-i2k(\omega)d}}, \quad (2.8)$$

$$b(\omega) = \frac{\sqrt{\epsilon} - 1}{\sqrt{\epsilon} + 1} e^{-i2k(\omega)d} f(\omega),$$

with

$$\sqrt{\epsilon} = ck(\omega) / \omega. \quad (2.9)$$

Then the electric field in the crystal is given by

$$[f(\omega) e^{-ik(\omega)z} + b(\omega) e^{ik(\omega)z}] e^{i\omega t} + \text{c.c.} \quad (2.10)$$

These results are obtained for the case of a monochromatic wave. When a pulse or wave packet is considered, the electric field can be decomposed into its Fourier components as

$$D(\omega, k) = \frac{\beta\omega_i^2}{\omega_i^2 - \omega^2 + \hbar\omega_i k^2/M + i\omega\Gamma(\omega)}. \quad (2.18)$$

The population grating with wave vector  $k_2 - k_1$  and frequency  $\omega_2 - \omega_1$  is calculated from (2.2) as

$$I(k_2 - k_1, \omega_2 - \omega_1) = \frac{2}{\hbar\omega_i} \int_0^\infty d\omega \int_0^\infty d\omega' \frac{\exp[i(\omega - \omega')t - i[k(\omega) - k^*(\omega')]z]}{\gamma_{||} + i(\omega - \omega')} G_2(\omega) G_1^*(\omega') f(\omega) f^*(\omega') \\ \times \left[ \left[ i\omega + \frac{\Gamma(\omega)}{2} \right] D(\omega, k(\omega)) + \left[ -i\omega' + \frac{\Gamma(\omega')}{2} \right] D^*(\omega', k(\omega')) \right]. \quad (2.19)$$

Then substitution of this population grating into the right-hand side of (2.1) yields the third-order nonlinear polarization  $P_{NL}^{(3)}$  with wave vector  $2k_2 - k_1$  and frequency  $2\omega_2 - \omega_1$  as

$$P_{NL}^{(3)}(2k_2 - k_1, 2\omega_2 - \omega_1) = -\frac{2}{\hbar\omega_i} \int_0^\infty d\omega \int_0^\infty d\omega' \int_0^\infty d\omega'' \frac{\exp\{i(\omega + \omega'' - \omega')t - i[k(\omega) + k(\omega'') - k^*(\omega')]z\}}{\gamma_{||} + i(\omega - \omega')} \\ \times D(\omega + \omega'' - \omega', k(\omega) + k(\omega'') - k^*(\omega')) G_2(\omega) G_2(\omega'') G_1^*(\omega') \\ \times f(\omega) f(\omega'') f^*(\omega') \left[ \left[ i\omega + \frac{\Gamma(\omega)}{2} \right] D(\omega, k(\omega)) + \left[ -i\omega' + \frac{\Gamma(\omega')}{2} \right] D^*(\omega', k(\omega')) \right]. \quad (2.20)$$

This nonlinear polarization will generate a signal electric field, acting as the source term on the right-hand side of (2.3), which is given by

$$E(2k_2 - k_1, 2\omega_2 - \omega_1) = -\frac{2}{\hbar\omega_i} \int_0^\infty d\omega \int_0^\infty d\omega' \int_0^\infty d\omega'' \frac{4\pi(\omega + \omega'' - \omega')^2 F(\omega, \omega', \omega'')}{-\epsilon_\infty(\omega + \omega'' - \omega')^2 + c^2[k(\omega) + k(\omega'') - k^*(\omega')]^2}, \quad (2.21)$$

where  $F(\omega, \omega', \omega'')$  denotes the whole integrand on the right-hand side of (2.20). This electric field is the field within the slablike crystal but not the signal field to be observed outside the crystal. The latter has to be calculated from the Maxwell equations and the associated boundary conditions.

Within the nonlinear crystal, the homogeneous electric fields are usually associated with the nonlinearly induced electric field whose wave vector is not necessarily identical to that of the homogeneous wave. These homogeneous fields arise as a due consequence of the Maxwell boundary conditions.<sup>14</sup> In Fig. 2 the configuration of the nonlinearly induced wave and the associated homogeneous waves is shown schematically, where the electric field corresponding to the backward-propagating nonlinear polarization is neglected owing to its smallness. Assuming the normal incidence of the laser beams the electric field for each wave in Fig. 2 can be written as

$$E_s e^{i(\omega t - K_s z)}, \quad E_r e^{i(\omega t + K_0 z)}, \quad E_t e^{i\omega t - iK_0(z-d)}, \\ E_f e^{i(\omega t - K_h z)}, \quad E_b e^{i(\omega t + K_h z)}, \quad (2.22)$$

with  $\omega = 2\omega_2 - \omega_1$ ,  $K_s = 2k(\omega_2) - k^*(\omega_1)$ ,  $K_0 = \omega/c$ , and  $K_h = k(\omega)$ , where  $E_s$ ,  $E_r$ , and  $E_t$  correspond to the nonlinearly induced field, the reflected field, and the electric field to be observed outside the crystal, respectively, and  $E_f$  and  $E_b$  correspond to the associated homogeneous waves. From the Maxwell boundary conditions at  $z=0$

and  $z=d$ , the four relations among  $E_s$ ,  $E_r$ ,  $E_t$ ,  $E_f$ , and  $E_b$  are obtained:

$$E_s + E_f + E_b = E_r, \quad n_s E_s + n(E_f - E_b) = -E_r, \\ E_s e^{-iK_s d} + E_f e^{-iK_h d} + E_b e^{iK_h d} = E_t, \\ n_s E_s e^{-iK_s d} + n(E_f e^{-iK_h d} - E_b e^{iK_h d}) = E_t, \quad (2.23)$$

where  $n_s$  and  $n$  are defined by

$$n_s = cK_s/\omega, \quad n = cK_h/\omega. \quad (2.24)$$

The amplitude  $E_t$  is calculated as

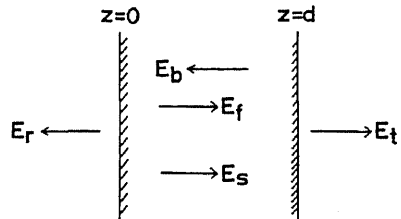


FIG. 2. Schematic representation of electric field amplitudes with frequency  $2\omega_2 - \omega_1$ .  $E_s$ ,  $E_r$ , and  $E_t$  represent the nonlinearly induced wave, the reflected wave, and the transmitted wave, respectively, and  $E_f$  and  $E_b$  are the forward- and backward-propagating homogeneous waves.

$$\frac{E_t}{E_s} = \frac{(1-n)(n-n_s)(e^{-i(K_s+K_h)d}-1) + (1+n)(n+n_s)(e^{-i(K_s-K_h)d}-1)}{(1+n)^2 e^{iK_h d} - (1-n)^2 e^{-iK_h d}} \quad (2.25)$$

or can be rewritten as

$$\frac{E_t}{E_s} = \frac{i(n^2-n_s^2)\omega/c}{(1+n)^2 e^{iK_h d} - (1-n)^2 e^{-iK_h d}} \int_0^d dz [(n+1)e^{-i(K_s-K_h)z} + (n-1)e^{-i(K_s+K_h)z}]. \quad (2.26)$$

Combining all the results, the expression of the electric field amplitude to be measured outside the crystal is given by

$$\begin{aligned} E_{\text{obs}}(R,t) = & -\frac{2i}{c\hbar\omega_t} \int_0^d dz \int_0^\infty d\omega \int_0^\infty d\omega' \int_0^\infty d\omega'' \left[ \frac{\omega_s(n^2-n_s^2)}{(1+n)^2 e^{iK_h d} - (1-n)^2 e^{-iK_h d}} \right] \\ & \times \left[ \frac{4\pi\omega_s^2}{[\gamma_{\parallel} + i(\omega-\omega')](c^2 K_s^2 - \epsilon_\infty \omega_s^2)} \right] G_2(\omega) G_1^*(\omega') \\ & \times G_2(\omega'') f(\omega) f^*(\omega') f(\omega'') D(\omega_s, K_s) \\ & \times \left[ \left[ i\omega + \frac{\Gamma(\omega)}{2} \right] D(\omega, k(\omega)) + \left[ -i\omega' + \frac{\Gamma(\omega')}{2} \right] D^*(\omega', k(\omega')) \right] \\ & \times [(n+1)e^{-i(K_s-K_h)z} + (n-1)e^{-i(K_s+K_h)z}] \exp \left[ i\omega_s \left[ t - \frac{R-d}{c} \right] \right], \end{aligned} \quad (2.27)$$

with

$$\begin{aligned} \omega_s &= \omega + \omega'' - \omega', \quad K_s = k(\omega) + k(\omega'') - k^*(\omega'), \\ K_h &= k(\omega_s), \quad n_s = cK_s/\omega_s, \quad n = cK_h/\omega_s, \end{aligned} \quad (2.28)$$

where  $R$  is the  $z$  coordinate of the observation point. This expression is quite general but contains a fourfold integral, which is a rather heavy task to perform straightforwardly. It is desirable to simplify the expression by introducing reasonable approximations. The integrations with respect to  $\omega$ ,  $\omega'$ , and  $\omega''$  are over the spectral width of the incident laser pulses. If a function contained in the

integrand is slowly varying over the region where the spectral function  $G_\alpha(\omega)$  takes significant values, it can be put outside the integral and replaced by its value at the peak position of  $G_\alpha(\omega)$ . In this spirit of simplification, all of the factors within the integrand on the right-hand side of (2.27) can be put outside the integral except for the exponential factors. This simplification can be justified under the condition that

$$\omega_1, \omega_2 \gg \Delta\omega, \quad \Delta\omega/v_g(\omega)k(\omega) \ll 1, \quad (2.29)$$

where  $\Delta\omega$  denotes the typical spectral width of the incident laser pulses, and  $v_g$  is the group velocity of the excitonic polariton. Then the expression (2.27) can be greatly simplified to

$$\begin{aligned} E_{\text{obs}}(R,t) \propto & \int_0^d dz \int_0^\infty d\omega \int_0^\infty d\omega' \int_0^\infty d\omega'' G_2(\omega) G_2(\omega'') G_1^*(\omega') \exp \left[ i(\omega + \omega'' - \omega') \left[ t - \frac{R-d}{c} \right] \right] \\ & \times [(\bar{n}+1)e^{-i(K_s-K_h)z} + (\bar{n}-1)e^{-i(K_s+K_h)z}], \end{aligned} \quad (2.30)$$

with

$$\bar{n} = ck(2\omega_2 - \omega_1)/(2\omega_2 - \omega_1),$$

where the unimportant multiplicative factors are omitted. At this stage the threefold frequency integral is reduced to a separable form and can be performed easily. The  $\omega$  dependence of  $k(\omega)$  in the exponent is expanded up to the first-order term as

$$k(\omega) = k(\bar{\omega}) + \frac{dk}{d\omega}(\omega - \bar{\omega}) + \dots = k(\bar{\omega}) + \frac{\omega - \bar{\omega}}{v_g(\bar{\omega})} + \dots, \quad (2.31)$$

where  $\bar{\omega}$  denotes the peak position of a spectral function  $G(\omega)$ . Then the threefold frequency integral in (2.30) can be simplified as

$$\begin{aligned}
E_{\text{obs}}(R, t) \propto & \exp[i(2\omega_2 - \omega_1)t_R] \\
& \times \int_0^d dz \int_0^\infty d\omega \int_0^\infty d\omega' \int_0^\infty d\omega'' G_2(\omega) G_1^*(\omega') G_2(\omega'') \exp\{-i[2k(\omega_2) - k^*(\omega_1)]z + i(\Delta + \Delta' - \Delta')t_R\} \\
& \times \{(\bar{n} + 1) \exp[ik_h z - i(1/v_2 - 1/v_h)(\Delta + \Delta')z + i(1/v_1 - 1/v_h)\Delta'z] \\
& + (\bar{n} - 1) \exp[-ik_h z - i(1/v_2 + 1/v_h)(\Delta + \Delta')z + i(1/v_1 + 1/v_h)\Delta'z]\}, \quad (2.32)
\end{aligned}$$

with the abbreviations:

$$\Delta = \omega - \omega_2, \quad \Delta' = \omega' - \omega_1, \quad \Delta'' = \omega'' - \omega_2, \quad v_1 = v_g(\omega_1), \quad v_2 = v_g(\omega_2), \quad (2.33)$$

$$v_h = v_g(2\omega_2 - \omega_1), \quad k_h = k(2\omega_2 - \omega_1), \quad \bar{n} = ck_h / (2\omega_2 - \omega_1), \quad t_R = t - \frac{R-d}{c}.$$

Making use of the relation

$$\int_0^\infty d\omega G_\alpha(\omega) e^{i\Delta t} = \int_0^\infty d\omega [g_\alpha(\omega + \omega_\alpha) + g_\alpha(\omega - \omega_\alpha)] e^{i(\omega - \omega_\alpha)t} \equiv \int_{-\infty}^\infty d\omega g_\alpha(\omega - \omega_\alpha) e^{i(\omega - \omega_\alpha)t} = E_\alpha(t), \quad (2.34)$$

one can further simplify (2.32) to

$$\begin{aligned}
E_{\text{obs}}(R, t) \propto & \int_0^d dz \exp\{-i[2k(\omega_2) - k^*(\omega_1)]z\} \\
& \times \{(\bar{n} + 1) e^{ik_h z} [E_2(t_R + (1/v_h - 1/v_2)z)]^2 E_1(t_R + (1/v_h - 1/v_1)z) \\
& + (\bar{n} - 1) e^{-ik_h z} [E_2(t_R - (1/v_h + 1/v_2)z)]^2 E_1(t_R - (1/v_h + 1/v_1)z)\}. \quad (2.35)
\end{aligned}$$

The second term in the second pair of curly brackets of (2.35) contains a factor which is rapidly oscillating with respect to  $z$  and gives a smaller contribution to  $E_{\text{obs}}$  than the first term. In the following only the first term will be considered. The physical quantity observed in the experiment is the integrated intensity of the signal field, namely,

$$\int_{-\infty}^\infty dt |E_{\text{obs}}(t)|^2. \quad (2.36)$$

The correlation trace is obtained by repeating the same measurement while changing the delay time  $\tau_d$  of the second pulse relative to the first pulse. When the shapes of the two pulses are identical, the signal field is given by

$$E_{\text{obs}}(R, t) \propto \int_0^d dz \exp\{i[k_h - 2k(\omega_2) + k^*(\omega_1)]z\} [E(t_R + (1/v_h - 1/v_2)z)]^2 E(t_R + \tau_d + (1/v_h - 1/v_1)z), \quad (2.37)$$

where  $E(t)$  is the common pulse envelope. The expression is remarkably simple and important in the analysis of the experimental data.

It is instructive to look into the limiting form of the correlation trace when all the incident pulses are  $\delta$ -function-like. In this case the signal field is calculated as

$$\begin{aligned}
E_{\text{obs}}(R, t) \propto & \int_0^d dz e^{i\Delta k z} [\delta(t_R + (1/v_h - 1/v_2)z)]^2 \delta(t_R + \tau_d + (1/v_h - 1/v_1)z) \\
& = \int_0^d dz e^{i\Delta k z} [\delta(t_R + (1/v_h - 1/v_2)z)]^2 \delta(\tau_d + (1/v_2 - 1/v_1)z) \\
& \propto \Theta(\tau_d) \Theta(d(1/v_1 - 1/v_2) - \tau_d) [\delta(t_R + (1/v_h - 1/v_2)\tau_d / (1/v_1 - 1/v_2))]^2 \exp[i\Delta k \tau_d / (1/v_1 - 1/v_2)], \quad (2.38)
\end{aligned}$$

with

$$\Delta k = k_h - 2k(\omega_2) + k^*(\omega_1),$$

where  $\Theta$  is the Heaviside step function and the inequality  $v_1 < v_2$  is implicitly assumed because  $\omega_2 < \omega_1 < \omega_1$  in the experiment. The integrated intensity of the signal field becomes

$$\int_{-\infty}^\infty dt |E_{\text{obs}}(t)|^2 \propto \Theta(\tau_d) \Theta(d(1/v_1 - 1/v_2) - \tau_d) \exp\{-2[2k_i(\omega_2) + k_i(\omega_1) - k_i(2\omega_2 - \omega_1)]\tau_d / (1/v_1 - 1/v_2)\}, \quad (2.39)$$

where  $k_i(\omega)$  is the imaginary part of the wave vector defined by

$$k(\omega) = k_r(\omega) - ik_i(\omega), \quad k_i(\omega) > 0. \quad (2.40)$$

Thus, the correlation trace is nonzero only within the range from  $\tau_d = 0$  to  $\tau_d = d(1/v_1 - 1/v_2)$  and shows a quite asymmetric form as depicted in Fig. 3. In this ideal limit, one can estimate  $2k_i(\omega_2) + k_i(\omega_1) - k_i(2\omega_2 - \omega_1)$

from the decay rate of the correlation trace. Furthermore, by varying  $\omega_1$  and  $\omega_2$  appropriately, one can determine  $k_i(\omega)$  at each  $\omega$  and accordingly  $\Gamma(\omega)$  in principle. The decay rate in (2.39) has a clear physical meaning. The length  $\tau_d / (1/v_1 - 1/v_2)$  is nothing but the depth in the crystal where the two  $\delta$ -function-like pulses meet and the nonlinear interaction occurs. Before the two pulses overlap spatially, each polariton wave suffers spatial damping

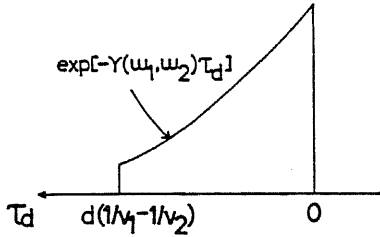


FIG. 3. A typical correlation trace of nondegenerate four-wave mixing under a limiting situation in which the two incident pulses are  $\delta$ -function-like.  $\gamma(\omega_1, \omega_2)$  is given by  $2[2k_i(\omega_2) + k_i(\omega_1) - k_i(2\omega_2 - \omega_1)] / (1/v_1 - 1/v_2)$ .

due to the imaginary part  $k_i$  of the wave vector. The generated nonlinear polarization emits the electromagnetic field, which is observed as a signal field outside the crystal. This signal field with frequency  $2\omega_2 - \omega_1$  propagates in the crystal as a polariton wave and suffers spatial damping during the passage from  $z = \tau_d / (1/v_1 - 1/v_2)$  to  $z = d$ , i.e., the rear surface of the sample. These spatial dampings lead to the decay rate in (2.39).

### III. ANALYSIS OF EXPERIMENTAL DATA

In this section the experimental data of the correlation trace are analyzed on the basis of the general theory developed in Sec. II and the dephasing relaxation constant

$\Gamma(\omega)$  of the excitonic polariton is determined as a function of energy. The electric field at the observation point is given by (2.37) and the integrated signal intensity is calculated as

$$\begin{aligned} I(\tau_d) &= \int_{-\infty}^{\infty} dt |E_{\text{obs}}(R, t)|^2 \\ &= \int_{-\infty}^{\infty} dt \int_0^d dz \int_0^d dz' e^{iKz - iK^*z'} E^2(t + \alpha z) \\ &\quad \times E(t + \tau_d + \beta z) E^2(t + \alpha z') \\ &\quad \times E(t + \tau_d + \beta z') \end{aligned} \quad (3.1)$$

with

$$K = k(2\omega_2 - \omega_1) - 2k(\omega_2) + k^*(\omega_1) = K_r + iK_i, \quad (3.2)$$

$$\alpha = 1/v_h - 1/v_2, \quad \beta = 1/v_h - 1/v_1,$$

where the real and imaginary parts of  $K$  are denoted by  $K_r$  and  $K_i$ , respectively. In the following the incident pulse envelope  $E(t)$  is supposed to be Gaussian:

$$E(t) \propto \exp(-t^2/2\sigma^2), \quad (3.3)$$

where  $\sigma$  characterizes the pulse width. Calculating the time integral in (3.1) first, and changing the integration variables  $z$  and  $z'$  to  $x$  and  $y$  defined by  $x = z + z'$  and  $y = z - z'$ , one obtains

$$\begin{aligned} I(\tau_d) &= \frac{\sigma}{2} \left[ \frac{\pi}{3} \right]^{1/2} \left[ \int_0^d dx \int_{-x}^x dy + \int_d^{2d} dx \int_{x-2d}^{2d-x} dy \right] \exp \left[ -\frac{[(\alpha - \beta)x - 2\tau_d]^2}{6\sigma^2} - K_i x - D \left( y - \frac{iK_r}{2D} \right)^2 - \frac{K_r^2}{4D} \right] \\ &= \left[ \frac{\pi\sigma^2}{3D} \right]^{1/2} \exp \left[ -\frac{(K_r)^2}{4D} \right] \text{Re} \left\{ \int_0^d dx \exp \left[ -\frac{[(\alpha - \beta)x - 2\tau_d]^2}{6\sigma^2} - K_i x \right] \text{erf} \left[ \sqrt{D} \left( x - \frac{iK_r}{2D} \right) \right] \right. \\ &\quad \left. + \int_d^{2d} dx \exp \left[ -\frac{[(\alpha - \beta)x - 2\tau_d]^2}{6\sigma^2} - K_i x \right] \text{erf} \left[ \sqrt{D} \left( 2d - x - \frac{iK_r}{2D} \right) \right] \right\} \end{aligned} \quad (3.4)$$

with

$$D = (2\alpha^2 + \beta^2)/4\sigma^2, \quad (3.5)$$

where the error function with complex argument  $z$  is defined by

$$\text{erf}[z] = \int_0^z dt \exp(-t^2), \quad (3.6)$$

and its real part is given by

$$\text{Re erf}[z = x + iy] = \text{erf}[x] + e^{-x^2} \int_0^{|y|} dt e^{-t^2} \sin 2xt. \quad (3.7)$$

It is now instructive to examine the case where the two incident pulses have the same energy, i.e.,  $\omega_1 = \omega_2$ . In this case the denominator  $\gamma_{\parallel} + i(\omega - \omega')$  in (2.27) cannot be simply put outside the integral because  $\omega - \omega'$  can become zero. Employing the Gaussian pulse envelope (3.3) and carrying out the frequency integral in (2.27), one obtains

$$E_{\text{obs}}(R, t) \propto \int_0^d dz \exp[-2k_i(\omega_1)z] \int_{-\infty}^{\infty} dx \frac{\exp[-\sigma^2 x^2/4 + ix(t_R + \tau_d/2)]}{\gamma_{\parallel} + ix}, \quad (3.8)$$

where  $t_R = t - (R - d)/c$  and  $k_i$  is defined by (2.40). The important point to be noted is that  $\tau_d$  and  $k_i(\omega)$  are contained in a separate manner. Thus,  $k_i(\omega)$  or equivalently  $\Gamma(\omega)$  cannot be determined from the correlation trace, i.e., from the  $\tau_d$  dependence of the integrated signal intensity. This confirms the importance of nondegenerate four-wave mixing in the study of the dephasing relaxation of the excitonic polariton as mentioned in the Introduction.

In the experiment the energy of the second pulse  $\omega_2$  is fixed at the transparent region of the crystal, while that of the first pulse  $\omega_1$  is varied over the resonance region as shown in Fig. 4. The energy of the nonlinearly mixed light  $2\omega_2 - \omega_1$  lies in the far off-resonance region. As seen from (3.2), the imaginary part  $K_i$  is dependent on  $\Gamma(\omega)$  at three energy points, namely,  $\Gamma(\omega_1)$ ,  $\Gamma(\omega_2)$ , and  $\Gamma(2\omega_2 - \omega_1)$ . The one of most interest is  $\Gamma(\omega_1)$ , since the others are values in the off-resonance region. The values of  $\Gamma(\omega_2)$  and  $\Gamma(2\omega_2 - \omega_1)$  are taken from the data of reflectivity and transmission measurements.<sup>15</sup> The value of  $\Gamma(\omega_1)$  is left as an adjustable parameter for the curve fitting. In the numerical calculation of the correlation trace, the dispersion relation of the excitonic polariton in CuCl is used; the dispersion relation has been studied recently in detail.<sup>10-13,16</sup> The parameter  $\sigma$  is determined from the experimental pulse width (full width at half maximum or FWHM) of 20 ps. The theoretical results are indicated by closed circles in Fig. 5. The spatial overlap between the two pulses and accordingly the integrated signal intensity become larger, in the case of a later arrival of the second pulse, than in the case of an earlier arrival, since the group velocity of the second pulse is quite large. The extreme case of this feature is demonstrated in Fig. 3 for  $\delta$ -function-like pulses. In reality, the incident pulse has a finite width and the correlation trace in Fig. 3 becomes broadened. The asymmetry of the correlation trace in Fig. 5 can be understood in this way. The values of  $\Gamma$  determined from the curve fitting are given in Fig. 6. The right-hand ordinate indicates the dephasing relaxation

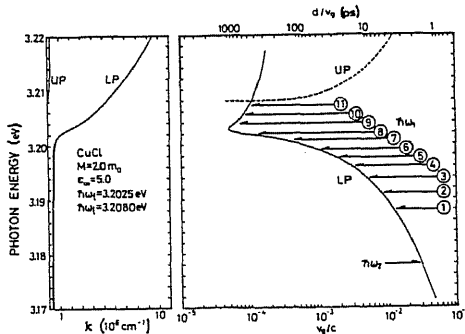


FIG. 4. Left: Dispersion relation of the excitonic polariton in CuCl, shown for both the upper- (UP) and lower- (LP) branch polaritons. Right: Group velocity of the excitonic polariton normalized by light velocity  $c$  in vacuum (lower abscissa) and the calculated transit time of the polariton pulse through a 14.15- $\mu\text{m}$ -thick CuCl crystal (upper abscissa). The energy  $\hbar\omega_1$  is varied from 1 to 11, whereas  $\hbar\omega_2$  is fixed at the transparent region.

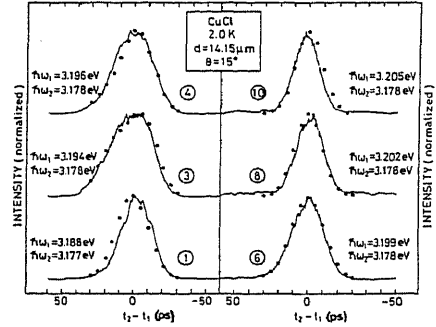


FIG. 5. Integrated intensity of the  $2\omega_2 - \omega_1$  beam emitted from a 14.15- $\mu\text{m}$ -thick CuCl crystal as a function of the relative time delay  $\tau_d = t_2 - t_1$  between  $\omega_2$  and  $\omega_1$  pulses.

time  $\hbar/(\Gamma/2)$  of the excitonic polariton. As seen in Fig. 6,  $\Gamma$  is of the order of 0.01 meV independent of the sample thickness and increases as the energy approaches the exciton resonance. When the energy  $\omega_1$  approaches the exciton resonance, the correlation trace becomes nearly symmetric with respect to  $\tau_d = 0$  and insensitive to the change of  $\omega_1$ . This feature can be understood on the basis of (3.4). In the resonance region the group velocity of the excitonic polariton is quite small and one can employ the following approximations:

$$\alpha - \beta \cong 1/v_1, \quad D \cong (4\sigma^2 v_1^2)^{-1}. \quad (3.9)$$

Since the ratio  $v_1/c$  is typically  $10^{-4}$ , the Gaussian factor

$$\exp\{-[(\alpha - \beta)x - 2\tau_d]^2 / 6\sigma^2\}$$

in (3.4) represents a very sharp distribution whose peak position and width are both of the order of 1  $\mu\text{m}$  or less. Thus, when the sample thickness  $d$  is about 20–30 mic-

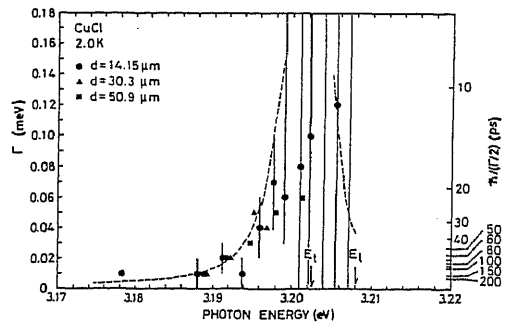


FIG. 6. Dephasing relaxation constant  $\Gamma$  as a function of energy of the excitonic polariton in CuCl. The three data symbols correspond to samples of different thicknesses. Long error bars above 3.200 eV mean that  $\Gamma$  cannot be determined precisely. The dashed line is the calculated energy dependence of  $\Gamma$  based on a model of polariton-polariton scattering (see text).

rons, the second integral in (3.4) can be neglected and one finds for positive  $\tau_d$

$$I(\tau_d) \propto \exp \left[ -\frac{K_r^2}{4D} - \frac{2K_i\tau_d}{\alpha - \beta} \right] \times \text{Re erf} \left[ \sqrt{D} \left[ \frac{2\tau_d}{\alpha - \beta} - \frac{iK_r}{2D} \right] \right]. \quad (3.10)$$

Substitution of (3.9) into (3.10) leads to

$$I(\tau_d) \propto \exp[ -(v_1\sigma K_r)^2 - 2v_1K_i\tau_d ] \text{Re erf}[\tau_d/\sigma - iv_1\sigma K_r]. \quad (3.11)$$

Since  $v_1\sigma K_r$  is large and typically of the order of  $10^2$ , one can use an approximate-formula derived from (3.7) for  $y \gg 1$ :

$$e^{-y^2} \text{Re erf}[x + iy] \cong e^{-x^2} \int_0^{|y|} dt \exp(t^2 - y^2) \sin 2xt. \quad (3.12)$$

Because the integral factor in (3.12) has only a weak dependence on  $x$ , the characteristic dependence of the correlation trace on  $\tau_d$  is given by

$$I(\tau_d) \propto \exp[ -2v_1K_i\tau_d - (\tau_d/\sigma)^2 ]. \quad (3.13)$$

For a typical value of  $K_i$  of about  $10^4 \text{ cm}^{-1}$  and for  $\sigma$  of the order of 10 ps, the  $\tau_d$  dependence of the correlation trace is dominated by the second exponent in (3.13) and the profile becomes insensitive to the change of  $\omega_1$  in the exciton resonance region. Thus, the value of  $K_i$  or equivalently  $\Gamma(\omega)$  cannot be determined precisely in the resonance region. However, even in a situation where the correlation trace is limited by the incident pulse width, the upper limit of  $\Gamma(\omega)$  can be estimated from the relation

$$\begin{aligned} \Gamma_{\text{imp}}(k) &= \frac{2\pi}{\hbar} |M|^2 \sum_q \delta(E(k+q) - E(k)) = \frac{|M|^2 V}{2\pi\hbar} \int_0^{2k} dq q^2 \int_0^\pi d\theta \sin\theta \delta(E((k^2+q^2-2kq\cos\theta)^{1/2}) - E(k)) \\ &= \frac{|M|^2 V}{2\pi\hbar^2 v_g(k)} \int_0^{2k} dq q = \frac{|M|^2 V k^2}{\pi\hbar^2 v_g(k)}, \end{aligned} \quad (4.1)$$

where  $V$  is the quantization volume and  $v_g(k)$  is the group velocity of the excitonic polariton with wave vector  $k$ . As seen from this expression,  $\Gamma_{\text{imp}}(k)$  shows an increase in the exciton resonance region due to the decrease of the group velocity and the increase of the wave vector  $k$ . The energy dependence of  $\Gamma_{\text{imp}}(k)$  is similar to the experimental result. On the other hand, the estimation of the absolute value of  $\Gamma_{\text{imp}}(k)$  cannot be precise since the magnitude of the matrix element  $M$  is uncertain. For a rough estimate, one may treat the scattering classically. The scattering cross section can be supposed to be the square of the exciton Bohr radius which is about 7 Å in CuCl.<sup>20</sup> The group velocity of the excitonic polariton in the off-resonance region is of the order of one hundredth of the light velocity in a vacuum. If the impurity concentration  $N_i$  is assumed to be  $10^{14} \text{ cm}^{-3}$ , one can estimate the order of  $\Gamma_{\text{imp}}$  as

$$2v_1K_i < \sigma^{-1}. \quad (3.14)$$

#### IV. MECHANISMS OF DEPHASING RELAXATION OF EXCITONIC POLARITONS

Let us now discuss the mechanism of the dephasing relaxation of excitonic polaritons. As mentioned in the Introduction, the relaxation to be observed in the experiment depends in general on the method of measurement. In the four-wave mixing experiment not only the incident laser beams but also the generated signal beam are spatially well collimated. Thus, any mechanism which causes a momentum change of the excitonic polariton will lead to the decay of the macroscopic polarization with a well-defined wave vector. Even elastic scattering leads to the decay of the polarization field, namely, the dephasing relaxation of the excitonic polariton in the case of four-wave mixing. This is in striking contrast to the case of induced absorption (IA).<sup>17-19</sup> In the case of IA all the polaritons that are scattered elastically into various directions can contribute to the absorption signal since only the energy is relevant in the absorption process and the direction of the polariton wave vector does not matter. The decay-time constant of IA reflects the energy relaxation of the ensemble of the injected polaritons. On the other hand, momentum relaxation by some mechanisms contributes to the dephasing relaxation of excitonic polaritons. The most likely mechanisms to cause such dephasing or momentum relaxation are (a) impurity scattering, (b) phonon scattering, and (c) polariton-polariton scattering.

Assuming the impurity-polariton scattering matrix element  $M$  to be independent of the momentum transfer, one can calculate the momentum relaxation rate due to the impurity scattering as

$$\Gamma_{\text{imp}} \cong (7 \text{ \AA})^2 v_g N_i = 1.5 \times 10^8 \text{ s}^{-1}. \quad (4.2)$$

This value is smaller by a few orders of magnitude than the experimentally estimated value. However, it is premature to rule out the impurity scattering as a mechanism of the dephasing relaxation of the excitonic polariton. To clarify the role of impurity scattering quantitatively, it is necessary to study the sample dependence of the dephasing relaxation constant by varying the impurity concentration systematically.

To examine the second possibility, the scattering probability is calculated for both the deformation potential coupling with longitudinal acoustic (ac) phonons and the Fröhlich interaction with longitudinal optic (op) phonons. The LA-phonon scattering rate via the deformation-potential coupling is given by

$$\Gamma_{ac}(k) = \frac{2\pi}{\hbar} \sum_q |V_{ac}(q)|^2 [n_q \delta(E(k) - E(k+q) + \hbar\omega_q) + (1+n_q) \delta(E(k) - E(k-q) - \hbar\omega_q)], \quad (4.3)$$

where the first term in the square brackets represents the contribution from the phonon absorption process and the second term that from the phonon emission process.  $E(k)$  denotes the energy dispersion of the excitonic polariton and  $\hbar\omega_q$  the acoustic phonon energy at wave vector  $q$ . For the case of a  $1s$  exciton, the exciton-phonon coupling constant  $V_{ac}(q)$  is given by<sup>21</sup>

$$V_{ac}(q) = \left[ \frac{\hbar q}{2\rho u V} \right]^{1/2} [D_c f_c(q) - D_v f_v(q)], \quad (4.4)$$

with

$$f_c(q) = 1/[1 + (\alpha_h a_B q/2)^2]^2 \quad (4.5)$$

and

$$f_v(q) = 1/[1 + (\alpha_e a_B q/2)^2]^2,$$

where  $\rho$ ,  $u$ ,  $V$ ,  $a_B$ , and  $D_c$  ( $D_v$ ) denote the mass density, the sound velocity of LA phonons, the quantization volume, the exciton Bohr radius, and the deformation potential constant for the conduction (valence) band, respectively, and  $\alpha_h$  and  $\alpha_e$  are defined by

$$\alpha_h = m_h/(m_h + m_e), \quad \alpha_e = m_e/(m_h + m_e) \quad (4.6)$$

with the electron (hole) effective mass  $m_e$  ( $m_h$ ). The coupling constant (4.4) is usually approximated in the small momentum limit as

$$V_{ac}(q) \cong \left[ \frac{\hbar q}{2\rho u V} \right]^{1/2} (D_c - D_v). \quad (4.7)$$

Strictly speaking, (4.3) should be multiplied by another factor relating to the exciton content in the polariton mode. However, the exciton content is a slowly varying function with respect to the polariton energy and is almost unity over a rather wide range of 50–60 meV around the exciton resonance in the case of CuCl. Thus, the factor of the exciton content in the polariton mode can be safely neglected. In the calculation the following

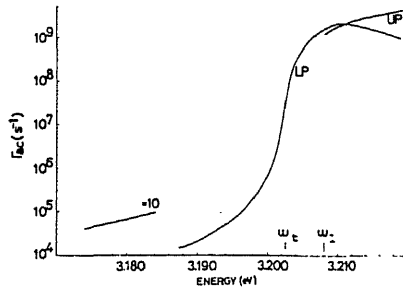


FIG. 7. Dephasing (momentum) relaxation rate of the excitonic polariton in CuCl due to the acoustic phonon scattering. Above the longitudinal exciton energy  $\omega_l$  the results are shown for both the upper- (UP) and lower- (LP) branch polaritons.

parameters are employed:  $u = 3.8 \times 10^5$  cm/s,<sup>22</sup>  $\rho = 4.16$  g/cm<sup>3</sup>,<sup>23</sup>  $D_c - D_v = -0.4$  eV,<sup>24</sup> and the temperature is taken to be 2 K. The calculated result is shown in Fig. 7. In the energy region above  $\omega_l$  the results are shown for both the upper- and lower-branch polaritons. The increasing trend of the LA-phonon scattering rate as the energy approaches the exciton resonance is in agreement with the experimental result in Fig. 6. However, the absolute value of the scattering rate is much smaller than the experimental value. Thus, it can be concluded that LA-phonon scattering is only a minor mechanism of the dephasing relaxation of the excitonic polariton.

Similarly the LO-phonon scattering rate can be calculated. In this case the exciton-phonon coupling is induced through the Fröhlich interaction and its explicit form is given by<sup>21</sup>

$$V_{op}(q) = \left[ \frac{2\pi e^2 \hbar \omega_{LO}}{V} \left( \frac{1}{\epsilon_\infty} - \frac{1}{\epsilon_0} \right) \right]^{1/2} [f_c(q) - f_v(q)]/q, \quad (4.8)$$

where  $\epsilon_\infty$  ( $\epsilon_0$ ) and  $\hbar\omega_{LO}$  are the optic (static) dielectric constant and the LO-phonon energy, respectively, and  $f_c$  and  $f_v$  are defined in (4.5). Taking into account only the phonon-emission process, one obtains the following scattering rate due to the LO phonon:

$$\Gamma_{op}(k) = \frac{2\pi}{\hbar} \sum_q |V_{op}(q)|^2 \delta(E(k) - E(k-q) - \hbar\omega_q). \quad (4.9)$$

The relevant parameters are chosen as  $\hbar\omega_{LO} = 26$  meV,<sup>25</sup>  $\epsilon_\infty = 5.0$ ,<sup>13</sup>  $\epsilon_0 = \epsilon_\infty \omega_l^2 / \omega_t^2$ ,  $\hbar\omega_l = 3.2080$  eV,<sup>13</sup> and  $\hbar\omega_t = 3.2025$  eV.<sup>13</sup> The calculated result is shown in Fig. 8. The general trend of the energy dependence is similar to that in Fig. 7. In this case also, the absolute value of  $\Gamma$  is too small to explain the experimental results. On the basis of these results one can conclude that phonon

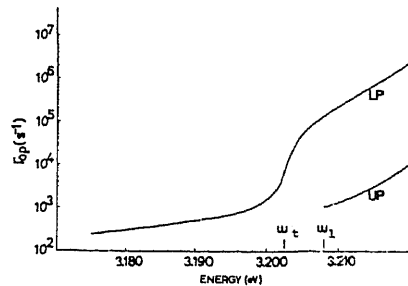


FIG. 8. Dephasing (momentum) relaxation rate of the excitonic polariton in CuCl due to the optic phonon scattering. Above the longitudinal exciton energy  $\omega_l$  the results are shown for both the UP and LP branch polaritons.

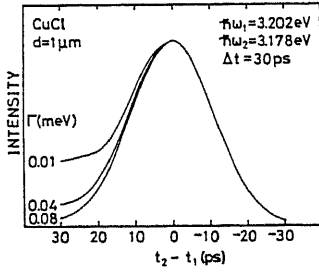


FIG. 9. Correlation traces of nondegenerate four-wave mixing for a 1- $\mu\text{m}$ -thick CuCl crystal. The pulse width  $\Delta t$  (FWHM) is chosen to be 30 ps and the dephasing relaxation constant  $\Gamma$  is varied at 0.01, 0.04, and 0.08 meV (see text in Sec. VI).

scattering makes a minor contribution to the momentum relaxation of the excitonic polariton and cannot explain quantitatively the experimental results.

Let us finally examine the possibility of polariton-polariton scattering. Even when a well-collimated laser beam is concerned, there is uncertainty with respect to the direction of the polariton wave vector of the order of  $0.1^\circ$ .

This broadening of the polariton wave vector may lead to mutual collisions among polaritons injected by an intense laser beam. The two colliding excitonic polaritons can scatter into various directions of the wave vector conserving the total energy and momentum. When the propagation direction of the scattered polariton is appreciably deflected from that of the incident polaritons, the scattered polariton cannot contribute to the signal intensity of the four-wave mixing. Even if the scattered polariton propagates in almost the same direction as the incident polaritons, the energy of the scattered polariton is not necessarily equal to that of the incident polariton. When detection is spatially well collimated and is also energetically well resolved, almost none of the scattered polaritons can contribute to the signal intensity. Thus, polariton-polariton scattering leads to the dephasing or momentum relaxation of the excitonic polariton. When the polariton-polariton scattering matrix element is written as

$$W(k_1, k_2; k_3, k_4) C_{k_1}^\dagger C_{k_2}^\dagger C_{k_3} C_{k_4}, \quad (4.10)$$

denoting the creation (annihilation) operator of the excitonic polariton with wave vector  $k$  by  $C_k^\dagger$  ( $C_k$ ), the momentum relaxation rate of an excitonic polariton with wave vector  $k$  is given by

$$\Gamma_c(k) = \frac{2\pi}{\hbar} \sum_{k_1, k_2, k_3} |W(k_1, k_2; k_3, k)|^2 (1 + N_{k_1})(1 + N_{k_2}) N_{k_3} \delta(k_1 + k_2 - k_3 - k) \delta(E(k_1) + E(k_2) - E(k_3) - E(k)), \quad (4.11)$$

where  $N(k)$  is the occupation number of the excitonic polariton with wave vector  $k$ . In (4.11)  $N_{k_1}$  and  $N_{k_2}$  can be neglected since the wave vector and energy of the scattered polaritons are in general different from those of the incident polaritons. The summation with respect to  $k_3$  is carried out over the distribution of the incident polaritons. As a result,  $\Gamma_c$  is proportional to the laser intensity. Expression (4.11) can be reduced to a more convenient form for numerical calculation. Taking the  $z$  axis in the direction of wave vector  $k + k_3$  and neglecting the wave-vector dependence of  $W$ , one can reduce (4.11) to

$$\begin{aligned} \Gamma_c(k) &= \frac{2\pi}{\hbar} |W|^2 \sum_{k_3} N_{k_3} \sum_{k_1} \delta(E(k_1) + E(k + k_3 - k_1) - E(k_3) - E(k)) \\ &= \frac{V}{2\pi\hbar^2} |W|^2 \sum_{k_3} N_{k_3} \int_0^\infty d|k_1| |k_1|^2 \int_0^\pi d\theta \sin\theta \sum_\alpha \frac{\delta(|k_1| - |k_1^\alpha|)}{|f(\theta, |k_1^\alpha|)|}, \end{aligned} \quad (4.12)$$

with

$$f(\theta, |k_1|) = v_g(|k_1|) + v_g(|k + k_3 - k_1|) (|k_1| - |k + k_3 \cos\theta|) / |k + k_3 - k_1|, \quad (4.13)$$

where  $v_g$  is the group velocity of the excitonic polariton,  $V$  the quantization volume, and the superscript  $\alpha$  indicates a number of solutions which satisfy the energy conservation implied by the  $\delta$  function. It is found numerically that the integral in (4.12) is not sensitive to the angle between  $k$  and  $k_3$  within a few degrees. Thus, it is permissible to replace the summation over  $k_3$  in (4.12) by the value for a typical  $k_3$  multiplied by the total number of incident polaritons. In the numerical estimate of the absolute value of  $\Gamma_c$ , the two colliding polaritons are assumed to have the same energy 3.188 eV ( $|k| = |k_3|$ )

and the angle between the two wave vectors is chosen typically as  $0.1^\circ$ . Using the recent results of the microscopic calculation of the collision matrix element of excitonic polaritons in CuCl,<sup>26</sup> one finds a typical value

$$WV = 4.8 \times 10^{-32} \text{ erg}, \quad (4.14)$$

and obtains

$$\Gamma_c^{\text{theor}}(3.188 \text{ eV}) = 3.6 \times 10^{10} \text{ s}^{-1}. \quad (4.15)$$

where the number density of the incident polaritons is

supposed to be  $10^{18} \text{ cm}^{-3}$ , estimated from the power, pulse width, beam diameter of the laser, and the crystal thickness. This value can be compared with the experimental result:

$$\Gamma_c^{\text{exp}}(3.188 \text{ eV}) = 1.5 \times 10^{10} \text{ s}^{-1}. \quad (4.16)$$

These two values agree well within a factor 3. However, this agreement should be considered as fortuitous since there remains uncertainty in the estimation of the number density of polaritons and other dynamical parameters. In the theoretical fitting the absolute value of  $\Gamma$  is adjusted to the experimental value at 3.188 eV and the energy dependence of  $\Gamma$  is determined by (4.12). The calculated result is shown by a dashed line in Fig. 6. As for the energy dependence of  $\Gamma$ , the agreement between theory and experiment is satisfactory, although the experimental values are ambiguous in the resonance region.

From the above arguments it may be concluded that the dephasing or momentum relaxation of the excitonic polariton is caused mainly by polariton-polariton scattering under our experimental conditions, although impurity scattering cannot be ruled out as a mechanism of the dephasing relaxation.

#### V. MICROSCOPIC DERIVATION OF EQUATIONS OF MOTION AND DEPHASING RELAXATION OF EXCITONIC POLARITONS

In Sec. II, the basic equations of motion for the excitonic polariton are taken from the familiar ones in laser theory which are derived on the picture of localized exci-

tations. However, the excitonic polariton is not a localized excitation but propagates throughout the crystal with a definite wave vector. In this section the basic equations of motion are derived from the microscopic point of view and it is confirmed that the same equations of motion as in laser theory are applicable for the case of excitonic polaritons with a small change to incorporate spatial dispersion. First of all let us derive the polarization field operator quantum mechanically from the electromagnetic interaction

$$\frac{e}{2mc}(\mathbf{p} \cdot \mathbf{A} + \mathbf{A} \cdot \mathbf{p}), \quad (5.1)$$

where  $\mathbf{A}$  is the vector potential and  $\mathbf{p}$  the momentum operator. In the second-quantized form the vector potential is written as

$$\mathbf{A}(r) = \sum_{q,\lambda} \left[ \frac{2\pi\hbar c}{|q|V} \right]^{1/2} \hat{\mathbf{e}}_{q\lambda} e^{iqr} (b_{q\lambda} + b_{-q\lambda}^\dagger), \quad (5.2)$$

where  $b_q$  ( $b_q^\dagger$ ),  $\hat{\mathbf{e}}_{q\lambda}$  and  $V$  are the annihilation (creation) operator of the photon with wave vector  $q$ , the polarization vector, and the quantization volume, respectively, and the polarization index  $\lambda$  indicates the transverse modes in the Coulomb gauge. Calculating the matrix element between the electron field operators, one obtains

$$\int d^3r \Psi^\dagger(r) \frac{e}{2mc}(\mathbf{p} \cdot \mathbf{A} + \mathbf{A} \cdot \mathbf{p}) \Psi(r) = \frac{ie}{mc} \left[ \frac{2\pi\hbar c}{V} \right]^{1/2} \sum_{k,q,\lambda} \frac{p_0 \cdot \hat{\mathbf{e}}_{q\lambda}}{|q|^{1/2}} (a_{c,k+q}^\dagger a_{vk} - a_{v,k+q}^\dagger a_{ck}) (b_{q\lambda} + b_{-q\lambda}^\dagger), \quad (5.3)$$

where  $a_{\alpha k}^\dagger$  ( $a_{\alpha k}$ ) is the creation (annihilation) operator of the  $\alpha$ -band electron with wave vector  $k$ . The real vector  $p_0$  is defined by

$$i p_0 = \frac{1}{v_0} \int_{v_0} d^3r u_{\alpha k}^*(r) p u_{\alpha k}(r), \quad (5.4)$$

where  $u_{\alpha k}(r)$  denotes the periodic part of the Bloch function of the  $\alpha$  band,  $v_0$  the volume of the unit cell, and the usual  $s$ - $p$  band combination is tacitly assumed for the conduction and valence bands. Here the wave-vector dependence of the matrix element is neglected. In the resonant-term approximation, (5.3) becomes

$$\frac{ie}{mc} \left[ \frac{2\pi\hbar c}{V} \right]^{1/2} \sum_{k,q,\lambda} \frac{p_0 \cdot \hat{\mathbf{e}}_{q\lambda}}{|q|^{1/2}} \times (a_{c,k+q}^\dagger a_{vk} b_{q\lambda} - a_{v,k+q}^\dagger a_{ck} b_{-q\lambda}^\dagger). \quad (5.5)$$

On the other hand, the electric field is given by

$$\begin{aligned} \mathbf{E}(r) &= -\frac{1}{c} \frac{\partial}{\partial t} \mathbf{A}(r) \\ &= \sum_{q,\lambda} i \left[ \frac{2\pi\hbar c}{V} |q| \right]^{1/2} \hat{\mathbf{e}}_{q\lambda} e^{iqr} (b_{q\lambda} - b_{-q\lambda}^\dagger) \\ &= \sum_q e^{iqr} [\mathbf{E}^-(q) + \mathbf{E}^+(q)] = \sum_q e^{iqr} \mathbf{E}(q), \end{aligned} \quad (5.6)$$

where the Fourier component of the electric field  $\mathbf{E}(q)$  is decomposed into the positive and negative frequency parts corresponding to  $b_{-q}^\dagger$  and  $b_q$ , respectively. With these notations (5.5) is written as

$$\frac{e p_0}{mc} \sum_{k,q} \frac{1}{|q|} [a_{c,k+q}^\dagger a_{vk} \mathbf{E}^-(q) + a_{v,k+q}^\dagger a_{ck} \mathbf{E}^+(q)]. \quad (5.7)$$

Supplementing the nonresonant terms, one obtains the second-quantized form of the electromagnetic interaction as

$$\frac{e}{mc} \sum_{k,q} \frac{p_0 \cdot \mathbf{E}(q)}{|q|} (a_{c,k+q}^\dagger a_{vk} + a_{v,k+q}^\dagger a_{ck}). \quad (5.8)$$

From the analogy to the electromagnetic interaction in the dipole approximation, the polarization field operator with wave vector  $q$  can be introduced by

$$p(q) = -\frac{e|p_0|}{mc|q|} \sum_k (a_{c,k+q}^\dagger a_{vk} + a_{v,k+q}^\dagger a_{ck}). \quad (5.9)$$

The prefactor of (5.9), having the dimensions of the electric dipole moment, will be denoted by  $\mu$ :

$$\mu = \frac{e|p_0|}{mc|q|}, \quad (5.10)$$

where the typical value of  $q$  is determined by the exciton energy  $\epsilon_x$  as

$$\hbar c|q| = \epsilon_x. \quad (5.11)$$

On the other hand, the quantity corresponding to the population inversion is defined by

$$I(r) = (a_{cr}^\dagger a_{cr} - a_{vr}^\dagger a_{vr})/v_0, \quad (5.12)$$

where  $a_{cr}^\dagger$  ( $a_{cr}$ ) is the creation (annihilation) operator of the  $\alpha$ -band electron in the Wannier representation and  $v_0$  is the volume of the unit cell. The Fourier component of the population inversion, defined by

$$\begin{aligned} \frac{d}{dt} a_{c,k+q}^\dagger a_{vk} &= \frac{i}{\hbar} [H, a_{c,k+q}^\dagger a_{vk}] = \frac{i}{\hbar} [E_c(k+q) - E_v(k)] a_{c,k+q}^\dagger a_{vk} \\ &\quad - \frac{ie|p_0|}{\hbar mc} \sum_{q'} (a_{c,k+q}^\dagger a_{c,k-q'} - a_{v,k+q}^\dagger a_{v,k-q'}) E^+(q')/|q'|, \end{aligned} \quad (5.17)$$

where  $E^+(q)$  is the positive frequency part of the electric field defined in (5.6). Hereafter, the electric field component parallel to  $p_0$  will be considered. Taking the sum over wave vector  $k$  on both sides of (5.17), replacing  $|q'|$  in the denominator on the right-hand side by a typical value given in (5.11), and introducing the replacement

$$E_c(k+q) - E_v(k) \equiv \epsilon_x(q) \quad (5.18)$$

with the exciton energy dispersion  $\epsilon_x(q)$ , one finds

$$\begin{aligned} \frac{d}{dt} \sum_k a_{c,k+q}^\dagger a_{vk} &= \frac{i}{\hbar} \epsilon_x(q) \sum_k a_{c,k+q}^\dagger a_{vk} \\ &\quad - \frac{i}{\hbar} \mu \sum_{q'} \sigma(q+q') E(q'), \end{aligned} \quad (5.19)$$

where the negative frequency part of the electric field is added to the second term on the right-hand side and the notation of (5.10) is used. In the same way one obtains

$$\frac{d}{dt} a_{c,k+q}^\dagger a_{ck} = \frac{i}{\hbar} [E_c(k+q) - E_c(k)] a_{c,k+q}^\dagger a_{ck} + \frac{ie|p_0|}{\hbar mc} \sum_{q'} \frac{1}{|q'|} [a_{v,k+q+q'}^\dagger a_{ck} E^+(q') - a_{c,k+q}^\dagger a_{v,k-q'} E^-(q')], \quad (5.23)$$

$$\frac{d}{dt} a_{v,k+q}^\dagger a_{vk} = \frac{i}{\hbar} [E_v(k+q) - E_v(k)] a_{v,k+q}^\dagger a_{vk} + \frac{ie|p_0|}{\hbar mc} \sum_{q'} \frac{1}{|q'|} [a_{c,k+q+q'}^\dagger a_{vk} E^-(q') - a_{v,k+q}^\dagger a_{c,k-q'} E^+(q')]. \quad (5.24)$$

$$\sigma(q) = \int d^3r e^{iqr} I(r), \quad (5.13)$$

can be written as

$$\sigma(q) = \sum_k (a_{c,k+q}^\dagger a_{ck} - a_{v,k+q}^\dagger a_{vk}) \quad (5.14)$$

by transforming the Wannier operators into the Bloch operators.

Now that the operators of the polarization field and of the population inversion are derived microscopically, the equations of motion for these variables will be considered. The Hamiltonian is assumed in the simplest form as

$$\begin{aligned} H &= \sum_k E_c(k) a_{ck}^\dagger a_{ck} + \sum_k E_v(k) a_{vk}^\dagger a_{vk} \\ &\quad + i \sum_{k,q,\lambda} g_\lambda(q) (a_{c,k+q}^\dagger a_{vk} b_{q\lambda} - a_{v,k+q}^\dagger a_{ck} b_{q\lambda}^\dagger), \end{aligned} \quad (5.15)$$

where  $E_c(k)$  is the energy dispersion of the  $\alpha$ -band electron and the electromagnetic coupling constant is defined by

$$g_\lambda(q) = \frac{e|p_0| \hat{e}_{q\lambda}}{mc} \left[ \frac{2\pi\hbar c}{V|q|} \right]^{1/2}. \quad (5.16)$$

A typical equation of motion is given as

$$\begin{aligned} \frac{d}{dt} \sum_k a_{v,k+q}^\dagger a_{ck} &= -\frac{i}{\hbar} \epsilon_x(q) \sum_k a_{v,k+q}^\dagger a_{ck} \\ &\quad + \frac{i}{\hbar} \mu \sum_{q'} \sigma(q+q') E(q'). \end{aligned} \quad (5.20)$$

The basic equations of motion for the polarization field operator are derived by adding (5.19) and (5.20) or by subtracting (5.20) from (5.19) as

$$\frac{d}{dt} p(q) = -\frac{i\mu}{\hbar} \epsilon_x(q) \sum_k (a_{c,k+q}^\dagger a_{vk} - a_{v,k+q}^\dagger a_{ck}), \quad (5.21)$$

$$\begin{aligned} \frac{d}{dt} \mu \sum_k (a_{c,k+q}^\dagger a_{vk} - a_{v,k+q}^\dagger a_{ck}) \\ = -\frac{i}{\hbar} \epsilon_x(q) p(q) - \frac{2i\mu^2}{\hbar} \sum_{q'} \sigma(q+q') E(q'), \end{aligned} \quad (5.22)$$

where  $p(q)$  is the magnitude of the vector in (5.9).

Next, the equation of motion for the population inversion is derived:

The first term on the right-hand side of each equation represents wavelike behavior due to the dispersion of the energy band. Since  $q$  denotes the wave vector of the population grating and is usually small, the first terms on the right-hand side can be safely neglected. By repeating the same procedure as in the derivation of (5.19) from (5.17), one obtains

$$\frac{d}{dt}\sigma(q) = -\frac{2i\mu}{\hbar}\sum_{q'}E(q')\sum_k(a_{c,k+q+q'}^\dagger a_{vk} - a_{v,k+q+q'}^\dagger a_{ck}). \quad (5.25)$$

Equations (5.21), (5.22), and (5.25) form the basis set for the dynamical description of the excitonic polariton. Let us now introduce the real-space field operators defined by

$$\begin{aligned} I(r) &= \frac{1}{V}\sum_q e^{-iqr}\sigma(q), \quad p(r) = \frac{1}{V}\sum_q e^{-iqr}p(q), \\ p^+(r) &= \frac{-\mu}{V}\sum_{k,q} e^{-iqr}a_{c,k+q}^\dagger a_{vk}, \\ p^-(r) &= \frac{-\mu}{V}\sum_{k,q} e^{-iqr}a_{v,k+q}^\dagger a_{ck}, \end{aligned} \quad (5.26)$$

where, of course, it holds that  $p(r) = p^+(r) + p^-(r)$ . Then the equations of motion for these operators are obtained as

$$\frac{d}{dt}p(r) = \frac{i}{\hbar}\epsilon_x(i\nabla)[p^+(r) - p^-(r)], \quad (5.27)$$

$$\frac{d}{dt}[p^+(r) - p^-(r)] = \frac{i}{\hbar}\epsilon_x(i\nabla)p(r) + \frac{2i\mu^2}{\hbar}I(r)E(r), \quad (5.28)$$

$$\frac{d}{dt}I(r) = \frac{2i}{\hbar}E(r)[p^+(r) - p^-(r)]. \quad (5.29)$$

Here the field quantities are scalars since, as mentioned before, the electric field component parallel to the polarization field is considered.

It is quite instructive to compare these equations with the density-matrix equations for a two-level atom. The latter are familiar in laser theory<sup>7,8</sup> and are given explicitly as

$$\frac{d}{dt}\rho_{12} = i\omega_0\rho_{12} + \frac{i\mu}{\hbar}E\sigma - \gamma_\perp\rho_{12}, \quad (5.30)$$

$$\frac{d}{dt}\sigma = \frac{i2\mu}{\hbar}E(\rho_{12} - \rho_{12}^*) + \gamma_\parallel(\sigma_0 - \sigma). \quad (5.31)$$

Here the upper (lower) level of a two-level atom is denoted by 2 (1) and  $\sigma$ ,  $\sigma_0$ ,  $\hbar\omega_0$ ,  $\mu$ , and  $\gamma_\parallel$  ( $\gamma_\perp$ ) are the population inversion defined by  $\rho_{22} - \rho_{11}$ , the equilibrium value of  $\sigma$ , the energy difference between the two levels, the electric dipole moment, and the longitudinal (transverse) relaxation constant, respectively. The polarization defined by

$$p = \mu(\rho_{12} + \rho_{12}^*), \quad (5.32)$$

satisfies the equation

$$\frac{d}{dt}p = -\gamma_\perp p + i\omega_0\mu(\rho_{12} - \rho_{12}^*). \quad (5.33)$$

Another relevant equation is derived from (5.30) and is given by

$$\frac{d}{dt}\mu(\rho_{12} - \rho_{12}^*) = i\omega_0 p + \frac{2i\mu^2}{\hbar}E\sigma - \gamma_\perp\mu(\rho_{12} - \rho_{12}^*). \quad (5.34)$$

It is easily seen that the equations of motion from (5.27) to (5.29) have a one-to-one correspondence with the set of equations (5.33), (5.34), and (5.31), if the relaxation terms in the latter are dropped and the following correspondence is supposed:

$$\mu\rho_{12} \leftrightarrow p^+(r), \quad \mu\rho_{12}^* \leftrightarrow p^-(r). \quad (5.35)$$

Thus, the equations of motion, which were originally derived in laser theory, turn out to be applicable in the case of excitonic polaritons with a small change to incorporate spatial dispersion. In fact Eqs. (2.1) and (2.2) can be derived from (5.27) and (5.29) with the replacement of  $2\omega_0\mu^2/\hbar$  by  $\beta\omega_0^2$ .

Next, the inclusion of the relaxation terms will be discussed from the microscopic point of view.<sup>27</sup> The relaxation phenomena result from the reversible dynamical equations of motion, when some kind of coarse graining is introduced which is closely related to the method of measurements; for example, the phonon state of the crystal lattice is not measured and the signal emitted in a particular direction is selectively observed. The procedure of coarse graining can be incorporated by means of the general method of projection<sup>28,29</sup> to derive the irreversibility from reversible dynamics. In the following let us derive the relaxation terms due to the polariton-phonon interaction and the polariton-polariton scattering. In the procedure of coarse graining the total system is divided into the relevant system and the rest, which is usually called the reservoir, and the dynamics of the total system are projected onto that of the relevant system by eliminating the degrees of freedom of the reservoir. To be more concrete, let us consider the reduced density operator defined by

$$\rho_r = P\rho, \quad (5.36)$$

where  $P$  is a suitable projection operator. The equation of motion for  $\rho_r$  is generally given by<sup>30</sup>

$$\begin{aligned} \frac{d}{dt}\rho_r(t) &= -\frac{i}{\hbar}L_S\rho_r(t) \\ &\quad - \frac{1}{\hbar^2}\int_0^t d\tau PL_{SR}e^{-i(1-P)L(t-\tau)/\hbar}L_{SR}\rho_r(\tau), \end{aligned} \quad (5.37)$$

where the Hamiltonian of the total system is divided into those of the relevant system ( $S$ ), the reservoir ( $R$ ) and their interaction ( $SR$ ) as

$$H = H_S + H_R + H_{SR}, \quad (5.38)$$

and the Liouville operators are defined, for any operator  $A$ , by

$$LA = [H, A], \quad L_S A = [H_S, A], \quad L_{SR} A = [H_{SR}, A]. \quad (5.39)$$

In the case of the polariton-phonon interaction, the relevant system and the reservoir correspond to the exci-

tonic polaritons and the phonon system, respectively. The suitable projection operator is given by

$$P\rho = \rho_{\text{ph}}^0 \text{Tr}_{\text{ph}} \rho = \rho_{\text{ph}}^0 \rho_S, \quad (5.40)$$

where  $\rho_{\text{ph}}^0$  denotes the thermal equilibrium state of the phonon system, the trace is over the phonon states, and  $\rho_S$  is the density operator only for the excitonic polaritons. It is convenient to use the polariton operator instead of the electron-hole excitation operator. Let  $C_{\lambda k}^\dagger$  ( $C_{\lambda k}$ ) denote the creation (annihilation) operator of the excitonic polariton with wave vector  $k$ , where the index  $\lambda$  specifies

the electron-hole relative motion. The polariton-phonon interaction Hamiltonian can be written as

$$H_{\text{ep}} = \sum_{k,q} \Xi(q) C_{k+q}^\dagger C_k (b_q + b_{-q}^\dagger), \quad (5.41)$$

where  $b^\dagger$  ( $b$ ) is the creation (annihilation) operator of phonons and  $\Xi(q)$  is the coupling strength dependent on the kind of phonons and on the exciton internal motion. Here the electron-hole relative motion is assumed to be the lowest  $1s$  state and the index  $\lambda$  is dropped. Then by substitution of  $H_{\text{ep}}$  for  $H_{\text{SR}}$ , the second term of (5.37) can be calculated up to the second-order perturbation with respect to  $H_{\text{SR}}$  as

$$-\frac{1}{\hbar^2} \sum_{k,k',q} |\Xi(q)|^2 \int_0^t d\tau \{ [n_q e^{-i\omega_q \sigma} + (1+n_q) e^{i\omega_q \sigma}] [C_{k'-q}^\dagger C_{k'} C_{k+q}^\dagger C_k(\sigma) e^{iH_S \sigma / \hbar} \rho_S(\tau) e^{-iH_S \sigma / \hbar}] \\ + [n_q e^{i\omega_q \sigma} + (1+n_q) e^{-i\omega_q \sigma}] [e^{iH_S \sigma / \hbar} \rho_S(\tau) e^{-iH_S \sigma / \hbar} C_{k+q}^\dagger C_k(\sigma) C_{k'-q}^\dagger C_{k'}] \}, \quad (5.42)$$

where  $\sigma = \tau - t$  and  $\omega_q$  and  $n_q$  denote the frequency and the occupation number of the phonon with wave vector  $q$ , respectively. The Heisenberg operator is defined in terms of  $H_S$  in (5.38), namely, the Hamiltonian of the excitonic polariton. Taking into account only the secular terms and employing the Markovian approximation,<sup>30</sup> one can further reduce (5.42) to

$$-\frac{2\pi}{\hbar} \sum_{k,q} |\Xi(q)|^2 \{ [n_q \delta(E(k+q) - E(k) - \hbar\omega_q) + (1+n_q) \delta(E(k+q) - E(k) + \hbar\omega_q)] [C_k^\dagger C_{k+q} C_{k+q}^\dagger C_k \rho_S(t)] \\ + [n_q \delta(E(k+q) - E(k) + \hbar\omega_q) + (1+n_q) \delta(E(k+q) - E(k) - \hbar\omega_q)] [\rho_S(t) C_{k+q}^\dagger C_k C_k^\dagger C_{k+q}] \} = \Gamma_{\text{ph}} \rho, \quad (5.43)$$

where the polariton dispersion is denoted by  $E(k)$  and the relaxation operator  $\Gamma_{\text{ph}}$  is defined by this equation. Consequently, the equation of motion for the reduced density operator  $\rho_S$  in (5.40) becomes

$$\frac{d}{dt} \rho_S(t) = -\frac{i}{\hbar} [H_S, \rho_S] + \Gamma_{\text{ph}} \rho_S. \quad (5.44)$$

In order to derive the equations of motion for physical quantities, the average value of some operator  $A$ , defined by

$$\langle A(t) \rangle = \text{Tr} A \rho_S(t), \quad (5.45)$$

will be considered. The equation of motion for the averaged quantity  $\langle A(t) \rangle$  is given as

$$\frac{d}{dt} \langle A(t) \rangle = \text{Tr} A \frac{d}{dt} \rho_S(t) = \frac{i}{\hbar} \text{Tr} \rho_S [H_S, A] + \text{Tr} A \Gamma_{\text{ph}} \rho_S. \quad (5.46)$$

The Fourier component of the polarization field with wave vector  $Q$  can be written in terms of the polariton operator as

$$p(Q) = -\mu (C_Q^\dagger + C_{-Q}). \quad (5.47)$$

The damping of the polarization field component  $p(Q)$  arising from the second term of (5.46) is calculated as

$$\frac{2\pi}{\hbar} \sum_q |\Xi(q)|^2 \{ [n_q \delta(E(Q) - E(Q-q) - \hbar\omega_q) + (1+n_q) \delta(E(Q) - E(Q-q) + \hbar\omega_q)] \langle C_{Q-q}^\dagger C_{Q-q} \rangle \\ - [n_q \delta(E(Q) - E(Q-q) + \hbar\omega_q) + (1+n_q) \delta(E(Q) - E(Q-q) - \hbar\omega_q)] \langle C_{Q-q} C_{Q-q}^\dagger \rangle \} p(Q), \quad (5.48)$$

where a decoupling approximation such as

$$\text{Tr} C_K^\dagger C_K C_Q \rho_S(t) \cong \langle C_Q \rangle \langle C_K^\dagger C_K \rangle, \quad (5.49)$$

is employed. When  $\langle C_k^\dagger C_k \rangle$  is regarded as the population of polaritons with wave vector  $k$ , the first term of (5.48) can be interpreted as the rate coming into the polariton

state with wave vector  $Q$ , whereas the second term can be interpreted as the rate leaving the same polariton state. If only the polariton state with wave vector  $Q$  is occupied in the initial state, only the second term of (5.48) does not vanish and gives exactly the same damping constant as in (4.3).

Now let us consider the relaxation term due to polariton-polariton scattering. In this case the relevant system is the ensemble of polaritons with a particular range of wave vectors contained in the incident beam; the reservoir corresponds to the other polaritons, which will be referred to as the reservoir polaritons. The suitable projection operator is given by

$$P\rho = |0'\rangle\langle 0'| \text{Tr}'\rho, \quad (5.50)$$

where  $|0'\rangle$  denotes the vacuum state with respect to the reservoir polaritons and the primed trace implies the trace operation over the reservoir polaritons. The polariton-polariton scattering Hamiltonian is given by (4.10). Then by a similar calculation as in (5.42), the relaxation operator in the Markovian approximation is derived:

$$\Gamma_c \rho = -\frac{2\pi}{\hbar} \sum_{k_1, k_2, k_3, k_4} \sum' \delta(E(k_1) + E(k_2) - E(k_3) - E(k_4)) |W(k_1, k_2; k_3, k_4)|^2 \{ [C_{k_1}^\dagger C_{k_2}^\dagger, C_{k_1} C_{k_2} \rho] + [\rho C_{k_1}^\dagger C_{k_2}^\dagger, C_{k_1} C_{k_2}] \}, \quad (5.51)$$

where the summation with respect to  $k_1$  and  $k_2$  is over the relevant polaritons, whereas the sum concerning  $k_3$  and  $k_4$  is over the reservoir polaritons and is indicated by a prime. The damping constant of the polarization field component  $p(Q)$  due to the relaxation operator  $\Gamma_c$  is calculated from (5.46) and (5.51) as

$$-\frac{2\pi}{\hbar} \sum_{k_1, k_3, k_4} \sum' |W(k_1, Q; k_3, k_4)|^2 N_{k_1} \times \delta(E(k_1) + E(Q) - E(k_3) - E(k_4)) \langle p(Q) \rangle, \quad (5.52)$$

where the decoupling approximation as in (5.49) is employed and  $N_k$  represents  $\langle C_k^\dagger C_k \rangle$ . This expression is exactly in agreement with (4.11) as it should be.

In summary, the basic equations of motion for the excitonic polariton are derived microscopically and given a firm basis. It is confirmed that the equations of motion familiar in laser theory are applicable also in the case of excitonic polaritons with the inclusion of spatial dispersion. At the same time, the damping of the polarization field that is identified with the dephasing relaxation of the excitonic polariton is derived by the standard statistical mechanical method using projection operators and it is confirmed that up to second-order perturbation the statistical mechanical method gives the same result as the golden-rule calculation.

## VI. SUMMARY AND DISCUSSION

The concept of the dephasing relaxation of the excitonic polariton has been clarified for the first time and the method of analysis of the experimental data of nondegenerate four-wave mixing has been established. The various mechanisms of the dephasing relaxation of the excitonic polariton are discussed and the most probable mechanism is identified as the polariton-polariton collision. The observed dephasing relaxation constant of the excitonic polariton in CuCl is of the order of 0.01 meV and increases as the energy approaches the exciton resonance.

The conceptual difference between the dephasing relaxation of the localized excitation and of the propagating elementary excitation has to be emphasized. In the former the dephasing relaxation or, in other words, the trans-

verse relaxation is related to the decay of the coherence of the relevant transition or of the off-diagonal component of the density matrix. In the latter case, however, the excitations are not localized but propagate throughout the crystal with a definite wave vector. Accordingly, the coherence of the relevant transition, which is usually related to the polarization field, has the degree of freedom of the wave vector. This degree of freedom is one of the salient features of the propagating elementary excitation which make a striking contrast with the case of the localized excitation. In addition to the wave vector the excitonic polariton has a degree of freedom of the exciton internal state, i.e., the electron-hole relative motion. The change of the exciton internal state may lead to the fluctuation and relaxation of the exciton coherence, since the oscillator strength of the exciton depends on the exciton internal state. The dephasing relaxation due to the change of the exciton internal state may be caused by a mutual collision among the excitonic polaritons under a rather high excitation. In this paper, however, the dephasing relaxation due to a change of wave vector has been discussed exclusively.

In the exciton resonance region, as mentioned in Sec. III, the correlation trace becomes insensitive to the dephasing relaxation constant  $\Gamma$  and the experimental value of  $\Gamma$  cannot be determined precisely. Let us make a few proposals to overcome this difficulty. The simplest one in principle is the use of a pulse with width comparable to the dephasing relaxation time. In the limit of infinitesimal pulse width, as shown in Sec. II, the correlation trace shows directly the decay due to the imaginary part of the wave vector. Thus, an improvement in the precision of measuring  $\Gamma$  can be expected by use of shorter pulses. A second proposal is to use a thinner sample. Let us consider a thin sample whose thickness is of the same order as the absorption length of the excitonic polariton, namely, the inverse of the imaginary part of the wave vector. In this case the simple expression (3.13) cannot be used and one has to calculate the full expression (3.4). The correlation trace can be expected to be sensitive to the value of  $\Gamma$ . In fact, for a 1- $\mu\text{m}$ -thick sample of CuCl one obtains correlation traces sensitive to the value of  $\Gamma$ , as shown in Fig. 9. Thus, the value of  $\Gamma$  can be fixed from curve fitting if the value lies within the range shown in the figure.

Finally let us point out a few interesting proposals for future study. The first one is the use of two-photon excitation of the upper-branch polariton. This excitation scheme was first devised by Fröhlich *et al.*<sup>31,32</sup> to measure the polariton dispersion in CuCl. By two-photon excitation an upper-branch polariton can be created almost uniformly in a sample because the fundamental photon energy lies in the transparent region of the crystal. Furthermore, this excitation scheme can create an upper-branch polariton selectively without excitation of the lower-branch polariton owing to wave-vector conservation. Thus, the troublesome additional boundary conditions (ABC) problem<sup>33</sup> can be avoided and the dephasing relaxation constant of the upper-branch polariton can be measured precisely, although the tunable energy range may be rather limited. A second proposal is the use of reflection-type four-wave mixing. As is well known, the pseudogap region is highly absorptive and shows a high

reflectivity. Thus, it is desirable to measure the four-wave mixing signal in reflection geometry rather than in transmission geometry. In fact, four-wave mixing in reflection geometry is successfully observed in CuCl (Ref. 34) using nanosecond laser pulses. Since the excitonic polariton in the pseudogap region has a very short penetration depth in the crystal, one can probe the relaxation of the excitonic polariton in the vicinity of the crystal surface by means of reflection-type four-wave mixing.

#### ACKNOWLEDGMENTS

The author would like to thank Professor S. Shionoya and Dr. Y. Masumoto for close collaboration and enlightening discussions. Thanks are also due to Professor T. Yajima, Professor Y. Toyozawa, Professor E. Hanamura, Professor M. Matsuoka, and Professor N. Nagasawa for enlightening discussions and critical comments.

- <sup>1</sup>Y. Masumoto, S. Shionoya, and T. Takagahara, *Phys. Rev. Lett.* **51**, 923 (1983).
- <sup>2</sup>T. Yajima and H. Souma, *Phys. Rev. A* **17**, 309 (1978).
- <sup>3</sup>T. Yajima, H. Souma, and Y. Ishida, *Phys. Rev. A* **17**, 324 (1978).
- <sup>4</sup>A. Laubereau and W. Kaiser, *Rev. Mod. Phys.* **50**, 607 (1978).
- <sup>5</sup>W. H. Hesselink and D. A. Wiersma, *Phys. Rev. Lett.* **43**, 1991 (1979).
- <sup>6</sup>I. D. Abella, N. A. Kurnit, and S. R. Hartmann, *Phys. Rev.* **141**, 391 (1966).
- <sup>7</sup>N. Bloembergen, *Nonlinear Optics* (Benjamin, New York, 1965).
- <sup>8</sup>K. Shimoda, T. Yajima, Y. Ueda, T. Shimizu, and T. Kasuya, *Quantum Electronics* (Shokabo, Tokyo, 1970) (in Japanese).
- <sup>9</sup>J. J. Hopfield and D. G. Thomas, *Phys. Rev.* **132**, 563 (1963).
- <sup>10</sup>T. Mita, K. Sotome, and M. Ueta, *Solid State Commun.* **33**, 1135 (1980).
- <sup>11</sup>T. Mita, K. Sotome, and M. Ueta, *J. Phys. Soc. Jpn.* **48**, 496 (1980).
- <sup>12</sup>Y. Segawa, Y. Aoyagi, K. Azuma, and S. Namba, *Solid State Commun.* **28**, 853 (1978).
- <sup>13</sup>Y. Masumoto, Y. Unuma, Y. Tanaka, and S. Shionoya, *J. Phys. Soc. Jpn.* **47**, 1844 (1979).
- <sup>14</sup>N. Bloembergen and P. S. Pershan, *Phys. Rev.* **128**, 606 (1962).
- <sup>15</sup>T. Mita and N. Nagasawa, *Solid State Commun.* **44**, 1003 (1982).
- <sup>16</sup>T. Itoh and T. Suzuki, *J. Phys. Soc. Jpn.* **45**, 1939 (1978).
- <sup>17</sup>R. Levy, B. Hönerlage, and J. B. Grun, *Solid State Commun.* **29**, 103 (1979).
- <sup>18</sup>Y. Segawa, Y. Aoyagi, and S. Namba, *Solid State Commun.* **39**, 535 (1981).
- <sup>19</sup>Y. Masumoto and S. Shionoya, *J. Phys. Soc. Jpn.* **51**, 181 (1982).
- <sup>20</sup>E. Hanamura, in *Excitons at High Density*, edited by H. Haken and S. Nikitine (Springer, Berlin, 1975), p. 43.
- <sup>21</sup>Y. Toyozawa, *Prog. Theor. Phys.* **20**, 53 (1958).
- <sup>22</sup>R. C. Hanson, K. Helliwell, and C. Schwab, *Phys. Rev. B* **9**, 2649 (1974).
- <sup>23</sup>T. H. K. Barron, J. A. Birch, and G. K. White, *J. Phys. C* **10**, 1617 (1977).
- <sup>24</sup>J. B. Anthony, A. D. Brothers, and D. W. Lynch, *Phys. Rev. B* **5**, 3189 (1972).
- <sup>25</sup>M. Kalm and Ch. Uihlein, *Phys. Status Solidi B* **87**, 575 (1978).
- <sup>26</sup>T. Takagahara and J. L. Birman, *Phys. Rev. B* **28**, 6161 (1983).
- <sup>27</sup>T. Takagahara, in *Semiconductors Probed by Ultrafast Laser Spectroscopy*, edited by R. R. Alfano (Academic, New York, 1984), p. 331.
- <sup>28</sup>S. Nakajima, *Prog. Theor. Phys.* **20**, 948 (1958).
- <sup>29</sup>R. Zwanzig, *Phys. Rev.* **124**, 983 (1961).
- <sup>30</sup>T. Takagahara, E. Hanamura, and R. Kubo, *J. Phys. Soc. Jpn.* **44**, 728 (1978).
- <sup>31</sup>D. Fröhlich, E. Mohler, and P. Wiesner, *Phys. Rev. Lett.* **26**, 554 (1971).
- <sup>32</sup>D. Fröhlich, E. Mohler, and Ch. Uihlein, *Phys. Status Solidi B* **55**, 175 (1973).
- <sup>33</sup>J. L. Birman, in *Excitons*, edited by E. I. Rashba and M. D. Sturge (North-Holland, Amsterdam, 1982), Chap. 2.
- <sup>34</sup>G. Mizutani and N. Nagasawa, *Opt. Commun.* **50**, 31 (1984).

## Picosecond energy-relaxation processes of excitons in CdSe

Yasuaki Masumoto and Shigeo Shionoya  
*The Institute for Solid State Physics, The University of Tokyo,  
 Roppongi 7-22-1, Minato-ku, Tokyo 106, Japan*

(Received 23 January 1984; revised manuscript received 4 May 1984)

Energy- and time-resolved luminescence of the one longitudinal optical-phonon Stokes sideband of the *A* exciton in CdSe has been studied in the picosecond time domain under the weak band-to-band excitation. Dynamic energy relaxation of excitons is directly visualized in the energy-time coordinates. The observed energy-relaxation rate of excitons is explained by a model taking into account three types of exciton-phonon interactions, that is, the deformation-potential-type, the piezoelectric-type, and the Fröhlich-type interaction. This result clearly demonstrates the applicability of the method used in this work to the analysis of the energy relaxation of excitons.

Recent advances of picosecond spectroscopy have enabled us to observe directly dynamic energy-relaxation processes of excitons.<sup>1-4</sup> In semiconductors the energy relaxation of excitons is considered to occur via three types of exciton-phonon interactions. They are the deformation-potential-type, the piezoelectric-type, and the Fröhlich-type interactions. However, so far there have been scarcely any experimental studies to reveal the role of these interactions in the energy relaxation of excitons.

In the present work the energy- and time-resolved luminescence of the one longitudinal optical-phonon (LO) Stokes sideband of the *A* exciton (*A*-LO) in CdSe is examined with picosecond time resolution under the rather weak band-to-band excitation. Because of the polariton effect, the luminescence line shape of the *A*-exciton zero-phonon band is related to the energy distribution function of excitons in a rather complicated manner. On the other hand, the line shape of the *A*-LO band directly reflects this distribution function.<sup>5</sup> Therefore, the analysis of the *A*-LO band is more favorable than that of the zero-phonon band to derive the distribution function. The group velocity of the excitonic polaritons in the *A*-LO band region is so fast ( $\frac{1}{3}$  of the light velocity in vacuum) that the time-resolved *A*-LO luminescence quickly follows the time evolution of the energy distribution of excitons. From the time evolution of the distribution thus observed, we clarify the role of the exciton-phonon interactions in the energy relaxation of excitons.

A platelet-type CdSe crystal was grown by the vapor-transport method. The crystal, having the *c* axis lying in its face, was directly immersed in liquid helium. Light pulses given by a Rhodamine-6G dye laser synchronously pumped by a mode-locked argon laser were used as the excitation source. Laser light with a pulse width of 1-2 ps and the output of 300 pJ/pulse was focused on the face of the CdSe crystal with the spot diameter of 200  $\mu$ m. The lasing photon energy, 2.072 eV, with the spectral width of 2 meV corresponds to the band-to-band excitation of CdSe.

The spectrally resolved temporal response of the luminescence was analyzed by using a system consisting of a 25-cm monochromator, a synchroscan streak camera (HTV-C1587), a silicon intensifier target (SIT) camera, and a computer. The spectral resolution was 1.4 meV. The time resolution of the combined system of the laser, the monochromator, and the streak camera was 70 ps, which is deter-

mined by the jitter and the finite slit width of the streak camera and the spread of the light path in the monochromator. Another 50-cm monochromator and an intensified SIT camera were used to obtain the time-integrated luminescence spectra with the spectral resolution of 0.2 meV.

In Fig. 1, time-integrated luminescence spectra of the *A*-exciton band and the *A*-LO sideband are shown. Under the

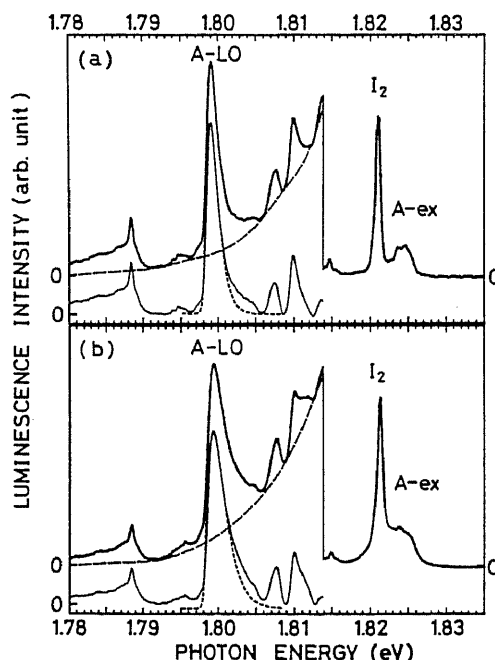


FIG. 1. Time-integrated luminescence of the *A*-exciton and *A*-LO bands of CdSe (a bold line) at 4.2 K under the irradiation of (a) the cw He-Ne laser (1.959 eV, 1 mW) and (b) the pulsed dye laser (2.072 eV, 1-2 ps, 300 pJ). The spectral resolution is 0.2 meV. Dashed lines show smooth backgrounds assumed and fine lines show the luminescence structures obtained by subtracting the backgrounds from the luminescence spectra. Theoretical fits on the basis of Eq. (2) are shown by dotted lines, assuming  $T_e = 9$  K for (a) and 14 K for (b).

excitation of the 1–2-ps (300-pJ) light pulses, the *A*-exciton and *A*-LO luminescence bands [Fig. 1(b)] are broadened compared with those under the excitation of 1-mW He-Ne cw laser light [Fig. 1(a)]. The line shapes of the *A*-LO and *A*-2LO bands have been considered to be expressed by

$$(\bar{E} - E_t + E_{LO})^{3/2} \exp[-(\bar{E} - E_t + E_{LO})/k_B T_e]$$

and

$$(\bar{E} - E_t + 2E_{LO})^{1/2} \exp[-(\bar{E} - E_t + 2E_{LO})/k_B T_e]$$

respectively.<sup>5,6</sup> Here,  $\bar{E}$  is the luminescence photon energy,  $E_t$  (=1.8242 eV)<sup>7</sup> the transverse *A*-exciton energy,  $E_{LO}$  (=26.3 meV)<sup>7</sup> the LO-phonon energy, and  $T_e$  the effective time-averaged temperature of the exciton ensemble. The line shape of the *A*-2LO band directly reflects the Maxwell-Boltzmann distribution of excitons. On the other hand, the line shape of the *A*-LO band reflects on both the energy distribution and the  $q$  dependence of the matrix element of the Fröhlich-type 1s exciton-LO-phonon interaction,<sup>8</sup>

$$V_F(q) = (1/q) [(2\pi E_{LO} e^2 / V) (\epsilon_{\infty} - 1 / \epsilon_0)]^{1/2} (q_e - q_h), \quad (1)$$

where

$$q_e (q_h) = \{1 + [(qa_B/2)m_{h(e)} / (m_e + m_h)]^2\}^{-2}.$$

$q$  is the wave vector of phonons,  $V$  the volume of the crystal,  $e$  the charge of an electron,  $\epsilon_{\infty(0)}$  the optical (static) dielectric constant,  $m_{h(e)}$  the mass of an electron (hole), and  $a_B$  is the Bohr radius of the 1s exciton. The extra factor  $(\bar{E} - E_t - E_{LO})$  in the line shape of the *A*-LO band arises from the asymptotic form ( $q \rightarrow 0$ ) of the matrix element, noting that

$$(1/q)(q_e - q_h) = (qa_B^2/2)(m_e - m_h)/(m_e + m_h)$$

when  $q < 1/a_B$ . This usual line-shape analysis includes a flaw, because the  $T_e$  obtained for the *A*-LO band was found to be slightly lower than that for the *A*-2LO band. This discrepancy is considered to arise because the condition  $q < 1/a_B$  does not hold at the high-energy side of the *A*-LO band.

For the refined line-shape analysis, we take the following procedure. In the procedure the polariton effect as well as the accurate  $q$  dependence of the Fröhlich-type interaction are taken into consideration. Excitons are assumed to be populated on the following polariton dispersion obeying the Boltzmann distribution  $\exp(-E/k_B T_e)$ .

$$(\hbar ck/E)^2 = \epsilon(k, E) = \epsilon_b [E_t(k)^2 - E^2] / [E_l(k)^2 - E^2],$$

where  $E_l(k) = E_t + \hbar^2 k^2 / 2M$  and  $E_t(k) = E_t + \hbar^2 k^2 / 2M$ . Here,  $E$  and  $k$  are the energy and the wave vector of an excitonic polariton,  $E_t = 1.8242$  eV,  $E_l = E_t + 0.50$  meV (Ref. 7),  $\epsilon_b = 8.4$  (Ref. 9), and  $M = m_e + m_h = 0.58m_0$  (electron mass).<sup>9</sup> From this dispersion relation, the density of states  $D(E)$  is obtained to be  $k^2 / (\pi^2 |dE/dk|)$ . Therefore, the luminescence line shape of the *A*-LO band is proportional to the product of  $D(E)$ ,  $\exp(-E/k_B T_e)$  and  $|V_F(q)|^2$  as follows:

$$I(\bar{E} = E - E_{LO}) \propto \exp(-E/k_B T_e) D(E) (1/k)^2 \times \{1/[1 + (\alpha_e k)^2] - 1/[1 + (\alpha_h k)^2]\}^2, \quad (2)$$

where

$$\alpha_{e(h)} = (a_B/2)m_{h(e)} / (m_e + m_h)$$

and  $q$  is replaced by  $k$  because  $q \cong k$ . The values of  $m_e$ ,  $m_h$ , and  $a_B$  are  $0.13m_0$ ,  $0.45m_0$ , and  $53.6 \text{ \AA}$ , respectively.<sup>10</sup> The line shapes fitted on the basis of Eq. (2) are shown in Fig. 1 by dotted lines, assuming  $T_e = 9$  K for (a) and 14 K for (b). The fitting is satisfactory. Using the same values of  $T_e$ , the line shapes of the *A*-2LO band were found to be also well explained by

$$I(\bar{E} = E - 2E_{LO}) \propto \exp(-E/k_B T_e) D(E).$$

Therefore, the line-shape analysis on the basis of Eq. (2) is precise enough.

Energy- and time-resolved luminescence are shown in Figs. 2 and 3. These figures are constructed from the spectrally resolved temporal response of luminescence. It can be seen from the figures that the rise of the luminescence is determined by the time resolution of the instrument at the high-energy extremity (1.806 eV). On the other hand, it takes more than 300 ps for the luminescence intensity to reach its maximum below 1.799 eV. Excitons relax toward lower-energy states losing their energy.

The luminescence intensity of the *A*-LO band is related to the energy- and time-dependent distribution function  $f(E, t)$  by the following equation:

$$I(\bar{E} = E - E_{LO}, t) \propto f(E, t) D(E) (1/k)^2 \times \{1/[1 + (\alpha_e k)^2] - 1/[1 + (\alpha_h k)^2]\}^2. \quad (3)$$

Using Eq. (3) and  $I(\bar{E}, t)$  which is directly displayed in Fig. 2, we can deduce  $f(E, t)$ . The obtained  $f(E, t)$  was found to be approximately described by a Boltzmann distribution. The average energy and the total number of excitons  $\langle E_e \rangle$  and  $N_e$  are calculated by

$$\langle E_e \rangle = \left( \sum_{i=1}^8 E_i f(E_i, t) D(E_i) \right) / \left( \sum_{i=1}^8 f(E_i, t) D(E_i) \right),$$

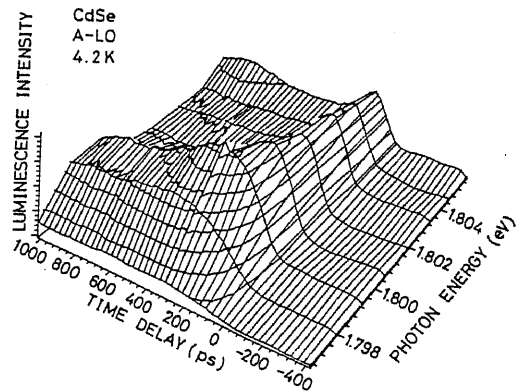


FIG. 2. Three-dimensional view of energy- and time-resolved luminescence intensity of the *A*-LO band in CdSe at 4.2 K.

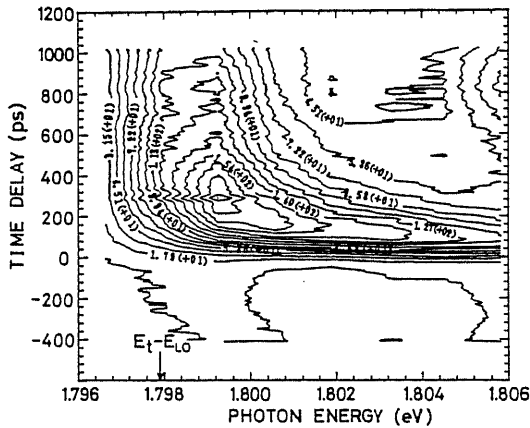


FIG. 3. Contour map of Fig. 2. Quantities in parentheses represent powers of ten by which the associated numbers are to be multiplied.

and

$$N_e = \sum_{i=1}^8 f(E_i, t) D(E_i).$$

Here,  $E_i$ 's ( $i=1-8$ ) minus  $E_{LO}$  are the photon energies where the temporal response of luminescence intensity is observed. The calculated  $\langle E_e \rangle$  and  $N_e$  are shown in Fig. 4. The result indicates that excitons lose their energy at the time constant  $\sim 150$  ps, which is much faster than their lifetime of 2.8 ns.

The kinetic energy loss rate of excitons can be calculated for three individual scattering processes: (i) the deformation-potential-type interaction with LA phonons; (ii) the piezoelectric-type interaction with LA or TA pho-

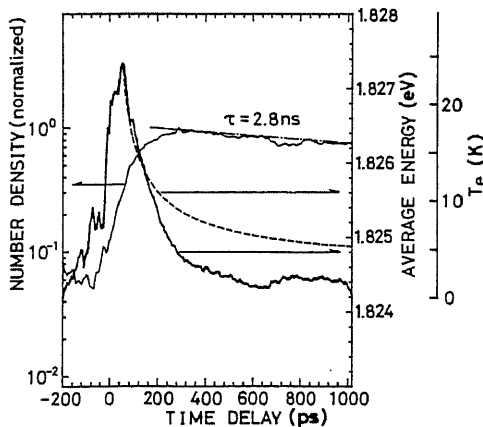


FIG. 4. Temporal change of the number density (a fine line) and the average energy (a bold line) of the A-exciton ensemble in CdSe at 4.2 K. The theoretical calculation on the basis of the model described in the text is shown by a dashed line.

sons; and (iii) the Fröhlich-type interaction with LO phonons. The matrix element of (iii) is given by Eq. (1), and those of (i) and (ii) are described by<sup>8,11</sup>

$$V_{dp}(q) = (\hbar/2\rho u_L)^{1/2} q^{1/2} (D_c q_e - D_v q_h),$$

and

$$V_{pe}(q) = (\hbar/2\rho u_{L(T)})^{1/2} \times [4\pi e \langle e_j^2 \rangle_{L(T)}^2 / (\epsilon_0 q^{1/2})] (q_e - q_h). \quad (4)$$

Here,  $D_{c(v)}$  is the deformation potential of the conduction (valence) band,  $\rho$  the density,  $\langle e_j^2 \rangle_{L(T)}$  the spherical average of the squares of the piezoelectric constant for the LA (TA) phonons, and  $u_{L(T)}$  the sound velocity of the LA (TA) phonons. Because the  $q$  dependence of  $V_{dp}(q)$ ,  $V_{pe}(q)$ , and  $V_F(q)$  are different from one another, the dominant energy-loss mechanism is alternated depending on the wave vector of excitons.

It is very difficult to derive the energy-loss rates of the excitons populated on the polariton dispersion using the exact forms of  $V_{dp}(q)$ ,  $V_{pe}(q)$ , and  $V_F(q)$ . The derivation can be performed only numerically. On the other hand, we can derive the analytical expression for the energy-loss rates of the excitons populated on the parabolic dispersion, taking the asymptotic forms of the matrix elements. As mentioned above, we have precisely treated the experimental results to derive the time-resolved average energy of excitons. In the following theoretical analysis, however, we take the parabolic exciton dispersion for simplicity and for good insight. We derive the energy-loss rates of the exciton ensemble obeying the Maxwell-Boltzmann distribution. They are given by the following equations for  $k < a_B^{-1} = 2$

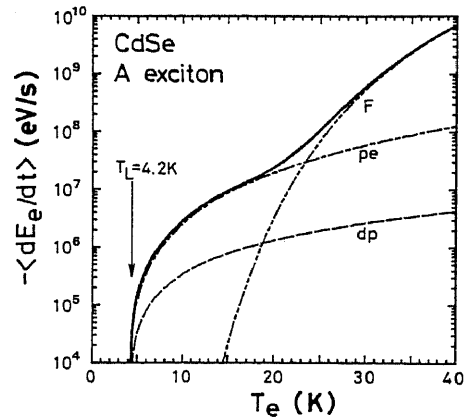


FIG. 5. Calculated energy-loss rates of excitons obeying the Maxwell-Boltzmann distribution with the exciton temperature  $T_e$ . Three individual energy-loss rates due to the deformation-potential-type, the piezoelectric-type, and the Fröhlich-type interactions are shown by a dashed line (dp), a dash-dotted line (pe), and a dash-double-dotted line (F), respectively. A bold solid line shows the total energy-loss rate which is a sum of the three individual loss rates.

$\times 10^6 \text{ cm}^{-1}$ .

$$\left\langle \frac{dE_e}{dt} \right\rangle_{dp} = - \frac{2^{7/2} D^2 M^{5/2}}{\pi^{3/2} \hbar^4 \rho} (k_B T_e)^{3/2} \left( \frac{T_e - T_L}{T_e} \right), \quad (5)$$

$$\left\langle \frac{dE_e}{dt} \right\rangle_{pe} = - \frac{512 (2\pi)^{1/2} e^2 \langle e_{ij}^2 \rangle M^{7/2}}{\hbar^6 \epsilon_0^2 \rho} \times \left( \frac{m_e - m_h}{m_e + m_h} \right)^2 a_{\beta}^2 (k_B T_e)^{5/2} \left( \frac{T_e - T_L}{T_e} \right), \quad (6)$$

and

$$\left\langle \frac{dE_e}{dt} \right\rangle_F = - \frac{2^{1/2} e^2 M^{5/2} E_{LO}^{7/2}}{\hbar^6} \left( \frac{1}{\epsilon_{\infty}} - \frac{1}{\epsilon_0} \right) \left( \frac{m_e - m_h}{m_e + m_h} \right)^2 \times a_{\beta}^2 \left[ \exp \left( - \frac{E_{LO}}{k_B T_e} \right) - \exp \left( - \frac{E_{LO}}{k_B T_L} \right) \right], \quad (7)$$

where  $D = |D_c - D_v| = 2 \text{ eV}$  is the deformation potential of the  $A$  exciton,<sup>9,12</sup>  $T_L = 4.2 \text{ K}$  the lattice temperature, and  $\langle e_{ij}^2 \rangle = \langle e_{ij}^2 \rangle_L + \langle e_{ij}^2 \rangle_T$ . These equations can be derived following the same procedures as are described by Conwell,<sup>13</sup> taking the asymptotic form ( $q \rightarrow 0$ ) of the matrix elements of Eqs. (1) and (4). The numerical values of the parameters are  $\rho = 5.81 \text{ g/cm}^3$ ,  $\langle e_{ij}^2 \rangle_{L(T)} = 0.0144 \text{ C}^2/\text{m}^4$  (LA),

$0.0189 \text{ C}^2/\text{m}^4$  (TA),<sup>14,15</sup>  $\epsilon_0 = 9.70$ ,<sup>15</sup> and  $\epsilon_{\infty} = 7.02$ .<sup>16</sup> The calculated energy-loss rates by using Eqs. (5)–(7) are shown in Fig. 5.

The overall energy-loss rate  $\langle dE_e/dt \rangle$  is given by the sum of  $\langle dE_e/dt \rangle_{dp}$ ,  $\langle dE_e/dt \rangle_{pe}$ , and  $\langle dE_e/dt \rangle_F$ . Thus, the temporal trajectory of the  $\langle dE_e/dt \rangle$  follows the curve of the overall energy-loss rate. Along this trajectory, the temporal change of  $\langle E_e \rangle$  can be calculated with the initial temperature  $T_e = 24.2 \text{ K}$ , noting that  $\langle E_e \rangle = E_i + (3/2)k_B T_e$ . The calculated result is shown by the dashed line in Fig. 4. The agreement with experiment is good except at the low-energy region. The piezoelectric-type exciton-phonon interaction plays the predominant role in the energy relaxation of excitons. Furthermore, it should be noted from Fig. 4 that the experimental average energy is lowered below  $E_i + (3/2)k_B T_L$  after 300 ps. This fact is not so surprising because excitons can be populated on the polariton dispersion even below  $E_i$ . Thus, it comes from the polariton effect. The numerical analysis taking account of the exact forms of  $V_{dp}(q)$ ,  $V_{pe}(q)$ , and  $V_F(q)$  as well as the polariton effect may give the full explanation of the experimental results. However, our essential conclusion concerning the energy-loss rates of excitons should still be valid. Instead, we should note that the simple calculation procedure mentioned above is useful to analyze the energy relaxation of excitons.

<sup>1</sup>P. Wiesner and U. Heim, Phys. Rev. B 11, 3071 (1975).

<sup>2</sup>Y. Masumoto and S. Shionoya, J. Phys. Soc. Jpn. 51, 181 (1982).

<sup>3</sup>T. Kushida, S. Kinoshita, F. Ueno, and T. Ohtsuki, J. Phys. Soc. Jpn. 52, 1838 (1983).

<sup>4</sup>F. Askary and P. Y. Yu, Phys. Rev. B 28, 6165 (1983).

<sup>5</sup>E. Gross, S. Permogorov, and B. Razbirin, J. Phys. Chem. Solids 27, 1647 (1966).

<sup>6</sup>V. A. Abramov, S. A. Permogorov, B. S. Razbirin, and A. I. Eki-mov, Phys. Status Solidi 42, 627 (1970).

<sup>7</sup>C. Hermann and P. Y. Yu, Phys. Rev. B 21, 3675 (1980).

<sup>8</sup>Y. Toyozawa, Progr. Theor. Phys. 20, 53 (1958).

<sup>9</sup>F. Askary and P. Y. Yu, Solid State Commun. 47, 241 (1983).

<sup>10</sup>B. Segall and D. T. F. Marple, in *Physics and Chemistry of II-VI Compounds*, edited by M. Aven and J. S. Prener (North-Holland,

Amsterdam, 1967), Chap. 3.

<sup>11</sup>C. Weisbuch and R. G. Ulbrich, in *Light Scattering in Solids III*, edited by M. Cardona and G. Gütherodt (Springer, Berlin, 1982), p. 207.

<sup>12</sup>D. W. Langer, R. N. Euwema, K. Era, and T. Koda, Phys. Rev. B 2, 4005 (1970).

<sup>13</sup>E. M. Conwell, in *Solid State Physics*, edited by F. Seitz, D. Turnbull, and H. Ehrenreich (Academic, New York, 1967), Suppl. 9, Chap. 3.

<sup>14</sup>A. R. Hutson, J. Appl. Phys. 32, 2287 (1961).

<sup>15</sup>D. Berlincourt, H. Jaffe, and L. R. Shiozawa, Phys. Rev. 129, 1009 (1963).

<sup>16</sup>R. E. Halsted, M. R. Lorenz, and B. Segall, J. Phys. Chem. Solids 22, 109 (1961).

## Picosecond time-resolved study of excitons in GaAs-AlAs multi-quantum-well structures

Yasuaki Masumoto and Shigeo Shionoya

*The Institute for Solid State Physics, The University of Tokyo, Roppongi 7-22-1, Minato-ku, Tokyo 106, Japan*

Hitoshi Kawaguchi

*Musashino Electrical Communication Laboratory, Nippon Telegraph and Telephone Public Corporation (NTT), Midori-machi 3-9-11, Musashino-shi, Tokyo 180, Japan*

(Received 1 December 1983)

Energy- and time-resolved measurements of luminescence of  $1s$  excitons ( $n=1, e-hh$ ) in GaAs-AlAs multi-quantum-well structures have been carried out for the first time in the picosecond time domain. Dynamical population changes of excitons are directly visualized in the energy-time coordinates. Results indicate that excitons lose their energy in the exciton band at a rate of  $1.0 \times 10^6$  eV/s. This rate is much slower than the calculated kinetic-energy-loss rate and is ascribed to the random nature of the well.

Excitons in multi-quantum-well (MQW) structures have prominent two-dimensional characters because of the quantum size effect.<sup>1</sup> Wave functions and binding energies of excitons in MQW are quite different from those of excitons in bulk crystals as a result of this effect.<sup>2-4</sup> In addition to the two-dimensional characters, excitons in MQW have an inhomogeneous character which is inevitably given in the process of the sample preparation.<sup>5,6</sup> The well thickness is considered to be fluctuated by an order of one atomic layer. This yields the fluctuation of the resonance energy of excitons. Thus excitons in MQW are considered as a typical example of the two-dimensional excitons in the random potential.

Energetical relaxation processes of excitons in the two-dimensional random well are expected to be quite different from those of excitons in three-dimensional regular crystals. However, to our knowledge, there exist no experimental as well as theoretical studies dealing with energetical relaxation processes of excitons in the two-dimensional random well. In this work, the energy- and time-resolved luminescence of weakly excited excitons in MQW has been studied for the first time. Energetical relaxation processes of excitons in MQW are discussed on the basis of the experimental results and of a simple calculation which takes account of the two-dimensional character of excitons.

The sample used in this experiment was grown by molecular beam epitaxy (MBE) on a GaAs (100) substrate. It consists of alternate 76-Å GaAs well layers and 33-Å AlAs barrier layers of the total thickness 2.98  $\mu\text{m}$ . A window was etched in the GaAs substrate for the optical absorption measurement.

A rhodamine 6-G dye laser synchronously pumped by a mode-locked argon laser was used, which gives 1-2-ps light pulses of 300 pJ. The pulse duration was continually monitored by using a rapid-scan autocorrelator.<sup>7</sup> The lasing photon energy was 2.063 eV with a spectral width of 3 meV. The laser beam was focused on a GaAs-AlAs MQW sample immersed in liquid helium with a spot size of 200  $\mu\text{m}$ . The spectrally resolved temporal response of the luminescence was analyzed by using a combined system of a 25-cm monochromator, a synchroscan streak camera (HTV-C1587), an SIT (silicon intensifier target) camera, and a computer. The

streak camera was synchronously operated with the mode-locked argon laser. The averaging at a high repetition rate (82 MHz) enabled us to observe directly the spectrally resolved [full width at half maximum (FWHM) = 1.1 meV] temporal response of the exciton luminescence from GaAs-AlAs MQW excited by only 300-pJ light pulses. Time resolution of the streak camera was found to be 30 ps. However, the time resolution of the combined system of the monochromator and the streak camera was lowered to 70 ps, because of the spread of the light path in the monochromator.

In Fig. 1, spectra of the absorption and time-integrated luminescence are shown. The absorption peak observed at 1.6225 eV with 7.5-meV width (FWHM) is ascribed to the  $1s$  exciton ( $n=1, e-hh$ ) composed of an electron and a heavy hole belonging to the lowest state ( $n=1$ ) in the quantum well. The observed spectral width is attributed to

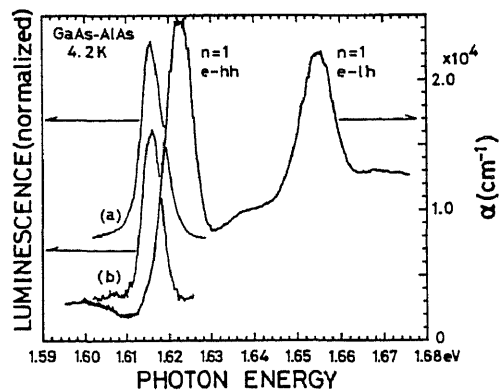


FIG. 1. Absorption coefficient and time-integrated luminescence spectra of GaAs-AlAs MQW (76-Å GaAs well, 33-Å AlAs barrier, 2.98  $\mu\text{m}$ ) at 4.2 K. The spectral resolution is 0.3 meV. Luminescence spectra were obtained under (a) pulsed dye laser (2.063 eV, 1-2 ps, 300 pJ) and (b) cw He-Ne laser (1.959 eV, 0.01 mW) excitation.

the fluctuation of the well thickness from the following discussion.<sup>5</sup> The energy of the  $1s$  exciton in the well measured from the bottom of the well (the band-gap energy of bulk GaAs) is  $E_{n-1}(1s) = 1.6225 \text{ eV} - E_g = 103.3 \text{ meV}$ , where  $E_g = 1.5192 \text{ eV}$  is the band-gap energy of GaAs.<sup>8</sup> Assuming the fluctuation of the well width to be the half of the lattice constant  $a$  of GaAs and noting that  $E_{n-1}(1s)$  is approximately proportional to the inverse square of the well thickness  $L_z$ ,<sup>2,3</sup> one can calculate the fluctuation of  $E_{n-1}(1s)$  in MQW as

$$\begin{aligned} \delta E_{n-1}(1s) &\cong 2E_{n-1}(1s)(\delta L_z/L_z) \\ &= 2E_{n-1}(1s)(a/2L_z) = 7.7 \text{ meV} . \end{aligned} \quad (1)$$

Here  $\delta E_{n-1}(1s)$  is the fluctuation of  $E_{n-1}(1s)$ ,  $L_z = 76 \text{ \AA}$  is the well thickness,  $\delta L_z$  is the fluctuation of  $L_z$ , and  $a = 5.64 \text{ \AA}$ .<sup>9</sup> Because this estimated value of  $7.7 \text{ meV}$  almost coincides with the measured value of  $7.5 \text{ meV}$ , it is concluded that the width of absorption arises from the fluctuation of the well width which is  $\sim a/2$ .<sup>10</sup>

A time-integrated luminescence band under the 1–2-ps pulse excitation is observed at the lower-energy side of the absorption band as shown in Fig. 1. Peaks of the luminescence and absorption spectra are separated by  $6.5 \text{ meV}$ . This fact indicates that photogenerated excitons are populated at the low-energy states in the exciton band, because the luminescence spectra reflect the energetical distribution of excitons. The excitation photon energy ( $= 2.063 \text{ eV}$ ) in the present case is above the band-gap energy of GaAs and below the indirect ( $= 2.229 \text{ eV}$ ;  $X$ ) as well as direct ( $= 3.13 \text{ eV}$ ;  $\Gamma$ ) excitonic band-gap energy of AlAs.<sup>11</sup> Therefore, only the GaAs well layers are photoexcited. The number of photoexcited layers is less than 20, because the absorption coefficient for  $2.063 \text{ eV}$  is above the detection limit ( $5 \times 10^4 \text{ cm}^{-1}$ ). The luminescence band changes little, even when the excitation level is reduced to  $0.01 \text{ mW}$  (CW) He-Ne laser excitation. Therefore, it is sure that the luminescence band observed under the 1–2-ps (300 pJ) pulse excitation arises from  $1s$  excitons. Any other luminescence bands, such as those due to  $2s$  excitons and  $1s$  excitons ( $n=1, e-hh$ ) in MQW, the AlAs barrier layers, and the GaAs substrate, were not observed.

The energy- and time-resolved results of luminescence are shown in Figs. 2 and 3. These figures are constructed from the spectrally resolved temporal response of luminescence. As is seen from the figures, the observed rise of the population of excitons is determined by the time resolution of the instrument at the high-energy extremity ( $1.6228 \text{ eV}$ ). On the other hand, it takes about  $400 \text{ ps}$  for the population of excitons lower than  $1.616 \text{ eV}$  to reach its maximum. Because the reflectivity in the relevant energy range was found not to change very much ( $\Delta R/R < 0.2$ ), the change of the refractive index also should be small. Thus the energy and time responses of luminescence can be regarded as directly reflecting the dynamics of the exciton population, because the energy dependence of the emission probability of excitons can be neglected. The temporal change of population is clearly observed in Fig. 3. Excitons drift toward lower-energy states losing their energy. The spectrally integrated luminescence does not show a single exponential decay. However, a characteristic time to decay to the  $1/e$  value of the maximum is about  $480 \text{ ps}$ . This decay characteristic does not depend on the excitation intensity down to 10%.

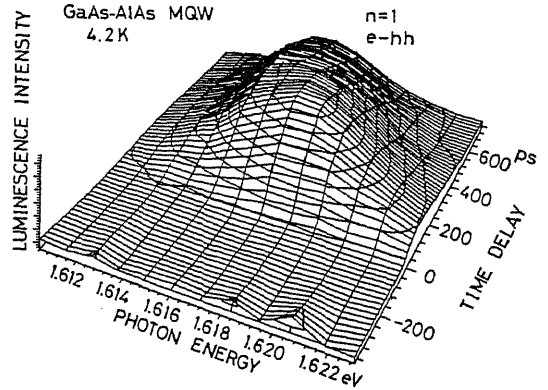


FIG. 2. A bird's-eye view of energy- and time-resolved luminescence intensity of the excitons ( $n=1, e-hh$ ) in GaAs-AlAs MQW at  $4.2 \text{ K}$ .

Therefore, we need not take account of the effect of the bimolecular recombination.

To discuss the energetical relaxation of excitons, the average energy  $\langle E(t) \rangle$  of the ensemble of excitons is defined as follows:

$$\langle E(t) \rangle = \frac{\left| \sum_{i=1}^{12} E_i f(E_i, t) \right|}{\left| \sum_{i=1}^{12} f(E_i, t) \right|} , \quad (2)$$

where  $f(E_i, t)$  is the spectrally resolved temporal response of the luminescence shown in Fig. 2, and  $E_i$ 's ( $i=1-12$ ) correspond to the observed photon energies. The temporal change of  $\langle E(t) \rangle$  is shown in Fig. 4. The result clearly shows that the average energy of excitons decreases at a constant rate of  $1.0 \times 10^6 \text{ eV/s}$ .

The kinetic energy decreasing rate of two-dimensional excitons via the deformation-potential-type interaction with LA phonons is calculated by the following equation, which is a direct extension of the expression describing the energy decreasing rate of two-dimensional hot electrons,<sup>12-14</sup>

$$\langle dE(t)/dt \rangle_{dp} = -(2M^2 D^2 / \hbar^3 \rho) [k_B T_e(t) - k_B T_L] , \quad (3)$$

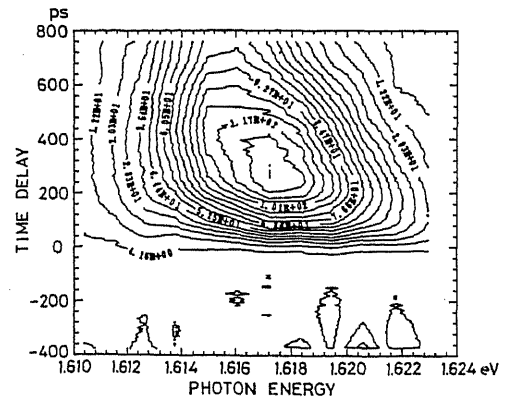


FIG. 3. A contour map of Fig. 2.

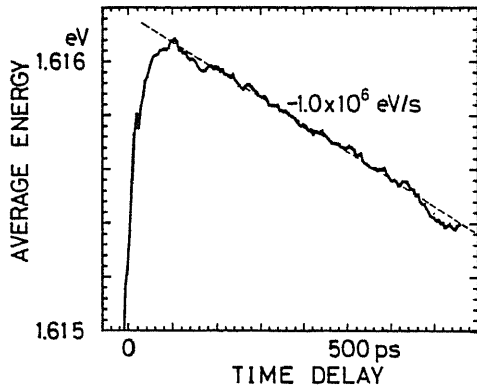


FIG. 4. Temporal change of the average energy of the excitons ( $n = 1, e-hh$ ) in GaAs-AlAs MQW at 4.2 K.

where  $M$  is the exciton translational mass,  $D$  is the exciton deformation potential,  $\rho$  is the areal mass density in a layer thickness  $L_z$ ,  $T_e(t)$  is the effective temperature of two-dimensional excitons, and  $T_L$  is the lattice temperature. The piezoelectric-type interaction with LA or TA phonons is considered to give the minor contribution to the energy-decreasing rate of two-dimensional excitons compared with the deformation-potential-type interaction in GaAs except at the large wave vector of excitons.<sup>15,16</sup> The Fröhlich-type interaction with LO phonons also does not contribute to the energy relaxation of excitons in the exciton band, because LO phonon energy ( $\approx 36.2$  meV) is larger than the observed luminescence bandwidth. Equation (3) is integrated as follows, because  $\langle E(t) \rangle = k_B T_e(t)$ :

$$T_e(t) = T_L + [T_e(0) - T_L] \exp[-(2M^2 D^2 / \hbar^3 \rho) t], \quad (4)$$

where  $T_e(0)$  is the initial temperature of the excitons. Using the values of  $M = 0.7m_0$  (electron mass),<sup>17</sup>  $D = 9.6$  eV,<sup>18</sup>  $\rho = \rho_{3\text{-dim}} L_z = (5.3 \text{ g/cm}^3) \times (76 \times 10^{-8} \text{ cm}) = 4.0 \times 10^{-6} \text{ g/cm}^2$ ,<sup>9</sup> and  $T_L = 4.2$  K, the exponent in Eq. (4) is obtained as  $-(2M^2 D^2 / \hbar^3 \rho) t = -(4.1 \times 10^{10} \text{ s}^{-1}) t$ . This indicates that two-dimensional excitons lose their kinetic energy at a time constant of 24 ps. This calculated decay rate is much faster than the observed one, if all the energy losses are attributed to the kinetic-energy loss.

In the above calculation, we have taken account only of the two dimensionality of excitons. In reality, not only the two dimensionality but also the randomness due to the fluctuation of the well width contributes to the energetical relaxation of excitons. In MQW there should be a number of clusters in which the well width is homogeneous. The lateral characteristic size  $l_c$  of the clusters is estimated to be an order of the exciton Bohr radius  $a_B = 136 \text{ \AA}$ ,<sup>19</sup> because the absorption spectrum of excitons does not show substructures. Because the excitation spot size of  $200 \mu\text{m}$  covers many (an order of  $10^8$ ) clusters, the statistical distribution of the lateral size of clusters in each photoexcited well structure is expected to be the same. Supposing the extreme case that the cluster lateral size is much larger than  $a_B$ , the exciton energy levels in each cluster are different from each other by the multiple of 7.7 meV in our sample, because the fluctuation of the well width is the multiple of

$a/2$ . Around the cluster boundaries, the intercluster translational motion of excitons is restricted, because the mismatch of the resonance energy of 1s excitons should be compensated by the emission or absorption of acoustic phonons. Thus excitons are localized in clusters with the loss of the kinetic energy and intercluster movement of excitons is weakly allowed with the emission or absorption of acoustic phonons.

Similarly to the three-dimensional case, photogenerated two-dimensional electron-hole pairs will quickly lose their energy to form excitons with the emission of a number of phonons within the present time resolution.<sup>20</sup> The calculation described in Eq. (4) shows that the kinetic energy loss of excitons is almost completed within the present time resolution. What process is responsible for the observed energy-loss rate of excitons? In the random well, there can be two channels for the energetic relaxation processes of excitons. On the one hand, excitons lose their kinetic energy via the acoustic-phonon interaction. On the other hand, excitons lose their energy migrating toward the lower-energy positions in an inhomogeneous well with the emission of acoustic phonons. After most of the kinetic energy is lost, the kinetic-energy-loss process works little because  $\langle dE(t)/dt \rangle_{dp}$  is proportional to the excess kinetic energy  $k_B T_e(t) - k_B T_L$ , so that excitons lose their energy mainly via the latter process. If this is correct, the estimation based on Eq. (3) and the result of Fig. 4 show that the alternation of the energy-loss channels occurs when the excess kinetic energy of excitons becomes smaller than 0.024 meV. Then the localization of the excitons is established with the loss of the kinetic energy. After that, excitons lose their energy slowly, migrating toward lower-energy positions in the inhomogeneous well with the emission of acoustic phonons. As stated above, the intercluster migration of excitons presumably interprets the observed slow energy-decreasing rate of excitons, although at present we cannot calculate quantitatively the energy-decreasing rate on the basis of this model. Detailed experiments on various samples having different degrees of two dimensionality and randomness are now in progress.

In summary, picosecond relaxation processes of 1s excitons ( $n = 1, e-hh$ ) in GaAs-AlAs MQW have been studied by observing the energy- and time-resolved luminescence. The decreasing rate of the average energy of excitons is constant and found to be  $1.0 \times 10^6$  eV/s. This rate is much slower than the kinetic-energy-loss rate calculated by taking account of the two dimensionality of excitons. Instead, the energetic relaxation process due to intercluster migration of excitons with the emission of acoustic phonons is proposed to interpret the observed slow rate.

#### ACKNOWLEDGMENTS

The authors wish to deeply thank Dr. H. Okamoto, Dr. Y. Horikoshi, and Dr. S. Tarucha at Musashino Electrical Communication Laboratory (Nippon Telegraph and Telephone Public Corporation) for providing high-quality samples and for valuable discussions. They thank Professor M. Matsuura at Yamaguchi University for sending them a report of work prior to publication. They also thank Dr. T. Takagahara at the University of Tokyo for valuable discussions and the critical reading of the manuscript.

- <sup>1</sup>R. Dingle, in *Festkörperprobleme XV*, edited by H. J. Queisser (Pergamon, New York, 1975), p. 21.
- <sup>2</sup>G. Bastard, E. E. Mendez, L. L. Chang, and L. Esaki, *Phys. Rev. B* **26**, 1974 (1982).
- <sup>3</sup>Y. Shinozuka and M. Matsuura, *Phys. Rev. B* **28**, 4878 (1983).
- <sup>4</sup>T. Ishibashi, S. Tarucha, and H. Okamoto, in *Gallium Arsenide and Related Compounds, 1981*, edited by T. Sugano (The Institute of Physics, London, 1982), p. 587.
- <sup>5</sup>C. Weisbuch, R. Dingle, A. C. Gossard, and W. Wiegmann, *Solid State Commun.* **38**, 709 (1981).
- <sup>6</sup>L. Goldstein, Y. Horikoshi, S. Tarucha, and H. Okamoto, *Jpn. J. Appl. Phys.* **22**, 1489 (1983).
- <sup>7</sup>Y. Ishida, T. Yajima, and Y. Tanaka, *Jpn. J. Appl. Phys.* **19**, L289 (1980).
- <sup>8</sup>D. D. Sell, *Phys. Rev. B* **6**, 3750 (1972).
- <sup>9</sup>M. Neuberger, in *III-V Semiconducting Compounds, Handbook of Electronic Materials*, edited by M. Neuberger, (Plenum, New York, 1971), Vol. 2, p. 45.
- <sup>10</sup>The observed resonance energy of 1s excitons ( $n=1, e-hh$ ) deviates from the calculation based on the finite-well model by 22.6 meV, while it coincides with the calculation based on the infinite-well model within an error of 1.4 meV. This suggests that excitons are completely confined in the well and that the transfer of the excitons between wells is negligible. Thus the broadening of the level by the tunneling is considered to be negligible. Even if one takes the multi-finite-well model, the calculation shows that the broadenings of the lowest-energy levels of electrons and holes by the tunneling through barriers are 0.56 and 0.039 meV, respectively. These values are much smaller than the observed spectral width of 7.5 meV.
- <sup>11</sup>B. Monemar, *Phys. Rev. B* **8**, 5711 (1973).
- <sup>12</sup>K. Hess and C. T. Sah, *Phys. Rev. B* **10**, 3375 (1974).
- <sup>13</sup>Y. Toyozawa, *Prog. Theor. Phys.* **20**, 53 (1958).
- <sup>14</sup>Y. Masumoto (unpublished).
- <sup>15</sup>R. G. Ulbrich and C. Weisbuch, in *Festkörperprobleme XVIII*, edited by J. Treusch (Vieweg, Braunschweig, 1978), p. 217.
- <sup>16</sup>C. Weisbuch and R. G. Ulbrich, in *Light Scattering in Solids III*, edited by M. Cardona and G. Güntherodt (Springer, Berlin, 1982), p. 207.
- <sup>17</sup>R. G. Ulbrich and C. Weisbuch, *Phys. Rev. Lett.* **38**, 865 (1977).
- <sup>18</sup>B. Welber, M. Cardona, C. K. Kim, and S. Rodriguez, *Phys. Rev. B* **12**, 5729 (1975).
- <sup>19</sup>D. D. Sell, S. E. Stokowski, R. Dingle, and J. V. DiLorenzo, *Phys. Rev. B* **7**, 4568 (1973).
- <sup>20</sup>C. V. Shank, R. L. Fork, R. Yen, J. Shah, B. I. Greene, A. C. Gossard, and C. Weisbuch, *Solid State Commun.* **47**, 981 (1983).

Reprint from

Proceedings of the 17th  
International Conference  
on the Physics of Semiconductors

Edited by J.D. Chadi and W.A. Harrison

---

© 1985 by Springer-Verlag New York, Inc.  
Printed in the United States of America.



Springer-Verlag  
New York Berlin Heidelberg Tokyo

SLOW ENERGY RELAXATION OF EXCITONS IN GaAs-AlAs  
MULTI-QUANTUM-WELL STRUCTURES

Yasuaki Masumoto, Shigeo Shionoya and Hiroshi Okamoto\*

The Institute for Solid State Physics, The University of Tokyo,  
Roppongi 7-22-1, Minato-ku, Tokyo 106, Japan  
\*Musashino Electrical Communication Laboratory,  
Nippon Telegraph and Telephone Public Corporation (NTT),  
Midori-machi 3-9-11, Musashino-shi, Tokyo 180, Japan

Picosecond energy relaxation processes of excitons in the well layers of GaAs-AlAs multi-quantum-well structures have been systematically studied for the first time. It has been observed that excitons lose their energy in the exciton band much more slowly than expected by the kinetic-energy-loss theory. The measured energy-loss-rate remarkably increases with the decrease of the GaAs well thickness. These facts suggest that excitons are localized in the disordered well and that slow energy relaxation is attributed to the phonon-assisted cross relaxation between localized exciton states.

1. Introduction

Excitons in multi-quantum-well structures (MQW) have inhomogeneous as well as two-dimensional characters. The resonance energy of excitons is spread, because the well thickness is laterally fluctuated by an order of one atomic layer. As a result, absorption, luminescence and excitation spectra of excitons in MQW are inhomogeneously broadened depending on the degree of the fluctuation [1-3]. The energy relaxation process of excitons in two-dimensional disordered systems provide one of the most important open subjects in semiconductor physics. The exciton in GaAs-AlAs MQW is suitable for this study, because two-dimensionality and disordered character in MQW are controllable by the recent semiconductor technology. In this work, we present for the first time a systematic study on the picosecond energy relaxation processes of excitons in GaAs-AlAs MQW made with changing the GaAs well thickness.

Sample Code	$L_z$ (Å)	$L_b$ (Å)	d (μm)	$E_{n=1}$ (eV)	$\delta E_{n=1}$ (meV)
#1	43	62	2.1	1.683	16
#2	53	50	2.3	1.672	20
#3	58	71	2.2	1.642	11
#4	76	33	3.0	1.622	7.5
#5	108	36	3.5	1.572	3.1

Table I. List of GaAs-AlAs MQW samples.  $L_z$ : GaAs well thickness;  $L_b$ : AlAs barrier thickness; d: total thickness of GaAs-AlAs MQW;  $E_{n=1}$ : energy of the absorption peak due to the 1s exciton ( $n = 1$ , e-hh) at 4.2 K;  $\delta E_{n=1}$ : line-width of the absorption spectrum at 4.2 K.

## 2. Experimental Procedures

In this work five samples grown by molecular beam epitaxy on GaAs substrates were used. Their properties are listed in Table I. They consist of alternate GaAs well layers and AlAs barrier layers. Window portions in the samples where the GaAs substrates were removed were used for the luminescence experiments as well as the absorption experiments.

As the excitation source a rhodamine 6-G dye laser synchronously pumped by a mode-locked argon laser was used. It gives 1-2 ps light pulses of 300 pJ. The laser beam was focused on GaAs-AlAs MQW samples immersed in liquid helium. The excitation photon energy is 2.0-2.1 eV which is above the lowest quantum state ( $n=1$ ) in GaAs well layers of all the samples and below the indirect ( $= 2.229$  eV; X) as well as direct ( $= 3.13$  eV;  $\Gamma$ ) excitonic band-gap energy of AlAs. Thus only the GaAs well layers were excited. The spectrally resolved (resolution = 1 meV) temporal response of the luminescence was analyzed by using a combined system of a 25 cm-monochromator, a synchroscan streak camera (Hamamatsu C1587), a silicon intensifier target camera and a computer. The time resolution of the system was 70 ps.

## 3. Experimental Results and Discussions

In Fig.1, spectra of the absorption and time-integrated luminescence

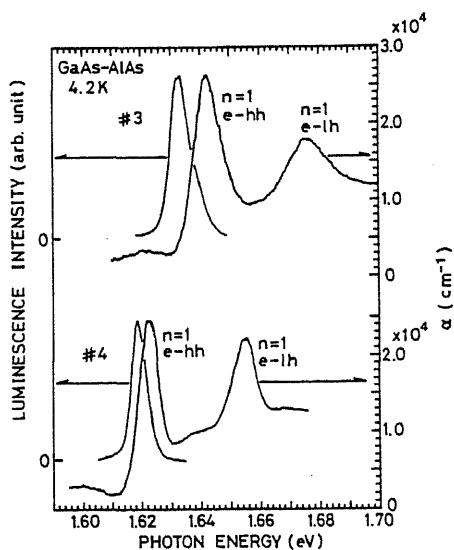


Fig.1. Absorption and time-integrated luminescence spectra of two GaAs-AlAs MQW samples, #3 and #4, at 4.2 K. Luminescence spectra were obtained under the irradiation of pulsed dye laser (2.063 eV, 1-2 ps, 300 pJ).

of typical two samples (#3 and #4) are shown. The absorption peak observed at 1.6420 eV with 11 meV width in #3 and that observed at 1.6225 eV with 7.5 meV width in #4 are ascribed to the 1s exciton ( $n=1$ , e-hh) composed of an electron and a heavy hole belonging to the lowest state ( $n=1$ ) in the quantum well. As is seen, the absorption spectral width is sample-dependent. This fact is not strange, because the origin of the spectral width is attributed to the fluctuation of the well thickness. As listed in Table I, the energy position of absorption peaks  $E_{n=1}$  and their spectral width  $\delta E_{n=1}$  are varied depending on the well thickness  $L_z$ . As the first approximation,  $E_{n=1} - E_g$  ( $E_g$  = band-gap energy of GaAs = 1.5192 eV) and  $\delta E_{n=1}$  are expected to be propor-

tional to  $L_z^{-2}$  and  $L_z^{-3}$ , respectively [1]. Actually, however,  $E_{n=1} - E_g$  and  $\delta E_{n=1}$  do not increase so much with the decrease of  $L_z$ .

Energy- and time-resolved results of luminescence of samples, #3 and #4, are shown in Figs.2 and 3. These figures are constructed from the spectrally resolved temporal response of luminescence by means of computer graphics. The energy and time response of luminescence directly reflects the population dynamics of excitons. Thus it is clearly observed from the figures that excitons drift toward lower energy states losing their energy in both of the samples. The temporal change of the average energy of the exciton ensemble is shown by bold dashed lines in the figures. It is found that the energy-loss-rate of excitons is sample-dependent. In #3, the energy-loss-rate varies from  $12.5 \times 10^6$  eV/s (at the initial stage) to  $3.7 \times 10^6$  eV/s (at the later stage), while it varies from  $4.5 \times 10^6$  eV/s to  $2.8 \times 10^6$  eV/s in #4.

In the disordered well, there can be two channels for the energy relaxation of excitons. These two channels are schematically shown in Fig.4. One channel is the kinetic-energy-loss process, in which excitons are scattered to smaller  $k$  states via the exciton-phonon interaction. The other channel is the cross relaxation process, in which excitons lose their energy migrating toward lower-energy positions in an inhomogeneously broadened exciton band accompanied by the emission of phonons. In MQW both the processes are expected to occur. The kinetic-energy-loss rate of two-dimensional excitons via the deformation-potential-type exciton-LA phonon interaction is calculated to be  $\langle dE/dt \rangle_d = -(2M^2 D^2 / \hbar^3 \rho) [k_B T_e(t) - k_B T_L]$  [3]. Here  $M$  is the exciton translational mass,  $D$  is the exciton

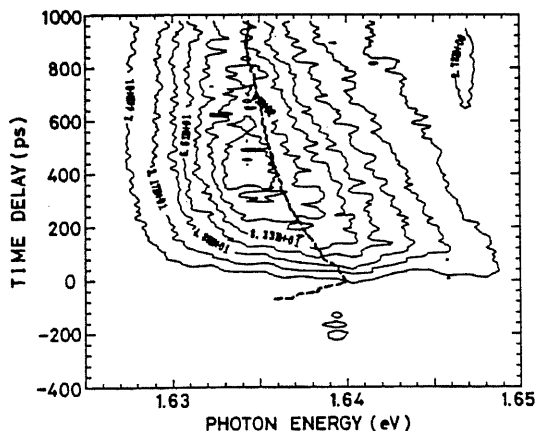


Fig.2. A contour map of the energy- and time-resolved luminescence intensity of the 1s excitons ( $n=1$ , e-hh) in a GaAs-AlAs MQW sample (#3) at 4.2 K. A bold dashed line shows the average energy of excitons.

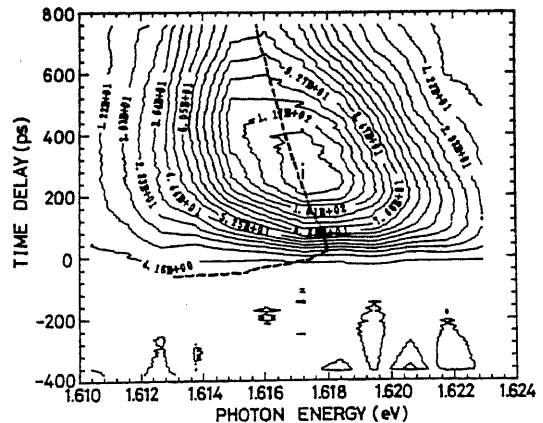


Fig.3. A contour map of the energy- and time-resolved luminescence intensity of the 1s excitons ( $n=1$ , e-hh) in a GaAs-AlAs MQW sample (#4) at 4.2 K. A bold dashed line shows the average energy of excitons.

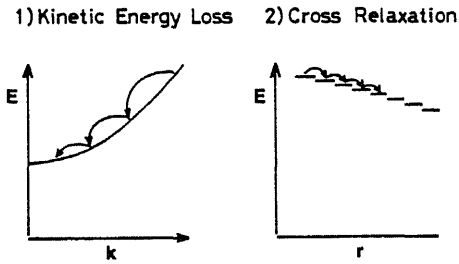


Fig.4. Two energy relaxation processes of excitons in the disordered system.

deformation potential,  $\rho$  is the areal mass density of well layers,  $T_e(t)$  is the effective temperature of two-dimensional excitons and  $T_L$  is the lattice temperature. From this equation it is derived that the average energy of excitons exponentially decay to reach the lattice temperature.

Using the values of  $M = 0.7 m_0$  (electron mass),  $D = -9.6$  eV,  $\rho = \rho_{3\text{-dim}L_z} = 3.1 \times 10^{-6}$  g/cm<sup>2</sup> (for #3),  $4.0 \times 10^{-6}$  g/cm<sup>2</sup> (for #4) and  $T_L = 4.2$  K,

the decay time constants are estimated to be 19 ps (for #3) and 24 ps (for #4), respectively.

From the above-mentioned simple calculation, it is concluded that the kinetic-energy-loss process is completed within our present time resolution (= 70 ps). In MQW it is considered that a well layer consists of a number of clusters in which the well width is homogeneous [1,2]. The lateral size of clusters is estimated to be an order of the exciton Bohr radius  $a_B = 136$  Å, because the absorption spectra of excitons do not show substructures [3]. With the loss of the kinetic energy, excitons are localized in respective clusters, because the intercluster translational motion of excitons is limited owing to the mismatch of the resonance energies of excitons in individual clusters. After that, excitons lose their energy slowly via the intercluster transfer process.

To describe this cross relaxation process, the localized exciton transfer model proposed by Cohen and Sturge [4] is helpful. This model was first proposed for the three-dimensional semiconductor alloys. Afterwards the model has been extended for the two-dimensional excitons in MQW by Takagahara [5]. Two-dimensional localized excitons lose their energy in the exciton band via the one-phonon-assisted transfer processes. Supposing the intercluster transfer Hamiltonian in the form of  $J(r) = J_0 \exp(-r/a_B)$ , the transfer rate from the a cluster to the b cluster due to the deformation-potential-type exciton-phonon interaction  $w_{ab}^d$  is expressed by

$$w_{ab}^d = \frac{8\pi^2}{\hbar} J_0^2 a_B^2 G_d^2 \left[ 1 - \frac{1}{(1+a_B^2 q^2)^{3/2}} \right] \exp\left(-\frac{q\xi}{2}\right) \frac{f(\Delta E_{ab})}{\Delta E_{ab}} g(E_b) \quad , \quad (1)$$

where  $G_d$  is the deformation-potential-type coupling constant which is proportional to  $L_z^{-1/2}$  and asymptotically depends on  $q^{1/2}$  ( $q \rightarrow 0$ ). Here  $q$  is the wavevector of phonons,  $\xi$  is the localization extent of excitons,  $\Delta E_{ab}$  is the difference between resonance energies of excitons localized in the a and b clusters,  $f(\Delta E_{ab})$  is the two-dimensional density of phonon

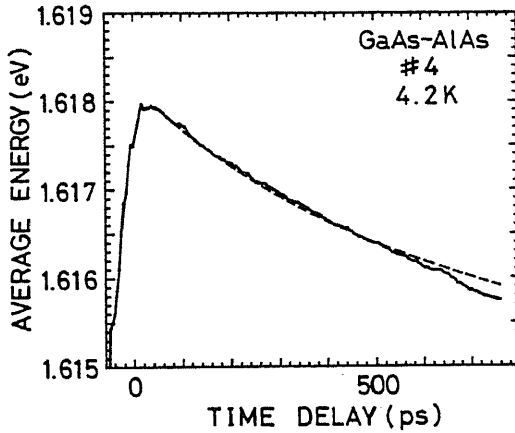


Fig.5. Experimental temporal change (a solid line) of the average energy of 1s excitons in a GaAs-AlAs MQW sample (#4) at 4.2 K and calculated change (a dashed line) based on the model described in the text. Here an adjustable parameter  $J_0$  is set to be 0.34 meV.

way is shown in Fig.5 by the dashed line. Fitting is satisfactory. The physical origin of the slow energy relaxation comes from the factor of  $\exp(-q^2\xi^2/2)$  in eq.(1). Localized excitons can only interact with phonons whose wavevectors are smaller than the inverse of the localization extent of excitons  $1/\xi$  which is estimated to be the inverse of the lateral cluster size. As a result, only small energy phonons ( $< 1$  meV) participate in the cross relaxation of localized excitons.

As stated above, the observed energy-loss-rate is sample-dependent. What characterizes the energy-loss-rate? To answer this question, we have measured the energy-loss-rates of five samples in Table I whose well thicknesses are different from one another. In Fig.6 the energy-loss-rate and the absorption line-width of the 1s excitons ( $n=1$ , e-hh) are plotted as a function of the well thickness  $L_z$ . It is obvious that the energy-loss-rate as well as the line-width increase with the decrease of  $L_z$ . The energy-loss-rate is approximately expressed by  $L_z^{-2}$ . At present we can not fully explain this dependence. However, the qualitative tendency observed is consistent with the theoretical model. We are considering two reasons to account for the  $L_z$  dependence of the energy-loss-rate. One reason is the  $L_z$  dependence of the transfer rate  $w_{ab}$ . With the decrease of  $L_z$ ,  $G_d^2$  and  $G_p^2$  in eq.(1) increase in proportion to  $1/L_z$ . Another reason is the increase of the absorption line-width with the decrease of  $L_z$ . As the slope of the density of exciton states  $g(E_b)$  at the low energy tail region decreases, the cross

states and  $g(E_b)$  is the density of exciton states for which we can substitute the absorption spectrum of the exciton. We obtain the expression for the transfer rate due to the piezoelectric-type interaction  $w_{ab}^p$  by substituting  $\pi^2/\hbar$  and  $G_p^2$  for  $8\pi^2/\hbar$  and  $G_d^2$ , respectively [5]. Here the piezoelectric-type coupling constant  $G_p$  is proportional to  $L_z^{-1/2}$  and asymptotically depends on  $q^{3/2}$  ( $q \rightarrow 0$ ). Using the transfer rate  $w_{ab} = w_{ab}^d + w_{ab}^p$ , the population dynamics of excitons are described by a rate equation. A numerical calculation is done based on this model adopting the GaAs parameters. The temporal development of average energy obtained by this

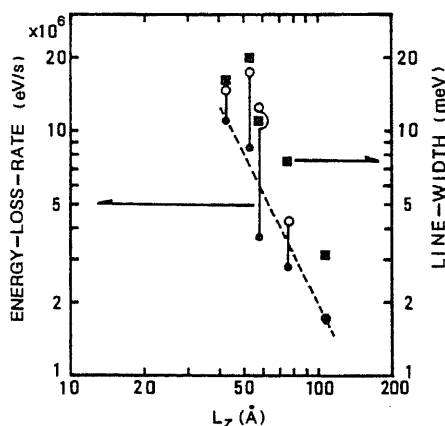


Fig.6. The energy-loss-rate (O,●) and the absorption line-width (■) of 1s excitons as a function of well thickness  $L_z$ . Open circles are the energy-loss-rates at the initial stage of time and closed circles are those at the later stage of time. A dashed line shows the  $L_z^{-2}$  dependence.

relaxation rate increases. Because we can substitute the absorption spectrum for the density of exciton states  $g(E_b)$ , the cross relaxation rate increases with the increase of the absorption line-width.

#### 4. Conclusion

We have systematically studied the energy relaxation processes of excitons in GaAs-AlAs MQW with changing the GaAs well thickness. Energy-loss-rate of excitons in the exciton band is much slower than the calculated kinetic-energy-loss rate. A new model describing the energy relaxation processes of two-dimensional localized excitons well explains the observed slow energy-loss-rate. The measured energy-loss-rate remarkably increases with the decrease of the well thickness.

#### Acknowledgments

This fact is considered to be a result of increased disordered character as well as two-dimensionality.

The authors wish to deeply thank Dr. H.Kawaguchi and Dr. S.Tarucha at Musashino Electrical Communication Laboratory (NTT) for providing high-quality samples and for valuable discussions. They also deeply thank Dr. T.Takagahara at the University of Tokyo for close collaboration in considering the theoretical problem.

#### References

- [1] C.Weisbuch, R.Dingle, A.C.Gossard and W.Wiegmann: Solid State Commun. **38**, 709 (1981).
- [2] L.Goldstein, Y.Horikoshi, S.Tarucha and H.Okamoto: Jpn. J. Appl. Phys. **22**, 1489 (1983).
- [3] Y.Masumoto, S.Shionoya and H.Kawaguchi: Phys. Rev. B **29**, 2324 (1984).
- [4] E.Cohen and M.D.Sturge: Phys. Rev. B **25**, 3828 (1982).
- [5] T.Takagahara: This Proceedings.

# GaAs-AlAs 超格子中の 二次元励起子系のピコ秒分光

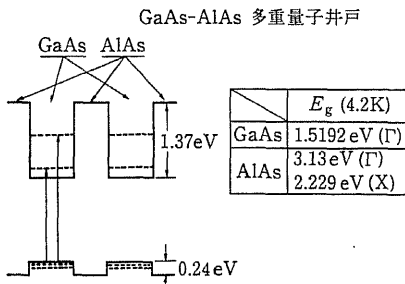
東京大学物性研究所 舛本 泰章

## §1 はじめに

半導体超格子とは、バンドギャップ・エネルギー  $E_g$  の異なる半導体超薄膜を交互に積層した構造のことである。この構造のため、伝導帯も価電子帯も周期的な凹凸のあるポテンシャルが形成される。例を GaAs-AlAs 超格子にとると、直接遷移の  $E_g$  は、低温 (4.2K) で GaAs では 1.5192 eV, AlAs では 3.13 eV であるため、第 1 図のように、GaAs 層はポテンシャル井戸 (量子井戸と呼ばれる) をつくり、AlAs はポテンシャル・バリアーをつくる。初等的な量子力学で明らかかなように、無限に深い井戸型ポテンシャル中の電子 (正孔) は、ポテンシャル井戸の底から測って離散的固有エネルギー

$$E_n^{e(h)} = \frac{\pi^2 \hbar^2 n^2}{2m_{e(h)}^* L_z^2}, \quad n=1, 2, 3, \dots \quad (1.1)$$

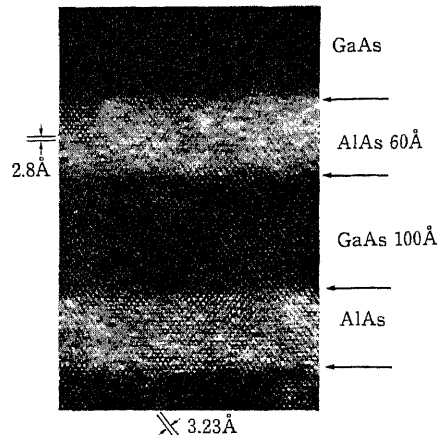
をもつ——量子サイズ効果<sup>1)</sup>。ここで、 $m_{e(h)}^*$  は電子 (正孔) の有効質量、 $L_z$  は井戸層の厚みである。この離散的エネルギー準位に属する電子と正孔



第 1 図 GaAs-AlAs 超格子 (多重量子井戸) 構造。GaAs と AlAs のバンドギャップ  $E_g$  は 4.2 K での値を示す。伝導帯と価電子帯の井戸の深さは、85%、15%の比で決まっている<sup>1)</sup>。

は、クーロン引力により励起子をつくる。量子サイズ効果は更に、励起子の envelope 波動関数に顕著な二次元性を与え、 $L_z \rightarrow 0$  の極限では、励起子の束縛エネルギーは三次元の場合の 4 倍になる<sup>2), 3)</sup>。そのため、量子井戸中の励起子は極めて安定であり、低温から室温まで光吸収スペクトル中に明瞭なピークとして観測される<sup>4)</sup>。

超格子 (多重量子井戸) 構造中の励起子は、このような顕著な二次元性をもっているが、この二次元性に加えて、もう一つの顕著な性質——不均一性——を併せもっている。超格子構造を作成する上で最も制御性に秀れた方法である分子線エピタキシー (MBE) 法は、半導体薄膜を 1 原子層程度の精度で膜厚制御をすることができる。第 2 図は MBE 法で作成された GaAs-AlAs 超格子構造の透過電子顕微鏡写真である。GaAs 層、AlAs 層とも、規則正しい結晶格子を組んでいるが、GaAs-AlAs



第 2 図 MBE 法で作られた GaAs-AlAs 超格子構造の透過電子顕微鏡写真 (岡本紘博士の好意による)。

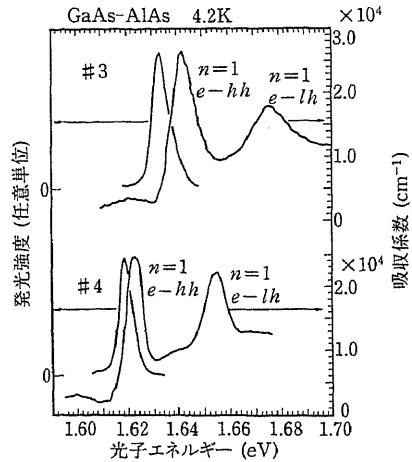
の界面の部分は、一原子層程度ゆらいでいるのが観察される。この層内における一原子層程度のゆらぎは、(1.1)式から推測できるように、励起子の吸収、発光および励起スペクトルにかなりの不均一広がりをもたらす<sup>5,6)</sup>。このため、超格子(多重量子井戸)中の励起子は、二次元不規則系の励起子の極めて良い例となっている。このような二次元不規則系の励起子の緩和は、三次元結晶での励起子の緩和とは大変異なった様相を示すことが予想できるが、未解決の問題であった。しかし、最新のピコ秒( $10^{-12}$ s)分光の手法により、超格子(多重量子井戸)中の励起子の緩和を直接に観測することが可能になってきた<sup>7,8)</sup>。本稿では、GaAs-AlAs超格子(多重量子井戸)中の励起子の緩和を調べた最新の実験データをもとに、どのような緩和過程が起こっているのか明らかにしよう。

## §2 励起子吸収帯の不均一広がりに

GaAs-AlAs界面のゆらぎが、励起子吸収帯の幅に、実際にどの程度寄与するのか示そう。第3図は典型的な二つのGaAs-AlAs超格子(多重量子井戸)試料の吸収および発光スペクトルを示す。#4の試料で1.6225 eVに幅7.5 meV、#3の試料で1.6420 eVに幅11 meVで観測される吸収ピークは、量子井戸の最低量子準位( $n=1$ )にある電子と重い正孔から成る励起子基底状態( $n=1, e-hh; 1s$ )である。いま、界面のゆらぎによる井戸層の厚みのゆらぎ $\delta L_z$ が一原子層すなわちGaAsの格子定数 $a$ ( $=5.64\text{\AA}$ )の半分程度だとすると、#4の試料( $L_z=76\text{\AA}$ )では、GaAsの $E_g$ から測った最低量子準位のエネルギーは $E_{n=1}=E_{n=1}^e+E_{n=1}^h\sim 100\text{ meV}$ なので、最低量子準位のエネルギーのゆらぎ $\delta E_{n=1}$ は、(1.1)式から

$$\delta E_{n=1} = E_{n=1} \left( \frac{2\delta L_z}{L_z} \right) = E_{n=1} \left( \frac{a}{L_z} \right) \sim 7.4\text{ meV} \quad (2.1)$$

となり、観測された幅7.5 meVとほぼ一致する。更に、より $L_z$ の薄い#3の試料( $L_z=58\text{\AA}$ )では、より吸収線幅は広くなり、(2.1)式の示す傾向と一致する。このように、井戸層の厚みのゆらぎが量子準位のエネルギーのゆらぎをひき起こし、こ



第3図 GaAs-AlAs超格子(多重量子井戸)試料#3(GaAs井戸厚 $L_z=58\text{\AA}$ , AlAsバリアー厚 $L_b=71\text{\AA}$ )と#4( $L_z=76\text{\AA}$ ,  $L_b=33\text{\AA}$ )の吸収スペクトルと時間積分発光スペクトル。

のエネルギーのゆらぎが実際に観測される吸収線幅を支配している。実際、ゆらぎがない場合の例として、バルクなGaAs結晶の励起子吸収帯の幅は、低温で0.4 meV程度であり極めて狭い<sup>9)</sup>。超格子(多重量子井戸)構造の井戸層の厚みのゆらぎの特徴としては、厚みが $a/2$ の整数倍ずつデジタルに変化するということがある。また、界面の凹凸の界面に沿った方向のスケールは原子のサイズであることは結晶成長論的に無理があるので、凹凸はかなり大きなスケール $\sim 100\text{\AA}$ 程度の島状になって起こっていると考えられている。井戸層の厚みの厚い島中の励起子の共鳴エネルギーは低く、厚みの薄い島中の共鳴エネルギーは高い。励起子の吸収線幅の広がりは、このような共鳴エネルギーの井戸層での場所による違いの集合によりできていると考えられ、不均一広がりである。

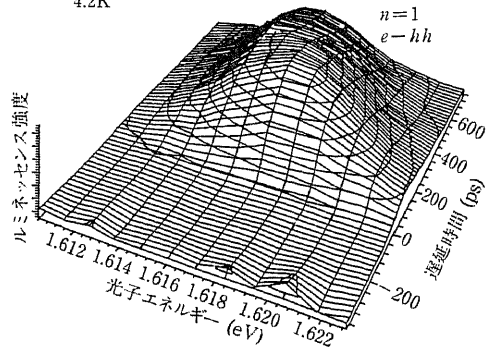
## §3 励起子発光のエネルギー、時間分解分光

直接許容遷移型半導体中の励起子の発光寿命は通例ナノ秒( $10^{-9}$ s)の程度であり、これより早い時間スケールで、エネルギー緩和をを起こし、発光消滅する。したがって、励起子のこうした高速のエネルギー緩和を直接観測するためには、ピコ秒

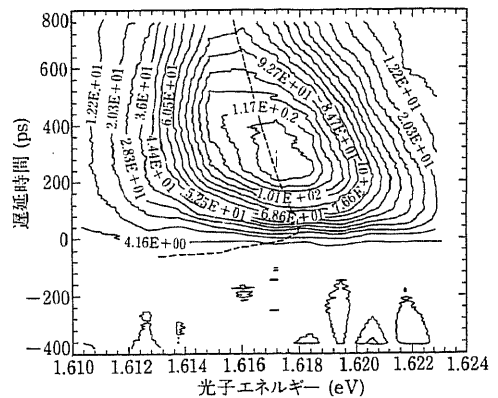
分光の助けをかりなければならぬ。実際、多重量子井戸層の励起子をピコ秒の光パルスで励起し、励起子発光をエネルギー、時間分解することにより励起子のエネルギー緩和を直接観測することができる<sup>2)</sup>。励起には、モード同期アルゴン・レーザーにより同期励起された色素レーザーを用いた。この色素レーザー(色素:ローダミン 6G)は、1~2 ps, 300 pJ の光パルス(2.0~2.1 eV)を安定に発生することができる。励起光のエネルギーはGaAs 井戸層の最低量子準位よりも高く、AlAsの $E_g$ よりも低く選ばれている。そのため励起は、GaAs 井戸層のみ選択的に行なわれている。励起子発光は、第3図に示されているように、最低エネルギー状態の励起子( $n=1, e-hh$ )のみが観測される。この励起子発光を分光器でエネルギー的に分解し、更に同期走査型ストリークカメラにより時間分解する。この方法で時間分解能は約70 psであった。得られた結果を鳥瞰図として第4図に示す。更にこの第4図の等高線図を第5図に示す。横軸は観測されるエネルギー、縦軸は時間の経過を示す。この図は、励起子発光強度の等高線図であり、曲線上の点は同じ発光強度を示し、各曲線は一定の強度ずつずれた点の集合を表わす。この図から励起子系が低いエネルギー状態に移りながら、発光消滅していることがわかる。励起子系の平均エネルギーは図中の太い破線で示されるような時間変化を示す。エネルギーの減少速度は、時間の初期には $4.5 \times 10^6$  eV/s、後期には $2.8 \times 10^6$  eV/sになる。また、励起子の全数は約480 psの時定数で消滅している。

さて、このような励起子系の挙動は、超格子試料でどの程度普遍的なものであるか? 第5図は#4の試料( $L_z=76\text{\AA}$ )についての励起子発光をエネルギー、時間分解した等高線図であるが、#3の試料( $L_z=58\text{\AA}$ )についての等高線図を第6図に示す。励起子系が低いエネルギー状態に移りながら発光消滅していく事情は同じである。しかし、第5図と第6図を比較してみると、#3の試料の方が、励起子系のエネルギーの減少速度がかなり速いことがわかり、エネルギーの減少速度は試料に依存している。(第6図の横軸のスケールは、第5図の横軸のスケールの約0.56倍に縮小してある。)

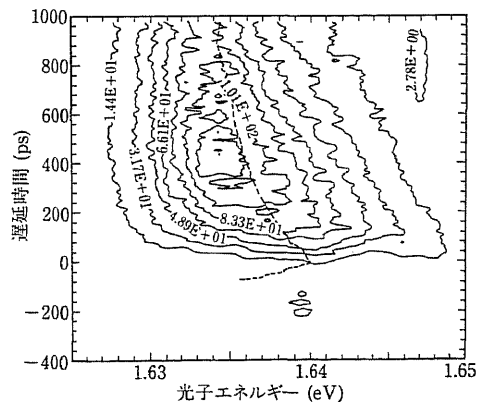
GaAs-AlAs 多重量子井戸  
4.2K



第4図 GaAs-AlAs 超格子(多重量子井戸) 試料#4の励起子発光をエネルギー・時間分解した鳥瞰図。



第5図 GaAs-AlAs 超格子(多重量子井戸) 試料#4の励起子発光をエネルギー・時間分解した等高線図。太い破線は励起子系の平均エネルギーの時間変化を示す。



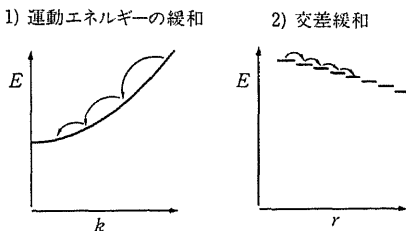
第6図 GaAs-AlAs 超格子(多重量子井戸) 試料#3の励起子発光をエネルギー・時間分解した等高線図。太い破線は励起子系の平均エネルギーの時間変化を示す。

## §4 不規則井戸中の励起子のエネルギー緩和

不規則系中の励起子のエネルギー緩和機構としては、第7図に示すような二通りのエネルギー緩和機構が考えられる。一つの機構は、運動エネルギーを失っていく過程であり、励起子は運動エネルギーを表わす分散曲線に沿って、フォノンを出しながら低いエネルギー状態に緩和していく。もう一つの機構は、不均一拡がりの中の交差緩和の過程であり、励起子は、フォノンを出しながら、不均一拡がりの中で、より低いエネルギー準位に遷移していく<sup>10)</sup>。すなわち、実空間では、励起子は、より低いエネルギー位置に移動していく過程である。量子井戸中の励起子系では、この両方の緩和機構が働いていると考えられる。二次元励起子系の運動エネルギーの減少速度は、変型ポテンシャル型の励起子格子相互作用を想定して計算でき、式

$$\langle dE/dt \rangle = -(2M^2D^2/\hbar^3\rho)[k_B T_e(t) - k_B T_L] \quad (4.1)$$

で評価できる<sup>7)</sup>。ここで  $\langle dE/dt \rangle$  は励起子系のエネルギーの減少速度、 $M$  は励起子の並進質量、 $D$  は励起子の変形ポテンシャル、 $\rho$  は井戸層の面密度、 $T_e(t)$  は二次元励起子系の有効温度、 $T_L$  は格子温度である。二次元励起子系では、励起子系の平均運動エネルギー  $\langle E \rangle$  は、 $\langle E \rangle = k_B T_e(t)$  と表わされるので、(4.1) から平均運動エネルギーは、指数関数的に減少し、格子温度に近づくことがわかる。 $M=0.7 m_0$  (電子質量)、 $D=-9.6$  eV および #4 の試料については、 $\rho=\rho_{a-dim}$   $L_z=4.0 \times 10^{-6}$  g/cm<sup>2</sup> のパラメータを使うと、平均運動エネルギーは減衰時定数  $\sim 24$  ps で格子温度に近づいてい



第7図 不規則系中の励起子のエネルギー緩和機構として考えられる二つの過程。

くことが示される。

この簡単な見積りから、運動エネルギーの緩和は、実験の時間分解能 (=70 ps) 以内に終わっていると結論できる。運動エネルギーを失った励起子は井戸層の中の島にゆるく局在化する。なぜなら、 $a/2$  ずつ異なる井戸厚の島では励起子の共鳴エネルギーの違いがかなりの大きさになり、このことが、励起子の層内での自由な運動をさまたげると考えられるからである。たとえば、島の大きさが、GaAs の励起子基底状態のボーア半径  $a_B$  (=136Å) よりも充分大きな場合には、(2.1) 式からわかるように、 $L_z=76$ Å のとき  $a/2$  厚みが異なる島では、7.4 meV ものエネルギーの違いができる。島中にゆるく局在化した励起子は、エネルギーの高い島から低い島へ、ゆっくりと移動することによってエネルギーを失っていく。

この交差緩和過程を記述するには、二次元局在励起子が、島から島へ、二つの島のエネルギー差を、一つのフォノンの出し入れにより補いながら、移動するというモデルが使える<sup>11,12)</sup>。距離  $r$  だけ離れた島の間を移動させる相互作用の行列要素を、 $J_0$  を定数として交換相互作用型の  $J(r) = J_0 \exp(-r/a_B)$  とすると、変型ポテンシャル型の励起子格子相互作用により、島  $a$  から島  $b$  に移動する速度  $w_{ab}^d$  は

$$w_{ab}^d = \frac{8\pi^2}{\hbar} J_0^2 a_B^2 G_d^2 \left[ 1 - \frac{1}{(1+a_B^2 q^2)^{3/2}} \right] \times \exp\left(-\frac{q^2 \xi^2}{2}\right) \frac{f(\Delta E_{ab})}{\Delta E_{ab}^2} g(E_b) \left\{ \frac{n}{n+1} \right\} \quad (4.2)$$

で表わされる<sup>12)</sup>。ここで、 $G_d$  は変型ポテンシャル型の結合定数で、 $L_z^{-1/2}$  に比例し、漸近的 ( $q \rightarrow 0$ ) に  $q^{1/2}$  に比例する。 $q$  はフォノンの波数、 $\xi$  は励起子の局在した拡がり、 $\Delta E_{ab}$  は島  $a$  と島  $b$  に局在した励起子のエネルギー差、 $f(\Delta E_{ab})$  はフォノンの二次元状態密度、 $g(E_b)$  は励起子状態密度、 $n$  は  $\Delta E_{ab}$  のフォノンの占有数で、 $n, n+1$  はそれぞれフォノンの吸収、放出に対応する。励起子状態密度  $g(E_b)$  としては、励起子の吸収スペクトルを充てることことができる。励起子格子相互作用には、他に圧電型のものがあり、圧電型相互作用による移動速度  $w_{ab}^p$  は、(4.2) の表式で、 $\pi^2/\hbar$  と  $G_d^2$  を  $8\pi^2/\hbar$  と  $G_d^2$  の代わりに代入することにより得

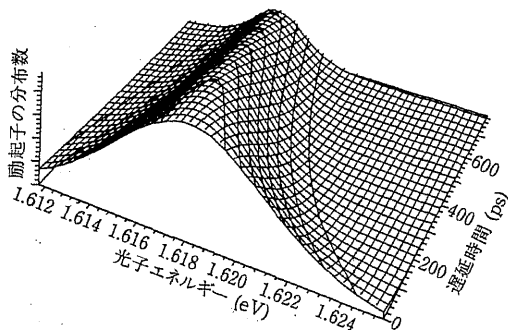
られる。ここで圧電型の結合定数  $G_p$  は  $L_z^{-1/2}$  に比例し、漸近的 ( $q \rightarrow 0$ ) に  $q^{3/2}$  に比例する。  $w_{ab}^d$  と  $w_{ab}^p$  の和,  $w_{ab} = w_{ab}^d + w_{ab}^p$  を用いて、励起子のエネルギー分布の時間変化は、

$$\frac{dP_a(t)}{dt} = -\frac{P_a(t)}{\tau} - \sum_b w_{ab} P_a(t) + \sum_b w_{ba} P_b(t) \quad (4.3)$$

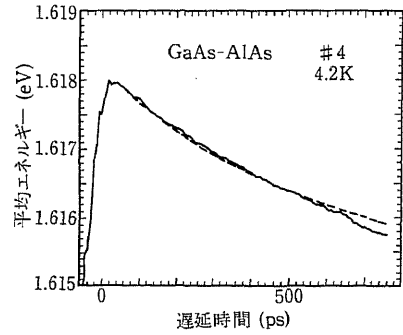
の速度方程式で記述できる。ここで  $P_a(t)$  は時刻  $t$  にエネルギー  $E_a$  にある励起子の分布,  $\tau$  は発光寿命を表わす。実験で得られた初期分布をもとに, (4.3)式により励起子のエネルギー分布の時間発展を計算した結果を第8図に示す。更に励起子系の平均エネルギーの時間変化は

$$\langle E \rangle = \frac{[\sum_a E_a P_a(t) g(E_a)]}{[\sum_a P_a(t) g(E_a)]}$$

で計算でき, 結果を第9図に示す。実験と計算結果との一致は良い。このゆっくりしたエネルギー緩和の物理的原因は, 式(4.2)中の  $\exp(-q^2 \xi^2/2)$  の因子にある。局在励起子は,  $1/\xi$  よりも小さな波数のフォノンとのみ相互作用する。  $\xi$  をほぼ島の大きさ ( $\sim 100\text{\AA}$ ) とみなせば,  $1\text{ meV}$  よりも小さなフォノンとのみ相互作用する。そのため, 励起子は, エネルギーの極めて近い励起子状態にしか遷移できず, 状態密度が小さくなる励起子帯の低エネルギー側の裾の領域では, エネルギーの減少速度にブレーキがかかる。計算によれば, 状態密度の大きな励起子吸収帯の中心では, 交差緩和の時定数は数ピコ秒程度であるが, 状態密度の小さな吸収帯の低エネルギー側の裾の付近では,  $1\text{ ns}$  程度にまでなる。

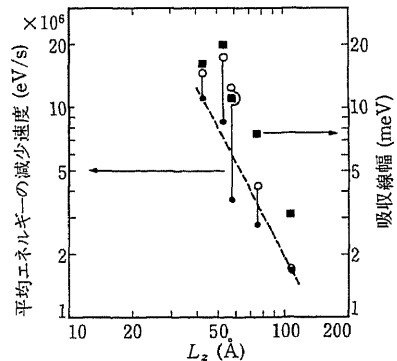


第8図 励起子系のエネルギー分布の時間発展(試料#4 についての計算結果)。

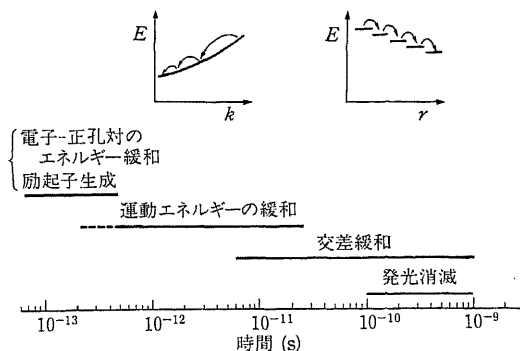


第9図 励起子系の平均エネルギーの時間変化。実線は試料#4での実験結果。破線は計算結果。

既に, 第5図と第6図で示したように, 励起子系の平均エネルギーの減少速度は試料に依存する。それでは, 何がエネルギーの減少速度を支配しているのだろうか? この疑問に答えるために, 互いに井戸層の異なる5個の試料について, 励起子系の平均エネルギーの減少速度を測定した<sup>9)</sup>。結果を, 第10図に示す。第10図には, 平均エネルギーの減少速度と, 励起子吸収スペクトルの吸収線幅とが,  $L_z$  の関数としてプロットしてある。減少速度, 吸収線幅とも,  $L_z$  の減少と共に増加している。観測されたこの傾向は, 定性的には次のように理解できる。一つの原因は, 移動速度  $w_{ab}$  が  $1/L_z$  に比例するからである<sup>12)</sup>。これは  $G_p^2$  および  $G_p^3$  が  $1/L_z$  に比例するからである。もう一つの原因は,  $L_z$  の減少と共に吸収線幅(状態密



第10図 励起子系 ( $n=1, e-hh$ ) の平均エネルギーの減少速度 (○, ●) および吸収線幅 (■) の井戸厚  $L_z$  依存性。○は時間の初期での減少速度, ●は時間の後期での減少速度を示す。破線は  $L_z^{-2}$  の依存性を示す。



第11図 GaAs-AlAs 超格子(多重量子井戸) 構造中の励起子系の緩和過程。

度のエネルギー幅)が増大するからである。励起子の状態密度の低エネルギー域の裾の傾きが小さくなると、 $E_a \rightarrow E_a - \Delta E$  (ただし  $\Delta E > 0$ ) の速度は大きくなり、逆に  $E_a \rightarrow E_a + \Delta E$  の速度は小さくなるからである。

以上説明してきたように、ピコ秒時間領域で観測された GaAs-AlAs 超格子(多重量子井戸) 構造中の励起子系のエネルギー緩和は、励起子の不均一幅の中での交差緩和の機構により説明できた。エネルギー緩和の様子、試料の井戸厚依存性とも、このモデルを支持する。第11図は、光励起された励起子系の緩和の様子をまとめて示す。光励起された電子・正孔対は、サブピコ秒以下の時間スケールで、最低量子準位まで緩和して励起子をつくる<sup>13)</sup>。つくられた励起子は、最初は動きまわるが、数十ピコ秒程度の時間スケールで運動エネルギーを失い、井戸層の厚みのゆらぎにとらえられて、ゆるく局在化する。ゆるく局在化した励起子は、井戸層の中で、より低エネルギーの場所にフォノンを出しながら移動するという交差緩和を十ピコ秒からナノ秒の時間スケールで起こし、最終的に、サブナノ秒の時間スケールで発光消滅する。

## §5 おわりに

以上述べてきたような、超格子(多重量子井戸) 構造中の励起子のピコ秒分光はまだ始まったばかりである。本稿では、励起子のエネルギー緩和をとりあげ、超格子構造のもつ二次元性、不規則性がエネルギー緩和にどのように影響を与えるのか

考察した。しかし、二次元性と不規則性を独立に変化させて、影響を調べる実験は今後に残されている。この問題以外にも、ピコ秒よりも速いフェムト秒 ( $10^{-15}$ s) の時間領域での測定が可能になりつつある現在では、光生成された電子・正孔対の初期緩和、励起子の位相緩和などの超高速現象が測定にかかってくるであろう<sup>14,15)</sup>。また、強磁場下、高圧下でのピコ秒、フェムト秒分光も二次元不規則系の励起子の挙動を調べる上で有用であろう。超格子試料としては、今後、充分制御された界面をもつ超格子、伝導帯の井戸層と価電子帯の井戸層の異なる、いわゆる第二種の超格子、格子不整合の大きな歪みを残した超格子などもピコ秒・フェムト秒分光の対象となり、発展が予想できる。

最後に、この研究に関しご協力、ご教示いただきました塩谷繁雄名誉教授、石田祐三氏、岡本紘博士、河口仁司博士、樽茶清悟氏および高河原俊秀博士に感謝いたします。

## 〔文 献〕

- 1) R. Dingle: *Festkörperprobleme XV*, edited by H. J. Queisser (Pergamon, New York, 1975) p. 21.
- 2) G. Bastard, E. E. Mendez, L. L. Chang and L. Esaki: *Phys. Rev. B* **26** (1982) 1974.
- 3) Y. Shinozuka and M. Matsuura: *Phys. Rev. B* **28** (1983) 4878.
- 4) T. Ishibashi, S. Tarucha and H. Okamoto: *Gallium Arsenide and Related Compounds*, 1981, edited by T. Sugano (The Institute of Physics, London, 1982) p. 587.
- 5) C. Weisbuch, R. Dingle, A. C. Gossard and W. Wiegmann: *Solid State Commun.* **38** (1981) 709.
- 6) L. Goldstein, Y. Horikoshi, S. Tarucha and H. Okamoto: *Jpn. J. Appl. Phys.* **22** (1983) 1489.
- 7) Y. Masumoto, S. Shionoya and H. Kawaguchi: *Phys. Rev. B* **29** (1984) 2324.
- 8) Y. Masumoto, S. Shionoya and H. Okamoto: to be published in *Proc. of the 17th Int. Conf. on the Physics of Semiconductors*, (San Francisco, 1984).
- 9) M. D. Sturge: *Excitons*, edited by E. I. Rashba and M. D. Sturge (North-Holland, Amsterdam, 1982) Chap. 1.

- 10) たとえば, T. Holstein, S. K. Lyo and R. Orbach: *Laser Spectroscopy of Solids*, edited by W. M. Yen and P. M. Selzer (Springer, Berlin, 1981) Chap. 2.
- 11) E. Cohen and M. D. Sturge: *Phys. Rev. B* **25** (1982) 3828.
- 12) T. Takagahara: to be published in *Proc. of the 17th Int. Conf. on the Physics of Semiconductors*, (San Francisco, 1984).
- 13) C. V. Shank, R. L. Fork, R. Yen, J. Shah, B. I. Greene, A. C. Gossard and C. Weisbuch: *Solid State Commun.* **47** (1983) 981.
- 14) D. J. Erskine, A. J. Taylor and C. L. Tang: *Appl. Phys. Lett.* **45** (1984) 54.
- 15) M. D. Sturge, J. Hegarty and L. Goldner: to be published in *Proc. of the 17th Int. Conf. on the Physics of Semiconductors*, (San Francisco, 1984).

## Localization and energy transfer of quasi-two-dimensional excitons in GaAs-AlAs quantum-well heterostructures

T. Takagahara

*Department of Applied Physics, The University of Tokyo, Bunkyo-ku, Tokyo 113 Japan*

(Received 21 November 1984)

A theory of energy transfer of the quasi-two-dimensional excitons in GaAs-AlAs quantum-well heterostructures is developed, and the recently observed slow and nonexponential energy relaxation of excitons is explained quantitatively in terms of the one-phonon-assisted transfer of localized excitons among islandlike structures within a quantum well. The nonexponential behavior of energy relaxation is clarified as a general feature to be observed in the low-energy tail of the density of states. The dependence of the energy relaxation rate on the quantum-well thickness is discussed along with the same dependence of the absorption bandwidth. The correlation between the energy relaxation rate and the absorption bandwidth is explained qualitatively on the basis of the scaling property of the rate equation for the exciton distribution function.

### I. INTRODUCTION

Recently, semiconductor quantum-well (QW) heterostructures have been extensively investigated because of interest in their fundamental physical properties as well as in their potential device applications. Optical techniques such as time-resolved photoluminescence<sup>1-3</sup> and resonant Raman<sup>4,5</sup> and Rayleigh scattering,<sup>6</sup> are quite promising to elucidate the salient features of the quasi-two-dimensional excitons in QW structures. Recently, Masumoto *et al.*<sup>3</sup> studied the time-resolved photoluminescence of 1s excitons ( $n=1$ ,  $e$ - $hh$ ) in GaAs-AlAs multiple-quantum-well structures and found the anomalously slow relaxation of the average energy of luminescence, which shows a nonexponential decay for about several hundred picoseconds after photoexcitation. In addition, the decreasing rate of the average energy of luminescence is too small to be accounted for in terms of the kinetic-energy relaxation on the dispersion curve of the quasi-two-dimensional exciton accompanied by emission of acoustic phonons. In the experiments of Masumoto *et al.* the GaAs layers are selectively excited by choosing the laser energy suitably and ensuring that the AlAs barrier layers are sufficiently thick to rule out the possibility of interlayer migration of excitons. On the other hand, it is well known that the topological disorder of the interface produces sizable optical effects. From the linewidth analysis of the luminescence and excitation spectra, and from transmission electron microscopy, an islandlike structure of the QW interface measuring one monolayer high and about 300 Å laterally was proposed.<sup>7-9</sup> On the basis of this model, a theory is developed to explain the experimental results of photoluminescence in terms of the intralayer migration of localized excitons among islandlike structures with different well thicknesses.

After photoexcitation, the generated electron-hole pairs quickly lose their energy and form excitons with emission of a number of phonons. At the next stage, the kinetic-energy relaxation on the dispersion curve of the quasi-

two-dimensional exciton takes place with a relaxation rate that is 1 order of magnitude faster than the observed rate. After these processes are completed, the anomalously slow energy relaxation begins showing nonexponential behavior. In this stage the lowest 1s exciton in the GaAs layer can be considered to be localized at some islandlike structure since the Bohr radius of the quasi-two-dimensional exciton in the sample of Ref. 3 is estimated to be about 100 Å according to recent theories<sup>10-12</sup> and is less than the average lateral size of the islandlike structures in a QW. Furthermore, the fluctuation of the well thickness of one monolayer produces the fluctuation of the exciton energy of about several meV.<sup>3</sup> This amount of energy fluctuation is sufficient to localize the excitons at the energetically local minimum sites. The localized excitons will then migrate among the local minimum sites in search of the lower-energy sites with emission of acoustic phonons. This intralayer migration of localized excitons is the key idea for explaining the anomalously slow energy relaxation. In fact, our theory explains the salient features of the experimental results quantitatively or qualitatively.

The paper is organized as follows. The two-dimensional aspects of the localized excitons and their interaction with acoustic phonons are essentially new and have not yet been investigated fully. In Sec. II the interaction Hamiltonian of the quasi-two-dimensional exciton with the acoustic phonons is derived microscopically for the first time. In Sec. III the kinetic-energy relaxation rate of the quasi-two-dimensional excitons is estimated on the basis of the result obtained in Sec. II and is shown to be 1 order of magnitude larger than the observed value. Thus the kinetic-energy relaxation is ruled out as the candidate which can explain the slow energy relaxation. In Sec. IV the one-phonon-assisted exciton transfer between localized sites is formulated from the microscopic point of view, making use of the perturbation theory with respect to the exciton-phonon interaction Hamiltonian and the intersite transfer Hamiltonian. In Sec. V the matrix element of the intersite transfer Hamiltonian of the localized excitons is calculated microscopically. In Sec. VI the exciton

citron transfer rate is estimated explicitly for both the deformation-potential coupling and the piezoelectric coupling, and for various cases of the localization form and the type of intersite transfer. In Sec. VII the rate equation for the distribution function of localized excitons is derived, neglecting the interlayer transfer of excitons and thus reducing the problem to that of a single QW. By integrating the rate equation numerically, the average energy of luminescence is calculated and compared with the experimental data. From the comparison between theory and experiment the constant of the exciton transfer integral is determined and found to be in good agreement with the theoretically estimated value. The experimentally observed nonexponential behavior of energy relaxation is clarified theoretically from a general point of view. Finally, in Sec. VIII the dependence of the energy relaxation rate on the QW thickness is discussed on the basis of the scaling property of the rate equation, and the observed correlation between the energy relaxation rate and the absorption bandwidth is explained in a qualitative way.

## II. INTERACTION OF QUASI-TWO-DIMENSIONAL EXCITONS WITH ACOUSTIC PHONONS

In this section the interaction Hamiltonian of the quasi-two-dimensional exciton with acoustic phonons is derived for both the deformation-potential and piezoelectric coupling. In the case of GaAs-AlAs QW structures, the electron and hole of the excitons are considered to be well confined within a QW since the band-gap discontinuity is quite large. On the other hand, the lattice properties of GaAs and AlAs, for example, the lattice constant and elastic moduli, are in close proximity.<sup>13</sup> Thus the acoustic phonons which interact with the quasi-two-dimensional exciton in a GaAs layer can be considered to have three-dimensional character. One can derive the interaction Hamiltonian of the quasi-two-dimensional exciton with acoustic phonons starting from the three-dimensional exciton-phonon interaction Hamiltonian.

$$f_{\lambda}(\mathbf{k}, \mathbf{k}'; \mathbf{K}_{\parallel}) = \frac{1}{L^2} \int d^2 r_{\parallel} \int dz_e \int dz_h F_{\lambda}(r_{\parallel}, z_e, z_h) \exp[i(\alpha_e \mathbf{K}_{\parallel} - \mathbf{k}_{\parallel}) \cdot r_{\parallel} - ik_e z_e + ik'_e z_h], \quad (2.6)$$

where  $\alpha_e$  and  $\alpha_h$  are defined by

$$\alpha_e = m_e / (m_e + m_h) \quad \text{and} \quad \alpha_h = m_h / (m_e + m_h). \quad (2.7)$$

The three-dimensional electron-phonon (*e-ph*) interaction for the deformation-potential (DF) coupling is written as<sup>14</sup>

$$H_{e-ph}^{DF} = \sum_{\mathbf{k}, \mathbf{q}} \left[ \frac{\hbar |q|}{2\rho u V} \right]^{1/2} (D_c a_{c, \mathbf{k}+\mathbf{q}}^{\dagger} a_{c, \mathbf{k}} + D_v a_{v, \mathbf{k}+\mathbf{q}}^{\dagger} a_{v, \mathbf{k}}) (b_{\mathbf{q}} + b_{-\mathbf{q}}^{\dagger}) \quad (2.8)$$

$$= \sum_{\mathbf{k}, \mathbf{q}} [\Xi_c(\mathbf{q}) a_{c, \mathbf{k}+\mathbf{q}}^{\dagger} a_{c, \mathbf{k}} + \Xi_v(\mathbf{q}) a_{v, \mathbf{k}+\mathbf{q}}^{\dagger} a_{v, \mathbf{k}}] (b_{\mathbf{q}} + b_{-\mathbf{q}}^{\dagger}), \quad (2.9)$$

where  $D_c$  ( $D_v$ ),  $\rho$ , and  $u$  are the deformation potential for the conduction (valence) band, the mass density, and the sound velocity of the longitudinal-acoustic (LA-) phonon mode, respectively, and the coupling functions  $\Xi_c$  and  $\Xi_v$  are introduced by (2.9) for later use. The interaction Hamiltonian of the quasi-two-dimensional exciton with acoustic phonons for the deformation-potential coupling is obtained by calculating the matrix element of  $H_{e-ph}^{DF}$  between two exciton states  $|\lambda, \mathbf{K}_{\parallel}\rangle$  and  $|\lambda, \mathbf{K}'_{\parallel}\rangle$ , where for simplicity, the change of the electron-hole internal motion is not taken into account. The result is given as

Let us now consider the quasi-two-dimensional exciton state with a total wave vector  $\mathbf{K}_{\parallel}$  and represent it as

$$|\lambda, \mathbf{K}_{\parallel}\rangle = \frac{v_0}{L} \sum_{\mathbf{r}_e, \mathbf{r}_h} e^{i\mathbf{K}_{\parallel} \cdot \mathbf{R}_{\parallel}} F_{\lambda}(r_{e\parallel} - r_{h\parallel}, z_e, z_h) a_{c, \mathbf{r}_e}^{\dagger} a_{v, \mathbf{r}_h} |0\rangle, \quad (2.1)$$

where  $v_0$  and  $L$  are, respectively, the volume of the unit cell and the linear dimension of the quantization volume,  $a_{\alpha r}^{\dagger}$  ( $a_{\alpha r}$ ) the creation (annihilation) operator of the  $\alpha$ th- (conduction- or valence-) band electron in the Wannier representation,  $|0\rangle$  the crystal ground state, and  $\mathbf{R}$  the coordinate of the exciton center of mass defined by

$$\mathbf{R} = (m_e \mathbf{r}_e + m_h \mathbf{r}_h) / (m_e + m_h), \quad (2.2)$$

with the electron (hole) effective mass  $m_e$  ( $m_h$ ). The envelope function for the  $\lambda$ th electron-hole internal motion is denoted by  $F_{\lambda}$ . In the following any position vector or wave vector will be decomposed into components parallel and perpendicular to the QW interface as  $\mathbf{r} = (r_{\parallel}, z)$  or  $\mathbf{k} = (k_{\parallel}, k_z)$ . Then, rewriting the operators in the Wannier representation with those in the Bloch representation by a well-known relation

$$a_{\alpha n} = \frac{1}{\sqrt{N}} \sum_{\mathbf{k}} e^{i\mathbf{k} \cdot \mathbf{r}_n} a_{\alpha \mathbf{k}}, \quad (2.3)$$

where  $N$  is the number of unit cells related to  $L$  by  $Nv_0 = L^3$ , and transforming the discrete sum over the lattice sites into a spatial integral by

$$\sum_{\mathbf{r}_e} \rightarrow \frac{1}{v_0} \int d^3 r_e, \quad (2.4)$$

one obtains

$$|\lambda, \mathbf{K}_{\parallel}\rangle = \sum_{\mathbf{k}, \mathbf{k}'} f_{\lambda}(\mathbf{k}, \mathbf{k}'; \mathbf{K}_{\parallel}) \delta_{\mathbf{k}_{\parallel} - \mathbf{k}'_{\parallel}, \mathbf{K}_{\parallel}} a_{c, \mathbf{k}}^{\dagger} a_{v, \mathbf{k}'} |0\rangle, \quad (2.5)$$

with

$$\begin{aligned} \langle \lambda, \mathbf{K}_{\parallel} | H_{e-ph}^{DF} | \lambda, \mathbf{K}_{\parallel} \rangle = & \sum_{\mathbf{k}, \mathbf{k}'} \sum_{l, l'} \Xi_c(l - \mathbf{k}) f_{\lambda}^*(l, l'; \mathbf{K}_{\parallel}) f_{\lambda}(\mathbf{k}, \mathbf{k}'; \mathbf{K}_{\parallel}) \delta_{l_{\parallel} - l'_{\parallel}, \mathbf{K}_{\parallel}} \delta_{\mathbf{k}_{\parallel} - \mathbf{k}'_{\parallel}, \mathbf{K}_{\parallel}} \delta_{\mathbf{k}, l'} \\ & - \sum_{\mathbf{k}, \mathbf{k}'} \sum_{l, l'} \Xi_v(\mathbf{k}' - l') f_{\lambda}^*(l, l'; \mathbf{K}_{\parallel}') f_{\lambda}(\mathbf{k}, \mathbf{k}'; \mathbf{K}_{\parallel}) \delta_{l_{\parallel} - l'_{\parallel}, \mathbf{K}_{\parallel}} \delta_{\mathbf{k}_{\parallel} - \mathbf{k}'_{\parallel}, \mathbf{K}_{\parallel}} \delta_{\mathbf{k}, l}. \end{aligned} \quad (2.10)$$

Substituting expression (2.6) and converting the discrete sum over  $\mathbf{k}$  into an integral by

$$\sum_{\mathbf{k}} \rightarrow \left[ \frac{L}{2\pi} \right]^3 \int d^3k, \quad (2.11)$$

one can reduce the first term as

$$\begin{aligned} \sum_{q_z} \Xi_c(\mathbf{K}_{\parallel} - \mathbf{K}_{\parallel}, q_z) \int d^2r_{\parallel} \int dz'_e \int dz'_h \int d^2r_{\parallel} \int dz_e \int dz_h F_{\lambda}^*(r'_{\parallel}, z'_e, z'_h) F_{\lambda}(r_{\parallel}, z_e, z_h) \\ \times \delta^{(2)}(r_{\parallel} - r'_{\parallel}) \delta(z_h - z'_h) \delta(z_e - z'_e) \exp[iq_z z_e - i\alpha_h(\mathbf{K}_{\parallel} - \mathbf{K}'_{\parallel}) \cdot r_{\parallel}] \\ = \sum_{q_z} \Xi_c(\mathbf{K}_{\parallel} - \mathbf{K}_{\parallel}, q_z) \int d^2r_{\parallel} \int dz_e \int dz_h |F_{\lambda}(r_{\parallel}, z_e, z_h)|^2 \exp[iq_z z_e - i\alpha_h(\mathbf{K}_{\parallel} - \mathbf{K}'_{\parallel}) \cdot r_{\parallel}], \end{aligned} \quad (2.12)$$

where the arguments of  $\Xi_c$  are written explicitly; the first argument is the component of the phonon wave vector parallel to the QW interface and the second is the perpendicular component. Similarly the second term in (2.10) can be reduced as

$$- \sum_{q_z} \Xi_v(\mathbf{K}'_{\parallel} - \mathbf{K}_{\parallel}, q_z) \int d^2r_{\parallel} \int dz_e \int dz_h |F_{\lambda}(r_{\parallel}, z_e, z_h)|^2 \exp[iq_z z_h + i\alpha_e(\mathbf{K}_{\parallel} - \mathbf{K}'_{\parallel}) \cdot r_{\parallel}]. \quad (2.13)$$

Thus the quasi-two-dimensional exciton-phonon interaction Hamiltonian  $H_{ex-ph}^{DF(Q2D)}$  for the deformation-potential coupling is given by

$$\begin{aligned} H_{ex-ph}^{DF(Q2D)} = & \sum_{\mathbf{K}_{\parallel}, \mathbf{K}'_{\parallel}, q_z} [\Xi_c(\mathbf{K}'_{\parallel} - \mathbf{K}_{\parallel}, q_z) H_{\lambda}(-\alpha_h(\mathbf{K}_{\parallel} - \mathbf{K}'_{\parallel}), q_z) \\ & - \Xi_v(\mathbf{K}_{\parallel} - \mathbf{K}'_{\parallel}, q_z) H_{\lambda}(\alpha_e(\mathbf{K}_{\parallel} - \mathbf{K}'_{\parallel}), q_z)] | \lambda, \mathbf{K}_{\parallel} \rangle \langle \lambda, \mathbf{K}_{\parallel} | (b_{\mathbf{K}'_{\parallel} - \mathbf{K}_{\parallel}, q_z} + b_{\mathbf{K}_{\parallel} - \mathbf{K}'_{\parallel}, -q_z}^{\dagger}), \end{aligned} \quad (2.14)$$

with

$$H_{\lambda}(\mathbf{Q}_{\parallel}, Q_z) = \int d^2r_{\parallel} \int dz_e \int dz_h |F_{\lambda}(r_{\parallel}, z_e, z_h)|^2 \exp(iQ_z z_e + i\mathbf{Q}_{\parallel} \cdot r_{\parallel}), \quad (2.15)$$

where the symmetry  $F_{\lambda}(r_{\parallel}, z_e, z_h) = F_{\lambda}(r_{\parallel}, z_h, z_e)$  is supposed to hold. This is a quite general expression for the deformation-potential coupling. To obtain a more explicit expression, the envelope function  $F_{\lambda}(r_{\parallel}, z_e, z_h)$  must be specified. For the lowest ( $1s$ ) exciton state, a variational envelope function was assumed as<sup>11</sup>

$$F_{1s}(r_{\parallel}, z_e, z_h) = N_n \exp\{-[\alpha^2 r_{\parallel}^2 + \beta^2 (z_e - z_h)^2]^{1/2}\} \cos\left[\frac{\pi z_e}{L_z}\right] \cos\left[\frac{\pi z_h}{L_z}\right], \quad (2.16)$$

where  $N_n$  is the normalization constant and  $\alpha$  and  $\beta$  are variational parameters to minimize the energy. Here the infinite band-gap discontinuity is assumed and the envelope function is zero outside the region of  $|z_e| \leq L_z/2$  and  $|z_h| \leq L_z/2$ . With use of this envelope function, the function  $H_{1s}(\mathbf{Q}_{\parallel}, Q_z)$  is calculated as

$$\begin{aligned} H_{1s}(\mathbf{Q}_{\parallel}, Q_z) = & \int d^2r_{\parallel} \int_{-L_z/2}^{L_z/2} dz_e \int_{-L_z/2}^{L_z/2} dz_h \exp(iQ_z z_e + i\mathbf{Q}_{\parallel} \cdot r_{\parallel}) |F_{1s}(r_{\parallel}, z_e, z_h)|^2 \\ = & N_n^2 \int d^2r_{\parallel} \int_{-L_z/2}^{L_z/2} dz_e \int_{-L_z/2}^{L_z/2} dz_h \exp\{iQ_z z_e + i\mathbf{Q}_{\parallel} \cdot r_{\parallel} - 2[\alpha^2 r_{\parallel}^2 + \beta^2 (z_e - z_h)^2]^{1/2}\} \cos^2\left[\frac{\pi z_e}{L_z}\right] \cos^2\left[\frac{\pi z_h}{L_z}\right]. \end{aligned} \quad (2.17)$$

By making the variables nondimensional, this can be reduced to

$$\frac{N_n^2 L_z^2}{\alpha^2} \int d^2r_{\parallel} \int_{-1/2}^{1/2} dz_e \int_{-1/2}^{1/2} dz_h \exp\{iQ_z L_z z_e + i\mathbf{Q}_{\parallel} \cdot r_{\parallel} / \alpha - 2[r_{\parallel}^2 + \beta^2 L_z^2 (z_e - z_h)^2]^{1/2}\} \cos^2(\pi z_e) \cos^2(\pi z_h). \quad (2.18)$$

Introducing the two-dimensional polar coordinate for  $r_{\parallel}$  and making use of the decomposition formula<sup>15</sup>

$$e^{iz \cos\theta} = \sum_{n=-\infty}^{\infty} J_n(z) \exp[in(\theta + \pi/2)], \quad (2.19)$$

one can further reduce (2.18) to

$$\frac{2\pi N_n^2 L_z^2}{\alpha^2} \int_0^\infty dr r J_0(br) \int_{-1/2}^{1/2} dz_e \int_{-1/2}^{1/2} dz_h \exp\{iQ_z L_z z_e - 2[r^2 + \beta^2 L_z^2 (z_e - z_h)^2]^{1/2}\} \cos^2(\pi z_e) \cos^2(\pi z_h), \quad (2.20)$$

where  $b = |Q_{||}|/\alpha$  and  $J_0$  is the zeroth-order Bessel function. By use of the formula<sup>15</sup>

$$\int_0^\infty dx x J_0(bx) \exp[-a(x^2 + y^2)^{1/2}] = \frac{a[1 + (a^2 + b^2)^{1/2}y]}{(a^2 + b^2)^{3/2}} \exp[-y(a^2 + b^2)^{1/2}], \quad (2.21)$$

the integral over  $r$  in (2.20) can be performed as

$$\begin{aligned} \frac{4\pi N_n^2 L_z^2}{\alpha^2(4+b^2)^{3/2}} \int_{-1/2}^{1/2} dz_e \int_{-1/2}^{1/2} dz_h \exp[iQ_z L_z z_e - (4+b^2)^{1/2} \beta L_z |z_e - z_h|] \\ \times [1 + (4+b^2)^{1/2} \beta L_z |z_e - z_h|] \cos^2(\pi z_e) \cos^2(\pi z_h) \\ = \frac{4\pi N_n^2 L_z^2}{\alpha^2(4+b^2)^{3/2}} G((4+b^2)^{1/2} \beta L_z, Q_z L_z), \end{aligned} \quad (2.22)$$

where the function  $G(\gamma, \delta)$  is defined by

$$G(\gamma, \delta) = \int_{-1/2}^{1/2} dz_e \int_{-1/2}^{1/2} dz_h \exp(i\delta z_e - \gamma |z_e - z_h|) (1 + \gamma |z_e - z_h|) \cos^2(\pi z_e) \cos^2(\pi z_h), \quad (2.23)$$

and the explicit expression of  $G$  is given in the Appendix. Consequently, one obtains

$$H_{1s}(Q_{||}, Q_z) = \frac{4\pi N_n^2 L_z^2}{\alpha^2(4+b^2)^{3/2}} G((4+b^2)^{1/2} \beta L_z, Q_z L_z), \quad (2.24)$$

with  $b = |Q_{||}|/\alpha$ .

Let us now determine the normalization constant  $N_n$  in (2.16). The quasi-two-dimensional exciton state given by (2.1) is normalized as

$$\begin{aligned} 1 = \langle \lambda, \mathbf{K}_{||} | \lambda, \mathbf{K}_{||} \rangle &= \frac{v_0^2}{L^2} \sum_{\mathbf{r}_e, \mathbf{r}_h} |F_\lambda(\mathbf{r}_e || - \mathbf{r}_h ||, z_e, z_h)|^2 \\ &= \frac{1}{L^2} \int d^3 r_e \int d^3 r_h |F_\lambda(\mathbf{r}_e || - \mathbf{r}_h ||, z_e, z_h)|^2, \end{aligned} \quad (2.25)$$

where the discrete sum is converted into an integral by (2.4). Substituting the variational envelope function (2.16), it is calculated as

$$\begin{aligned} 1 &= N_n^2 \int d^2 r_{||} \int_{-L_z/2}^{L_z/2} dz_e \int_{-L_z/2}^{L_z/2} dz_h \exp\{-2[\alpha^2 r_{||}^2 + \beta^2 (z_e - z_h)^2]^{1/2}\} \cos^2\left[\frac{\pi z_e}{L_z}\right] \cos^2\left[\frac{\pi z_h}{L_z}\right] \\ &= 2\pi N_n^2 \int_0^\infty dr r \int_{-L_z/2}^{L_z/2} dz_e \int_{-L_z/2}^{L_z/2} dz_h \exp\{-2[\alpha^2 r^2 + \beta^2 (z_e - z_h)^2]^{1/2}\} \cos^2\left[\frac{\pi z_e}{L_z}\right] \cos^2\left[\frac{\pi z_h}{L_z}\right]. \end{aligned} \quad (2.26)$$

By use of the partial integration, the  $r$  integration can be performed as

$$\int_0^\infty dr r \exp[-2(\alpha^2 r^2 + \Delta^2)^{1/2}] = e^{-2|\Delta|} (1 + 2|\Delta|) / 4\alpha^2, \quad (2.27)$$

where  $\Delta$  is independent of  $r$ . Then the normalization condition is reduced to

$$1 = \frac{\pi N_n^2 L_z^2}{2\alpha^2} \int_{-1/2}^{1/2} dz_e \int_{-1/2}^{1/2} dz_h (1 + 2\beta L_z |z_e - z_h|) \exp(-2\beta L_z |z_e - z_h|) \cos^2(\pi z_e) \cos^2(\pi z_h), \quad (2.28)$$

where the variables are made nondimensional. Let us introduce an integral  $I(\gamma)$  defined by

$$I(\gamma) = \frac{1}{2} \int_{-1/2}^{1/2} dz_e \int_{-1/2}^{1/2} dz_h (1 + \gamma |z_e - z_h|) e^{-\gamma |z_e - z_h|} \cos^2(\pi z_e) \cos^2(\pi z_h), \quad (2.29)$$

whose explicit expression is given in the Appendix. Finally, the normalization condition becomes

$$1 = \pi N_n^2 L_z^2 I(2\beta L_z) / \alpha^2, \quad (2.30)$$

and the normalization constant  $N_n$  is determined as

$$N_h = \frac{\alpha}{L_z [\pi I (2\beta L_z)]^{1/2}}. \quad (2.31)$$

Summarizing all the results, the quasi-two-dimensional exciton-phonon interaction for the deformation-potential coupling is obtained as

$$\begin{aligned} H_{\text{ex-ph}}^{\text{DF (Q2D)}} = & \frac{1}{2} \sum_{\mathbf{K}_{||}, \mathbf{K}'_{||}, q_z} \left[ \frac{\hbar [(\mathbf{K}_{||} - \mathbf{K}'_{||})^2 + q_z^2]^{1/2}}{2\rho\mu V} \right]^{1/2} \\ & \times \left[ \frac{D_c G((4+b_h^2)^{1/2}\beta L_z, q_z L_z)}{[1+(b_h/2)^2]^{3/2}} - \frac{D_v G((4+b_e^2)^{1/2}\beta L_z, q_z L_z)}{[1+(b_e/2)^2]^{3/2}} \right] / I(2\beta L_z) \\ & \times |1s, \mathbf{K}'_{||}\rangle \langle 1s, \mathbf{K}_{||}| (b_{\mathbf{K}'_{||}-\mathbf{K}_{||}, q_z} + b_{\mathbf{K}_{||}-\mathbf{K}'_{||}, -q_z}^\dagger), \end{aligned} \quad (2.32)$$

with

$$b_h = \alpha_h |\mathbf{K}_{||} - \mathbf{K}'_{||}| / \alpha, \quad b_e = \alpha_e |\mathbf{K}_{||} - \mathbf{K}'_{||}| / \alpha,$$

where  $\alpha_e$  and  $\alpha_h$  are defined in (2.7) and  $\alpha$  and  $\beta$  are the variational parameters in (2.16). This expression is rather complicated, and thus it is instructive to look into the expression under a few limiting situations. When the QW thickness  $L_z$  is zero, namely in the extremely two-dimensional case,  $H_{\text{ex-ph}}^{\text{DF (Q2D)}}$  may be simplified to

$$\begin{aligned} H_{\text{ex-ph}}^{\text{DF (2D)}} = & \lim_{L_z \rightarrow 0} H_{\text{ex-ph}}^{\text{DF (Q2D)}} = \sum_{\mathbf{K}_{||}, \mathbf{K}'_{||}} \left[ \frac{\hbar |\mathbf{K}_{||} - \mathbf{K}'_{||}|}{2\rho\mu S} \right]^{1/2} \left[ \frac{D_c}{[1+(b_h/2)^2]^{3/2}} - \frac{D_v}{[1+(b_e/2)^2]^{3/2}} \right] \\ & \times |1s, \mathbf{K}'_{||}\rangle \langle 1s, \mathbf{K}_{||}| (b_{\mathbf{K}'_{||}-\mathbf{K}_{||}} + b_{\mathbf{K}_{||}-\mathbf{K}'_{||}}^\dagger), \end{aligned} \quad (2.33)$$

where the component  $q_z$  of the phonon wave vector is set equal to zero, the quantization volume  $V$  is replaced by the quantization area  $S$ , and use is made of the relation

$$G(0,0) = 2I(0) = \frac{1}{4}. \quad (2.34)$$

Secondly, let us consider the three-dimensional limit where  $L_z$  becomes infinite. Since in this case there is no preferential spatial direction,  $q_z$  is set equal to zero and the subscript  $||$  on  $\mathbf{K}$  is dropped. It is seen that

$$G(\gamma,0) = 2I(\gamma), \quad (2.35)$$

and the limiting form of (2.29) is given as

$$\lim_{\gamma \rightarrow \infty} I(\gamma) = 3/4\gamma. \quad (2.36)$$

Then, when the QW thickness  $L_z$  is infinite, i.e., in the three-dimensional case,  $H_{\text{ex-ph}}^{\text{DF (Q2D)}}$  may be simplified to

$$\begin{aligned} H_{\text{ex-ph}}^{\text{DF (3D)}} = & \lim_{L_z \rightarrow \infty} H_{\text{ex-ph}}^{\text{DF (Q2D)}} = \sum_{\mathbf{K}, \mathbf{K}'} \left[ \frac{\hbar |\mathbf{K} - \mathbf{K}'|}{2\rho\mu V} \right]^{1/2} \\ & \times \left[ \frac{D_c}{[1+(b_h/2)^2]^2} - \frac{D_v}{[1+(b_e/2)^2]^2} \right] |1s, \mathbf{K}'\rangle \langle 1s, \mathbf{K}| (b_{\mathbf{K}'-\mathbf{K}} + b_{\mathbf{K}-\mathbf{K}'}^\dagger). \end{aligned} \quad (2.37)$$

This is exactly the well-known result for the three-dimensional exciton.<sup>14</sup> Comparing (2.33) and (2.37), it is found that the most striking difference between the two- and three-dimensional cases consists in the power law in the second set of large parentheses. For the long-wavelength phonons, this difference may not be significant since the quantities in the second sets of large parentheses of (2.33) and (2.37) are both essentially  $D_c - D_v$ . On the other hand, when the short-wavelength phonons are concerned, the difference in the power law will lead to a significant difference in the optical and transport properties.

So far, the deformation-potential coupling has been discussed exclusively. However, it is known that the contribution from the piezoelectric coupling is not negligible in GaAs. The piezoelectric coupling arises from the longitudinal electric field induced by the strain field associated with acoustic-phonon modes. The piezoelectric electron-phonon interaction Hamiltonian for the zinc-blende type crystal with  $T_d$  symmetry is given by<sup>16</sup>

$$H_{\text{ex-ph}}^{\text{PZ}} = \sum_{\mathbf{k}, \mathbf{q}, \sigma} \frac{8\pi e e_{14}}{\epsilon_0 q^2} \left[ \frac{\hbar}{2\rho\omega_\sigma(\mathbf{q})V} \right]^{1/2} (\xi_x q_y q_z + \xi_y q_x q_z + \xi_z q_x q_y) (a_{c, \mathbf{k}+\mathbf{q}}^\dagger a_{c, \mathbf{k}} + a_{v, \mathbf{k}+\mathbf{q}}^\dagger a_{v, \mathbf{k}}) (b_{\mathbf{q}\sigma} + b_{-\mathbf{q}\sigma}^\dagger), \quad (2.38)$$

where  $e_{14}$ ,  $\epsilon_0$ , and  $\xi_\alpha$  are the piezoelectric constant, the longitudinal dielectric constant without the piezoelectric contribution, and the  $\alpha$ th component of the phonon polarization vector, respectively, and the subscript  $\sigma$  specifies the longitudinal-acoustic (LA) or transverse-acoustic (TA) phonon mode. The Cartesian components in (2.38) are referred to with respect to the cubic crystallographic axes of the zinc-blende type crystal. The derivation of the piezoelectric exciton-phonon interaction for the quasi-two-dimensional exciton is straightforward. Repeating the same procedure as in (2.10)–(2.15), one obtains

$$H_{\text{ex-ph}}^{\text{PZ(Q2D)}} = \frac{4\pi e e_{14}}{\epsilon_0} \sum_{\mathbf{K}_\parallel, \mathbf{K}'_\parallel, q_z, \sigma} \left[ \frac{\hbar}{2\rho u_\sigma V (|\mathbf{K}_\parallel - \mathbf{K}'_\parallel|^2 + q_z^2)^{5/2}} \right]^{1/2} \\ \times [\xi_x (\mathbf{K}'_\parallel - \mathbf{K}_\parallel)_y q_z + \xi_y (\mathbf{K}'_\parallel - \mathbf{K}_\parallel)_x q_z + \xi_z (\mathbf{K}'_\parallel - \mathbf{K}_\parallel)_x (\mathbf{K}'_\parallel - \mathbf{K}_\parallel)_y] \\ \times \left[ \frac{G((4+b_h^2)^{1/2} \beta L_z, q_z L_z)}{[1+(b_h/2)^2]^{3/2}} - \frac{G((4+b_e^2)^{1/2} \beta L_z, q_z L_z)}{[1+(b_e/2)^2]^{3/2}} \right] / I(2\beta L_z) \\ \times |1s, \mathbf{K}'_\parallel\rangle \langle 1s, \mathbf{K}_\parallel| (b_{\mathbf{K}'_\parallel - \mathbf{K}_\parallel, q_z, \sigma} + b_{\mathbf{K}_\parallel - \mathbf{K}'_\parallel, -q_z, \sigma}^\dagger), \quad (2.39)$$

where the functions  $G$  and  $I$  are the same as in (2.32), and  $b_e$  and  $b_h$  are given under (2.32). In this case the factor within the small square brackets of (2.39) gives rise to the anisotropic effect. If the extremely two-dimensional case is considered and  $q_z$  is set equal to zero, the anisotropic factor becomes  $\xi_x (\mathbf{K}'_\parallel - \mathbf{K}_\parallel)_x (\mathbf{K}'_\parallel - \mathbf{K}_\parallel)_y$ , which simply implies that the piezoelectric coupling is possible only with the TA-phonon mode having the polarization vector in the  $z$  direction. On the other hand, in the limit  $L_z = \infty$  expression (2.39) exactly reproduces the well-known result<sup>16</sup> for the three-dimensional exciton as

$$H_{\text{ex-ph}}^{\text{PZ(3D)}} = \lim_{L_z \rightarrow \infty} H_{\text{ex-ph}}^{\text{PZ(Q2D)}} = \sum_{\mathbf{K}, \mathbf{q}, \sigma} \frac{8\pi e e_{14}}{\epsilon_0 q^2} \left[ \frac{\hbar}{2\rho\omega_\sigma(\mathbf{q})V} \right]^{1/2} (\xi_x q_y q_z + \xi_y q_x q_z + \xi_z q_x q_y) \\ \times \left[ \frac{1}{[1+(\alpha_h |\mathbf{q}|/2\alpha)^2]^2} - \frac{1}{[1+(\alpha_e |\mathbf{q}|/2\alpha)^2]^2} \right] |1s, \mathbf{K} + \mathbf{q}\rangle \langle 1s, \mathbf{K}| (b_{\mathbf{q}\sigma} + b_{-\mathbf{q}\sigma}^\dagger). \quad (2.40)$$

Thus, Eq. (2.32) for  $H_{\text{ex-ph}}^{\text{DF(Q2D)}}$  and Eq. (2.39) for  $H_{\text{ex-ph}}^{\text{PZ(Q2D)}}$  give quite general expressions of the exciton-phonon interaction for the quasi-two-dimensional exciton that reduce smoothly (as  $L_z \rightarrow \infty$ ) to those for the three-dimensional exciton.

### III. KINETIC-ENERGY RELAXATION OF QUASI-TWO-DIMENSIONAL EXCITONS

We now discuss the kinetic-energy relaxation on the dispersion curve of the quasi-two-dimensional exciton, adapting Conwell's argument,<sup>17</sup> which was originally developed for the three-dimensional case. It will be shown that the kinetic-energy relaxation is too fast to explain the experimentally observed energy relaxation rate. The quasi-two-dimensional exciton state with a total wave vector  $\mathbf{K}_\parallel$  is denoted by  $|K_\parallel\rangle$ , assuming the lowest  $1s$  state for the electron-hole internal motion. The matrix element of the exciton-phonon interaction derived in Sec. II will be denoted by  $H_{\text{ex-ph}}(\mathbf{Q}_\parallel, \mathbf{Q}_z)$  for the phonon wave

vector  $\mathbf{Q}$  defined by  $\mathbf{Q} = (\mathbf{Q}_\parallel, \mathbf{Q}_z)$ . The increasing rate of the number of phonons with wave vector  $(\mathbf{Q}_\parallel, \mathbf{Q}_z)$  due to phonon emission by excitons is given by

$$\frac{2\pi}{\hbar} \sum_{\mathbf{K}_\parallel} |H_{\text{ex-ph}}(\mathbf{Q}_\parallel, \mathbf{Q}_z)|^2 (1+n_{\mathbf{Q}}) f(\mathbf{K}_\parallel + \mathbf{Q}_\parallel) \\ \times \delta(E(\mathbf{K}_\parallel + \mathbf{Q}_\parallel) - E(\mathbf{K}_\parallel) - \hbar\omega_{\mathbf{Q}}), \quad (3.1)$$

where  $n$  and  $f$  are the phonon occupation number and the exciton distribution function, respectively,  $E(\mathbf{K}_\parallel)$  the parabolic two-dimensional exciton energy, and  $\hbar\omega_{\mathbf{Q}}$  the energy of acoustic phonon with wave vector  $\mathbf{Q}$ . Similarly, the decreasing rate of the number of phonons with wave vector  $(\mathbf{Q}_\parallel, \mathbf{Q}_z)$  is given by

$$\frac{2\pi}{\hbar} \sum_{\mathbf{K}_{\parallel}} |H_{\text{ex-ph}}(\mathbf{Q}_{\parallel}, Q_z)|^2 n_{Q'} f(\mathbf{K}_{\parallel}) \times \delta(E(\mathbf{K}_{\parallel}) - E(\mathbf{K}_{\parallel} + \mathbf{Q}_{\parallel}) + \hbar\omega_Q). \quad (3.2)$$

The common argument of the  $\delta$  functions in (3.1) and (3.2) can be written as

$$E(\mathbf{K}_{\parallel} + \mathbf{Q}_{\parallel}) - E(\mathbf{K}_{\parallel}) - \hbar\omega_Q = \hbar^2(2\mathbf{K}_{\parallel} \cdot \mathbf{Q}_{\parallel} + Q_{\parallel}^2)/2M - \hbar\omega_Q, \quad (3.3)$$

$$\frac{dN_Q}{dt} = \frac{4\pi}{\hbar} |H_{\text{ex-ph}}(\mathbf{Q}_{\parallel}, Q_z)|^2 \frac{L^2}{(2\pi)^2} \int_{K_Q}^{\infty} dK_{\parallel} K_{\parallel} \int_0^{\pi} d\theta \frac{M\delta(\theta - \theta_0)}{\hbar^2 |\mathbf{K}_{\parallel} \cdot \mathbf{Q}_{\parallel} \sin\theta|} [(1+n_Q)f(\mathbf{K}_{\parallel} + \mathbf{Q}_{\parallel}) - n_Q f(\mathbf{K}_{\parallel})], \quad (3.5)$$

where  $\theta_0$  is the angle between  $\mathbf{K}_{\parallel}$  and  $\mathbf{Q}_{\parallel}$  satisfying the energy-conservation condition and  $L$  is the linear dimension of quantization volume defined in Sec. II. In the following let us assume that

$$Mu/\hbar \ll |\mathbf{Q}_{\parallel}|/2, \quad (3.6)$$

where  $u$  is the sound velocity of acoustic-phonon modes and rewrite the integral over  $\mathbf{K}_{\parallel}$  in (3.5) with that over the energy defined by  $E = \hbar^2 K_{\parallel}^2/2M$ . Then it is calculated as

$$\frac{dN_Q}{dt} = \frac{4\pi}{\hbar} \frac{L^2}{(2\pi)^2} \left[ \frac{M}{\hbar^2} \right]^2 \frac{|H_{\text{ex-ph}}(\mathbf{Q}_{\parallel}, Q_z)|^2}{|\mathbf{Q}_{\parallel}|} \frac{\hbar}{\sqrt{2M}} \times \int_{E_Q}^{\infty} dE [(1+n_Q)f(E + \hbar\omega_Q) - n_Q f(E)] / \sqrt{E} |\sin\theta_0|, \quad (3.7)$$

with

$$E_Q = \hbar^2 K_Q^2/2M \cong \hbar^2 Q_{\parallel}^2/8M.$$

By the inequality (3.6), one may approximate as

$$\cos\theta_0 = (2M\omega_Q/\hbar - Q_{\parallel}^2)/2 |\mathbf{K}_{\parallel} \cdot \mathbf{Q}_{\parallel}| \cong -|\mathbf{Q}_{\parallel}|/2 |\mathbf{K}_{\parallel}|, \quad (3.8)$$

and one has

$$|\sin\theta_0| \cong (1 - E_Q/E_K)^{1/2}, \quad (3.9)$$

where  $E_K$  is defined by  $\hbar^2 K_{\parallel}^2/2M$ . Equation (3.7) is the general expression for the increasing rate of phonon numbers. In the following, the exciton distribution function is assumed to follow the Boltzmann statistics, namely

$$f(E) = f_0 \exp(-\beta_e E), \quad (3.10)$$

with

$$\beta_e = 1/k_B T_e,$$

where  $T_e$  is the effective temperature of excitons and  $f_0$  is some constant. In fact, the experimentally determined exciton distribution function can be described by the Boltzmann statistics fairly well, as will be shown in Sec. VII. This situation may be attained by frequent collisions among excitons. Then, calculating the integral

where  $M$  is the exciton translational mass. The energy-conservation condition leads to the condition that the magnitude of exciton wave vector  $\mathbf{K}_{\parallel}$  must satisfy

$$|\mathbf{K}_{\parallel}| \geq |2M\omega_Q/\hbar - Q_{\parallel}^2|/2 |\mathbf{Q}_{\parallel}| = K_Q, \quad (3.4)$$

where  $K_Q$  is defined by the right-hand side. Then the total increasing rate of the number of phonons with wave vector  $(\mathbf{Q}_{\parallel}, Q_z)$  is calculated as

$$\frac{dN_Q}{dt} = \frac{4\pi}{\hbar} |H_{\text{ex-ph}}(\mathbf{Q}_{\parallel}, Q_z)|^2 \frac{L^2}{(2\pi)^2} \int_{K_Q}^{\infty} dK_{\parallel} K_{\parallel} \int_0^{\pi} d\theta \frac{M\delta(\theta - \theta_0)}{\hbar^2 |\mathbf{K}_{\parallel} \cdot \mathbf{Q}_{\parallel} \sin\theta|} [(1+n_Q)f(\mathbf{K}_{\parallel} + \mathbf{Q}_{\parallel}) - n_Q f(\mathbf{K}_{\parallel})], \quad (3.5)$$

$$\int_{E_Q}^{\infty} dE \frac{e^{-\beta_e E}}{\sqrt{E} (1 - E_Q/E)^{1/2}} = \left[ \frac{\pi}{\beta_e} \right]^{1/2} e^{-\beta_e E_Q}, \quad (3.11)$$

one obtains

$$\frac{dN_Q}{dt} = \frac{4\pi}{\hbar} \frac{L^2}{(2\pi)^2} \left[ \frac{M}{\hbar^2} \right]^2 \frac{\hbar\sqrt{\pi}}{(2M\beta_e)^{1/2}} \frac{|H_{\text{ex-ph}}(\mathbf{Q}_{\parallel}, Q_z)|^2}{|\mathbf{Q}_{\parallel}|} \times f_0 e^{-\beta_e E_Q} [(1+n_Q) \exp(-\beta_e \hbar\omega_Q) - n_Q]. \quad (3.12)$$

The average energy relaxation rate of excitons is given by

$$\left\langle \frac{dE}{dt} \right\rangle = -\frac{1}{N} \sum_Q \hbar\omega_Q \frac{dN_Q}{dt}, \quad (3.13)$$

where  $N$  is the total number of excitons defined by

$$N = \sum_{\mathbf{K}_{\parallel}} f(E(\mathbf{K}_{\parallel})) = \frac{f_0 M L^2}{2\pi\beta_e \hbar^2}. \quad (3.14)$$

The explicit expression of (3.13) is written as

$$\left\langle \frac{dE}{dt} \right\rangle = -\frac{(2\pi M\beta_e)^{1/2}}{\hbar^2} \times \sum_Q \frac{|H_{\text{ex-ph}}(\mathbf{Q}_{\parallel}, Q_z)|^2}{|\mathbf{Q}_{\parallel}|} \hbar\omega_Q \times e^{-\beta_e E_Q} [(1+n_Q) \exp(-\beta_e \hbar\omega_Q) - n_Q]. \quad (3.15)$$

To obtain a more explicit result, the deformation-potential coupling derived in Sec. II will be substituted for the exciton-phonon interaction  $H_{\text{ex-ph}}$ . Since the function  $G$  in (2.32) is a slowly varying function with respect to  $|\mathbf{Q}_{\parallel}|$  and  $Q_z$  for the physically important range of parameters, one may safely set  $Q_z = 0$ , i.e.,  $|\mathbf{Q}_{\parallel}| = |\mathbf{Q}|$  in  $G$  to obtain

$$H_{\text{ex-ph}}^{\text{DF}}(Q_{\parallel}, Q_z) \cong \left[ \frac{\hbar |Q|}{2\rho u V} \right]^{1/2} \left[ \frac{D_c}{[1+(\alpha_h |Q|/2\alpha)^2]^{3/2}} - \frac{D_v}{[1+(\alpha_e |Q|/2\alpha)^2]^{3/2}} \right] \\ \cong \left[ \frac{\hbar |Q|}{2\rho u V} \right]^{1/2} (D_c - D_v), \quad (3.16)$$

where to simplify the algebraic manipulations, it is supposed that  $b_h$  and  $b_e$  in (2.32) are small, and that  $(4+b_h^2)^{1/2}$  and  $(4+b_e^2)^{1/2}$  are nearly equal to 2. Substituting this expression into (3.15), one obtains

$$\left\langle \frac{dE}{dt} \right\rangle = -(2\pi M \beta_e)^{1/2} \frac{(D_c - D_v)^2}{4\pi^2 \rho} \\ \times \int_0^\infty dQ Q^3 e^{-\beta_e E_Q} \\ \times [(1+n_Q) \exp(-\beta_e \hbar \omega_Q) - n_Q], \quad (3.17)$$

with

$$E_Q = \hbar^2 Q^2 / 8M.$$

By using the experimental data

$$T_e \cong 20 \text{ K} \quad \text{and} \quad T_L = 4.2 \text{ K},$$

where  $T_L$  is the lattice temperature and, choosing the material parameters of GaAs given in detail in Sec. VII, the energy relaxation rate is calculated as

$$\left\langle \frac{dE}{dt} \right\rangle \cong 20 \times 10^6 \text{ eV/s}. \quad (3.18)$$

This value is 1 order of magnitude larger than the observed value of  $(2-3) \times 10^6$  eV/s. Furthermore, it can be shown that the effective temperature of excitons decreases from 20 to 4.2 K within several tens of picoseconds. Since there is an additional relaxation mechanism due to the piezoelectric coupling, the theoretical value of the energy relaxation rate becomes larger and the discrepancy increases. Thus it is concluded that the observed slow energy relaxation cannot be explained by the kinetic-energy relaxation on the dispersion curve of the quasi-two-dimensional exciton. When the excitons relax on the two-dimensional dispersion curve and accumulate on the low-energy portion of the density of states, the excitons become more and more immobile and can be considered

as distributed among the energetically local minimum sites which are induced by the well-thickness fluctuation in the lateral direction of a QW. Under such a situation the energy relaxation occurs through the exciton migration in search of the lower-energy sites, and the exciton system eventually approaches the energetically global minimum state. This process of energy relaxation is considered slow compared to the kinetic-energy relaxation and, in fact, explains quantitatively the experimental energy relaxation rate.

#### IV. ONE-PHONON-ASSISTED TRANSFER OF LOCALIZED QUASI-TWO-DIMENSIONAL EXCITONS

Let us now consider the quasi-two-dimensional exciton transfer among localized sites, such as the islandlike structures in a QW that are induced by the well-thickness fluctuation in the lateral direction. A general theory will be developed without recourse to the details of the localized sites, namely the microscopic structure of the disorder. In the process of exciton transfer the energy mismatch of excitons is compensated for by acoustic phonons. At low temperatures only the one-phonon-assisted process needs to be taken into account, since the relevant energy mismatch is less than 1 meV and rather small. The exciton state localized at site  $\mathbf{R}_a$  will be denoted by  $|\mathbf{R}_a\rangle$ , assuming the lowest  $1s$  state for the electron-hole internal motion. The relevant Hamiltonians for the phonon-assisted exciton transfer are the exciton-phonon interaction Hamiltonian denoted by  $H_{\text{ex-ph}}$  and the intersite transfer Hamiltonian denoted by  $H_{\text{ss}}$ . Then there are three possibilities for the exciton transfer from site  $\mathbf{R}_a$  to site  $\mathbf{R}_b$ , namely

$$(a) |\mathbf{R}_a; n_Q\rangle \xrightarrow{H_{\text{ex-ph}}} |\mathbf{R}_b; n_Q \pm 1\rangle, \quad (4.1)$$

$$(b) |\mathbf{R}_a; n_Q\rangle \xrightarrow{H_{\text{ex-ph}}} |\mathbf{R}_a; n_Q \pm 1\rangle \xrightarrow{H_{\text{ss}}} |\mathbf{R}_b; n_Q \pm 1\rangle, \quad (4.2)$$

$$(c) |\mathbf{R}_a; n_Q\rangle \xrightarrow{H_{\text{ss}}} |\mathbf{R}_b; n_Q\rangle \xrightarrow{H_{\text{ex-ph}}} |\mathbf{R}_b; n_Q \pm 1\rangle, \quad (4.3)$$

where  $n_Q$  represents the occupation number of phonons relevant to the exciton transfer. Term (a) arises from the first-order perturbation process with respect to  $H_{\text{ex-ph}}$ , whereas terms (b) and (c) are the contributions from the second-order perturbation process using both  $H_{\text{ex-ph}}$  and  $H_{\text{ss}}$  once for each.<sup>18</sup> As will be seen later, term (a) is possible through the overlap of exciton wave functions and is short ranged in nature, while terms (b) and (c) are effective over a long range, in general. The transition amplitude of the exciton transfer for each process in (4.1)–(4.3) is given as follows:

$$(a) \langle \mathbf{R}_b; n_Q \pm 1 | H_{\text{ex-ph}} | \mathbf{R}_a; n_Q \rangle, \quad (4.4)$$

$$(b) \frac{\langle \mathbf{R}_b; n_Q \pm 1 | H_{\text{ss}} | \mathbf{R}_a; n_Q \pm 1 \rangle \langle \mathbf{R}_a; n_Q \pm 1 | H_{\text{ex-ph}} | \mathbf{R}_a; n_Q \rangle}{\mp \hbar \omega_Q}, \quad (4.5)$$

$$(c) \frac{\langle \mathbf{R}_b; n_Q \pm 1 | H_{\text{ex-ph}} | \mathbf{R}_b; n_Q \rangle \langle \mathbf{R}_b; n_Q | H_{\text{ss}} | \mathbf{R}_a; n_Q \rangle}{\pm \hbar \omega_Q}, \quad (4.6)$$

where  $\omega_Q$  is the phonon frequency with wave vector  $Q$ . The intersite exciton transfer Hamiltonian  $H_{ex}$  arises from the electron-electron interaction Hamiltonian, and the matrix element is independent of the phonon state. Thus it can be written as

$$J(\langle \mathbf{R}_a - \mathbf{R}_b |) = \langle \mathbf{R}_b | H_{ex} | \mathbf{R}_a \rangle. \quad (4.7)$$

The explicit calculation of  $J(\mathbf{R})$  will be given in Sec. V. To calculate the matrix element of  $H_{ex-ph}$ , the localized exciton state must be specified more explicitly.

The localized quasi-two-dimensional exciton state can be represented as

$$|\mathbf{R}_a\rangle = v_0 \sum_{\mathbf{r}_e, \mathbf{r}_h} G(\mathbf{R}_{||} - \mathbf{R}_a) F_{1s}(\mathbf{r}_{e||} - \mathbf{r}_{h||}, z_e, z_h) \times a_{c\mathbf{r}_e}^\dagger a_{v\mathbf{r}_h} |0\rangle, \quad (4.8)$$

where the  $1s$  exciton envelope function  $F_{1s}$  is given in (2.16) and the function  $G$  describes the two-dimensional localization of the exciton center of mass  $\mathbf{R}$  defined by (2.2). The notations  $v_0$ ,  $a_{c\mathbf{r}_e}$ , and  $a_{v\mathbf{r}_h}$  are given in Sec. II. The function  $G$  is normalized as

$$\int d^2 R_{||} |G(\mathbf{R}_{||} - \mathbf{R}_a)|^2 = 1, \quad (4.9)$$

$$\begin{aligned} |\mathbf{R}_a\rangle &= v_0 \sum_{\mathbf{r}_e, \mathbf{r}_h} G(\mathbf{R}_{||} - \mathbf{R}_a) F_{1s}(\mathbf{r}_{e||} - \mathbf{r}_{h||}, z_e, z_h) a_{c\mathbf{r}_e}^\dagger a_{v\mathbf{r}_h} |0\rangle \\ &= \int d^2 K_{||} g(\mathbf{K}_{||}, \mathbf{R}_a) v_0 \sum_{\mathbf{r}_e, \mathbf{r}_h} e^{i\mathbf{K}_{||} \cdot \mathbf{R}_{||}} F_{1s}(\mathbf{r}_{e||} - \mathbf{r}_{h||}, z_e, z_h) a_{c\mathbf{r}_e}^\dagger a_{v\mathbf{r}_h} |0\rangle \\ &= L \int d^2 K_{||} g(\mathbf{K}_{||}, \mathbf{R}_a) |\mathbf{K}_{||}\rangle. \end{aligned} \quad (4.14)$$

where use is made of (2.1). Thus, evidently, the localized exciton state consists of the superposition of extended exciton states. The explicit expression of  $g$  is given as follows: (1) Gaussian case,

$$g(\mathbf{K}_{||}, \mathbf{R}_a) = \frac{\xi}{2\pi\sqrt{\pi}} \exp(-i\mathbf{K}_{||} \cdot \mathbf{R}_a - \xi^2 K_{||}^2 / 2), \quad (4.15)$$

and (2) exponential case,

$$\langle \mathbf{R}_b; n_Q \pm 1 | H_{ex-ph} | \mathbf{R}_a; n_Q \rangle = L^2 \int d^2 K'_{||} \int d^2 K_{||} g^*(\mathbf{K}'_{||}, \mathbf{R}_b) g(\mathbf{K}_{||}, \mathbf{R}_a) \langle \mathbf{K}'_{||}; n_Q \pm 1 | H_{ex-ph} | \mathbf{K}_{||}; n_Q \rangle. \quad (4.18)$$

The matrix element on the right-hand side is taken between the two-dimensionally extended exciton states and can be written as

$$\langle \mathbf{K}'_{||}; n_Q \pm 1 | H_{ex-ph} | \mathbf{K}_{||}; n_Q \rangle = \delta_{\mathbf{K}'_{||} \pm \mathbf{Q}_{||}, \mathbf{K}_{||}} \langle \mathbf{K}'_{||} | H_{ex-ph} | \mathbf{K}_{||} \rangle_Q = \frac{(2\pi)^2}{L^2} \delta^{(2)}(\mathbf{K}'_{||} \pm \mathbf{Q}_{||} - \mathbf{K}_{||}) H_{ex-ph}(\mathbf{Q}_{||}, \mathbf{Q}_z), \quad (4.19)$$

where in the second equality the Kronecker  $\delta$  function is changed to the Dirac  $\delta$  function and a factor related to the phonon absorption or emission is not written explicitly by incorporating the factor in  $H_{ex-ph}(\mathbf{Q}_{||}, \mathbf{Q}_z)$ . As shown in Sec. II, the matrix element  $\langle \mathbf{K}'_{||} | H_{ex-ph} | \mathbf{K}_{||} \rangle_Q$  depends only on the phonon momentum  $Q$  and thus is written as  $H_{ex-ph}(\mathbf{Q}_{||}, \mathbf{Q}_z)$ . Then, in the case of Gaussian localization one obtains

and thus the localized exciton state  $|\mathbf{R}_a\rangle$  is normalized correctly

$$\langle \mathbf{R}_a | \mathbf{R}_a \rangle = 1. \quad (4.10)$$

The functional form of  $G$  depends on the details of microscopic configuration of the localized state. Until now, there has been no systematic study of this subject. However, the dynamical properties of the system, such as the energy relaxation, are not expected to be very sensitive to the microscopic details of localization, but may be characterized by only a few parameters, such as the localization length. In this paper two typical cases of exciton localization will be examined, namely (1) the Gaussian case,

$$G(\mathbf{R}_{||}) = \frac{1}{\sqrt{\pi\xi}} \exp(-R_{||}^2 / 2\xi^2), \quad (4.11)$$

and (2) the exponential case,

$$G(\mathbf{R}_{||}) = \frac{1}{\sqrt{2\pi\xi}} \exp(-|\mathbf{R}_{||}| / 2\xi), \quad (4.12)$$

where  $\xi$  is the characteristic localization length. Then, introducing the two-dimensional Fourier transform of the localization function by

$$G(\mathbf{R}_{||} - \mathbf{R}_a) = \int d^2 K_{||} e^{i\mathbf{K}_{||} \cdot \mathbf{R}_{||}} g(\mathbf{K}_{||}, \mathbf{R}_a), \quad (4.13)$$

one obtains

$$\begin{aligned} g(\mathbf{K}_{||}, \mathbf{R}_a) &= \frac{e^{-i\mathbf{K}_{||} \cdot \mathbf{R}_a}}{2\pi\sqrt{2\pi\xi}} \int_0^\infty dR R J_0(K_{||}R) \exp(-R/2\xi) \\ &= \frac{e^{-i\mathbf{K}_{||} \cdot \mathbf{R}_a}}{\pi\sqrt{2\pi}} \frac{2\xi}{[1 + (2\xi K_{||})^2]^{3/2}}, \end{aligned} \quad (4.16)$$

where  $(K_{||} = |\mathbf{K}_{||}|)$ ,  $J_0(x)$  is the zeroth-order Bessel function, and the following formula<sup>15</sup> is used:

$$\int_0^\infty dx x e^{-ax} J_0(bx) = \frac{a}{(a^2 + b^2)^{3/2}}. \quad (4.17)$$

The matrix element of the exciton-phonon interaction can be calculated by using the expression (4.14) as

$$\langle \mathbf{R}_b; n_Q \pm 1 | H_{\text{ex-ph}} | \mathbf{R}_a; n_Q \rangle = \exp \left[ -i \frac{\mathbf{Q}_{\parallel} \cdot (\mathbf{R}_a + \mathbf{R}_b)}{2} - \frac{\xi^2 Q_{\parallel}^2}{4} - \frac{(\mathbf{R}_a - \mathbf{R}_b)^2}{4\xi^2} \right] H_{\text{ex-ph}}(\mathbf{Q}_{\parallel}, Q_z), \quad (4.20)$$

while, in the case of exponential localization, the result is given as

$$\langle \mathbf{R}_b; n_Q \pm 1 | H_{\text{ex-ph}} | \mathbf{R}_a; n_Q \rangle = \frac{8\xi^2}{\pi} \exp[-i\mathbf{Q}_{\parallel} \cdot (\mathbf{R}_a + \mathbf{R}_b)/2] \times \int d^2K_{\parallel} \frac{\exp[i\mathbf{K}_{\parallel} \cdot (\mathbf{R}_b - \mathbf{R}_a)]}{[1 + (2\xi |\mathbf{K}_{\parallel} - \mathbf{Q}_{\parallel}/2|)^2]^{3/2} [1 + (2\xi |\mathbf{K}_{\parallel} + \mathbf{Q}_{\parallel}/2|)^2]^{3/2}} H_{\text{ex-ph}}(\mathbf{Q}_{\parallel}, Q_z). \quad (4.21)$$

Now, the transition amplitude of the exciton transfer from site  $\mathbf{R}_a$  to site  $\mathbf{R}_b$  for the case of Gaussian localization is calculated as

$$\langle \mathbf{R}_b | T | \mathbf{R}_a \rangle_Q = e^{-i\mathbf{Q}_{\parallel} \cdot (\mathbf{R}_a + \mathbf{R}_b)/2} \exp \left[ -\frac{\xi^2 Q_{\parallel}^2}{4} - \frac{(\mathbf{R}_a - \mathbf{R}_b)^2}{4\xi^2} \right] H_{\text{ex-ph}}(\mathbf{Q}_{\parallel}, Q_z) + \frac{J(|\mathbf{R}_a - \mathbf{R}_b|)}{E_a - E_b} (e^{-i\mathbf{Q}_{\parallel} \cdot \mathbf{R}_b} - e^{-i\mathbf{Q}_{\parallel} \cdot \mathbf{R}_a}) \exp \left[ -\frac{\xi^2 Q_{\parallel}^2}{4} \right] H_{\text{ex-ph}}(\mathbf{Q}_{\parallel}, Q_z). \quad (4.22)$$

The first term on the right-hand side is the contribution from process (a) in (4.1) and the second term combines the contribution from processes (b) and (c) in (4.2) and (4.3). The first term contains the Gaussian factor  $\exp[-(\mathbf{R}_a - \mathbf{R}_b)^2/4\xi^2]$  arising from the overlap integral between two localized exciton states and has a short-range character. On the other hand, the second term in (4.22) depends on the distance  $|\mathbf{R}_a - \mathbf{R}_b|$  through the function  $J(|\mathbf{R}_a - \mathbf{R}_b|)$  and the coherence factor

$$\exp(-i\mathbf{Q}_{\parallel} \cdot \mathbf{R}_b) - \exp(-i\mathbf{Q}_{\parallel} \cdot \mathbf{R}_a),$$

which are generally effective over a long range. The common factor  $\exp(-\xi^2 Q_{\parallel}^2/4)$  implies that the magnitude of the wave vector of phonons which can interact with the localized exciton is limited within a few times the inverse localization length. In the case of exponential localization, the transition amplitude shows similar features, although its expression is more complicated. When the

transition amplitude is obtained, the exciton transfer rate can be calculated by

$$T(|E_a - E_b|, |\mathbf{R}_a - \mathbf{R}_b|) = \frac{2\pi}{\hbar} \sum_{\mathbf{Q}} |\langle \mathbf{R}_b | T | \mathbf{R}_a \rangle_Q|^2 \times \delta(E_a - E_b \pm \hbar\omega_{\mathbf{Q}}). \quad (4.23)$$

In the absolute square of the transition amplitude, there appears the interference between two terms in (4.22). However, this interference term will be neglected since the relevant spatial range of the two terms is quite different and the contribution from the interference term may be small. To calculate the exciton transfer rate more explicitly, the matrix element of the intersite transfer Hamiltonian  $H_{ss}$  must be calculated. This matrix element,  $J(R)$ , will be studied in the next section.

## V. INTERSITE TRANSFER MATRIX ELEMENT FOR LOCALIZED QUASI-TWO-DIMENSIONAL EXCITONS

In this section the matrix element  $J(R)$  of the intersite transfer Hamiltonian  $H_{ss}$  is calculated, and it is shown that  $J(R)$  behaves like the dipole-dipole interaction at a distance much longer than the exciton Bohr radius and the localization length. As given in (4.8), the localized quasi-two-dimensional exciton state can be represented as

$$|\mathbf{R}_a\rangle = v_0 \sum_{\mathbf{r}_e, \mathbf{r}_h} \tilde{F}(\mathbf{r}_e, \mathbf{r}_h; \mathbf{R}_a) a_{c\mathbf{r}_e}^\dagger a_{v\mathbf{r}_h} |0\rangle = v_0 \sum_{\mathbf{r}_e, \mathbf{r}_h} G(\mathbf{R}_{\parallel} - \mathbf{R}_a) F_{1s}(\mathbf{r}_{e\parallel}, \mathbf{r}_{h\parallel}, z_e, z_h) a_{c\mathbf{r}_e}^\dagger a_{v\mathbf{r}_h} |0\rangle. \quad (5.1)$$

The intersite transfer Hamiltonian  $H_{ss}$  is given by the electron-electron interaction Hamiltonian, namely

$$H_{ss} = \frac{1}{2} \int d^3r \int d^3r' \psi^\dagger(\mathbf{r}) \psi^\dagger(\mathbf{r}') \frac{e^2}{\epsilon_0 |\mathbf{r} - \mathbf{r}'|} \psi(\mathbf{r}') \psi(\mathbf{r}), \quad (5.2)$$

where  $\epsilon_0$  and  $\psi(\mathbf{r})$  are the dielectric constant and the electron-field operator, respectively. Then the matrix element is calculated as

$$\begin{aligned} J(|\mathbf{R}_a - \mathbf{R}_b|) &= \langle \mathbf{R}_b | H_{ss} | \mathbf{R}_a \rangle \\ &= v_0^2 \sum_{\mathbf{r}'_e, \mathbf{r}'_h} \sum_{\mathbf{r}_e, \mathbf{r}_h} \tilde{F}^*(\mathbf{r}'_e, \mathbf{r}'_h; \mathbf{R}_b) \tilde{F}(\mathbf{r}_e, \mathbf{r}_h; \mathbf{R}_a) \langle 0 | a_{v\mathbf{r}'_h}^\dagger a_{c\mathbf{r}'_e} H_{ss} a_{c\mathbf{r}_e}^\dagger a_{v\mathbf{r}_h} | 0 \rangle \\ &= v_0^2 \sum_{\mathbf{r}'_e, \mathbf{r}'_h} \sum_{\mathbf{r}_e, \mathbf{r}_h} \tilde{F}^*(\mathbf{r}'_e, \mathbf{r}'_h; \mathbf{R}_b) \tilde{F}(\mathbf{r}_e, \mathbf{r}_h; \mathbf{R}_a) [V(c\mathbf{r}'_e, v\mathbf{r}_h; c\mathbf{r}_e, v\mathbf{r}'_h) - V(c\mathbf{r}'_e, v\mathbf{r}_h; v\mathbf{r}'_h, c\mathbf{r}_e)], \end{aligned} \quad (5.3)$$

with

$$V(\alpha_1 n_1, \alpha_2 n_2; \alpha_3 n_3, \alpha_4 n_4) = \frac{1}{2} \int d^3 r \int d^3 r' \phi_{\alpha_1 n_1}^*(\mathbf{r}) \phi_{\alpha_2 n_2}^*(\mathbf{r}') \frac{e^2}{\epsilon_0 |\mathbf{r} - \mathbf{r}'|} \phi_{\alpha_3 n_3}(\mathbf{r}') \phi_{\alpha_4 n_4}(\mathbf{r}), \quad (5.4)$$

where  $\phi_{\alpha n}(\mathbf{r})$  is the Wannier function of the  $\alpha$ th band at site  $n$ . When the intersite distance is longer than the localization length  $\xi$  and the two-dimensional exciton Bohr radius  $a_B^{2D}$ , i.e.,

$$|\mathbf{R}_a - \mathbf{R}_b| \gg \xi, a_B^{2D}, \quad (5.5)$$

it turns out that the exchange term, namely the first term in square brackets on the right-hand side of (5.3), is dominant. Then, by using the usual multipole expansion of the Coulomb interaction,<sup>19</sup> one obtains

$$J(|\mathbf{R}_a - \mathbf{R}_b|) = \frac{v_0^2}{2 |\mathbf{R}_a - \mathbf{R}_b|^3} \mu^\dagger (1 - 3\mathbf{n} \cdot \mathbf{n}) \mu \sum_{\mathbf{r}_e, \mathbf{r}_h} \sum_{\mathbf{r}'_e, \mathbf{r}'_h} \delta_{\mathbf{r}_e, \mathbf{r}_h} \delta_{\mathbf{r}'_e, \mathbf{r}'_h} \tilde{F}^*(\mathbf{r}'_e, \mathbf{r}'_h; \mathbf{R}_b) \tilde{F}(\mathbf{r}_e, \mathbf{r}_h; \mathbf{R}_a), \quad (5.6)$$

with

$$\mu = e \int d^3 r \phi_{\nu \mathbf{r}_e}^*(\mathbf{r}) (\mathbf{r} - \mathbf{r}_e) \phi_{c \mathbf{r}_e}(\mathbf{r}) \quad \text{and} \quad \mathbf{n} = (\mathbf{R}_a - \mathbf{R}_b) / |\mathbf{R}_a - \mathbf{R}_b|, \quad (5.7)$$

where the Wannier functions are assumed to be well localized at each site. To calculate (5.6) more explicitly, the Gaussian localization in (4.11) will be employed as

$$\tilde{F}(\mathbf{r}_e, \mathbf{r}_h; \mathbf{R}_a) = \frac{1}{\sqrt{\pi} \xi} \exp(-|\mathbf{R}_a - \mathbf{r}_e|^2 / 2\xi^2) F_{1s}(\mathbf{r}_e - \mathbf{r}_h, z_e, z_h). \quad (5.8)$$

Using the normalization factor  $N_n$  in (2.31), one obtains

$$\begin{aligned} v_0^2 \sum_{\mathbf{r}_e, \mathbf{r}_h} \sum_{\mathbf{r}'_e, \mathbf{r}'_h} \tilde{F}^*(\mathbf{r}'_e, \mathbf{r}'_h; \mathbf{R}_b) \tilde{F}(\mathbf{r}_e, \mathbf{r}_h; \mathbf{R}_a) \delta_{\mathbf{r}_e, \mathbf{r}_h} \delta_{\mathbf{r}'_e, \mathbf{r}'_h} \\ = \left[ \frac{1}{\sqrt{\pi} \xi} \int d^2 r_{\parallel} \exp(-|\mathbf{r}_{\parallel} - \mathbf{R}|^2 / 2\xi^2) \right]^2 \int_{-L_z/2}^{L_z/2} dz'_e \int_{-L_z/2}^{L_z/2} dz'_e F_{1s}^*(0, z'_e, z'_e) F_{1s}(0, z_e, z_e) \\ = N_n^2 \pi \xi^2 L_z^2 = (\alpha \xi)^2 / I(2\beta L_z), \end{aligned} \quad (5.9)$$

where the function  $I(x)$  is defined in (2.29). Then the matrix element in (5.6) becomes

$$J(|\mathbf{R}_a - \mathbf{R}_b|) = \frac{(\alpha \xi)^2}{2I(2\beta L_z)} \frac{\mu^\dagger (1 - 3\mathbf{n} \cdot \mathbf{n}) \mu}{|\mathbf{R}_a - \mathbf{R}_b|^3}. \quad (5.10)$$

This is a typical form of the dipole-dipole interaction. In the following the angular dependence in (5.10) is dropped and the isotropic form will be assumed as

$$J(|\mathbf{R}_a - \mathbf{R}_b|) = \frac{\mu^2 (\alpha \xi)^2 A}{2I(2\beta L_z) |\mathbf{R}_a - \mathbf{R}_b|^3}, \quad (5.11)$$

with

$$A = [\langle (1 - 3\mathbf{n} \cdot \mathbf{n})^2 \rangle]^{1/2} = (\frac{11}{8})^{1/2}, \quad (5.12)$$

where the angular brackets denote the angular average. As is well known, the longitudinal-transverse (LT) splitting of excitons at the zone center is given by<sup>19</sup>

$$\Delta_{LT}(\mathbf{k}=0) = \frac{4\mu^2}{a_B^3}, \quad (5.13)$$

where  $a_B$  is the Bohr radius of the three-dimensional exciton. Finally, one arrives at the expression

$$\begin{aligned} J(|\mathbf{R}_a - \mathbf{R}_b|) \\ = \frac{\Delta_{LT} a_B^3 (\alpha \xi)^2 A}{8I(2\beta L_z) |\mathbf{R}_a - \mathbf{R}_b|^3} = \frac{\tilde{J}}{|\mathbf{R}_a - \mathbf{R}_b|^3}. \end{aligned} \quad (5.14)$$

By choosing the values  $\Delta_{LT} = 0.08 \text{ meV}$ ,<sup>20</sup>  $a_B = 136 \text{ \AA}$ ,<sup>21</sup>  $\xi = 150 \text{ \AA}$ ,  $\alpha^{-1} = 100 \text{ \AA}$ , and  $\beta L_z = 0.37$ ,<sup>11</sup> it is calculated as

$$\tilde{J}(\text{theor}) = 5.3 \times 10^2 \text{ eV \AA}^3. \quad (5.15)$$

This value will be compared with that which gives the best fit of theory to experiment for the energy relaxation in Sec. VII.

So far, the behavior of  $J(R)$  has been studied at long distances, i.e., under the condition of (5.5). In the intermediate range, in which the intersite distance is comparable to the exciton Bohr radius and/or the localization length, the calculation of  $J(R)$  is a rather involved problem. In this range, an exponential-type tunneling transfer is usually assumed without a rigorous theoretical basis.<sup>22</sup> Some interpolation between tunneling-type transfer and dipole-dipole type transfer may be appropriate to simulate the true behavior of  $J(R)$ . However, the details of the distance dependence of the intersite transfer do not affect sensitively the energy relaxation of localized excitons, since the energy relaxation rate is determined by the spatial integral of  $J^2(R)$  multiplied by other functions. In this paper both cases, dipole-dipole type transfer and tunneling-type transfer, will be examined.

## VI. ESTIMATION OF EXCITON TRANSFER RATE

Now that the matrix elements of the quasi-two-dimensional exciton-phonon interaction and the intersite transfer Hamiltonian have been determined, the exciton transfer rate can be estimated explicitly. The transition amplitude is given by (4.22) for the case of Gaussian localization. As mentioned there, the interference between the two terms in (4.22) will be neglected. Then one has

$$|\langle \mathbf{R}_b | T | \mathbf{R}_a \rangle_Q|^2 \cong \exp \left[ -\frac{\xi^2 Q_{\parallel}^2}{2} - \frac{|\mathbf{R}_a - \mathbf{R}_b|^2}{2\xi^2} \right] |H_{\text{ex-ph}}(Q_{\parallel}, Q_z)|^2 + \frac{J^2(|\mathbf{R}_a - \mathbf{R}_b|)}{|E_a - E_b|^2} |e^{-iQ_{\parallel} \cdot \mathbf{R}_b} - e^{-iQ_{\parallel} \cdot \mathbf{R}_a}|^2 \exp \left[ -\frac{\xi^2 Q_{\parallel}^2}{2} \right] |H_{\text{ex-ph}}(Q_{\parallel}, Q_z)|^2, \quad (6.1)$$

where the exciton-phonon matrix element is abbreviated as  $H_{\text{ex-ph}}$ , and the arguments  $Q_{\parallel}$  and  $Q_z$  are the components of the phonon wave vector parallel and perpendicular to the QW interface, respectively. In the second term, there appears the coherence factor  $|\exp(-iQ_{\parallel} \cdot \mathbf{R}_b) - \exp(-iQ_{\parallel} \cdot \mathbf{R}_a)|^2$  due to the interference between phonon emission or absorption at different sites. The matrix element of the quasi-two-dimensional exciton-phonon interaction for the deformation-potential coupling is given by (2.32) as

$$H_{\text{ex-ph}}^{\text{DF(Q2D)}}(Q_{\parallel}, Q_z) = \frac{1}{2} \left[ \frac{\hbar(Q_{\parallel}^2 + Q_z^2)^{1/2}}{2\rho u V} \right]^{1/2} \left[ D_c \frac{G((4+b_h^2)^{1/2}\beta L_z, Q_z L_z)}{[1+(b_h/2)^2]^{3/2}} - D_v \frac{G((4+b_e^2)^{1/2}\beta L_z, Q_z L_z)}{[1+(b_e/2)^2]^{3/2}} \right] / I(2\beta L_z) \quad (6.2)$$

$$= \Xi_D(|Q_{\parallel}|, Q_z) / \sqrt{V}, \quad (6.3)$$

with

$$b_h = \alpha_h |Q_{\parallel}| / \alpha \quad \text{and} \quad b_e = \alpha_e |Q_{\parallel}| / \alpha,$$

where a factor related to the phonon absorption or emission is omitted and  $\Xi_D$  is defined by (6.3). In the summation over  $\mathbf{Q}=(Q_{\parallel}, Q_z)$  in (4.23), the magnitude  $|Q|=(Q_{\parallel}^2 + Q_z^2)^{1/2}$  is fixed by the energy-conservation factor and only the angular integration remains. The integration of the coherence factor over the polar angle  $\phi$  results in

$$\int_0^{2\pi} d\phi |e^{-iQ_{\parallel} \cdot \mathbf{R}_b} - e^{-iQ_{\parallel} \cdot \mathbf{R}_a}|^2 = 4\pi [1 - J_0(|Q_{\parallel}| |\mathbf{R}_a - \mathbf{R}_b|)], \quad (6.4)$$

where  $J_0$  is the zeroth-order Bessel function. Then the transition probability for the deformation-potential (DF) coupling is calculated as

$$T_{\text{DF}}(|E_a - E_b|, |\mathbf{R}_a - \mathbf{R}_b|) = \frac{2\pi}{\hbar} \sum_Q |\langle \mathbf{R}_b | T | \mathbf{R}_a \rangle_Q|^2 \delta(E_a - E_b \pm \hbar\omega_Q)$$

$$= \frac{Q^2}{2\pi \hbar^2 u} \exp \left[ -\frac{|\mathbf{R}_a - \mathbf{R}_b|^2}{2\xi^2} \right] \int_0^{\pi} d\theta \sin\theta \exp \left[ -\frac{\xi^2 Q^2 \sin^2\theta}{2} \right] \Xi_D^2(Q \sin\theta, Q \cos\theta)$$

$$+ \frac{Q^2}{\pi \hbar^2 u} \frac{J^2(|\mathbf{R}_a - \mathbf{R}_b|)}{|E_a - E_b|^2} \int_0^{\pi} d\theta \sin\theta \exp \left[ -\frac{\xi^2 Q^2 \sin^2\theta}{2} \right]$$

$$\times [1 - J_0(Q |\mathbf{R}_a - \mathbf{R}_b| \sin\theta)] \Xi_D^2(Q \sin\theta, Q \cos\theta), \quad (6.5)$$

where the magnitude of phonon wave vector  $Q$  is denoted simply by  $Q$  and is given by  $|E_a - E_b| / \hbar u$  with the sound velocity  $u$  of the longitudinal-acoustic phonon mode. Similarly, in the case of exponential localization, one has

$$T_{\text{DF}}(|E_a - E_b|, |\mathbf{R}_a - \mathbf{R}_b|) = \frac{Q^2}{(2\pi)^2 \hbar^2 u} \int_0^{2\pi} d\phi \int_0^{\pi} d\theta \sin\theta K^2(Q_{\parallel}, \mathbf{R}_a - \mathbf{R}_b) \Xi_D^2(Q \sin\theta, Q \cos\theta)$$

$$+ \frac{Q^2}{\pi \hbar^2 u} \frac{J^2(|\mathbf{R}_a - \mathbf{R}_b|)}{|E_a - E_b|^2} \int_0^{\pi} d\theta \sin\theta I^2(Q \sin\theta) [1 - J_0(Q |\mathbf{R}_a - \mathbf{R}_b| \sin\theta)]$$

$$\times \Xi_D^2(Q \sin\theta, Q \cos\theta), \quad (6.6)$$

where

$$I(|Q_{\parallel}|) = \frac{8\xi^2}{\pi} \int d^2 K_{\parallel} \frac{1}{[1+(2\xi|K_{\parallel}-Q_{\parallel}/2|)^2]^{3/2} [1+(2\xi|K_{\parallel}+Q_{\parallel}/2|)^2]^{3/2}}, \quad (6.7)$$

$$K(Q_{\parallel}, \mathbf{R}_a - \mathbf{R}_b) = \frac{8\xi^2}{\pi} \int d^2K_{\parallel} \frac{\exp[i\mathbf{K}_{\parallel} \cdot (\mathbf{R}_b - \mathbf{R}_a)]}{[1 + (2\xi |\mathbf{K}_{\parallel} - Q_{\parallel}/2|)^2]^{3/2} [1 + (2\xi |\mathbf{K}_{\parallel} + Q_{\parallel}/2|)^2]^{3/2}}. \quad (6.8)$$

Here,  $I$  is a function of only the magnitude of  $Q_{\parallel}$ , while the function  $K$  is dependent also on the angle between  $Q_{\parallel}$  and  $\mathbf{R}_a - \mathbf{R}_b$ . These are the complete expressions of the exciton transfer rate for the case of deformation-potential coupling. In practice, however, the calculation of the angular integrals in (6.5) and (6.6) is rather cumbersome, and it is desirable to simplify these expressions by introducing a reasonable approximation. It is confirmed numerically that the function  $\Xi_D(|Q_{\parallel}|, Q_z)$  is a slowly varying function with respect to  $|Q_{\parallel}|$  and  $Q_z$  for a physically important range of parameters, where  $|Q_{\parallel}|, |Q_z| \leq 10^6 \text{ cm}^{-1}$  and  $L_z \leq 100 \text{ \AA}$ . Thus one may safely set  $\theta = \pi/2$  in  $\Xi_D(Q \sin\theta, Q \cos\theta)$  and put it outside the integral and further replace the integral over  $\theta$  by  $\pi$  times the arithmetic mean of the values of the integrand at  $\theta = 0$  and  $\theta = \pi/2$ . Then the transition probability in (6.5) can be approximated as

$$T_{\text{DF}}(|E_a - E_b|, |\mathbf{R}_a - \mathbf{R}_b|) \cong \frac{Q^2}{4\hbar^2 u} \exp\left[-\frac{|\mathbf{R}_a - \mathbf{R}_b|^2}{2\xi^2} - \frac{\xi^2 Q^2}{2}\right] \Xi_D^2(Q, 0) \\ + \frac{Q^2}{2\hbar^2 u} \frac{J^2(|\mathbf{R}_a - \mathbf{R}_b|)}{|E_a - E_b|^2} \exp\left[-\frac{\xi^2 Q^2}{2}\right] [1 - J_0(Q|\mathbf{R}_a - \mathbf{R}_b|)] \Xi_D^2(Q, 0). \quad (6.9)$$

With use of relation (2.35),  $\Xi_D(Q, 0)$  can be written as

$$\Xi_D(Q, 0) = \left[\frac{\hbar Q}{2\rho u}\right]^{1/2} \left[\frac{D_c I((4+b_h^2)^{1/2} \beta L_z)}{[1+(b_h/2)^2]^{3/2}} - \frac{D_v I((4+b_e^2)^{1/2} \beta L_z)}{[1+(b_e/2)^2]^{3/2}}\right] / I(2\beta L_z). \quad (6.10)$$

Noting that  $b_e \cong b_h \leq 1$  for the wave vector  $|Q| \leq 10^6 \text{ cm}^{-1}$ , it can be approximated as

$$\Xi_D(Q, 0) \cong \left[\frac{\hbar Q}{2\rho u}\right]^{1/2} \left[\frac{D_c}{[1+(b_h/2)^2]^{3/2}} - \frac{D_v}{[1+(b_e/2)^2]^{3/2}}\right]. \quad (6.11)$$

In a similar way, one can simplify (6.6) for the case of exponential localization. As seen from (6.8), the function  $K^2(Q_{\parallel}, \mathbf{R})$  is sensitively dependent on the angle between  $Q_{\parallel}$  and  $\mathbf{R}$ . However, when integrated spatially over  $\mathbf{R}$ , the angular dependence vanishes and the result depends weakly on  $|Q_{\parallel}|$ . In the rate equation for the exciton distribution function, as will be shown later, the spatial integral of  $K^2$  is physically relevant. Thus, in anticipation of their later use in the rate equation, the  $\theta$  and  $\phi$  integrations in (6.6) can be simplified as

$$T_{\text{DF}}(|E_a - E_b|, |\mathbf{R}_a - \mathbf{R}_b|) \cong \frac{Q^2}{4\hbar^2 u} K^2(Q, \mathbf{R}_a - \mathbf{R}_b) \Xi_D^2(Q, 0) \\ + \frac{Q^2}{2\hbar^2 u} \frac{J^2(|\mathbf{R}_a - \mathbf{R}_b|)}{|E_a - E_b|^2} I^2(Q) [1 - J_0(Q|\mathbf{R}_a - \mathbf{R}_b|)] \Xi_D^2(Q, 0). \quad (6.12)$$

Equations (6.9) and (6.12) with (6.11) are the basic expressions of the exciton transfer rate via the deformation-potential coupling that will be used in the rate equation.

Next, the probability of exciton transfer via the piezoelectric coupling will be calculated. In this case the coupling is highly anisotropic. Let us introduce a piezoelectric coupling function  $\Xi_P^{\sigma}(|Q_{\parallel}|, Q_z)$  defined by

$$\Xi_P^{\sigma}(|Q_{\parallel}|, Q_z) = \frac{4\pi e e_{14}}{\epsilon_0} \left[\frac{\hbar}{2\rho u_{\sigma} (Q_{\parallel}^2 + Q_z^2)^{1/2}}\right]^{1/2} \left[\frac{G((4+b_h^2)^{1/2} \beta L_z, Q_z L_z)}{[1+(b_h/2)^2]^{3/2}} - \frac{G((4+b_e^2)^{1/2} \beta L_z, Q_z L_z)}{[1+(b_e/2)^2]^{3/2}}\right] / I(2\beta L_z), \quad (6.13)$$

where the functions  $G$  and  $I$  and the variables  $b_h$  and  $b_e$  are the same as in (2.32) and the suffix  $\sigma$  specifies the longitudinal-acoustic (LA-) or transverse-acoustic (TA-) phonon mode. Then, for the case of Gaussian localization the exciton transfer rate via the piezoelectric coupling is calculated as

$$\begin{aligned}
T_{\text{PZ}}(|E_a - E_b|, |\mathbf{R}_a - \mathbf{R}_b|) &= \frac{2\pi}{\hbar} \sum_Q |\langle \mathbf{R}_b | T | \mathbf{R}_a \rangle_Q|^2 \delta(E_a - E_b \pm \hbar\omega_Q) \\
&= \frac{1}{(2\pi\hbar)^2} \exp\left[-\frac{|\mathbf{R}_a - \mathbf{R}_b|^2}{2\xi^2}\right] \sum_{\sigma} \frac{Q_{\sigma}^2}{u_{\sigma}} \int_0^{2\pi} d\phi \int_0^{\pi} d\theta \sin\theta \exp\left[-\frac{\xi^2 Q_{\sigma}^2 \sin^2\theta}{2}\right] \\
&\quad \times [\Xi_{\text{P}}^{\sigma}(Q_{\sigma} \sin\theta, Q_{\sigma} \cos\theta)]^2 A_{\sigma}^2(\theta, \phi) \\
&+ \frac{1}{(2\pi\hbar)^2} \frac{J^2(|\mathbf{R}_a - \mathbf{R}_b|)}{|E_a - E_b|^2} \sum_{\sigma} \frac{Q_{\sigma}^2}{u_{\sigma}} \int_0^{2\pi} d\phi \int_0^{\pi} d\theta \sin\theta \exp\left[-\frac{\xi^2 Q_{\sigma}^2 \sin^2\theta}{2}\right] \\
&\quad \times |e^{-i\mathbf{Q}_{\sigma} \cdot \mathbf{R}_b} - e^{-i\mathbf{Q}_{\sigma} \cdot \mathbf{R}_a}|^2 [\Xi_{\text{P}}^{\sigma}(Q_{\sigma} \sin\theta, Q_{\sigma} \cos\theta)]^2 A_{\sigma}^2(\theta, \phi), \quad (6.14)
\end{aligned}$$

where the magnitude of phonon wave vector  $Q_{\sigma}$  is determined by  $|E_a - E_b|/\hbar u_{\sigma}$  with the sound velocity  $u_{\sigma}$  for  $\sigma$  (LA or TA) phonon mode, and the anisotropy factor  $A_{\sigma}(\theta, \phi)$  is given as

$$A_{\text{LA}}(\theta, \phi) = \frac{1}{2} \sin^2\theta \cos\theta \sin 2\phi, \quad (6.15)$$

$$A_{\text{TA}}(\theta, \phi) = \frac{1}{8}(\sin\theta - 3\sin 3\theta) \sin 2\phi \quad \text{or} \quad \frac{1}{2} \sin 2\theta \cos 2\phi, \quad (6.16)$$

where the results are shown for two possibilities of the polarization direction of the TA mode. Formula (6.14) is quite general, but its calculation is rather complicated. Thus it is desirable to simplify the expression by introducing the same kind of approximation as to reduce (6.5) to (6.9). As noted before, the function  $G$  in (6.13) is a slowly varying function with respect to  $|Q_{\parallel}|$  and  $Q_z$  for the physically important range of parameters, and thus  $\Xi_{\text{P}}^{\sigma}(|Q_{\parallel}|, Q_z)$  is also such a function. Furthermore, since the main contribution to the transfer rate comes from the range  $\xi Q \leq 1$ , the localization factor  $\exp(-\xi^2 Q^2 \sin^2\theta/2)$  may be regarded as slowly varying with respect to  $\theta$ . Thus one may suppose that  $\theta = \pi/2$  in both  $\Xi_{\text{P}}^{\sigma}$  and the localization factor and put these factors outside the integral. The piezoelectric coupling function is reduced to

$$\Xi_{\text{P}}^{\sigma}(Q, 0) = \frac{8\pi e e_{14}}{\epsilon_0} \left[ \frac{\hbar}{2\rho u_{\sigma} Q} \right]^{1/2} \left[ \frac{I((4+b_h^2)^{1/2}\beta L_z)}{[1+(b_h/2)^2]^{3/2}} - \frac{I((4+b_e^2)^{1/2}\beta L_z)}{[1+(b_e/2)^2]^{3/2}} \right] / I(2\beta L_z), \quad (6.17)$$

with

$$b_h = \alpha_h Q/\alpha \quad \text{and} \quad b_e = \alpha_e Q/\alpha.$$

By noting that  $b_h \cong b_e \leq 1$ , the piezoelectric coupling function is further simplified to

$$\Xi_{\text{P}}^{\sigma}(Q, 0) \cong \frac{8\pi e e_{14}}{\epsilon_0} \left[ \frac{\hbar}{2\rho u_{\sigma} Q} \right]^{1/2} \left[ \frac{1}{[1+(b_h/2)^2]^{3/2}} - \frac{1}{[1+(b_e/2)^2]^{3/2}} \right]. \quad (6.18)$$

Then performing the angular integration of the anisotropic factor and the coherence factor, one obtains

$$\begin{aligned}
T_{\text{PZ}}(|E_a - E_b|, |\mathbf{R}_a - \mathbf{R}_b|) &\cong \frac{1}{(2\pi\hbar)^2} \exp\left[-\frac{|\mathbf{R}_a - \mathbf{R}_b|^2}{2\xi^2}\right] \sum_{\sigma} \frac{Q_{\sigma}^2}{u_{\sigma}} \exp\left[-\frac{\xi^2 Q_{\sigma}^2}{2}\right] [\Xi_{\text{P}}^{\sigma}(Q_{\sigma}, 0)]^2 B_{\sigma} \\
&+ \frac{1}{(2\pi\hbar)^2} \frac{J^2(|\mathbf{R}_a - \mathbf{R}_b|)}{|E_a - E_b|^2} \sum_{\sigma} \frac{Q_{\sigma}^2}{u_{\sigma}} \exp\left[-\frac{\xi^2 Q_{\sigma}^2}{2}\right] [\Xi_{\text{P}}^{\sigma}(Q_{\sigma}, 0)]^2 f_{\sigma}, \quad (6.19)
\end{aligned}$$

with

$$\begin{aligned}
B_{\text{LA}} &= 12\pi/35, \quad B_{\text{TA}} = 16\pi/35, \\
f_{\text{LA}} &= 2B_{\text{LA}} - \frac{9\pi}{2} \int_0^{\pi} d\theta \sin^5\theta \cos^2\theta [J_0(Q_{\text{LA}} R_{ab} \sin\theta) - J_4(Q_{\text{LA}} R_{ab} \sin\theta) \cos(4\phi_{ab})], \quad (6.20) \\
f_{\text{TA}} &= 2B_{\text{TA}} - \frac{\pi}{2} \int_0^{\pi} d\theta \sin^3\theta (\sin^2\theta - 2\cos^2\theta)^2 [J_0(Q_{\text{TA}} R_{ab} \sin\theta) - J_4(Q_{\text{TA}} R_{ab} \sin\theta) \cos(4\phi_{ab})] \\
&\quad - \frac{\pi}{2} \int_0^{\pi} d\theta \sin\theta \sin^2 2\theta [J_0(Q_{\text{TA}} R_{ab} \sin\theta) + J_4(Q_{\text{TA}} R_{ab} \sin\theta) \cos(4\phi_{ab})],
\end{aligned}$$

where  $J_0$  and  $J_4$  are the zeroth- and fourth-order Bessel function, respectively, and  $R_{ab} = |\mathbf{R}_a - \mathbf{R}_b|$  and  $\phi_{ab}$  is the angle between  $\mathbf{R}_a - \mathbf{R}_b$  and one of the crystallographic axes in the QW interface plane. These formulas are sufficiently simple to be useful in practical calculation of the exciton transfer rate.

For the sake of completeness, the results for the case of exponential localization will be given. The general formula is given as

$$T_{\text{PZ}}(|E_a - E_b|, |\mathbf{R}_a - \mathbf{R}_b|) = \frac{1}{(2\pi\hbar)^2} \sum_{\sigma} \frac{Q_{\sigma}^2}{u_{\sigma}} \int_0^{2\pi} d\phi \int_0^{\pi} d\theta \sin\theta K^2(Q_{\sigma}, \mathbf{R}_a - \mathbf{R}_b) [\Xi_{\sigma}^g(Q_{\sigma} \sin\theta, Q_{\sigma} \cos\theta)]^2 A_{\sigma}^2(\theta, \phi) \\ + \frac{1}{(2\pi\hbar)^2} \frac{J^2(|\mathbf{R}_a - \mathbf{R}_b|)}{|E_a - E_b|^2} \\ \times \sum_{\sigma} \frac{Q_{\sigma}^2}{u_{\sigma}} \int_0^{2\pi} d\phi \int_0^{\pi} d\theta \sin\theta I^2(Q_{\sigma} \sin\theta) \\ \times |e^{-iQ_{\sigma} \cdot \mathbf{R}_b} - e^{-iQ_{\sigma} \cdot \mathbf{R}_a}|^2 [\Xi_{\sigma}^g(Q_{\sigma} \sin\theta, Q_{\sigma} \cos\theta)]^2 A_{\sigma}^2(\theta, \phi). \quad (6.21)$$

Introducing the same kind of approximation as used in reducing (6.14) to (6.19), one can simplify (6.21) to

$$T_{\text{PZ}}(|E_a - E_b|, |\mathbf{R}_a - \mathbf{R}_b|) \cong \frac{1}{(2\pi\hbar)^2} \sum_{\sigma} \frac{Q_{\sigma}^2}{u_{\sigma}} K^2(Q_{\sigma}, \mathbf{R}_a - \mathbf{R}_b) [\Xi_{\sigma}^g(Q_{\sigma}, 0)]^2 B_{\sigma} \\ + \frac{1}{(2\pi\hbar)^2} \frac{J^2(|\mathbf{R}_a - \mathbf{R}_b|)}{|E_a - E_b|^2} \sum_{\sigma} \frac{Q_{\sigma}^2}{u_{\sigma}} I^2(Q_{\sigma}) [\Xi_{\sigma}^g(Q_{\sigma}, 0)]^2 f_{\sigma}, \quad (6.22)$$

where  $B_{\sigma}$  and  $f_{\sigma}$  are the same as defined in (6.20), and the meaning of  $K^2(Q, \mathbf{R})$  is given above (6.12).

In the rate equation for the exciton distribution function, there appears the two-dimensional spatial integration of the transfer probability  $T(|E_a - E_b|, |\mathbf{R}_a - \mathbf{R}_b|)$ . Let us now calculate the spatial integral assuming a suitable form for the inter-site matrix element  $J(R)$ . In Sec. V, it is shown that  $J(R)$  behaves as

$$J(R) = \tilde{J}/R^3, \quad (6.23)$$

like the dipole-dipole interaction in the region where  $R$  is larger than both the localization length and the Bohr radius of the two-dimensional exciton. However, it is quite difficult to derive, theoretically, the behavior of  $J(R)$  over the entire range of  $R$ . Thus a dipole-dipole type transfer will be assumed for  $J(R)$ , with a lower cutoff at the localization length  $\xi$ . As another choice, the tunneling-type transfer given by

$$J(R) = \tilde{J} \exp(-\delta R/2) \quad (6.24)$$

will be examined, where  $\delta^{-1}$  is the order of the two-dimensional exciton Bohr radius and  $\tilde{J}$  is a phenomenological constant. In this case it is not necessary to introduce a cutoff. Since there appear a few types of spatial dependence on  $|\mathbf{R}_a - \mathbf{R}_b|$  in the exciton transfer rate, it is sufficient to give the results for typical terms. In the integration the spatial distribution function  $F(R)$  of nearest-neighbor sites at a distance  $R$  must be included. In the two-dimensional case,  $F(R)$  is given by

$$F(R) = \exp(-\pi R^2/\sigma_0), \quad (6.25)$$

where  $\sigma_0^{-1}$  is the areal number density of islandlike structures. Since  $\sigma_0$  is of the order of  $10^{-11} \text{ cm}^2$ ,  $F(R)$  can often be neglected, in comparison with other more rapidly decaying functions. Then the typical spatial integrals are calculated as

$$\int d^2R \exp(-R^2/2\xi^2) = 2\pi\xi^2, \quad (6.26)$$

$$\int d^2R K^2(Q_{\parallel}, \mathbf{R}) = 256\xi^4 \int d^2K_{\parallel} \frac{1}{[1 + (2\xi |K_{\parallel} - Q_{\parallel}/2|)^2]^3 [1 + (2\xi |K_{\parallel} + Q_{\parallel}/2|)^2]^3}. \quad (6.27)$$

For the dipole-dipole type transfer (6.23), one obtains

$$\int_{\xi}^{\infty} dR R \int_0^{2\pi} d\phi J^2(R) F(R) [1 - J_0(QR)] = \int_{\xi}^{\infty} dR R \int_0^{2\pi} d\phi J^2(R) F(R) [1 - J_0(QR) + \cos(4\phi) J_4(QR)] \\ = \frac{2\pi\tilde{J}^2}{\xi^4} \left[ \frac{\pi^2\xi^4}{2\sigma_0^2} \Gamma(-2, \pi\xi^2/\sigma_0) - H(Q\xi) \right], \quad (6.28)$$

with

$$H(x) = x^4 \int_x^{\infty} dz J_0(z) \exp(-\pi z^2/\sigma_0 Q^2)/z^5, \quad (6.29)$$

where  $\Gamma(z, p)$  is the incomplete  $\Gamma$  function defined by

$$\Gamma(z, p) = \int_p^\infty dt e^{-t} t^{z-1}. \quad (6.30)$$

Here, the nearest-neighbor site distribution function  $F(R)$  is included explicitly, because both the dipole-dipole type transfer  $J(R)$  and the zeroth-order Bessel function  $J_0(QR)$  show rather slow spatial decay. Similarly, for the tunneling-type transfer (6.24) the above quantity is calculated as

$$\int d^2R J^2(R)[1 - J_0(QR)] = \frac{2\pi\bar{J}^2}{\delta^2} \left[ 1 - \frac{1}{[1 + (Q/\delta)^2]^{3/2}} \right], \quad (6.31)$$

where formula (4.17) is used. By combining all of the results, the exciton transfer rate and its spatial integration can be calculated for both the deformation-potential and piezoelectric coupling, for both cases of the Gaussian and exponential localization, and for both cases of the dipole-dipole type and tunneling-type transfer.

Finally, for illustrative purposes, let us calculate the spatially integrated transfer rate for the simplest case of Gaussian localization and tunneling-type transfer. For the deformation-potential coupling, making use of (6.9), (6.11), and (6.31), one obtains

$$\begin{aligned} \int d^2R T_{DF}(E, R) &= \frac{\pi Q^3}{2\hbar\rho u_{LA}^2} \left[ \frac{\xi^2}{2} + \frac{\bar{J}^2}{\delta^2 E^2} \left[ 1 - \frac{1}{[1 + (Q/\delta)^2]^{3/2}} \right] \right] \exp \left[ -\frac{\xi^2 Q^2}{2} \right] \\ &\times \left[ \frac{D_c}{[1 + (\alpha_h Q/2\alpha)^2]^{3/2}} - \frac{D_v}{[1 + (\alpha_e Q/2\alpha)^2]^{3/2}} \right]^2. \end{aligned} \quad (6.32)$$

Similarly, for the case of piezoelectric coupling, it is calculated as

$$\begin{aligned} \int d^2R T_{PZ}(E, R) &= \frac{1}{4\pi\hbar\rho} \left[ \frac{8\pi e e_{14}}{\epsilon_0} \right]^2 \sum_\sigma \left[ \xi^2 B_\sigma + \frac{\bar{J}^2 \bar{f}_\sigma}{\delta^2 E^2} \right] \frac{Q_\sigma}{u_\sigma^2} \exp \left[ -\frac{\xi^2 Q_\sigma^2}{2} \right] \\ &\times \left[ \frac{1}{[1 + (\alpha_h Q_\sigma/2\alpha)^2]^{3/2}} - \frac{1}{[1 + (\alpha_e Q_\sigma/2\alpha)^2]^{3/2}} \right]^2, \end{aligned} \quad (6.33)$$

with

$$\begin{aligned} B_{LA} &= 12\pi/35, \quad B_{TA} = 16\pi/35, \\ \bar{f}_{LA} &= \frac{9\pi}{2} \int_0^\pi d\theta \sin^5\theta \cos^2\theta \left[ 1 - \frac{1}{[1 + (Q_{LA} \sin\theta/\delta)^2]^{3/2}} \right], \\ \bar{f}_{TA} &= \frac{\pi}{2} \int_0^\pi d\theta \sin^3\theta (9 \sin^4\theta - 16 \sin^2\theta + 8) \left[ 1 - \frac{1}{[1 + (Q_{TA} \sin\theta/\delta)^2]^{3/2}} \right], \end{aligned} \quad (6.34)$$

where the suffix  $\sigma$  indicates the LA- or TA-phonon mode. The material parameters chosen in the numerical calculation are given in Sec. VII. The results are shown in Fig. 1. It is found that the contribution from the piezoelectric coupling is smaller than that from the deformation-potential coupling, but it is not negligible. The energy dependence is similar for both cases of the deformation-potential and piezoelectric coupling. Roughly speaking, the peak position is determined by the localization factor  $\exp(-\xi^2 Q_\sigma^2/2)$ , namely  $E \cong \hbar u_\sigma \xi^{-1}$ . In fact, this estimate gives the right order of 0.3–0.4 meV. The overall features in Fig. 1 are preserved for other cases of combination of the Gaussian and exponential localization, and the tunneling- and dipole-dipole type transfers.

## VII. RATE EQUATION FOR EXCITON DISTRIBUTION FUNCTION AND NONEXPONENTIAL BEHAVIOR OF ENERGY RELAXATION

Now that the transition probability of the exciton transfer is derived, one can set up the rate equation for the exciton distribution function. In the following the inter-

layer transfer of excitons through the AlAs barrier layer is neglected and only the exciton transfer within a QW will be taken into account. Thus the problem is reduced to that of a single QW. As noted in the Introduction, due to the fluctuation of the well thickness in the lateral direction of a QW, the quasi-two-dimensional excitons can be localized at such islandlike structures. The energy relaxation occurs through the exciton migration in search of lower-energy sites. Now for simplicity an assumption will be introduced that the line broadening is microscopic,<sup>22</sup> i.e., that there is no correlation between the energy of the localized exciton and its position in space. Thus the energy distribution of the localized exciton at any particular site depends only on the overall density of states but not on the nearby configuration of the localized site. In addition, the density of states of localized excitons is assumed to be proportional to the absorption spectrum at low temperatures. This assumption is reasonable because in the low-energy tail of the density of states the contribution from the localized excitons is dominant. Under these assumptions the rate equation for the distribution function  $f(E, t)$  of the localized exciton with energy  $E$  is derived as

$$\begin{aligned} \frac{d}{dt}f(E,t) = & -\gamma_0 f(E,t) - \sigma_0^{-1} \int d^2R F(R) \int dE' D(E') f(E',t) \{n(E'-E)\Theta(E'-E) \\ & + [1+n(E-E')]\Theta(E-E')\} T(|E-E'|,R) \\ & + \sigma_0^{-1} \int d^2R F(R) \int dE' D(E') f(E',t) \{n(E-E')\Theta(E-E') \\ & + [1+n(E'-E)]\Theta(E'-E)\} T(|E-E'|,R), \end{aligned} \quad (7.1)$$

where  $\gamma_0$ ,  $\sigma_0^{-1}$ ,  $n$ ,  $T$ , and  $\Theta$  are the generally energy-dependent decay rate including both the radiative and nonradiative contributions, the areal number density of islandlike structures, the phonon occupation number, the exciton transfer rate calculated in Sec. VI, and the Heaviside step function, respectively;  $F(R)$  is the distribution function of nearest-neighbor sites given by (6.25) and  $D(E)$  is the density of states of localized excitons normalized as

$$\int dE D(E) = 1. \quad (7.2)$$

$$\begin{aligned} \rho = 5.3 \text{ g/cm}^3 \text{ (Ref. 23)}, \quad u_{LA} = 4.81 \times 10^5 \text{ cm/s (Ref. 20)}, \quad u_{TA} = 3.34 \times 10^5 \text{ cm/s (Ref. 13)}, \\ L_z = 76 \text{ \AA (Ref. 3)}, \quad a_B = 136 \text{ \AA (Ref. 21)}, \quad \xi = 150 \text{ \AA}, \quad \sigma_0 = 10^{-11} \text{ cm}^2, \\ \alpha = 10^6 \text{ cm}^{-1} \text{ (Ref. 11)}, \quad D_b = 3.1 \text{ eV (Ref. 24)}, \quad D_c = -6.5 \text{ eV (Ref. 25)}, \quad m_e = 0.067m_0 \text{ (Ref. 26)}, \\ m_h = 0.45m_0 \text{ (Ref. 26)}, \quad e_{14} = 1.6 \times 10^{-5} \text{ C/cm}^2 \text{ (Ref. 27)}, \quad \epsilon_0 = 12.56 \text{ (Ref. 28)}, \quad \gamma_0^{-1} = 480 \text{ ps (Ref. 29)}, \end{aligned} \quad (7.4)$$

where  $m_0$  is the free-electron mass and  $\gamma_0$  is determined from the experimental decay curve of the spectrally integrated luminescence intensity<sup>29</sup> and is assumed to be energy independent, for simplicity. The transfer-integral constant  $\bar{J}$  in (6.23) or (6.24) is left as an adjustable parameter. The density of states  $D(E)$  is approximated by a Gaussian with a peak at 1.6225 eV and a half-width of 7.5 meV. The initial distribution function is taken from the experimental data of the time-resolved luminescence spectrum. In Fig. 2 the time-resolved luminescence spectrum divided by the absorption spectrum is plotted on the logarithmic scale.<sup>29</sup> This figure can be considered as

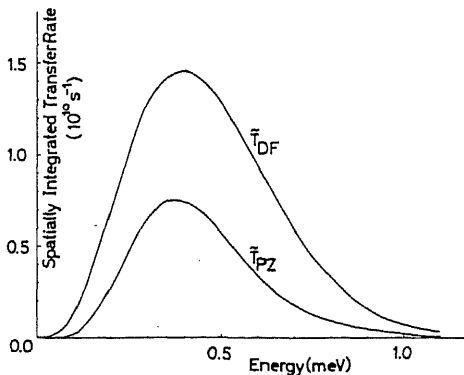


FIG. 1. Energy dependence of the spatially integrated one-phonon-assisted transfer rate of excitons for deformation-potential coupling (DF) and piezoelectric coupling (PZ).

The second and third terms in (7.1) represent the probability leaving and coming into the exciton state with energy  $E$ , respectively. For the exciton transfer rate  $T(E,R)$ , the contributions from both the deformation-potential and piezoelectric coupling are taken into account, namely

$$T(E,R) = T_{DF}(E,R) + T_{PZ}(E,R). \quad (7.3)$$

In the numerical integration of the rate equation (7.1), the following parameters are chosen:

representing the exciton distribution function  $f(E,t)$ . Surprisingly enough, the experimental  $f(E,t)$  can be described by the Boltzmann distribution fairly well, especially in the higher-energy region  $E \geq 1.614$  eV. The Boltzmann statistics may be maintained by the frequent collisions among excitons. As for the initial distribution function in the numerical integration of the rate equation, the effective temperature of excitons is assumed to be 20 K above 1.614 eV and  $-10$  K below that energy, respectively, to simulate the experimental distribution function at  $t=100$  ps. The calculated average energy of luminescence shows a nonexponential behavior, i.e., decay with an

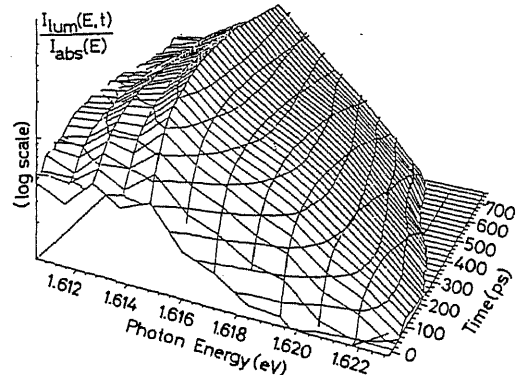


FIG. 2. Experimental data of the time-resolved luminescence spectrum divided by the absorption spectrum which can be considered as representing the exciton distribution function.

almost constant rate. At first, let us assume for  $J(R)$  the dipole-dipole type transfer in (6.23). In Fig. 3 the theoretical result for the case of Gaussian localization is compared with the experimental data of Ref. 30. The best fit is obtained by adjusting  $\bar{J}$  as

$$\bar{J}(\text{Gaussian}) = 11.7 \times 10^2 \text{ eV \AA}^3. \quad (7.5)$$

A similar result is obtained in the case of exponential localization by taking

$$\bar{J}(\text{exponential}) = 10.2 \times 10^2 \text{ eV \AA}^3. \quad (7.6)$$

In the latter case the magnitude of the wave vector of phonons participating in the exciton transfer, or, equivalently, the possible energy mismatch of excitons, is larger than that in the former case, as seen from (4.15) and (4.16). This leads to the faster energy relaxation in the case of exponential localization than in the case of Gaussian localization for the same localization length  $\xi$ , and thus the smaller value of  $\bar{J}$  is obtained in the former case. For the tunneling-type transfer in (6.24), the parameter  $\delta$  is assumed to be  $10^6 \text{ cm}^{-1}$ , which is on the order of the inverse Bohr radius of the quasi-two-dimensional exciton. From the fitting to the experimental curve, the phenomenological constant  $\bar{J}$  is determined as 0.44 and 0.31 meV for the case of Gaussian localization and exponential localization, respectively. These values are on the same order as those of the dipole-dipole type transfer in (6.23) estimated at  $R \cong \xi$ . For the case of dipole-dipole-type transfer, the agreement within a factor of 2 or 3 between the theoretical value in (5.15) and the values estimated from the experiment in (7.5) and (7.6) is quite satisfactory in view of ambiguities in the material parameters. This confirms the adequacy of both our model for the localized excitons in QW heterostructures and our theory of the energy transfer.

Let us now explain the observed nonexponential behavior of energy relaxation. Experimentally, the average energy of luminescence showed decay with an almost constant rate. The average energy of luminescence at time  $t$  is defined by

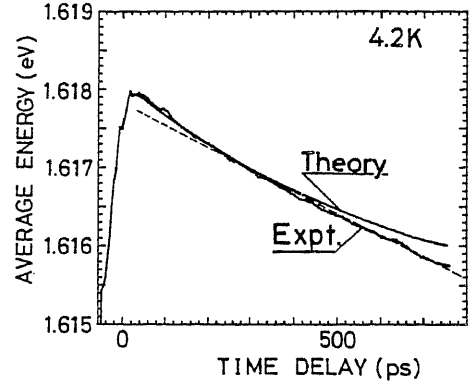


FIG. 3. Comparison of the theoretical calculation of the average energy of luminescence with the experimental data cited from Ref. 30.

$$\langle E \rangle(t) = \int dE E D(E) f(E, t) / \int dE D(E) f(E, t), \quad (7.7)$$

where  $D(E)f(E, t)$  is proportional to the intensity of luminescence with energy  $E$  at time  $t$ . The energy relaxation rate is then calculated by  $d\langle E \rangle/dt$ . On the basis of the analytical expression of  $d\langle E \rangle/dt$ , the nonexponential behavior of energy relaxation will be clarified. To simplify the rate equation (7.1), the spatial integral of the exciton transfer rate will be denoted by  $\bar{T}$ , namely

$$\bar{T}(|E - E'|) = \sigma_0^{-1} \int d^2R T(|E - E'|, R) F(R). \quad (7.8)$$

Furthermore, the time dependence due to the radiative and nonradiative decay processes will be separated out by setting

$$f(E, t) = e^{-\gamma_0 t} \tilde{f}(E, t). \quad (7.9)$$

Then the rate equation for  $\tilde{f}(E, t)$  can be written as

$$\begin{aligned} \frac{d}{dt} \tilde{f}(E, t) = & - \int dE' D(E') \tilde{f}(E', t) \bar{T}(|E - E'|) \{ n(E' - E) \Theta(E' - E) + [1 + n(E - E')] \Theta(E - E') \} \\ & + \int dE' D(E') \tilde{f}(E', t) \bar{T}(|E - E'|) \{ n(E - E') \Theta(E - E') + [1 + n(E' - E)] \Theta(E' - E) \}. \end{aligned} \quad (7.10)$$

It is easily found that

$$\frac{d}{dt} \int dE D(E) \tilde{f}(E, t) = 0, \quad (7.11)$$

and, correspondingly,

$$\int dE D(E) \tilde{f}(E, t) = D_0, \quad (7.12)$$

where  $D_0$  is the initial value of the total exciton population. This relation implies simply that the total luminescence intensity or the total exciton population decreases with the decay rate  $\gamma_0$ . Next, by multiplying  $ED(E)$  on both sides of (7.10) and by integrating over  $E$ , one obtains

$$\frac{d}{dt} \left[ \int dE ED(E)\tilde{f}(E,t) \right] = \int dE \int dE' D(E)D(E')\tilde{f}(E',t)(E-E')\tilde{T}(|E-E'|) \\ \times \{n(E-E')\Theta(E-E') + [1+n(E'-E)]\Theta(E'-E)\}. \quad (7.13)$$

As shown in Fig. 1, the function  $\tilde{T}(E)$  is a rapidly decreasing function compared to the density of states  $D(E)$  and the phonon occupation number  $n(E)$ . This is simply due to the exciton localization factors in (6.5), (6.6), (6.14), and (6.21). Thus it is allowed to expand as

$$D(E) = D(E') + \frac{dD(E')}{dE'}(E-E') + \dots \quad (7.14)$$

Substituting this expansion into the integrand on the right-hand side of (7.13) and changing the integration variables from  $(E, E')$  to  $(E', E-E')$ , one finds

$$\frac{d}{dt} \left[ \int dE ED(E)\tilde{f}(E,t) \right] = - \int dE' D^2(E')\tilde{f}(E',t) \int_0^\infty dE E\tilde{T}(|E|) \\ + \int dE' D(E') \frac{dD(E')}{dE'} \tilde{f}(E',t) \int_0^\infty dE E^2 \tilde{T}(|E|) [1+2n(E)] + \dots \quad (7.15)$$

The average energy of luminescence defined by (7.7) can be rewritten as

$$\langle E \rangle(t) = \frac{\int dE ED(E)\tilde{f}(E,t)}{\int dE D(E)\tilde{f}(E,t)} \\ = D_0^{-1} \int dE ED(E)\tilde{f}(E,t), \quad (7.16)$$

where the equation (7.12) is used. Then the energy relaxation rate is calculated as

$$-\frac{d\langle E \rangle}{dt} = -D_0^{-1} \frac{d}{dt} \left[ \int dE ED(E)\tilde{f}(E,t) \right] \\ \cong D_0^{-1} \int_0^\infty dE E\tilde{T}(|E|) \int dE' D^2(E')\tilde{f}(E',t), \quad (7.17)$$

where only the first term on the right-hand side of (7.15) is retained. As shown in (7.12), the integral  $\int dE D(E)\tilde{f}(E,t)$  is exactly time independent. Thus it is expected that the right-hand side of (7.17) is almost time independent, if the functional form of  $D^2(E)$  is not very different from that of  $D(E)$ . This may be the case because at the later stage, after photoexcitation, the excitons have accumulated on the low-energy tail of the density of states. In this energy region,  $D(E)$  is a smooth function and one may approximate (7.17) as

$$-\frac{d\langle E \rangle}{dt} = W \int dE' D^2(E')\tilde{f}(E',t) \\ \cong W\bar{D} \int dE' D(E')\tilde{f}(E',t) \\ = \bar{D} \int_0^\infty dE E\tilde{T}(E), \quad (7.18)$$

with

$$W = D_0^{-1} \int_0^\infty dE E\tilde{T}(E),$$

where  $\bar{D}$  is a representative value of  $D(E)$  at the peak region of  $\tilde{f}(E,t)$ . The final expression is exactly time independent. This explains qualitatively the observed nonexponential behavior of energy relaxation. In fact, expression (7.18) gives the right order of the observed energy

relaxation rate. The generality of the above argument suggests that the nonexponential behavior of energy relaxation is a universal feature to be observed in the tail region of optical transitions which is induced by any kind of inhomogeneity or disorder.

#### VIII. DEPENDENCE OF ENERGY RELAXATION RATE ON THE QUANTUM-WELL THICKNESS

Here the dependence of energy relaxation rate on the QW thickness  $L_z$  is discussed. Experimentally, the dependence of  $L_z^{-2}$  is observed along with the same dependence of the absorption bandwidth, as shown in Fig. 4.<sup>30</sup> This experimental result suggests that there is some kind of correlation between the energy relaxation rate and the absorption bandwidth. In fact, according to (7.18), the  $L_z$  dependence of the energy relaxation rate arises from  $\bar{D}$

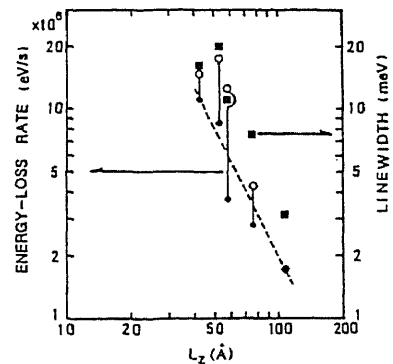


FIG. 4. Observed dependence on the quantum-well thickness  $L_z$  of the energy relaxation rate and the absorption bandwidth of the 1s exciton. The dashed line shows the  $L_z^{-2}$  dependence. The open circles represent the energy relaxation rates at the initial stage after photoexcitation, while the solid circles are those at the later stage.

since the integral factor  $\int dE E \tilde{T}(E)$  is only weakly dependent on  $L_z$ . When the width of the density of states is increased, the value  $\tilde{D}$  at the low-energy tail becomes larger, since the density of states is normalized by (7.2). Thus the above correlation can be understood qualitatively. To investigate in more detail the relationship between the energy relaxation rate and the absorption bandwidth,

$$\begin{aligned} \frac{d}{dt} \tilde{f}(E, \sigma, t) = & - \int dE' D(E', \sigma) \tilde{f}(E', \sigma, t) \tilde{T}(|E - E'|) \{ n(E' - E) \Theta(E' - E) + [1 + n(E - E')] \Theta(E - E') \} \\ & + \int dE' D(E', \sigma) \tilde{f}(E', \sigma, t) \tilde{T}(|E - E'|) \{ n(E - E') \Theta(E - E') + [1 + n(E' - E)] \Theta(E' - E) \}, \end{aligned} \quad (8.1)$$

where  $\tilde{T}(E)$  is defined by (7.8) and is not dependent on  $\sigma$ . Since the density of states  $D(E, \sigma)$  is normalized as

$$\int dE D(E, \sigma) = 1, \quad (8.2)$$

the following scaling relation can be postulated,

$$\sigma D(\sigma E, \sigma) = \tilde{D}(E), \quad (8.3)$$

where  $\tilde{D}$  is a universal function independent of  $\sigma$ . By scaling the variables  $(E, E')$  as  $(\sigma E, \sigma E')$  and using (8.3), one finds

$$\begin{aligned} \frac{d}{dt} \tilde{f}(\sigma E, \sigma, t) = & - \int dE' \tilde{D}(E') \tilde{f}(\sigma E', \sigma, t) \tilde{T}(\sigma |E - E'|) \{ n(\sigma(E' - E)) \Theta(E' - E) + [1 + n(\sigma(E - E'))] \Theta(E - E') \} \\ & + \int dE' \tilde{D}(E') \tilde{f}(\sigma E', \sigma, t) \tilde{T}(\sigma |E - E'|) \{ n(\sigma(E - E')) \Theta(E - E') + [1 + n(\sigma(E' - E))] \Theta(E' - E) \}. \end{aligned} \quad (8.4)$$

Furthermore, the transfer rate  $\tilde{T}$  is supposed to be scaled as

$$\tilde{T}(\sigma |E - E'|) = \sigma^\alpha U(|E - E'|), \quad (8.5)$$

where  $U$  is a universal function that is independent of, or weakly dependent on, the scaling parameter  $\sigma$ . Consequently, (8.4) can be rewritten as

$$\begin{aligned} \frac{d}{dt} \tilde{f}(\sigma E, \sigma, t) = & - \sigma^\alpha \left[ \int dE' K(E, E') \tilde{f}(\sigma E', \sigma, t) \right. \\ & \left. - \int dE' L(E, E') \tilde{f}(\sigma E', \sigma, t) \right]. \end{aligned} \quad (8.6)$$

Here,  $K$  and  $L$  are the integral kernels corresponding to each term on the right-hand side of (8.4) which can be regarded as universal functions since the parameter  $\sigma$  included in the phonon occupation number  $n$  gives rise to only a weak dependence on  $\sigma$ . Scaling the time variable as

$$t \rightarrow t/\sigma^\alpha, \quad (8.7)$$

one finally arrives at the universal rate equation,

$$\begin{aligned} \frac{d}{dt} \tilde{f}(\sigma E, \sigma, t/\sigma^\alpha) = & - \int dE' K(E, E') \tilde{f}(\sigma E', \sigma, t/\sigma^\alpha) \\ & + \int dE' L(E, E') \tilde{f}(\sigma E', \sigma, t/\sigma^\alpha). \end{aligned} \quad (8.8)$$

Since the integral kernels  $K$  and  $L$  are universal functions,

one can make full use of the scaling property of the rate equation.

The characteristic width of the density of states of excitons will be denoted by  $\sigma$ , which is identified here with the absorption bandwidth. Then, by expressing the  $\sigma$  dependence explicitly, the rate equation (7.10) can be written as

the solution of the rate equation (8.8) can also be regarded as universal, namely

$$\tilde{f}(\sigma E, \sigma, t/\sigma^\alpha) = G(E, t), \quad (8.9)$$

where  $G$  is a universal function independent of  $\sigma$ . This is an important consequence of the scaling property of the rate equation.

Now the average energy of luminescence is calculated by

$$\langle E \rangle_\sigma = \frac{\int dE E D(E, \sigma) \tilde{f}(E, \sigma, t)}{\int dE D(E, \sigma) \tilde{f}(E, \sigma, t)}. \quad (8.10)$$

Scaling the integration variable  $E$  as  $\sigma E$  and using the relation (8.3), it is rewritten as

$$\begin{aligned} \langle E \rangle_\sigma &= \frac{\sigma \int dE E \tilde{D}(E) \tilde{f}(\sigma E, \sigma, t)}{\int dE \tilde{D}(E) \tilde{f}(\sigma E, \sigma, t)} \\ &= \frac{\sigma \int dE E \tilde{D}(E) G(E, \sigma^\alpha t)}{\int dE \tilde{D}(E) G(E, \sigma^\alpha t)}, \end{aligned} \quad (8.11)$$

where the scaling property (8.9) is used. Then the energy relaxation rate is calculated as

$$\frac{d}{dt} \langle E \rangle_\sigma = \sigma^{1+\alpha} \frac{d}{du} \left[ \frac{\int dE E \tilde{D}(E) G(E, u)}{\int dE \tilde{D}(E) G(E, u)} \right] \Bigg|_{u=\sigma^\alpha t}. \quad (8.12)$$

Here the derivative term with respect to  $u$  is a universal function since  $\tilde{D}$  and  $G$  are universal functions. It can be

expected that the derivative term is a smooth function with respect to  $u$  at the large argument, and that it takes an almost constant value independent of  $\sigma$  at large  $t$ . Thus the energy relaxation rate can be scaled as

$$\frac{d}{dt}\langle E \rangle_{\sigma} \propto \sigma^{1+\alpha}, \quad (8.13)$$

in terms of the absorption bandwidth  $\sigma$ , where the exponent  $\alpha$  is determined by the scaling property of the transfer rate as shown in (8.5). The exponent  $\alpha$  can be estimated, in principle, from the dependence of the transfer rate on the energy or the phonon wave vector. However, as investigated in Sec. VI, the expression of the transfer rate contains these variables in a rather complicated way and the determination of the exponent  $\alpha$  is not straightforward. The exponent  $\alpha$  should be determined in the energy region in which  $\bar{T}(E)$  takes a significant value and from which the contribution to the exciton transfer process is dominant. For example, in Fig. 1, where  $\bar{T}_{DF}(E)$  and  $\bar{T}_{PZ}(E)$  are shown for the case of Gaussian localization and for tunneling-type transfer, the relevant energy region is considered to be  $0.2 \leq E \leq 0.8$  meV. In this region the exponent  $\alpha$  can be considered to be 0 since there is no definite power-law dependence on energy. The same situation holds for other cases of combinations of the Gaussian and exponential localization and the tunneling-type and dipole-dipole-type transfer. Consequently, it can be concluded that  $\alpha=0$  and that

$$\frac{d}{dt}\langle E \rangle_{\sigma} \propto \sigma. \quad (8.14)$$

The scaling argument successfully explains the observed correlation between the energy relaxation rate and the absorption bandwidth, though in a qualitative way. On the other hand, the observed dependence of the absorption bandwidth on the QW thickness  $L_z$  is different from the expected one. Since the kinetic energy of the electron and hole confined in a QW is approximately proportional to  $L_z^{-2}$ ,<sup>31</sup> the fluctuation of the exciton energy is proportional to  $L_z^{-3}$  if the amount of well-thickness fluctuation is independent of  $L_z$ . In reality, however, the bandwidth of

excitons is determined by the details of atomic-scale disorder of the QW interface and a naive theory fails to predict the observed dependence on  $L_z$ . A detailed theory based on the microscopic morphology of the QW interface will be necessary to explain the  $L_z^{-2}$  dependence of the absorption bandwidth.

## IX. SUMMARY

The slow energy relaxation of the quasi-two-dimensional excitons in GaAs-AlAs QW heterostructures is explained quantitatively in terms of the intralayer migration of excitons localized at the energetically local minimum sites induced by the fluctuation of the well thickness along the QW interface. The nonexponential behavior of energy relaxation is clarified theoretically as a general feature to be observed in the low-energy tail of the density of states. The dependence of the energy relaxation rate on the QW thickness is discussed along with the same dependence of the absorption bandwidth. The correlation between the energy relaxation rate and the absorption bandwidth is explained qualitatively on the basis of the scaling property of the rate equation.

Finally, let us briefly comment on the energy relaxation of excitons in three dimensions, such as the excitons in mixed semiconductors. The underlying physics is analogous to that in the quasi-two-dimensional case discussed in this paper, although the origin of the inhomogeneity or disorder is different in two cases. In fact, the slow and nonexponential energy relaxation of excitons in the band-edge region was observed recently in mixed semiconductors.<sup>32</sup> This can be regarded as one of the experimental verifications of the general feature of the nonexponential relaxation clarified in Sec. VII.

## ACKNOWLEDGMENTS

The author would like to thank Dr. Y. Masumoto and Professor E. Hanamura for enlightening discussions and especially the former for supplying unpublished experimental data.

## APPENDIX

The explicit expressions of  $I(\gamma)$  defined by (2.29) and  $G(\gamma, \delta)$  defined in (2.23) are given in the following. The argument  $\delta$  of  $G$  is changed to  $2\delta$  for simplicity of expression:

$$I(\gamma) = \frac{1}{4\gamma^2(\gamma^2 + 4\pi^2)^3} [3\gamma^7 + 28\pi^2\gamma^5 + 96\pi^4\gamma^3 - 112\pi^4\gamma^2 + 128\pi^6\gamma - 192\pi^6 + 16\pi^4 e^{-\gamma}(\gamma^3 + 7\gamma^2 + 4\pi^2\gamma + 12\pi^2)], \quad (A1)$$

$$G(\gamma, 2\delta) = \int_{-1/2}^{1/2} dz_e \int_{-1/2}^{1/2} dz_h \exp(i2\delta z_e - \gamma |z_e - z_h|) (1 + \gamma |z_e - z_h|) \cos^2(\pi z_e) \cos^2(\pi z_h) \quad (A2)$$

$$= \frac{\pi^2}{2\delta} \left[ \frac{P(\gamma, \delta; 0) \sin \delta + Q(\gamma, \delta; 0) \cos \delta}{\pi^2 - \delta^2} + \frac{P(\gamma, \delta; \pi) \sin \delta + Q(\gamma, \delta; \pi) \cos \delta}{(\pi + \delta)(4\pi + 2\delta)} \right. \\ \left. + \frac{P(\gamma, \delta; -\pi) \sin \delta + Q(\gamma, \delta; -\pi) \cos \delta}{(\pi - \delta)(4\pi - 2\delta)} \right], \quad (A3)$$

with

$$P(\gamma, \delta; x) = \frac{1}{(\gamma^2 + 4x^2)^2 [\gamma^2 + 4(x + \delta)^2]^2} (2\gamma^7 + 8[x^2 + (x + \delta)^2]\gamma^5 + 16[x^4 + (x + \delta)^4]\gamma^3 - 2\delta(2x + \delta)e^{-\gamma} \{ \gamma^6 + 4\gamma^5 + 4[x^2 + (x + \delta)^2]\gamma^4 + 8[\delta^2 + 2x(x + \delta)]\gamma^3 + 16x^2(x + \delta)^2\gamma^2 \} , \quad (\text{A4})$$

$$Q(\gamma, \delta; x) = \frac{1}{(\gamma^2 + 4x^2)^2 [\gamma^2 + 4(x + \delta)^2]^2} \times (-3(2x + \delta)\gamma^6 - 4[(x + \delta)^3 + 6x(x + \delta)^2 + 6x^2(x + \delta) + x^3]\gamma^4 - 16[3x(x + \delta)^4 + 2x^2(x + \delta)^3 + 2x^3(x + \delta)^2 + 3x^4(x + \delta)]\gamma^2 - 64x^3(x + \delta)^4 - 64x^4(x + \delta)^3 + (2x + \delta)e^{-\gamma} \{ \gamma^7 + 3\gamma^6 + 4[x^2 + (x + \delta)^2 + x(x + \delta)]\gamma^5 + 4[x^2 + (x + \delta)^2 + 5x(x + \delta)]\gamma^4 + 16x(x + \delta)[x^2 + (x + \delta)^2 + x(x + \delta)]\gamma^3 + 16x(x + \delta)[x^2 + (x + \delta)^2 + 3x(x + \delta) + 2\delta^2]\gamma^2 + 64x^3(x + \delta)^3\gamma + 64x^3(x + \delta)^3 \} ) . \quad (\text{A5})$$

- <sup>1</sup>C. V. Shank, R. L. Fork, R. Yen, J. Shah, B. I. Greene, A. C. Gossard, and C. Weisbuch, *Solid State Commun.* **47**, 981 (1983).
- <sup>2</sup>E. O. Göbl, H. Jung, J. Kuhl, and K. Ploog, *Phys. Rev. Lett.* **51**, 1588 (1983).
- <sup>3</sup>Y. Masumoto, S. Shionoya, and H. Kawaguchi, *Phys. Rev. B* **29**, 2324 (1984). Figure 4 in this reference is not correct and should be replaced by Fig. 5 of Ref. 30.
- <sup>4</sup>A. Pinczuk, J. Shah, A. C. Gossard, and W. Wiegmann, *Phys. Rev. Lett.* **46**, 1341 (1981).
- <sup>5</sup>J. E. Zucker, A. Pinczuk, D. S. Chemla, A. Gossard, and W. Wiegmann, *Phys. Rev. Lett.* **51**, 1293 (1983).
- <sup>6</sup>J. Hegarty, M. D. Sturge, C. Weisbuch, A. C. Gossard, and W. Wiegmann, *Phys. Rev. Lett.* **49**, 930 (1982).
- <sup>7</sup>P. M. Petroff, A. C. Gossard, W. Wiegmann, and A. Savage, *J. Cryst. Growth* **44**, 5 (1978).
- <sup>8</sup>C. Weisbuch, R. Dingle, A. C. Gossard, and W. Wiegmann, *Solid State Commun.* **38**, 709 (1981).
- <sup>9</sup>L. Goldstein, Y. Horikoshi, S. Tarucha, and H. Okamoto, *Jpn. J. Appl. Phys.* **22**, 1489 (1983).
- <sup>10</sup>G. Bastard, E. E. Mendez, L. L. Chang, and L. Esaki, *Phys. Rev. B* **26**, 1974 (1982).
- <sup>11</sup>Y. Shinozuka and M. Matsuura, *Phys. Rev. B* **28**, 4878 (1983); *B* **29**, 3717(E) (1984).
- <sup>12</sup>R. L. Greene and K. K. Bajaj, *Solid State Commun.* **45**, 831 (1983).
- <sup>13</sup>*Physics of Group IV Elements and III-V Compounds*, Vol. 17a of *Landolt-Börnstein*, edited by O. Madelung, M. Schulz, and H. Weiss (Springer, Berlin, 1982).
- <sup>14</sup>A. I. Anselm and Yu. A. Firsov, *Zh. Eksp. Teor. Fiz.* **28**, 151 (1955) [*Sov. Phys.—JETP* **1**, 139 (1955)]; Y. Toyozawa, *Prog. Theor. Phys.* **20**, 53 (1958).
- <sup>15</sup>M. Abramowitz and I. A. Stegun, *Handbook of Mathematical Functions*, 10th ed. (Dover, New York, 1972).
- <sup>16</sup>G. D. Mahan, in *Polarons in Ionic Crystals and Polar Semiconductors*, edited by J. T. Devreese (North-Holland, Amsterdam, 1972), p. 553; C. Weisbuch and R. G. Ulbrich, in *Light Scattering in Solids III*, edited by M. Cardona and G. Güntherodt (Springer, Berlin, New York, 1982), p. 207.
- <sup>17</sup>E. M. Conwell, *High Field Transport in Semiconductors*, Suppl. 9 to *Solid State Physics* (Academic, New York, 1967).
- <sup>18</sup>T. Holstein, S. K. Lyo, and R. Orbach, in *Laser Spectroscopy of Solids*, edited by W. M. Yen and P. M. Selzer (Springer, Berlin, 1981), p. 39.
- <sup>19</sup>R. S. Knox, *Theory of Excitons*, Suppl. 5 to *Solid State Physics* (Academic, New York, 1963).
- <sup>20</sup>R. G. Ulbrich and C. Weisbuch, *Phys. Rev. Lett.* **38**, 865 (1977).
- <sup>21</sup>D. D. Sell, S. E. Stokowski, R. Dingle, and J. V. DiLorenzo, *Phys. Rev. B* **7**, 4568 (1973).
- <sup>22</sup>E. Cohen and M. D. Sturge, *Phys. Rev. B* **25**, 3828 (1982).
- <sup>23</sup>M. Neuberger, *III-V Semiconductor Compounds*, Vol. 2. of *Handbook of Electronic Materials* (Plenum, New York, 1971).
- <sup>24</sup>J. D. Wiley, *Solid State Commun.* **8**, 1865 (1970).
- <sup>25</sup>B. Welber, M. Cardona, C. K. Kim, and S. Rodriguez, *Phys. Rev. B* **12**, 5729 (1975).
- <sup>26</sup>Q. H. F. Vrehen, *J. Phys. Chem. Solids* **29**, 129 (1968).
- <sup>27</sup>G. Arlt and P. Quadflieg, *Phys. Status Solidi A* **25**, 323 (1968).
- <sup>28</sup>G. E. Stillmann, D. M. Larsen, C. M. Wolfe, and R. C. Brandt, *Solid State Commun.* **9**, 2245 (1971).
- <sup>29</sup>Y. Masumoto (private communication).
- <sup>30</sup>Y. Masumoto, S. Shionoya, and H. Okamoto, in *Proceedings of the 17th International Conference on the Physics of Semiconductors* (San Francisco, 1984) (unpublished).
- <sup>31</sup>R. Dingle, in *Festkörperprobleme XV*, edited by H. J. Queisser (Pergamon/Vieweg, Braunschweig, 1975), p. 21.
- <sup>32</sup>J. A. Kash, A. Ron, and E. Cohen, *Phys. Rev. B* **28**, 6147 (1983).

## Direct experimental observation of two-dimensional shrinkage of the exciton wave function in quantum wells

Yasuaki Masumoto

*The Institute for Solid State Physics, The University of Tokyo, Roppongi, Minato-ku, Tokyo 106, Japan*

Mitsuru Matsuura

*Department of Applied Science, Faculty of Engineering, Yamaguchi University, Tokiwadai, Ube 755, Japan*

Seigo Tarucha and Hiroshi Okamoto

*Musashino Electrical Communication Laboratory, Nippon Telegraph and Telephone Corporation,*

*Midori-machi, Musashino-shi, Tokyo 180, Japan*

(Received 1 July 1985)

We have studied the oscillator strength of the lowest 1s heavy excitons in GaAs-AlAs quantum wells as a function of well-layer thickness by means of optical absorption. The oscillator strength of the lowest 1s heavy excitons is largely enhanced with the decrease of well-layer thickness. The result is the first full experimental observation of two-dimensional shrinkage of the exciton wave function in quantum wells.

It is interesting to clarify experimentally the form of the exciton wave function in semiconductor quantum wells, both from the viewpoint of general physics as well as from that of semiconductor physics. This is because excitons in quantum wells are excellent analogues of hydrogen atoms in one-dimensional square wells.<sup>1</sup> By reducing the well thickness, we can continuously change the wave functions of excitons or hydrogen atoms from the three-dimensional to the two-dimensional state. Recent advances in semiconductor technology allow us to study experimentally this dimensional problem for excitons by creating quantum wells whose thickness is comparable to the exciton Bohr radius. The effect of dimensionality on the oscillator strength of the exciton<sup>2-4</sup> as well as on the binding energy of the exciton has been extensively studied by theorists.<sup>2-6</sup> The recent magnetoabsorption experiment has revealed the binding energy of excitons in quantum wells.<sup>7,8</sup> However, there has been no full experimental study of the oscillator strength.

Compared with the binding energy, the oscillator strength is a more direct probe for the investigation of the nature of the wave function of excitons. This is because the oscillator strength is directly proportional to the square of the amplitude of the exciton wave function at the point where the two constituents of the exciton, an electron and a hole, overlap. It is expected that the overlap amplitude of the electron and the hole rapidly increases with the decrease of the well-layer thickness  $L_z$ , when  $L_z$  is smaller than the exciton Bohr radius  $a_B$ . Then the oscillator strength of excitons will rapidly increase. Some authors have reported the enhancement of the exciton oscillator strength with the decrease of well-layer thickness by comparing the lifetime of excitons.<sup>9,10</sup> However, the lifetime of excitons does not always reflect the oscillator strength, owing to the considerable contribution of the nonradiative processes. In fact, the observed reduction of the lifetime is too small compared with the enhancement of the oscillator strength directly presented in this paper.<sup>11</sup> In this work, we systematically study the oscillator strength of the lowest 1s heavy excitons in GaAs-AlAs quantum wells as a function of well thickness by means of optical absorption. The results give the first full experimental observation of the nature of the exciton

wave function in quantum wells.

In this work ten multi-quantum-well samples grown by molecular-beam epitaxy on GaAs(100) substrates were used. Their characters are listed in Table I. Samples (GaAs-AlAs, QW1-QW10) consist of alternate undoped GaAs well layers and undoped AlAs barrier layers. The thickness of the GaAs well layers ranges from 30 to 254 Å. A hole in the GaAs substrate of all the samples was made by means of selective chemical etching. Samples were directly immersed in superfluid helium. For the optical-absorption measurement, an incandescent lamp and a 50-cm monochromator were used. The light beam was carefully set to pass vertically through the hole in each GaAs substrate and the quantum-well layers.

In Fig. 1 absorption spectra  $\alpha(E)$  of six representative samples are shown. Here the absorption coefficient is defined as  $\alpha(E) = -\ln(I/I_0)/d(\text{GaAs})$ , where  $I_0$  and  $I$  are the incident and transmitted light intensities, respectively. The total thickness of the GaAs,  $d(\text{GaAs})$ , is equal to the well-layer thickness  $L_z$  multiplied by the number of GaAs

TABLE I. List of samples.  $L_z$  is the GaAs well thickness,  $L_b$  the AlAs barrier thickness,  $d(\text{GaAs})$  the total thickness of GaAs, and  $E_{n=1}$  the energy of the absorption peak due to the lowest 1s heavy-exciton state at 2.0 K.

GaAs-AlAs sample numbers	$L_z$ (Å)	$L_b$ (Å)	$d(\text{GaAs})$ (μm)	$E_{n=1}$ (eV)
QW1	30	40	0.30	1.845
QW2	43	62	0.86	1.683
QW3	53	50	1.18	1.672
QW4	58	71	0.99	1.642
QW5	76	33	2.08	1.622
QW6	83	93	1.43	1.579
QW7	96	91	0.96	1.571
QW8	108	36	2.63	1.572
QW9	154	131	2.00	1.540
QW10	254	122	2.03	1.524

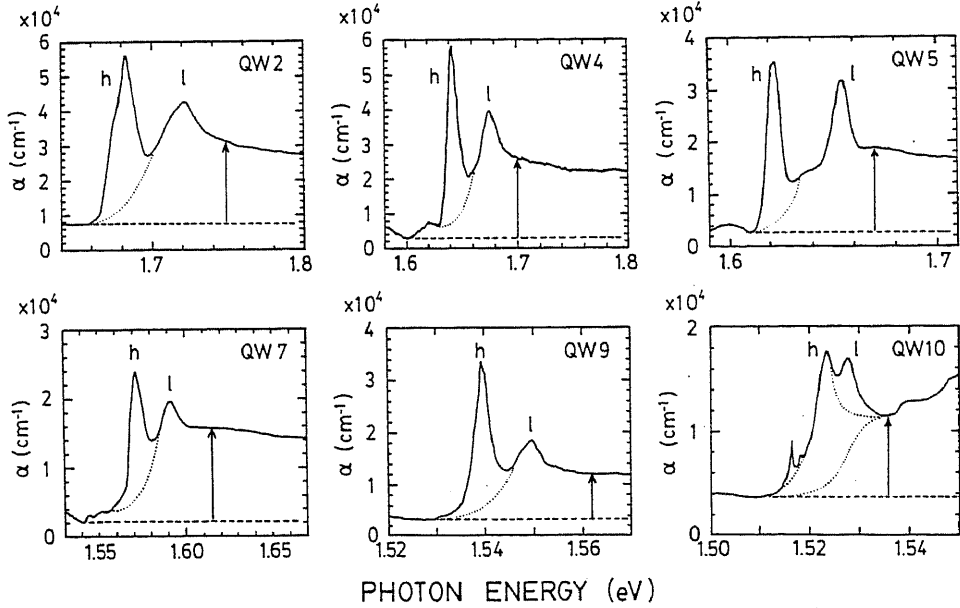


FIG. 1. Absorption spectra of the lowest heavy and light excitons in six representative GaAs-AlAs multi-quantum-well samples at 2.0 K. Heavy and light excitons are denoted by *h* and *l*, respectively. The background comes from the reflection loss, which is shown by dashed lines. Absorption areas of the heavy excitons plotted in Fig. 2 are those surrounded by solid lines and dotted lines. Absorption coefficient at the continuum plotted in the inset of Fig. 2 are indicated by arrows.

well layers. Observed absorption peaks located at the lowest energy are ascribed to the 1s heavy exciton ( $n=1$ , *e*-HH), which is composed of an electron and a heavy hole belonging to the lowest state ( $n=1$ ) in the quantum well. The absorption peaks located at the higher energy are ascribed to the 1s light exciton ( $n=1$ , *e*-LH), composed of an electron and a light hole. The absorption spectra are steplike above the 1s light-exciton energy. They correspond to the continuum transition from both the heavy and light valence bands to the conduction band. Steplike absorption spectra reflect the steplike two-dimensional density of states of the conduction and valence bands in a quantum well. The absorption coefficient at the continuum-band positions increases with the decrease of well-layer thickness  $L_z$ .<sup>12</sup> Simultaneously, the integrated areas of the absorption peaks due to heavy and light excitons increase.

The integrated areas of the absorption peaks are directly proportional to the oscillator strength  $f$  as follows:

$$\int_{E_1}^{E_2} \alpha(E) dE = \frac{2\pi^2 e^2 \hbar}{m_0 c \sqrt{\epsilon_b}} f, \quad (1)$$

where  $m_0$  is the mass of electron,  $e$  is the charge of electron,  $c$  is the light velocity,  $\epsilon_b$  is the background dielectric constant, and the lower and upper limits of the integral,  $E_1$  and  $E_2$ , cover the absorption peaks. Thus, we can directly estimate the oscillator strength  $f$  from the absorption area. The oscillator strength  $f$  of excitons in quantum wells is considered to vary spatially, because quantum wells consist of many islandlike clusters whose thickness fluctuates by the height of a monolayer.<sup>13</sup> The exciton in each cluster has

the oscillator strength for that cluster. Therefore, the oscillator strength  $f$  in Eq. (1) is regarded as the spatially averaged one.

In Fig. 2, the obtained absorption areas of the heavy-exciton peaks are shown as a function of  $L_z$ . In the inset of Fig. 2, the absorption coefficients at the continuum positions indicated by arrows in Fig. 1 are plotted.<sup>14</sup> From Fig. 2, one can find that the absorption coefficient at the continuum and the absorption area of the heavy-exciton peaks are strongly enhanced with the decrease of  $L_z$ . The absorption coefficient is proportional to  $1/L_z$ , while the absorption area of heavy-exciton peaks is enhanced much more with the decrease of  $L_z$ .

From the same variational calculation described previously, we can obtain the oscillator strength of 1s excitons in an infinite square well.<sup>3,4</sup> Dropping the plane-wave term, we take the following trial function for the 1s exciton wave function:

$$\Psi = N \cos(\pi z_e / L_z) \cos(\pi z_h / L_z) \times \exp\{-[\alpha^2(x^2 + y^2) + \beta^2(z_e - z_h)^2]^{1/2}\}. \quad (2)$$

Here two variational parameters  $\alpha$  and  $\beta$  are related to the spatial extent of the exciton in directions parallel ( $x, y$ ) and perpendicular ( $z$ ) to the well layer, respectively. The quantum well is assumed to have infinite wall at  $z = \pm L_z/2$  and the  $z$  coordinates of the electrons and holes are  $z_e$  and  $z_h$ , respectively.  $N$  is determined by the normalization condition. This trial function contains that used by Bastard, Mendez, Chang, and Esaki as a special case.<sup>5</sup> The oscillator

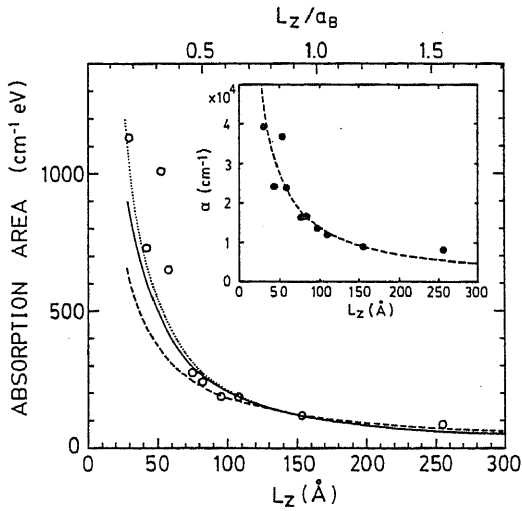


FIG. 2.  $L_z$  dependence of the absorption area (○) of the lowest 1s heavy exciton. The solid and dotted lines are the oscillator strength calculated on the basis of Eq. (3) with and without taking account of the energy dependence of the optical transition, respectively. The dashed line shows the  $1/L_z$  dependence. Calculated lines are normalized to fit the experimental data of QW9. In the inset the  $L_z$  dependence of the absorption coefficient (●) at the continuum indicated by arrows in Fig. 1 is plotted. The dashed line shows  $1/L_z$  dependence.

strength of 1s excitons is calculated by

$$f = (L_z N^2 / 2 m_0 \hbar \omega) |M_{cv}|^2 F(k_z L_z / 2), \quad (3)$$

where  $M_{cv}$  is the matrix element of the optical transition from the valence to the conduction band,  $\hbar\omega$  is the optical transition energy, and  $k_z$  is the  $z$  component of the photon wave vector in the well layers. A factor  $F(x) = [(\sin x/x)\pi^2/(x^2 - \pi^2)]^2$  arises from the wave-vector mismatch between excitons and photons. Because the relation  $k_z L_z / 2 < 0.35$  holds in all the samples, it is exact enough to regard  $F(k_z L_z / 2)$  in Eq. (3) as 1.0 for the analysis of the experiment. As  $L_z$  approaches zero, Eq. (3) converges to  $(4\alpha^2 / \pi m_0 \hbar \omega L_z) |M_{cv}|^2$ . In the limit of small  $L_z$ ,  $\alpha$  goes to  $2/a_B$ . Then expression (3) agrees with the well-known formula  $(16/\pi m_0 \hbar \omega L_z a_B^2) |M_{cv}|^2$  for the two-dimensional exciton.<sup>2</sup> As is shown by Chang and Schulman,<sup>15</sup> the square of the optical matrix element  $|M_{cv}|^2$  can be regarded as independent of  $L_z$  in the present range (30 Å <  $L_z$  < 254 Å). Thus we calculated the relative oscillator strength regarding the term  $|M_{cv}|^2$  in Eq. (3) as a constant. The calculated oscillator strength is shown as a function of  $L_z$  by solid and dotted lines in Fig. 2. The solid and dotted lines are calculated with and without taking into account the energy dependence of the optical transition energy  $\hbar\omega$  ( $=E_n - 1$  in Table I), respectively. Here we have adopted the values of static dielectric constant  $\epsilon_0 = 12.5$  and the reduced mass of exciton in the  $x,y$  directions  $\mu = 0.04 m_0$ , so that the Bohr radius  $a_B = \epsilon_0 \hbar^2 / \mu e^2$  is taken to be 165 Å. The calculated curves are normalized to fit the absorption area of the 1s heavy exciton in the QW9 sample. As a result of normalization, the calculated curves depend little

on the values of  $\epsilon_0$ ,  $\mu$ , and  $a_B$ . The agreement between the experimental values and the calculated curve is fairly good unless the well thickness is thinner than 60 Å. It is noted that almost the same calculated curves have been obtained even with other forms of trial functions by Bastard *et al.*<sup>5</sup> or Greene and Bajaj,<sup>6</sup> although the present trial function in Eq. (2) gives the largest binding energy for excitons.

It is instructive to compare the  $L_z$  dependence of the absorption area of the heavy-exciton peaks with that of the absorption coefficient at the continuum. With the decrease of  $L_z$ , the absorption coefficient grows larger in proportion to  $1/L_z$ . This dependence comes from the fact that the square of the overlap amplitude of the wave functions of the electrons and holes is proportional to  $1/L_z$ , because the unbound states of electrons and holes are confined in the well of thickness  $L_z$  in the  $z$  direction but are extended in the  $x,y$  directions, while the 1s exciton wave function shrinks in both the  $z$  and  $x,y$  directions. In the  $z$  direction, the exciton wave function shrinks in proportion to  $L_z$ , while in the  $x,y$  directions, the exciton wave function shrinks in proportion to  $1/\alpha$ . In the limit of small  $L_z$ ,  $1/\alpha a_B$  goes to  $1/2$ . This fact explains the more drastic increase of the absorption area of the heavy-exciton peak compared with the increase of the absorption coefficient at the continuum. Thus, the enhancement character of absorption area presents direct experimental verification of the two-dimensional shrinkage of the exciton wave function in quantum wells. In the case that the well layer is thinner than 60 Å, the experimental values are much larger than the calculated ones. The present experiment presents the relative increase of the oscillator strength of excitons in quantum wells. The calculated curve varies little even if we change the value of the Bohr radius  $a_B$  from 100 to 200 Å. This is because the calculated curve is normalized to fit the experimental data of the QW9 sample. Thus the disagreement between experiment and calculation is unavoidable.

The experimental data definitely show that the exciton wave function shrinks much more than calculated for the infinite-well model. This deviation is enhanced even more if we take the finite-well model. Then the exciton wave function does not shrink as much with the decrease of  $L_z$ , because the wave function penetrates somewhat into the barrier layer. The effect of the image force on excitons somewhat enhances the oscillator strength with the decrease of  $L_z$ . However, the enhancement explains only a part of the deviation.<sup>16</sup> If we assume that the reduced mass  $\mu$  of the exciton is enhanced by  $\approx 20\%$  below  $L_z \approx 60$  Å, the oscillator strength increases by  $\approx 40\%$ , so that the deviation is canceled. This is because the Bohr radius  $a_B$  is proportional to  $1/\mu$ , and because the oscillator strength of the two-dimensional exciton is enhanced in proportion to the enhancement of  $1/a_B^2$ . In this connection, we note the recent magneto-optical experiments.<sup>7,8</sup> The enhancement of the reduced mass of excitons deduced from our present experiment qualitatively agrees with that deduced from the magneto-optical experiments. The nonparabolicity of the heavy-hole subband probably explains the increase of the reduced mass with the decrease of  $L_z$ , because the hole states with larger wave vectors contribute to the exciton wave function with its shrinkage.

In summary, the oscillator strength of the lowest 1s heavy excitons in GaAs-AlAs quantum wells is studied as a function of well-layer thickness by means of optical absorption.

The oscillator strength of the lowest 1s heavy excitons is largely enhanced with the decrease of well-layer thickness. The enhancement character gives the full experimental verification of two-dimensional shrinkage of the exciton wave function in quantum wells. The exciton wave function shrinks much more than the calculated one when the quantum well is thinner than 60 Å. This fact suggests that the reduced mass of excitons is then enhanced by  $\approx 20\%$ .

The authors wish to thank Professor M. Matsuoka for fruitful discussions and continuous encouragement. This work was in part supported by the Scientific Research Grant-in-Aid No. 59460024 and the Scientific Research Grants-in-Aid No. 60222017 and No. 60222033 for Special Project Research on "Alloy Semiconductor Electronics" from the Ministry of Education, Science and Culture of Japan.

- <sup>1</sup>R. Dingle, in *Festkörperprobleme*, edited by H. J. Queisser, *Advances in Solid State Physics*, Vol. XV (Pergamon, New York, 1975), p. 21.
- <sup>2</sup>M. Shinada and S. Sugano, *J. Phys. Soc. Jpn.* **21**, 1936 (1966).
- <sup>3</sup>Y. Shinozuka and M. Matsuura, *Phys. Rev. B* **28**, 4878 (1983); **29**, 3717(E) (1984).
- <sup>4</sup>M. Matsuura and Y. Shinozuka, *J. Phys. Soc. Jpn.* **53**, 3138 (1984).
- <sup>5</sup>G. Bastard, E. E. Mendez, L. L. Chang, and L. Ésaki, *Phys. Rev. B* **26**, 1974 (1982).
- <sup>6</sup>R. L. Greene and K. K. Bajaj, *Solid State Commun.* **45**, 831 (1983).
- <sup>7</sup>S. Tarucha, H. Okamoto, Y. Iwasa, and N. Miura, *Solid State Commun.* **52**, 815 (1984).
- <sup>8</sup>J. C. Maan, G. Belle, A. Fasolino, M. Altarelli, and K. Ploog, *Phys. Rev. B* **30**, 2253 (1984).
- <sup>9</sup>E. O. Göbel, H. Jung, J. Kuhl, and K. Ploog, *Phys. Rev. Lett.* **51**, 1588 (1983).
- <sup>10</sup>J. Christen, D. Bimberg, A. Steckenborn, and G. Weimann, *Appl. Phys. Lett.* **44**, 84 (1983).
- <sup>11</sup>The ratio of the exciton lifetime in two samples, 2.85, observed by Göbel *et al.* (Ref. 9) is too small compared with the theoretical value, 3.8, and the experimentally observed ratio, 5.5, of the oscillator strength of excitons which are shown in Fig. 2. A similar conclusion holds for the result of Christen *et al.* (Ref. 10).
- <sup>12</sup>H. Iwamura, H. Kobayashi, and H. Okamoto, *Jpn. J. Appl. Phys.* **23**, L795 (1984).
- <sup>13</sup>C. Weisbuch, R. Dingle, A. C. Gossard, and W. Wiegmann, *Solid State Commun.* **38**, 709 (1981).
- <sup>14</sup>The absorption area of heavy excitons and the continuum-band positions shown by arrows in Fig. 1 are determined by the following guidelines. (1) The absorption line profile of heavy excitons is determined so as to be symmetric. (2) The absorption line profile of heavy excitons and that of light excitons are assumed to be the same because a common origin, that is, fluctuation of the well-layer thickness broadens these absorption lines. The continuum absorption coefficient is estimated at the positions where the contribution of absorption due to 1s light excitons is negligible. The continuum absorption coefficient thus estimated corresponds to the sum of absorption coefficients of heavy and light continuum bands. If we adopt other guidelines, the estimated absorption area of heavy excitons differs from the present value at most by  $\approx 25\%$ . Then, however, the relative values normalized by the value of the QW9 sample vary at most by  $\approx 10\%$ . Thus, the conclusion of this paper does not depend on the selection of guidelines.
- <sup>15</sup>Y. C. Chang and J. N. Schulman, *Appl. Phys. Lett.* **43**, 536 (1983); *Phys. Rev. B* **31**, 2069 (1985).
- <sup>16</sup>M. Matsuura (unpublished); the calculated oscillator strength of excitons for  $L_z = 50$  Å normalized by that for  $L_z = 154$  Å increases by about 10%, taking into account the effect of image force.

## Localization and homogeneous dephasing relaxation of quasi-two-dimensional excitons in quantum-well heterostructures

T. Takagahara

*Department of Applied Physics, The University of Tokyo, Bunkyo-ku, Tokyo 113, Japan*

(Received 6 August 1985)

The mechanisms of dephasing relaxation (homogeneous linewidth) of quasi-two-dimensional excitons in quantum-well heterostructures are clarified for both localized and delocalized excitons. The recently observed energy and temperature dependences of the homogeneous linewidth  $\Gamma_h$  are explained quantitatively. Furthermore, a new exponent for the temperature dependence of  $\Gamma_h$  of the localized excitons at low temperatures, the energy dependence of  $\Gamma_h$  of the delocalized excitons, and the dependence of  $\Gamma_h$  on the quantum-well thickness are predicted.

Recently, the homogeneous linewidth and the diffusion constant of quasi-two-dimensional excitons in GaAs-Al<sub>x</sub>Ga<sub>1-x</sub>As multiple-quantum-well structures have been measured by Hegarty, Goldner, and Sturge<sup>1</sup> with various techniques, such as resonant Rayleigh scattering, hole burning, and the transient grating method. Their measurements revealed the salient features of the energy and temperature dependence of the homogeneous linewidth of quasi-two-dimensional excitons. They found that the homogeneous linewidth increases sharply as the exciton energy increases through the center of the absorption line, and that below the line center the homogeneous linewidth is thermally activated. These experimental results suggest the existence of the mobility edge for the quasi-two-dimensional excitons in quantum-well heterostructures. From the linewidth analysis of the luminescence and its excitation spectra,<sup>2</sup> and independently from transmission electron microscopy,<sup>3,4</sup> it was suggested that the quantum-well interface has a kind of disorder, namely, islandlike structures having a height of one monolayer and a lateral size of about 300 Å. In the low-energy region the excitons can be localized at one of these islandlike structures since the exciton energy changes by several meV because of the one monolayer difference of the quantum-well thickness, and the Bohr radius of the quasi-two-dimensional exciton is about 100 Å for a typical well thickness of 100 Å.<sup>5-7</sup> The excitons localized at such islands of local minima in energy will migrate among the islands toward the lower-energy sites emitting acoustic phonons. The phonon-assisted migration of excitons among localized sites within a quantum-well layer was the key to understanding the behavior of energy relaxation in the low-energy region of photoluminescence spectra.<sup>8,9</sup>

In this paper the energy and temperature dependence of the homogeneous linewidth, which will be referred to as the dephasing relaxation constant hereafter, of the quasi-two-dimensional exciton and its absolute value are explained

quantitatively on the basis of the same model. In the following calculation the dephasing relaxation rate is identified with the rate at which the exciton state changes some of its degrees of freedom, for example, energy, momentum, site, and polarization.<sup>10</sup>

First of all, the mechanisms of dephasing relaxation should be identified.<sup>11</sup> In the localized regime the excitons can tunnel to other localized sites accompanying absorption or emission of acoustic phonons in order to compensate for the energy mismatch. As another mechanism contributing to the homogeneous linewidth, one can consider the phonon-assisted transition to the extended (delocalized) exciton states. The latter mechanism is effective in the intermediate temperature range ( $\geq 10$  K) because the transition is associated with phonon absorption. Obviously this mechanism leads to the activation-type behavior of the temperature dependence of the homogeneous linewidth ( $\Gamma_h$ ), which was observed experimentally.<sup>1</sup> On the other hand, the tunneling mechanism is working even at low temperatures ( $\sim 1$  K) and leads to the variable-range-hopping<sup>12</sup> behavior of  $\Gamma_h$ , which was also claimed to be observed.<sup>1</sup> As for the delocalized exciton state, dephasing relaxation is caused by acoustic phonon scattering on the two-dimensional dispersion curve. In fact, the phonon scattering rate is found to be enhanced by two orders of magnitude over that for the three-dimensional case because the phonon momentum perpendicular to the quantum-well interface can be arbitrary in the scattering. Another mechanism of dephasing relaxation of the delocalized exciton is elastic scattering by the potential fluctuation due to the layer-thickness fluctuation within a layer.

Now let us discuss the dephasing relaxation in the localized regime. The homogeneous linewidth of the localized exciton state with energy  $E$  due to phonon-assisted tunneling is calculated by

$$\Gamma_h^l(E) = \int dE' D(E') \tilde{T}(|E-E'|) \{ n(E'-E) \Theta(E'-E) + [1 + n(E-E')] \Theta(E-E') \}, \quad (1)$$

where  $D$  is the density of states of the localized exciton state,  $n$  is the phonon occupation number, and  $\tilde{T}(|E-E'|)$  denotes the spatially integrated exciton transfer rate whose expression is given in Ref. 9. The dephasing relaxation rate due to the activation process is given by

$$\Gamma_h^d(E) = \frac{2\pi}{\hbar} \sum_{K_{\parallel}} \sum_Q |\langle K_{\parallel} | H_{\text{ex-ph}} | R_a \rangle_Q|^2 n_Q \delta(E_a - E_{K_{\parallel}} + \hbar\omega_Q), \quad (2)$$

where  $|K_{\parallel}\rangle$  is the delocalized exciton state with a wave vector  $K_{\parallel}$  parallel to the quantum-well interface,  $|R_a\rangle$  is the local-

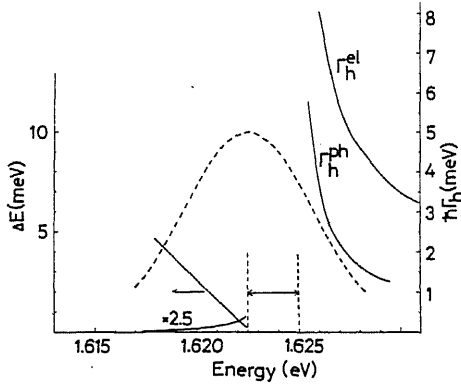


FIG. 1. The calculated homogeneous linewidth  $\Gamma_h$  and activation energy  $\Delta E$  as functions of exciton energy. The dashed line indicates the assumed exciton absorption spectrum. The region indicated by a double arrow is the supposed transition region between the localized and the delocalized regimes.

ized exciton state at site  $R_d$ , and  $H_{\text{ex-ph}}$  denotes the quasi-two-dimensional exciton-phonon interaction derived in Ref. 9. As for the envelope function of the localized exciton, it is found that a Gaussian form is not adequate because the energy dependence of the calculated  $\Gamma_h^{\text{lc}}$  is too sharp to explain the experimental results. Instead, an exponential function is adopted for the localization envelope. Calculated dephasing relaxation constants are shown in Fig. 1. The density of states of the exciton is assumed to be proportional to the absorption spectrum and the mobility edge is set at the center of the absorption line. The absolute value of the exciton energy in the figure has no particular meaning. The quantum-well thickness is taken as 80 Å and the infinite-barrier model is adopted for the exciton state. The temperature is 5 K and other material parameters, e.g., the exciton-phonon coupling constants, are the same as chosen in Ref. 9. Below the center of the absorption line, the calculated  $\Gamma_h$  is of the order of 0.1 meV and increases with the exciton energy. This is in good agreement with the experimental results. The temperature dependence of  $\Gamma_h$  is examined in this energy region. The Arrhenius plots of  $\Gamma_h$  at various exciton energies are given in Fig. 2. The activation energies determined from the temperature dependence in Fig. 2(a) are plotted in Fig. 1 as  $\Delta E$  on the left ordinate axis. As seen from Fig. 2(b), in the temperature region about 10 K there occurs a crossover in the dephasing mechanism from thermal activation to phonon-assisted tunneling because the latter mechanism is effective even at low temperatures ( $\sim 1$  K). Accordingly, the temperature dependence of  $\Gamma_h$  experiences a crossover between activation-type behavior and the behavior exhibited by  $\Gamma_h^{\text{ll}}$ . From the least-squares fit in the temperature range between 2 and 0.5 K,  $\Gamma_h^{\text{ll}}$  is found to obey the temperature dependence

$$\Gamma_h^{\text{ll}}(T) = \Gamma_0 \exp[B/T^\alpha], \quad (3)$$

where  $B$  is positive and the exponent  $\alpha$  is estimated to be

$$\Gamma_h^{\text{ll}}(K_{\parallel}) = \frac{2\pi}{\hbar} \sum_Q | \langle K_{\parallel} \pm Q_{\parallel} | H_{\text{ex-ph}} | K_{\parallel} \rangle_Q |^2 [n_Q \delta(E_{K_{\parallel}+Q_{\parallel}} - E_{K_{\parallel}} - \hbar\omega_Q) + (1+n_Q) \delta(E_{K_{\parallel}-Q_{\parallel}} - E_{K_{\parallel}} + \hbar\omega_Q)]. \quad (4)$$

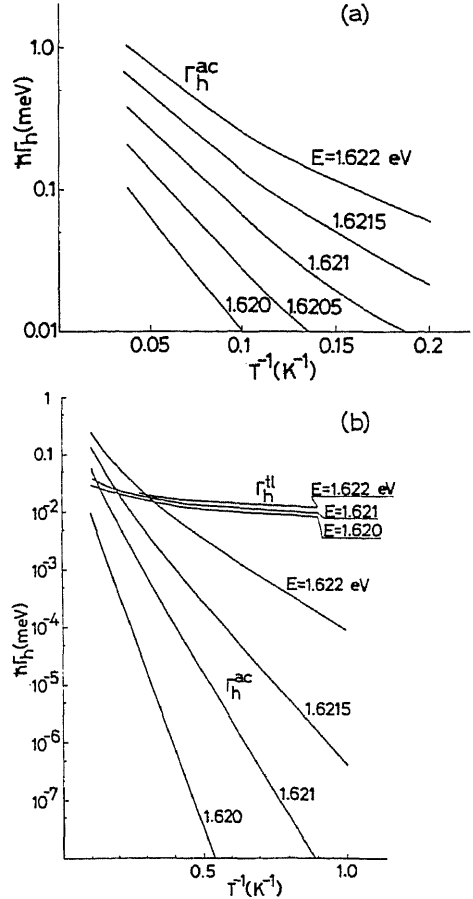


FIG. 2. Arrhenius plot of the homogeneous linewidth  $\Gamma_h$  at various exciton energies in the localized regime; (a) for  $\Gamma_h^{\text{lc}}$  and (b) for both  $\Gamma_h^{\text{lc}}$  and  $\Gamma_h^{\text{ll}}$ .

about  $(-1.7)$ – $(-1.6)$ , depending weakly on the exciton energy. This exponent is different from that for variable range hopping in two dimensions.<sup>12</sup> This difference arises essentially from the difference in the quantity to be measured. The hopping conductivity is induced by the activation of electrons near the Fermi surface by phonon absorption, while both the phonon absorption and emission processes contribute to the dephasing relaxation rate. Thus it is not very surprising that we found a new exponent different from that for variable range hopping.

Next, the dephasing relaxation constant of the delocalized exciton state will be discussed. As mentioned before, dephasing relaxation is partly caused by acoustic phonon scattering on the two-dimensional dispersion curve and partly by elastic scattering by the potential fluctuation. The contribution from the phonon scattering is given by

The calculated results are shown by  $\Gamma_h^{ph}$  in Fig. 1. The dispersion of the delocalized exciton state is assumed to begin from 2.5 meV above the mobility edge. This choice is rather arbitrary but does not seriously affect the qualitative features of the energy dependence of  $\Gamma_h$ . The dephasing relaxation rate due to elastic scattering by the potential fluctuation is calculated as follows. The fluctuation of the exciton energy is caused mainly by the fluctuation of the sub-band energy, since the binding energy of excitons is affected little by one monolayer change of the well thickness.<sup>5-7</sup> Within the effective-mass approximation the fluctuation of the exciton energy due to the fluctuation of the quantum-well thickness  $\delta L_z$  is given as

$$\delta E \approx \hbar^2 \pi^2 \delta L_z / \mu L_z^3, \quad (5)$$

where  $\mu$  is the reduced mass of the exciton. Assuming the scattering potential due to the exciton energy fluctuation to be a cylindrical one with radius  $\xi$ , the dephasing relaxation rate is calculated as

$$\Gamma_h^e(K_{\parallel}) = \frac{8\pi M \xi^2 (\delta E)^2}{\hbar^3 \sigma_0} \int_0^{\pi/2} d\theta \left( \frac{J_1(2K_{\parallel} \xi \cos \theta)}{2K_{\parallel} \cos \theta} \right)^2, \quad (6)$$

where  $M$ ,  $\delta E$ , and  $\sigma_0^{-1}$  are the exciton total mass, the potential fluctuation, and the areal number density of the scattering potential, respectively, and  $J_1$  denotes the first-order Bessel function. The calculated results are depicted as  $\Gamma_h^e$  in Fig. 1. The employed material parameters are again the same as in Ref. 9. The absolute values of  $\Gamma_h^{ph}$  and  $\Gamma_h^e$  are both of the order of meV in agreement with the experimental results, whereas they tend to decrease in the higher-energy region. This is because the magnitude of the wave vector of the participating phonons increases with the exciton energy in the case of  $\Gamma_h^{ph}$  and because of the  $K_{\parallel}^{-2}$  behavior of (6) in the case of  $\Gamma_h^e$ , respectively. Experimentally the value of  $\Gamma_h$  in this energy region has not yet been studied in detail.

The dependence of the dephasing relaxation rate on the quantum-well thickness will now be discussed. In the localized regime both  $\Gamma_h^{ac}$  and  $\Gamma_h^l$  depend on  $L_z$  through the matrix element of the exciton-phonon interaction. In the delocalized regime  $\Gamma_h^e$  in (6) is found to be inversely proportional to the sixth power of  $L_z$ , while  $\Gamma_h^{ph}$  in (4) depends on  $L_z$

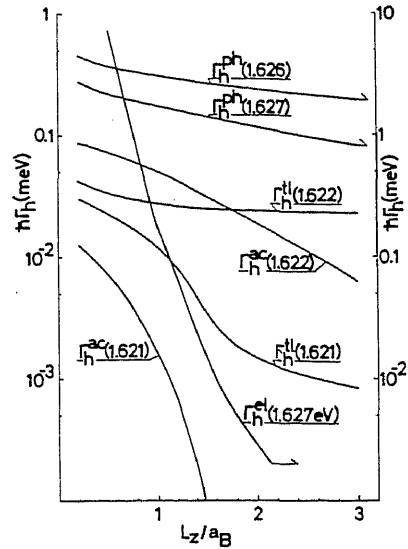


FIG. 3. Dependence of the homogeneous linewidth  $\hbar\Gamma_h$  on the quantum-well thickness. The fixed energies of exciton are indicated in parentheses and  $a_B$  denotes the Bohr radius of the three-dimensional exciton.

through the exciton-phonon matrix element. Typical variations of  $\Gamma_h$  at various exciton energies at 5 K are plotted in Fig. 3. It is seen that the  $L_z$  dependence of  $\Gamma_h$  in the localized regime is rather sensitive to the exciton energy. On the other hand,  $\Gamma_h^{ph}$  in the delocalized regime is insensitive to the exciton energy and is dependent on  $L_z$  only weakly. These features will be useful to identify the mechanism of dephasing relaxation, and systematic experimental study on the  $L_z$  dependence is highly desired.

In the energy region of transition between the localized and the delocalized regimes, it is difficult to describe the exciton state precisely and the calculation of  $\Gamma_h$  is left for future study.

<sup>1</sup>J. Hegarty, L. Goldner, and M. D. Sturge, Phys. Rev. B 30, 7346 (1984).

<sup>2</sup>C. Weisbuch, R. Dingle, A. C. Gossard, and W. Wiegmann, Solid State Commun. 38, 709 (1981).

<sup>3</sup>P. M. Petroff, A. C. Gossard, W. Wiegmann, and A. Savage, J. Cryst. Growth 44, 5 (1978).

<sup>4</sup>L. Goldstein, Y. Horikoshi, S. Tarucha, and H. Okamoto, Jpn. J. Appl. Phys. 22, 1489 (1983).

<sup>5</sup>G. Bastard, E. E. Mendez, L. L. Chang, and L. Esaki, Phys. Rev. B 26, 1974 (1982).

<sup>6</sup>R. L. Greene and K. K. Bajaj, Solid State Commun. 45, 831 (1983).

<sup>7</sup>Y. Shinozuka and M. Matsuura, Phys. Rev. B 28, 4878 (1983); 29, 3717(E) (1984).

<sup>8</sup>Y. Masumoto, S. Shionoya, and H. Kawaguchi, Phys. Rev. B 29, 2324 (1984).

<sup>9</sup>T. Takagahara, Phys. Rev. B 31, 6552 (1985).

<sup>10</sup>T. Takagahara, Phys. Rev. B 31, 8171 (1985).

<sup>11</sup>J. Hegarty and M. D. Sturge, J. Opt. Soc. Am. B2, 1143 (1985).

<sup>12</sup>N. F. Mott and E. A. Davis, *Electronic Processes in Noncrystalline Materials*, 2nd ed. (Oxford Univ. Press, New York, 1979).

## Tunneling dynamics of photogenerated carriers in semiconductor superlattices

Yasuaki Masumoto

*Institute for Solid State Physics, University of Tokyo, Roppongi 7-22-1, Minato-ku, Tokyo 106, Japan*

Seigo Tarucha and Hiroshi Okamoto

*Musashino Electrical Communication Laboratory, Nippon Telegraph and Telephone Corporation,**Midori-machi 3-9-11, Musashino-shi, Tokyo 180, Japan*

(Received 2 December 1985)

The tunneling dynamics of photogenerated carriers in GaAs-Al<sub>0.29</sub>Ga<sub>0.71</sub>As multiple-quantum-well structures are studied using picosecond spectroscopy with an electric field perpendicular to the well layers. Drastic changes, such as an increase in the photocurrent, a decrease in the exciton luminescence, and a change in the exciton lifetime, take place simultaneously for electric fields of  $\sim 5.0 \times 10^3$  V/cm. These changes are ascribed to the onset of exciton dissociation and electron tunneling through the Al<sub>0.29</sub>Ga<sub>0.71</sub>As barrier layers. The electron tunneling rate is determined to be 1/(430 ps) and is compared with calculations.

BMR306 1986 PACS numbers 73.40.Gk 71.35.+z 73.40.Lq

Recently, the dynamics of carriers in semiconductor superlattices has attracted growing interest. There are two directions of motion of the carriers in semiconductor superlattices. One is motion in the plane of heterostructures and the other is motion across the heterostructures. So far, the former has been studied extensively in two-dimensional carrier systems by means of transport experiments. However, *the study of the latter* have been relatively scarce and limited to current-voltage characteristics since the first observation of resonant tunneling of electrons.<sup>1</sup> This technique could be used to clarify the energy levels in superlattices but not the dynamical aspects. Therefore, new techniques have been required.

In this work, picosecond spectroscopy has been used to study the motion of photogenerated carriers in the direction of the superlattice. We probed the exciton luminescence in GaAs-Al<sub>0.29</sub>Ga<sub>0.71</sub>As multiple-quantum-well structures (MQW's) in an electric field applied in the direction of the superlattice. Exciton luminescence quenching and the change in the exciton lifetime have already been observed in a GaAs-Al<sub>x</sub>Ga<sub>1-x</sub>As MQW in an electric field.<sup>2-4</sup> It has been pointed out that these phenomena are possibly correlated with the field-induced separation of electrons from holes in a well or the tunneling of electrons or holes across the barrier potential. In the study, definitive evidence of the tunneling was not produced. In addition, the electric field in the MQW was not accurately determined, so that the experimental data could not be compared with the calculation. This is because the electric field is screened, to some extent, by the excess photogenerated carriers. We have overcome this difficulty. We have determined the electric field in the MQW by the peak shift of the heavy-exciton luminescence. In addition, we found that the exciton lifetime is surely dominated by the tunneling of electrons across the Al<sub>0.29</sub>Ga<sub>0.71</sub>As barrier above a certain critical electric field because the tunneling rate of electrons becomes faster than the decay rate of the exciton population, due to the other processes including radiative recombination. Then, the tunneling rate can be estimated by transient measurement of the exciton luminescence. The tunneling rate thus obtained is compared with the calculated one on the basis of the precise knowledge of the electric field in the MQW.

The sample is a *p-i-n* diode structure grown by molecular-beam epitaxy.<sup>5</sup> The main part consists of 100 alternate periods of undoped 120-Å GaAs well layers and undoped 58-Å Al<sub>0.29</sub>Ga<sub>0.71</sub>As barrier layers. The MQW's are surrounded by the *p*-type and *n*-type Al<sub>0.54</sub>Ga<sub>0.46</sub>As cladding layers 1  $\mu$ m thick. The MQW and cladding layers are sandwiched between the *p*<sup>+</sup>-type GaAs cap layer (0.5  $\mu$ m thick) and the *n*-type GaAs substrate. Electrical Ohmic contacts are made on both the *p*<sup>+</sup>-GaAs cap layer and *n*-GaAs substrate. With the sample in a perpendicular electric field at 4.2 K, we made measurements of the photoconductivity, the photocurrent-voltage characteristics, the exciton luminescence, the exciton-luminescence-voltage characteristics, and the picosecond transient response of the exciton luminescence.

For all measurements except photoconductivity, a dye laser synchronously pumped by a cw mode-locked Nd<sup>3+</sup>:YAG laser (Quantronix 416) (where YAG is yttrium aluminum garnet) is used as the excitation source. The dye laser gives 1-2-ps light pulses with a repetition rate of 82 MHz. The laser dyes Rhodamine 6G and DCM are used to generate 605-nm (2.05-eV) and 678-nm (1.83-eV) light pulses, respectively. The band-gap energies of Al<sub>0.54</sub>Ga<sub>0.46</sub>As, Al<sub>0.29</sub>Ga<sub>0.71</sub>As, and GaAs are 2.15 eV ( $X$ ), 1.88 eV ( $\Gamma$ ), and 1.519 eV ( $\Gamma$ ), respectively.<sup>6</sup> Therefore, neither 605- nor 678-nm light excites the Al<sub>0.54</sub>Ga<sub>0.46</sub>As cladding layers. The 605-nm light excites both the well layers and the barrier layers, while the 678-nm light excites only the well layers. No significant difference was found in the results, including the time-resolved result, whether the barrier layers were excited or not. Therefore, only the results for the 605-nm light excitation are presented in this paper. The laser beam is loosely focused on a *p-i-n* diode sample immersed in liquid helium. To reduce the electrical screening by photogenerated carriers, the excitation laser intensity is reduced to being as weak as possible for the picosecond time-resolved study. The excitation density is about 10 mW/cm<sup>2</sup>. The luminescence spectra are recorded by using a 50-cm monochromator. The exciton luminescence is temporally analyzed by using a synchroscan streak camera with 140- $\mu$ m slit width. Then the time resolution is 42 ps.

The energy shift of the heavy exciton can be used to

determine the electric field in the MQW as described below. We measured the photoconductivity spectra of the sample in the electric field by using the incandescent lamp. The result is shown in the inset of Fig. 1. In the photoconductivity spectra, the heavy excitons in the quantum wells produce a peak. The heavy-exciton peak shifts toward lower energy with the increase in the applied electric voltage. The shifts do not vary with further reduction of the excitation light level. The built-in voltage  $V_{bi}$  was determined to be 1.8 V from the curve of the current-voltage characteristics. The sample has no buffer layers. Therefore, the field is simply calculated to be  $F = (V_{ext} + V_{bi})/d$ , where  $V_{ext}$  is the externally applied voltage and  $d = 1.78 \mu\text{m}$  is the total thickness of the MQW. Following the calculation of Bastard for an infinite well, the energy shift of the lowest transition between the electron and hole sublevels,  $\Delta E$ , is proportional to the square of the electric field  $F$  as follows:<sup>7</sup>

$$\Delta E = -2.135 \times 10^{-3} (m_e^* + m_{hh}^*) e^2 F^2 L_z^4 / \hbar^2, \quad (1)$$

where  $e$  is the charge of electron, the  $z$  axis is along the superlattice direction,  $L_z$  is the well layer thickness, and  $m_e^*$  ( $= 0.655m_0$ ) and  $m_{hh}^*$  ( $= 0.45m_0$ ) are effective masses of the electron and the heavy hole, respectively. The change of the exciton binding energy is neglected because it is smaller than  $\Delta E$  by an order of magnitude.<sup>8</sup> In fact, Eq. (1) explains the energy shift of the excitons in a strikingly complete manner, as is shown in Fig. 1. Conversely, the

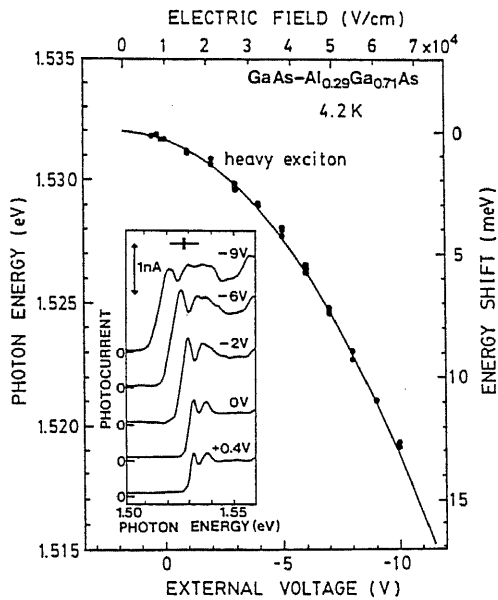


FIG. 1. Peak shift of the heavy excitons observed in photoconductivity spectra as a function of the applied electric voltage  $V_{ext}$ . Experimental data are shown by solid circles. The built-in voltage  $V_{bi}$  is +1.8 V. Electric field in the MQW is calculated to be  $(V_{ext} + V_{bi})/d$ . The solid line is the calculated one on the basis of Eq. (1). In the inset, photoconductivity spectra under the externally applied voltage are shown. The lowest-energy peak corresponds to heavy excitons.

electric field in the MQW can be determined from the peak shift of excitons.

Under the picosecond laser excitation, the exciton-luminescence energy shifts toward lower energy with an increase in the externally applied voltage as is shown in the inset of Fig. 2. Then, however, the peak shift is not so large as expected. We attribute this disagreement to the screening of the electric field by the high density of photo-generated carriers<sup>3</sup> because we observe that the peak shift is reduced with an increase in the exciton intensity. Therefore, we do not estimate the electric field from the applied voltage. Instead, we determine the electric field from the peak shift on the basis of Eq. (1). In Fig. 2, both the exciton-luminescence intensity and the photocurrent across the superlattices are plotted as a function of electric field thus estimated. A sudden change is observed at a field of  $F_c \sim 5.0 \times 10^3$  V/cm. At this value, the exciton-luminescence intensity decreases and the photocurrent increases. These facts indicate that the excitons dissociate at this field and that electrons or holes tunnel through the potential barriers and contribute to the photocurrent. At the field of  $F_c \sim 5.0 \times 10^3$  V/cm, the field gain for the electrons or holes amounts to 9 meV when they move by a superlattice period

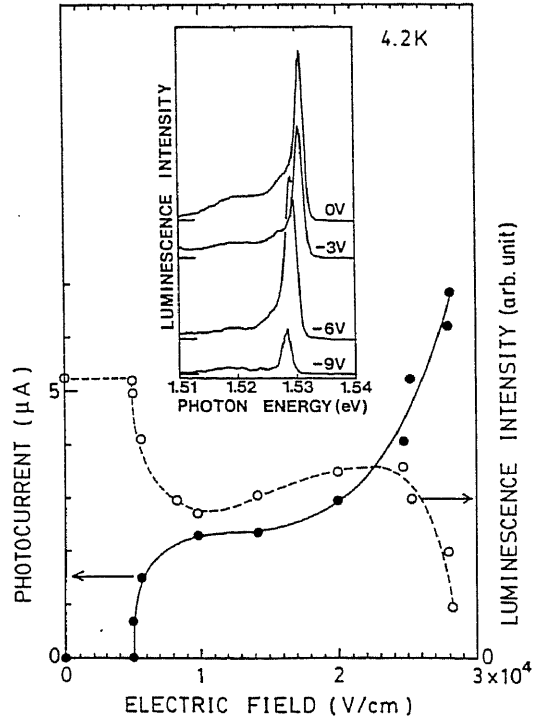


FIG. 2. Luminescence intensity of heavy excitons (O) and photocurrent (●) as a function of the electric field in the MQW. Solid and dashed lines are guides for the eyes. The inset shows heavy-exciton luminescence spectra under externally applied voltage. The peak shifts of heavy excitons indicate that applied voltages 0, -3, -6, and -9 V correspond to electric fields  $5.0 \times 10^3$ ,  $9.8 \times 10^3$ ,  $2.5 \times 10^4$ , and  $2.8 \times 10^4$  V/cm, respectively.

( $\approx 178 \text{ \AA}$ ). The field gain is almost equal to the exciton binding energy in 120-Å quantum wells (10 meV) derived from the magneto-optical measurements.<sup>9</sup> The field gain compensates for the binding energy. Therefore, it is quite reasonable for excitons to dissociate at a field of  $F_i \sim 5.0 \times 10^3$  V/cm. Curves of photocurrent and luminescence intensity show a plateau between  $\sim 1.0 \times 10^4$  and  $\sim 2.0 \times 10^4$  V/cm. With the further increase in the electric field up to  $\sim 2.8 \times 10^4$  V/cm, the photocurrent increases and the exciton luminescence decreases.

The transient response of the exciton luminescence is shown in Fig. 3. At the field of  $F_i \sim 5.0 \times 10^3$  V/cm, the temporal profile of the exciton luminescence changes drastically. Below  $F_i$ , the exciton luminescence exponentially decays with a time constant of 1.52 ns. Above  $F_i$ , the exciton-luminescence decay seems to consist of two components. The fast decay has a time constant of 430 ps. The slow one has a long time constant which has not been determined in this experiment. We determine that the change of the temporal profile comes from the tunneling of the electrons or holes because the luminescence decrease and the photocurrent increase take place at the common electric field of  $F_i \sim 5.0 \times 10^3$  V/cm. Then, the fast decay of exciton luminescence is dominated by the tunneling of electrons or holes across the potential barriers. Therefore the tunneling rate can be estimated to be  $1/(430 \text{ ps}) = 2.3 \times 10^9 \text{ s}^{-1}$ . At a field of  $\sim 2.8 \times 10^4$  V/cm, the slow-decay component of the exciton luminescence vanishes completely and the exciton luminescence exponentially decays with a time constant of 430 ps.

It is not easy to estimate the dissociation rate of excitons in the MQW. To estimate it, we must calculate the rates of at least two processes, the dissociation of excitons, and the tunneling of electrons or holes across the barrier potential. If the excitons are not in the quantum wells and are in the

electric field  $F$ , the dissociation rate of excitons,  $w_1$ , is given by the following formula which also describes the ionization rate of hydrogen atoms.<sup>10</sup>

$$w_1 = (16R^2/\hbar e F a_B) \exp(-4R/3e F a_B), \quad (2)$$

where  $R$  ( $= 4.2 \text{ meV}$ ) is the Rydberg energy and  $a_B$  ( $= 136 \text{ \AA}$ ) is the exciton Bohr radius. The dissociation rate reaches  $2.8 \times 10^{13} \text{ s}^{-1}$  at an electric field of  $F_i \sim 5.0 \times 10^3$  V/cm. The rate is much faster than the observed rate.

Compared with the above-mentioned dissociation rate, the tunneling rate of electrons or holes across the barrier potential is expected to be slow because the  $\text{Al}_{0.29}\text{Ga}_{0.71}\text{As}$  barrier potential is much higher than the Coulomb barrier. The experimental results corresponds exactly with this expectation. In the Wentzel-Kramers-Brillouin approximation, the tunneling rate of electrons or heavy holes across the barrier potential  $w_2$  is estimated to be<sup>11</sup>

$$w_2 = (\pi\hbar/2m_{e^*}^*(\text{hh})L_z^2) \exp[-(2/\hbar)\sqrt{2m_{e^*}^*(\text{hh})(U-E)}d_b], \quad (3)$$

if the Coulomb interaction between the electrons and heavy holes is neglected. Here,  $E$  is the band discontinuity,  $U$  is the confinement energy of the lowest sublevel, and  $d_b$  ( $= 58 \text{ \AA}$ ) is the barrier thickness. The factor  $2m_{e^*}^*(\text{hh})L_z^2/\pi\hbar$  is the classical period of the electron (heavy-hole) motion in the quantum well,<sup>11</sup> because the  $z$  component of the velocity of electrons (heavy holes) in the lowest sublevel is  $\hbar k/m_{e^*}^*(\text{hh}) = \pi\hbar/m_{e^*}^*(\text{hh})L_z$ . Equation (3) is the expression in the case of zero applied electric field. However, this equation approximately holds under the condition  $eFd \ll U - E$ , even when the electric field is applied.

The rate calculated on the basis of Eq. (3) is not altered much when the confinement energy  $U$  is neglected because  $U$  is smaller than the band discontinuity  $E$  by an order of magnitude. Therefore  $U$  is neglected for simplicity. If the band-gap discontinuity split of 85:15 is correct,<sup>12</sup> the conduction-band discontinuity  $E_c$  is 307 meV and the valence-band discontinuity  $E_v$  is 54 meV. Then, the tunneling rate of electrons is  $3.9 \times 10^9 \text{ s}^{-1}$  and that of holes is  $2.7 \times 10^8 \text{ s}^{-1}$ . On the other hand, the tunneling rate of electrons is  $1.8 \times 10^{10} \text{ s}^{-1}$  and that of holes is  $4.3 \times 10^9 \text{ s}^{-1}$ , if the band-gap discontinuity split of 57:43 ( $E_c = 206 \text{ meV}$ ,  $E_v = 155 \text{ meV}$ ) is correct.<sup>13</sup> In both the cases, tunneling of electrons dominates the field dissociation rate of excitons across the barrier potential. The calculated tunneling rates are faster than the experimental value. However, disagreement is within an order of magnitude, although the calculation is the simplest one.

The simple calculation well explains the experimental characteristics that the tunneling rate is not affected by the electric field between  $5.0 \times 10^3$  and  $2.8 \times 10^4$  V/cm. In fact, unlike the earlier experiments,<sup>2,3</sup> the condition  $eFd \ll U - E$  holds in our experiment. Nevertheless, excitons are stripped of electrons and electrons tunnel across barrier potentials critically at the field  $F_i \sim 5.0 \times 10^3$  V/cm, because the field gain can compensate for the binding energy of excitons. It is not easy to consider the tunneling of electrons through both the Coulomb barrier and the barrier potential. In fact, there is no available theoretical study of this problem. The slow-decay component observed between  $\sim 5.6 \times 10^3$  and  $\sim 2.8 \times 10^4$  V/cm may be due to nongeminate excitons made of stripped electrons and holes. With

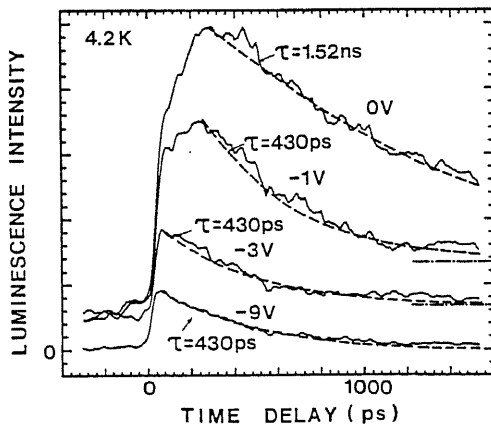


FIG. 3. Temporal profile of the heavy-exciton luminescence intensity in the perpendicular electric field. The estimated electric fields in the MQW are  $5.0 \times 10^3$ ,  $5.6 \times 10^3$ ,  $9.8 \times 10^3$ , and  $2.8 \times 10^4$  V/cm for the applied voltages of 0, -1, -3, and -9 V, respectively. Dashed lines show exponential decay with respective time constant  $\tau$ . Dash-dotted lines show long-lived component. The background observed before 0 ps comes from the stray of 6-ns-lived luminescence which is peculiar to the synchroscan streak camera.

the increase in the electric field, the slow-decay component decreases and the photocurrent increases. We may attribute this change to the onset of successive tunneling of electrons through many barriers. However, these processes remain to be clarified by future study.

In summary, the tunneling dynamics of photogenerated carriers in GaAs-Al<sub>0.29</sub>Ga<sub>0.71</sub>As multiple-quantum-well structures have been studied in an electric field perpendicular to the well layers. Drastic changes, such as an increase in the photocurrent, a decrease in the exciton luminescence, and a change of the exciton lifetime take place simultaneously at the critical electric field of  $\sim 5.0 \times 10^3$  V/cm. The changes are ascribed to the dissociation of excitons and the tunneling of electrons through the Al<sub>0.29</sub>Ga<sub>0.71</sub>As potential barriers. These processes take place when the field gain can compensate for the exciton binding energy. The tunneling rate of the electrons is determined to be 1/(430 ps), slower than the simple estimation.

*Note added.* A recent work by Pollard *et al.* [Phys. Rev. Lett. 55, 2610 (1985)] covers similar ground treated in the present work. Contrary to the present results, they have observed that the lifetime of excitons is prolonged with an increase in the electric field. The contradiction probably comes from a difference in the quantum-well structures, especially with respect to the thickness of barriers.

The authors wish to thank Professor M. Matsuoka for valuable discussions and continuous encouragement. The picosecond laser system used in this work was developed by one of the authors (Y.M.) in collaboration with Professor M. Matsuoka and Dr. M. Baba, whom authors wish to thank. This work was supported in part by Scientific Research Grant-in-Aid No. 59460024 and Scientific Research Grant-in-Aid No. 60222017 from the Ministry of Education, Science and Culture of Japan.

---

<sup>1</sup>L. L. Chang, L. Esaki, and R. Tsu, Appl. Phys. Lett. 24, 593 (1974).  
<sup>2</sup>E. E. Mendez, G. Bastard, L. L. Chang, L. Esaki, H. Morkoc, and R. Fisher, Phys. Rev. B 26, 7101 (1982).  
<sup>3</sup>J. A. Kash, E. E. Mendez, and H. Morkoc, Appl. Phys. Lett. 46, 173 (1985).  
<sup>4</sup>Y. Horikoshi, A. Fischer, and K. Ploog, Phys. Rev. B 31, 7859 (1985).  
<sup>5</sup>H. Iwamura, T. Saku, and H. Okamoto, Jpn. J. Appl. Phys. 24, 104 (1985).  
<sup>6</sup>H. C. Casey, Jr. and M. B. Panish, *Heterostructure Lasers* (Academic, New York, 1978), Part A, Chap. 4.  
<sup>7</sup>G. Bastard, E. E. Mendez, L. L. Chang, and L. Esaki, Phys. Rev. B 28, 3241 (1983).

<sup>8</sup>D. A. B. Miller, D. S. Chemla, T. C. Damen, A. C. Gossard, W. Wiegmann, T. H. Wood, and C. A. Burrus, Phys. Rev. Lett. 53, 2173 (1984); Phys. Rev. B 32, 1043 (1985).  
<sup>9</sup>S. Tarucha, H. Okamoto, Y. Iwasa, and N. Miura, Solid State Commun. 52, 815 (1984).  
<sup>10</sup>L. D. Landau and E. M. Lifshitz, *Quantum Mechanics*, 3rd ed. (Pergamon, New York, 1977), Chap. 10.  
<sup>11</sup>D. Bohm, *Quantum Theory* (Prentice-Hall, Englewood Cliffs, 1951), Chap. 12.  
<sup>12</sup>R. Dingle, in *Festkörperprobleme*, Advances in Solid State Physics, Vol. XV, edited by H. J. Queisser (Pergamon, New York, 1975), p. 21.  
<sup>13</sup>R. C. Miller, D. A. Kleinman, and A. C. Gossard, Phys. Rev. B 29, 7085 (1984).